Norwegian University of Life Sciences
Faculty of Chemistry, Biotechnology and Food Science

Philosophiae Doctor (PhD)
Thesis 2022:27

An investigation of the interplay between *in situ* hydrogen peroxide production and catalytic efficiency in lytic polysaccharide monooxygenase reactions

En studie av samspillet mellom *in situ* hydrogenperoksidproduksjon og katalytisk effektivitet i lytisk polysakkarid monooksygenase-reaksjoner

Anton Stepnov

An investigation of the interplay between *in situ* hydrogen peroxide production and catalytic efficiency in lytic polysaccharide monooxygenase reactions

En studie av samspillet mellom *in situ* hydrogenperoksidproduksjon og katalytisk effektivitet i lytisk polysakkarid monooksygenase-reaksjoner

Philosophiae Doctor (PhD) Thesis

Anton Stepnov

Norwegian University of Life Sciences
Faculty of Chemistry, Biotechnology and Food Science

Ås (2022)

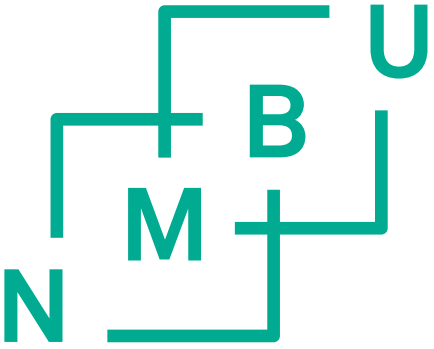

Thesis number 2022:27
ISSN 1894-6402
ISBN 978-82-575-1900-1

Table of contents

* - the chapter contains excerpts from a review previously published by the author [1]

Acknowledgements

The work described in this thesis was carried out at the Protein Engineering and Proteomics (PEP) group at the Norwegian University of Life Sciences and was supported by the Research Council of Norway under Grant no. 269408 (Centre for Digital Life Norway, project OxyMod).

I would like to express my gratitude to all my supervisors for the incredible support and guidance that I have received. **Vincent**, thank you very much for giving me an exciting opportunity to get back into science after 10 long years of gap. I have learned so much through our discussions! **Morten** and **Åsmund**, thank you for backing me up with your expertise. A wise advice on chemistry is a thing a biologist like me can always use. **Zarah**, we both know that working with LPMOs can be really scary. Thank you for giving me the best course in LPMO survival. It helped a lot.

Special thanks to all the people at KBM for being friends and great colleagues. **Amanda**, **Aniko**, **AnneCath**, **Eirik**, **Geir**, **Gustav**, **Heidi**, **Ivan**, **Kelsi**, **Lasse**, **Live**, **Lukas, Ole, Olav** and **Tamil**, thank you very much for many hours of interesting conversations and your support. I also wish to thank my co-authors at NTNU and SINTEF for a very productive collaboration.

Last but not least, I would like to say thank you to my parents, **Irina** and **Igor**, and to my wife **Daria**. You make this Universe such a great place to be!

Summary

Lytic polysaccharide monooxygenases (LPMOs) are mono-copper enzymes that catalyze oxidative depolymerization of recalcitrant carbohydrate substrates, such as chitin and cellulose. LPMOs have received much attention from academia and industry due to their remarkable ability to act on the crystalline surfaces of their target substrates, rather than on isolated polysaccharide chains. Despite a large amount of research, there are still many unknowns regarding the mechanism and kinetics of LPMO-catalyzed reactions. LPMOs were previously thought to use molecular oxygen as a co-substrate, but later it was shown that these enzymes prefer hydrogen peroxide, thus operating as peroxygenases rather than strict monooxygenases. Importantly, peroxygenase reactions are likely to occur even in the absence of exogenous hydrogen peroxide, since H_2O_2 can be produced *in situ* in most aerobic reaction set-ups with LPMOs, for example through oxidase activity of the LPMO itself. This study was focused on the complex interplay between H_2O_2-generating reactions and the catalytic efficiency of LPMOs acting on cellulose in the presence of oxygen and various low-molecular weight reductants.

Paper I presents the biochemical characterization of a novel bacterial LPMO discovered by mining the genome of a marine Actinomycete. We used this enzyme as a model to study how free copper affects LPMO activity in reactions with two reductants that are commonly used to drive LPMO catalysis, ascorbic acid and gallic acid. The results indicate that ascorbate-driven reactions are sensitive to sub-micromolar concentrations of free copper because copper promotes enzyme-independent H_2O_2 production. Consequently, copper not only speeds up the (peroxygenase) reaction but also leads to increased autocatalytic enzyme inactivation due to excess H_2O_2. On the other hand, using gallic acid as an electron donor allows for controlled and more stable reactions showing no dependency on free copper in the system. Importantly, we describe how LPMO preparations devoid of free copper can be prepared and how the concentration of non-enzyme-bound Cu(II) can be assessed using a simple assay. Last but not least, the data presented in

Paper I suggest that the apparent monooxygenase reactions observed for this bacterial model LPMO in standard reaction set-ups, without added H_2O_2 and with minimized levels of free copper, are in fact peroxygenase reactions driven by reductant auto-oxidation.

Paper II builds on the observation, presented in Paper I, that *in situ* H_2O_2 production fuels LPMO reactions at standard aerobic conditions. This paper describes a novel LPMO from the phytopathogenic bacterium *Streptomyces scabies* and documents a strong correlation between the enzyme catalytic rate and the rate of H_2O_2 generation in the reaction mixture, for three reductants (ascorbic acid, gallic acid or L-cysteine). Unexpectedly, the results show that the oxidized form of ascorbic acid (dehydroascorbic acid, DHA) is also able to drive LPMO reactions. Based on kinetic studies and NMR analysis, it is shown that DHA is unstable and converts into multiple derivatives, some of which are redox active and can sustain the LPMO reaction by reducing the active site copper and promoting H_2O_2 production.

Paper III provides insight into the complex interplay between multiple LPMOs, which can arise as a result of *in situ* H_2O_2 generation and consumption. Such insight was obtained by comparing properties of full length two-domain *Sc*LPMO10C and its truncated form (*Sc*LPMO10C-AA10), lacking the C-terminal cellulose-binding module (CBM). The results show that truncation of the CBM leads to elevated H_2O_2 production by the enzyme, which again leads to higher catalytic activity and decreased operational stability. Furthermore, the results show that combining *Sc*LPMO10C and *Sc*LPMO10C-AA10 allows for synergistic and steady depolymerization of cellulose. Being an efficient hydrogen peroxide producer, *Sc*LPMO10C-AA10 is able to enhance cellulose oxidation by the full-length enzyme. At the same time, *Sc*LPMO10C protects the truncated LPMO from fast auto-catalytic inactivation by consuming H_2O_2. Importantly, the results described in this paper indicate that, in reactions with ascorbic acid, release of copper ions as a consequence of oxidative damage to the LPMO active site triggers a self-reinforcing chain reaction leading to increased enzyme-independent H_2O_2 generation, rapid enzyme inactivation and reductant depletion, which will eventually stop the LPMO reaction.

Paper IV presents a kinetic investigation of two fungal LPMOs (*Nc*LPMO9C and *Ls*LPMO9A) capable of acting on soluble oligosaccharides. To dig deeper into

LPMO-catalyzed peroxygenase reactions, we obtained Michaelis-Menten parameters for cellopentaose oxidation by *Nc*LPMO9C. The results show that both enzymes are fast and specific peroxygenases capable of achieving unprecedented catalytic rates, which, for *Nc*LPMO9C reach about 100 s^{-1} at 4 °C. Importantly, when acting on the rapidly diffusing cellopentaose substrate, the LPMOs were capable of stoichiometric productive conversion of high starting amounts of exogenous H_2O_2.

In conclusion, this thesis provides novel insights into many factors that affect LPMO performance and shows that, under optimal conditions, LPMOs can be very efficient enzymes. Based on the results presented here, it seems unlikely that the monooxygenase reaction plays a significant role in biomass turnover by LPMOs.

Sammendrag

Lytisk polysakkarid monooksygenaser (LPMOer) er mono-kobberenzymer som kan katalysere oksidativ depolymerisering av krystallinske substrater som kitin og cellulose. LPMOer er av høy interesse for både forskere og industri på grunn av deres unike evne til å virke på den krystallinske overflaten til substratene fremfor på de isolerte polysakkaridkjedene. Selv om mye forskning er gjennomført, er det fremdeles mye usikkerhet forbundet med mekanismen og kinetikken av LPMO-katalyserte reaksjoner. Opprinnelig trodde man at LPMOer benytter molekylært oksygen som ko-substrat, men i senere tid er det blitt vist at enzymene foretrekker hydrogenperoksid og at de derfor fungerer som peroksygenaser istedenfor monooksygenaser. Peroksygenasereaksjonen vil trolig skje selv ved fravær av tilsatt H_2O_2 fordi de fleste aerobe reaksjonsbetingelsene vil føre til at det dannes H_2O_2 *in situ*, for eksempel som følge av LPMOenes oksidaseaktivitet. Denne studien har satt søkelys på det komplekse samspillet mellom H_2O_2-genererende reaksjoner og den katalytiske effektiviteten til LPMOer som bryter ned cellulose i reaksjoner med oksygen og et utvalg av reduktanter.

Artikkel I presenterer biokjemisk karakterisering av en nyoppdaget bakteriell LPMO som ble funnet gjennom utforsking av genomet til en marin Actinomycete. Dette enzymet ble brukt som en modell til å undersøke hvordan fritt kobber påvirker LPMO-aktivitet i reaksjoner med to av de vanligste reduktantene brukt til å drive LPMO katalyserte reaksjoner: gallussyre og askorbinsyre. Resultatene indikerer at askorbinsyredrevne reaksjoner er sensitive for mikromolare konsentrasjoner av fritt kobber på grunn av høy produksjon av H_2O_2 gjennom enzymuavhengig kobberkatalyserte reaksjoner. Derfor vil kobber både øke hastigheten til (peroksygenase) reaksjonen og øke auto-katalysert enzyminaktivering som er en følge av et overskudd av H_2O_2. I motsetning til reaksjoner med askorbinsyre viser reaksjoner med gallussyre en kontrollert og stabil reaksjon, som er uavhengig av fritt kobber i systemet. Artikkel I beskriver en fremgangsmåte for hvordan LPMOer kan prepareres uten kobber kontaminering, og viser hvordan konsentrasjonen av fritt

kobber i enzympreparater kan analyseres ved bruk av en enkel metode. Sist, men ikke minst, viser resultatene i Artikkel I at de tidligere antatte monooksygenasereaksjonene observert i standardreaksjoner med den bakterielle LPMOen, uten tilsatt H_2O_2 og i fravær av signifikante mengder av fritt kobber, faktisk er peroksygenase reaksjoner som drives av auto-oksidering av reduktanten.

Artikkel II bygger på observasjonene presentert i Artikkel I, som tyder på at *in situ* produksjon av H_2O_2 driver LPMO-reaksjoner ved standard aerobe betingelser. Denne artikkelen beskriver en nyoppdaget LPMO fra den patogene bakterien *Streptomyces scabies* og viser en klar korrelasjon mellom den enzymkatalyserte nedbryting av cellulose og mengden H_2O_2 produsert i reaksjonen, for reduktantene askorbinsyre, gallussyre og L-cysteine. Overraskende viser resultatene at den oksiderte formen av askorbinsyre (dehydroaskorbinsyre, DHA) også kan drive LPMO reaksjoner. Basert på både kinetiske analyser og NMR analyser, vises det at DHA er ustabil og omgjøres til flere derivater, hvorav noen er redoksaktive og kan opprettholde LPMO reaksjoner ved å redusere det aktive kobbersetet og øke produksjonen av H_2O_2.

Artikkel III gir innsikt i det komplekse samspillet mellom flere LPMOer som kan oppstå som et resultat av *in situ* produksjon og konsumpsjon av H_2O_2. I denne artikkelen sammenligner vi to-domene enzymet *Sc*LPMO10C med den trunkerte formen (*Sc*LPMO10C-AA10) som mangler den C-terminale cellulose bindene modulen (CBM). Resultatene viser at trunkering av CBMen fører til at enzymet produserer mer H_2O_2, og som igjen fører til økt katalytisk aktivitet og redusert operasjonell stabilitet. Videre viser resultatene at man ved å blande *Sc*LPMO10C og *Sc*LPMO10C-AA10 oppnår synergistisk og stabil de-polymerisering av cellulose. Ved å være en effektiv produsent av H_2O_2 vil *Sc*LPMO10C-AA10 kunne øke den celluloseoksiderende aktiviteten av full-lengde enzymet. Samtidig vil full-lengde enzymet beskytte den trunkerte LPMOen fra rask auto-katalytisk inaktivering ved å fjerne H_2O_2 fra reaksjonsblandingen. Et viktig resultat av arbeidet beskrevet i denne artikkelen er at det vises at oksidativ skade til det aktive setet i LPMOer kan sette i gang en kjedereaksjon som gjør at enzymaktivitet raskt opphører. Slik skade fører til at kobber slippes ut, og i reaksjoner med askorbinsyre vil dette føre til økt enzym-

uavhengig H_2O_2 produksjon, raskere inaktivering av enzymet, og rask konsumpsjon av reduktanten.

Artikkel IV presenterer en kinetisk undersøkelse av to fungale LPMOer (*Nc*LPMO9C og *Ls*LPMO9A) som kan fungere på løselige oligosakkarider og som ble testet i reaksjoner med tilsatt H_2O_2. For å få en bedre forståelse av peroksygenasereaskjonen katalysert av disse LPMO, ble det utført en Michaelis-Menten kinetisk analyse av aktiviteten til *Nc*LPMO9C på cellopentaose. Resultatene viser at begge enzymene er raske og spesifikke peroksygenaser som kan oppnå hastigheter av opp til 100 s^{-1} ved 4 °C. En annen vesentlig observasjon er at når LPMOen virker på dette substratet, så er enzymene i stand til å omdanne store mengder H_2O_2 som ble tilsatt ved starten av reaksjonen, til støkiometriske mengder av oksidert substrat.

Til sammen gir resultatene av denne studien nye innsikter i flere av faktorene som påvirker LPMO reaksjoner og viser at LPMOer kan være effektive enzymer under godt kontrollerte reaksjonsbetingelser. Basert på disse resultater virker det usannsynlig at monooksygenase reaksjonen spiller en vesentlig rolle når LPMOer bryter ned biomasse**.**

Abbreviations

AA – auxiliary activities
CBM – carbohydrate-binding module
CMC - carboxymethyl cellulose
DHA – dehydroascorbic acid
HPAEC-PAD – high performance anion exchange chromatography with pulsed amperometric detection
HRP – horseradish peroxidase
ICP-MS – inductively coupled plasma mass spectrometry
LPMO – lytic polysaccharide monooxygenase
Ls - *Lentinus similis*
MALDI-ToF MS – matrix assisted laser desorption/ionization – time-of-flight mass spectrometry
Nc – *Neurospora crassa*
PASC – phosphoric acid-swollen cellulose
PDB – Protein Data Bank
Sc – *Streptomyces coelicolor*
Ssc – *Streptomyces scabies*

List of papers

Paper I: Stepnov AA, Forsberg Z, Sørlie M, Nguyen GS, Wentzel A, Røhr ÅK, Eijsink VG. Unraveling the roles of the reductant and free copper ions in LPMO kinetics. *Biotechnology for biofuels.* 2021 Dec; 14(1): 1-4.

Paper II: Stepnov AA, Christensen IA, Forsberg Z, Aachmann FL, Courtade G, Eijsink VG. The impact of reductants on the catalytic efficiency of a lytic polysaccharide monooxygenase and the special role of dehydroascorbic acid. *FEBS letters.* 2022 Jan; 596(1): 53-70.

Paper III: Stepnov AA, Eijsink VG, Forsberg Z. Enhanced *in situ* H_2O_2 production explains synergy between an LPMO with a cellulose-binding domain and a single-domain LPMO. Submitted to *Scientific Reports*.

Paper IV: Rieder L, **Stepnov AA**, Sørlie M, Eijsink VG. Fast and specific peroxygenase reactions catalyzed by fungal mono-copper enzymes. *Biochemistry.* 2021 Nov 5; 60(47): 3633-43.

Other papers on LPMOs by the author:

Forsberg Z, **Stepnov AA**, Nærdal GK, Klinkenberg G, Eijsink VG. Engineering lytic polysaccharide monooxygenases (LPMOs). In *Methods in Enzymology* 2020 Jan 1 (Vol. 644, pp. 1-34). Academic Press.

Manavalan T, **Stepnov AA**, Hegnar OA, Eijsink VG. Sugar oxidoreductases and LPMOs–two sides of the same polysaccharide degradation story? *Carbohydrate Research.* 2021 Jul 1; 505: 108350.

1 Introduction

1.1 Cellulose, hemicelluloses and lignin

Cellulose is a naturally occurring linear homopolymer composed of D-anhydroglucose units connected through β-1,4 glycosidic bonds (Fig. 1) [2]. Cellulose is the major structural component of plant cell walls, but it is also produced by some bacteria (e.g., *Acetobacter*), green algae (*Valonia*) and even invertebrate animals (*Tunicata*) [3,4]. It has been estimated that approximately 10^{11}-10^{12} tons of cellulose are generated annually by photosynthetic organisms, making cellulose the most abundant biopolymer on Earth [5]. Cellulose is an attractive source of renewable energy, but its effective utilization is complicated by a remarkable recalcitrance [6].

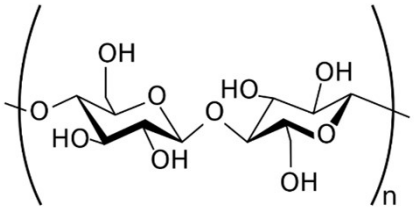

Figure 1. Chemical structure of cellulose. The repeating cellobiose unit is formed by two D-glucose monomers connected through a β-1,4-glucosidic bond.

In plant biomass, individual cellulose chains have a high degree of polymerization (about 1500-5000 [7]) and are organized into microfibrils. These insoluble microfibrils are stabilized by a network of hydrogen and Van der Waals bonds [2] resulting in a densely packed crystalline structure. Due to this arrangement, cellulose is hard to access. To complicate things further, cellulose fibrils are surrounded by hemicelluloses and lignin in plants. These

amorphous polymers provide additional layers of protection to the cell wall (Fig. 2). Cellulose may represent up to 50% of the plant biomass on dry weight basis, whereas hemicelluloses (20-30%) and lignin (5-30%) are the next largest fractions [8].

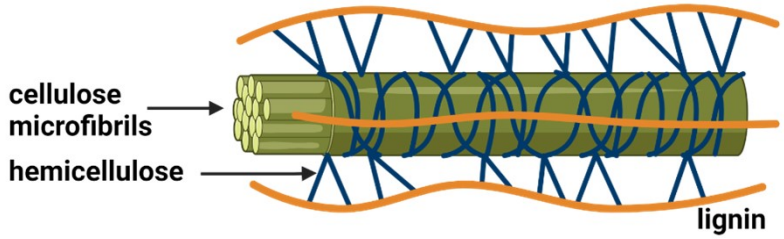

Figure 2. Schematic representation of plant cell wall. The figure shows a cluster of cellulose microfibrils covered with hemicellulose and lignin.

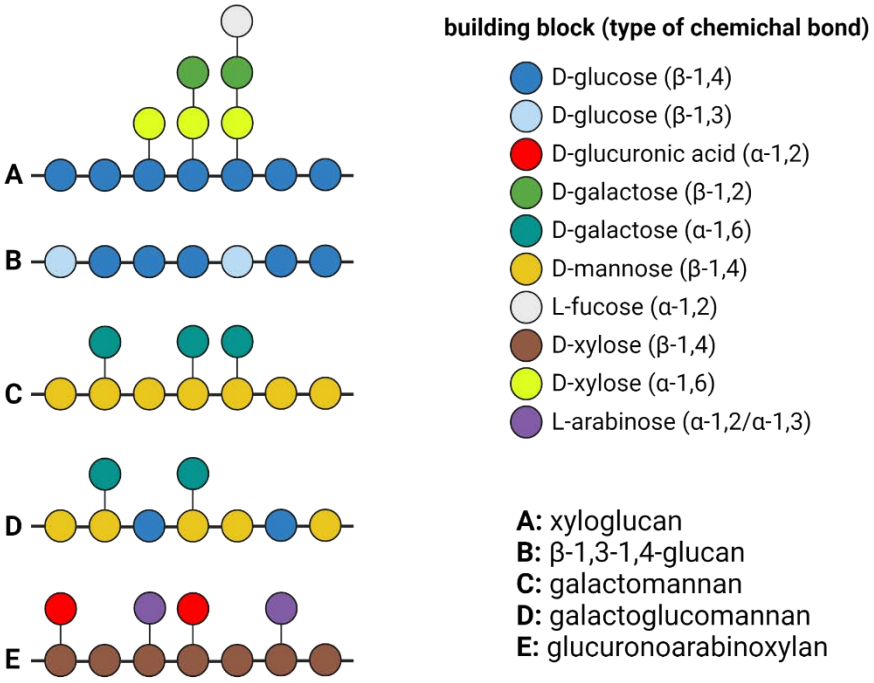

Figure 3. Structural variation of hemicelluloses. The figure shows a schematic representation of commonly occurring types of backbones and side-chain decorations in hemicellulosic polymers. The figure was adapted from [9].

In contrast to cellulose, hemicelluloses are heteropolymers that contain various pentoses (β-D-xylose, α-L-arabinose), hexoses (β-D-mannose, β-D-glucose, α-D-galactose) and sugar derivatives (e.g., α-D-glucuronic-, α-D-4-O-methylgalacturonic- and α-D-galacturonic acids) [10]. Other sugars may also present in hemicellulose in small amounts. Hemicelluloses vary in structure and composition between plant species. Typically, these polymers are branched and have a relatively low molecular weight with a degree of polymerization of 80-200 [11]. The four main types of hemicelluloses are xylans, xyloglucans, mannans and mixed-linkage β-glucans (Fig. 3) [12]. Hemicelluloses form hydrogen bonds with crystalline cellulose and covalent bonds with lignin (predominantly, α-benzyl ether linkages) [11].

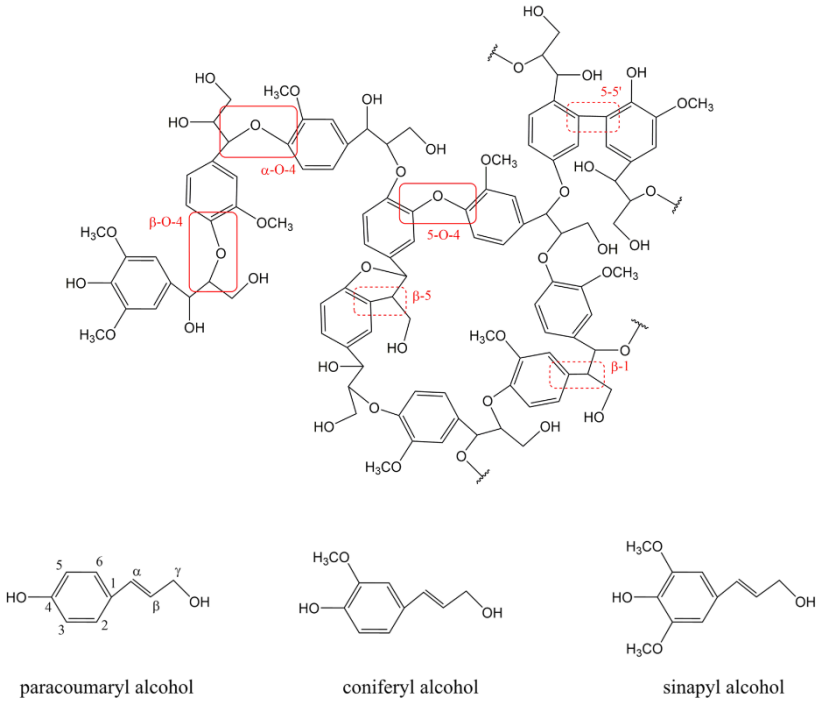

Figure 4. Chemical structure of lignin and its three main precursors. Dot boxes indicate condensed linkages whereas solid boxes indicate ether linkages. The figure was taken from [13].

Lignin is a phenolic heteropolymer composed of 4-hydroxypropanoids connected through ether- and carbon-carbon linkages. The three major

precursors of lignin are p-coumaryl alcohol, coniferyl alcohol and sinapyl alcohol (Fig. 4) [13]. In cells, lignin is synthesized as the result of multiple free-radical reactions [14], hence its structure is complex and highly variable. Being a rather hydrophobic compound, lignin is thought to be one of the key factors determining water permeability in plant tissues [15].

Cellulose microfibrils coated with layers of hemicellulose and lignin comprise a very strong composite biomaterial. Its chemical degradation typically involves harsh conditions, such as treatment with mineral acids at high (90-240 °C) temperature and, sometimes, at high pressure (e.g., 20 bar) [16].

1.2 Enzymatic depolymerization of plant biomass

In Nature, depolymerization of lignocellulosic biomass is carried out by the synergistic action of hydrolytic and oxidative enzymes that target cellulose, hemicelluloses, lignin and other compounds in the plant cell wall. Bacteria and fungi are advanced degraders of plant biomass, however there are data suggesting that some animals (such as isopods and nematodes) are also capable of producing cellulolytic enzymes [17,18], most likely as a result of horizontal gene transfer from microorganisms. Aerobic bacteria and fungi rely on enzyme cocktails that are released into the environment when these microbes encounter lignocellulosic substrates. In contrast, anaerobic bacteria tend to depend on cellulosomes. Cellulosomes are multi-enzyme complexes that are usually anchored to the cell wall and are capable of binding and degrading biomass [19]. The utilization of cellulosomes, instead of protein cocktails, may allow anaerobes to re-use their enzymes, which may provide a significant advantage in an energy-poor anoxic environment [20]. Of note, cellulosomes contain multiple enzyme activities, including hemicellulases.

The many carbohydrate-modifying and -degrading enzymes involved in plant biomass turnover are classified based on sequence similarity in the CAZy database. Enzymes that hydrolytically break glycosidic bonds occur in the glycoside hydrolase (GH) families, whereas redox enzymes acting on carbohydrates and associated materials (lignin) occur in the auxiliary activity (AA) families. The substrate-binding domains occurring in many of these enzymes are classified in families of carbohydrate-binding modules (CBMs).

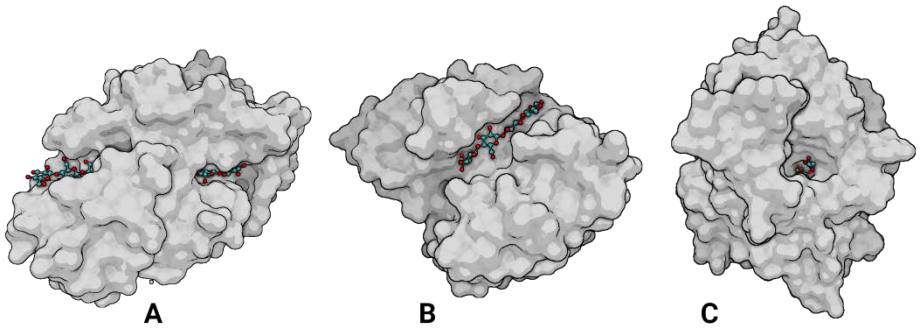

Figure 5. Topology of cellulases. The figure shows surface topologies commonly occurring among exocellulases (A, "tunnel"), endocellulases (B, "open cleft") and β-glucosidases (C, "pocket"). A, exocellulase from *Trichoderma reesei* in complex with two molecules of cellotetraose (PDB: 5CEL, [21]); B, endocellulase from *Termobifida fusca* in complex with cellotetraose (PDB: 2BOF, [22]); C, β-glucosidase from *Thermotoga maritima* in complex with transition state mimic (PDB: 5N6T, [23]). Enzyme structures were visualized using BioRender.

Getting for plant biomass to fermentable glucose requires the action of cellulases (Fig. 5). Cellulases are a well-studied class of hydrolytic enzymes that target the most abundant compound in plant biomass. These enzymes catalyze cleavage of the β-1,4-glycosidic bonds in cellulose via a general acid/base mechanism, which leads to either inversion or retention of the anomeric configuration [24]. Cellulases may be divided into three functional groups that have distinct active site topologies. Exocellulases attack the reducing or non-reducing ends of cellulose chains and release cellobiose (or

other short oligosaccharides) into solution. Most studied exocellulases are thought to be processive, which means that they catalyze multiple consecutive reactions before dissociating from the cellulose chain [25]. The common structural feature of exocellulases is a tunnel-shaped active site (Fig. 5A)[26,27]. In contrast to exocellulases, endocellulases are able to randomly bind accessible sites inside a cellulose chain generating products with various degrees of polymerization. The active sites of endocellulases show an open-cleft topology (Fig. 5B) [26,27]. Last but not least, cellulolytic enzyme systems comprise β-glucosidases, which hydrolyze cellobiose (and, sometimes, other short oligosaccharides) to yield glucose. Accumulation of cellobiose may inhibit both endo- and exocellulases, hence β-glucosidases play a very important role in controlling and promoting the overall cellulose depolymerization rate [28]. The catalytic residues of cellobiases are situated inside a pocket that can accommodate the non-reducing end of a cello-oligomer (Fig. 5C) [29].

The genomes of aerobic cellulolytic bacteria and fungi typically encode for multiple cellulases that are secreted together. For instance, the cellulolytic arsenal of the model plant-degrading bacterium *Thermobifida fusca* includes two exocellulases (*Cel*6B and *Cel*48A), five endocellulases (*Cel*5A, *Cel*5B, *Cel*6A, *Cel*9A, *Cel*9B) and a β-glucosidase (*Bgl*C)[30]. These enzymes are well-characterized and are known to work in a synergistic fashion [31]. The synergy between cellulases is thought to be due to certain enzyme types creating access sites for other enzyme types. For example, disruption of the cellulose surface by processive exocellulases may expose new regions that are susceptible to endocellulase action. At the same time, exocellulases will act on new chain ends generated by endocellulases, to produce cellobiose. A schematic representation of all three classes of cellulases working in cooperation is shown on Fig. 6.

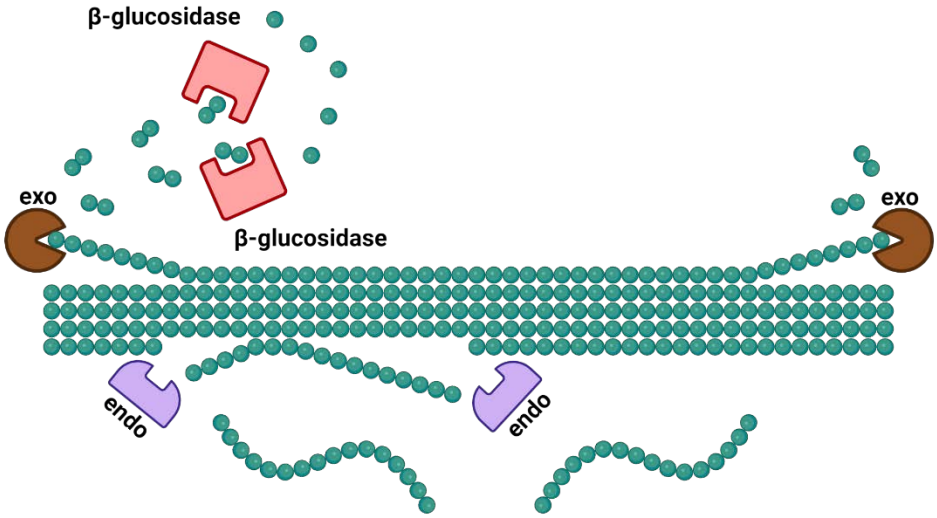

Figure 6. Cooperative depolymerization of cellulose by hydrolytic enzymes. "Exo", exocellulase; "endo", endocellulase.

In addition to cellulases, many other types of enzymes are required to efficiently process lignocellulosic biomass. Hemicellulases are hydrolytic enzymes targeting various hemicelluloses. They are capable of cleaving the polysaccharide backbones or removing the side-chain decorations of their substrates. More than 25 types of distinct hemicellulase activities are known at the current time [32].

Microbes produce a large and diverse group of redox enzymes acting on lignin, including laccases, lignin peroxidases (LiP), manganese-dependent peroxidases (MnP), versatile peroxidases (VP) and dye-decolorizing peroxidases (DyP). The common feature of these enzymes is low specificity [13]. Peroxidases and laccases oxidize and cleave lignin at random points rather than at specific positions, using H_2O_2 or molecular oxygen as the final electron acceptor, respectively.

Previously, it was thought that oxidative enzymatic degradation of plant biomass was limited to the lignin fraction. However, relatively recently, a new class of unique mono-copper redox enzymes called lytic polysaccharide

monooxygenases (LPMOs) was discovered [33-37]. LPMOs act on crystalline surfaces [33,38], rather than on single polysaccharide chains and rely on redox chemistry to break glycosidic bonds. By oxidizing recalcitrant polymers such as cellulose, LPMOs significantly boost the efficiency of canonical hydrolytic enzymes [33,39,40]. The discovery of LPMOs has revolutionized our understanding of enzymatic degradation of plant biomass. Modern commercial cellulolytic cocktails used in industry are now benefiting from the inclusion of LPMOs [41-43].

1.3 Lytic polysaccharide monooxygenases (LPMOs)

1.3.1 History of discovery

For a long time, hydrolytic enzymes were thought to be the only class of proteins involved in polysaccharide depolymerization. In 1954, Rees et al. were studying enzymatic degradation of cotton fibers and proposed that cellulases may depend on unknown biocatalytic system ("C_1 factor"), that carries out initial decrystallization of substrate chains [44]. In 1974, Eriksson et al. observed that cellulose degradation by fungal secretomes is more efficient in the presence of oxygen, compared to anaerobic conditions [45]. Therefore, they speculated that the hypothetical "C_1 factor" is an oxidative enzyme. It took the field about 35 years to substantiate this idea (Fig. 7). Of note, in the meantime, most attention was devoted to cellobiose dehydrogenase [46], a redox enzyme that indeed may play a role in cellulose conversion [47] but which we now know is not the "C_1 factor".

In 1993, Schnellmann and colleagues described a small (18.7 kDa) chitin-binding protein from the chitinolytic soil bacterium *Streptomyces olivaceoviridis* [48] and called it "CHB1". CHB1 was found to be secreted but

seemed to lack catalytic activity. A few years later, a CHB1 homolog was discovered in *Serratia marcescens* and designated as "CBP21", for chitin-binding protein of 21 kDa [49]. The growing group of CHB1-like proteins was later classified as a new family of carbohydrate-binding modules, CBM33 [50]. In 1997, Saloheimo et al. reported the discovery of a novel (and rather weak) fungal cellulase from *Trichoderma reesei* that was called EGIV and became the founding member of a new GH family, GH61 [51]. X-ray structures of CBP21 and a GH61 from *Hypocrea jecorina* became available in 2005 and 2008, respectively, both showing the same fold that had never been observed before among CBMs or carbohydrate-active enzymes [52,53]. Importantly, in 2005, it became evident that CBP21 boosts the activity of chitinases [39], and similar effects were reported for a GH61 in 2007 [54], but the mechanisms behind these, in some cases truly remarkable, synergies remained enigmatic.

In 2010, Vaaje-Kolstad and colleagues demonstrated that CBP21 is a redox enzyme, catalyzing oxidative depolymerization of crystalline chitin in a reductant-dependent fashion [33]. Experiments with isotopically labeled O_2 revealed that CBP21 inserts an oxygen atom at the C1 of the β(1-4) glycosidic bonds in chitin, which results in bond cleavage, and led to naming CBP21 a monooxygenase. This pioneering discovery attracted much attention, and soon bacterial and fungal monooxygenases targeting cellulose were reported [34-36,55,56]. In 2011, Quinlan at al. provided essential insight into the active site of these new enzymes, showing they contain a single copper atom coordinated by two histidine residues [35]. Finally, in 2012, the name "lytic polysaccharide monooxygenase" was coined [37]. GH61 and CBM33 proteins were reclassified as LPMOs and reassigned to new CAZy families (AA9 and AA10, respectively) [57].

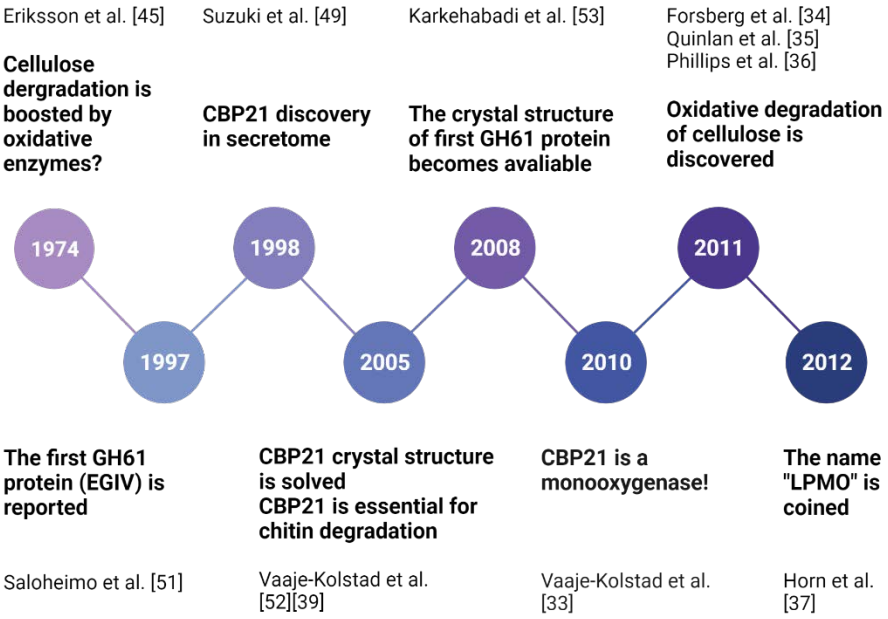

Figure 7. Early milestones in LPMO research. The figure was adapted from [58].

1.3.2 Classification, occurrence and structure

Since the discovery of LPMOs in 2010, researchers have been much focusing on exploring novel LPMOs, including LPMOs belonging to novel families according to the CAZy classification and LPMOs with novel functionalities, i.e., novel substrates. Today, eight CAZy families of LPMOs have been founded containing enzymes with varying substrate specificities (AA9-AA11, AA13-AA17; Table 1).

The AA9 family comprises LPMOs of fungal origin primarily targeting cellulose and hemicelluloses with β-1,4-linked glucose backbones, such as glucomannans and xyloglucans. Furthermore, activity towards xylan has been reported for a few representatives of AA9 family [59-61]. Importantly, several of these hemicellulolytic activities only occur when the hemicellulose is

bound to cellulose [59,60,62], which is compatible with the notion that LPMOs have evolved to act on surfaces, including co-polymeric plant cell wall structures. Some AA9 LPMOs can bind and oxidize short soluble cello-oligosaccharides (e.g., cellopentaose or cellohexaose) [63,64]. While these reactions may be highly efficient ([65]; Paper IV in this thesis), the biological role of LPMO activity on soluble substrates is not clear.

Family 10 (AA10) LPMOs are known to oxidize cellulose or chitin and, in some cases, both these polysaccharides. The founding member of this family is CBP21, the first LPMO to be discovered. The AA10 family predominantly includes enzymes of bacterial origin, with a few notable exceptions, such as LPMOs from the fern *Tectaria macrodonta* [66] and from entomopoxviruses [67].

The AA11 and AA13 families are exclusively composed of fungal enzymes. AA11 LPMOs are active on chitin or chito-oligomers [68-71]. Very few of these enzymes were characterized so far. AA13 LPMOs have the unique ability to oxidize starch (i.e., cleave α-1,4 glycosidic bonds). The first LPMO of this type was reported in 2014 by Vu et al. [72].

The AA14 - AA17 LPMO families are the most recently discovered. The AA14 family was founded in 2018 and comprises fungal LPMOs that are thought to be active on cellulose-bound xylan [73]. AA15 LPMOs target cellulose and/or chitin and are found in various organisms, including oomycetes and insects. The two founding family members were characterized in 2018 from the insect *Thermobia domestica* that is known to be capable of digesting crystalline cellulose [74]. The AA16 family of LPMOs was first described in 2019 [75] and its members are cellulose-active and found in fungi and oomycetes. Finally, the AA17 family was described in 2021 [76] and comprises LPMOs from oomycetes with the unique ability to oxidatively cleave homogalacturonan and oligogalacturonides, which are constituents of pectin, a component of plant cell walls.

Table 1. Overview of LPMO classification, occurrence and known substrates.

Family	Occurrence	Known substrates*	Number of characterized members**	Number of reported structures**
AA9	Fungi	cellulose, hemicelluloses	34	18
AA10	Bacteria, plants, viruses	cellulose, chitin	30	23
AA11	Fungi	chitin	1	1
AA13	Fungi	starch	4	1
AA14	Fungi	xylan	2	1
AA15	Metazoa, Oomycota, Alveolata, Rhodophyta, Chlorophyta, Haptophyta, Ichthyosporea, Phaeophyceae, Bacillariophyceae, viruses	cellulose, chitin	3	1
AA16	Fungi, Oomycota	cellulose	1	-
AA17	Oomycota	pectin	3	1

* Note that not all characterized LPMOs have been tested on all possible substrates
** The data were retrieved from the database of carbohydrate-active enzymes (CAZy; http://www.cazy.org) in February 2022.

It is worth noting that despite more than a decade of research, the amount of well-studied LPMOs remains relatively low even for the members of the two oldest families of these enzymes (AA9, AA10; see Table 1). Therefore, characterization of novel LPMOs is of interest and may reveal new types of activities and biological functions. As an example, recent data suggest that some LPMOs may play essential roles in host-pathogen interactions, promoting infections in mammals [77] and plants [76]. The active site of all known LPMOs is formed by two fully conserved histidine residues coordinating a single cooper atom (the so-called "histidine brace"; Fig. 8) [35]. Note that while being rare, this motif is not exclusive to LPMOs and occurs in a few other (non-catalytic) proteins, such as CopC copper chaperones [78] and family X325 proteins (whose biological function is still unclear) [79].

Importantly, one of the two histidine residues making up the copper site is always the N-terminal residue of the polypeptide chain [80] and this residue contributes with two of the in total three nitrogen ligands of the copper (Fig. 8). Therefore, proper processing of LPMOs (i.e., correct cleavage of signal peptides during secretion) is essential for enzymatic activity. In fungal LPMOs, the N-terminal histidine residue is methylated. This posttranslational modification is thought to protect the active site from auto-catalytic oxidation [81]. In fungal LPMOs, the active site contains a tyrosine residue in what may be referred to as the proximate axial coordination position (Fig. 8), whereas bacterial LPMOs may have a tyrosine or, more commonly, a phenylalanine in this position.

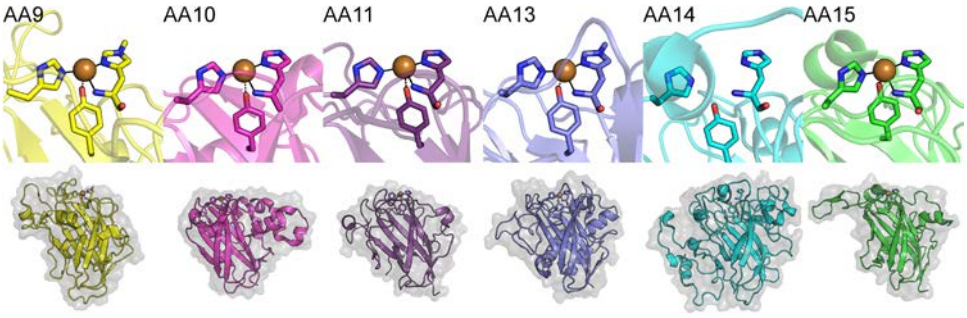

Figure 8. Topology and active site configuration of LPMOs from various families. The histidine residues of the copper-binding site and the associated tyrosine residue are shown using stick representation. In most AA10 LPMOs the tyrosine residue is replaced by a phenylalanine residue. The copper atom is rendered as an orange sphere. The crystal structure of the AA14 family LPMO presented in figure was solved without copper, however copper binding to the active site was confirmed by EPR [73]. The AA9 structure shows methylation of the N-terminal histidine. In the oxidized LPMO [Cu(II)], the copper ion would normally also be coordinated by two water molecules [82,83]; in the copper-binding proteins with seemingly no catalytic activity one of these coordination positions is occupied by an amino acid side chain. The enzyme models were rendered based on the following PDB entries: 5ACH (AA9), 5OPF (AA10), 4MAI (AA11), 4OPB (AA13), 5NO7 (AA14) and 5MSZ (AA15). The figure was taken from [84].

The overall fold of all LPMOs, regardless of the family, is conserved and represents an immunoglobulin-like β-sandwich core structure consisting of

two β-sheets comprising seven or eight β-strands in total (Fig. 8) [80]. In most LPMOs (e.g., AA9, AA10), the catalytic surface accommodating the histidine brace is characteristically flat, which reflects the unique ability of these enzymes to act directly on the crystalline surface of their substrates. However, some enzymes have more rugged surfaces, for example AA13 family members that act on starch. The surfaces of these latter LPMOs show a groove and are likely adapted to binding individual polysaccharide chains of the substrate rather than the surface as a whole [85]. The structural diversity of the LPMO substrate-binding surfaces is determined by helices and loops that connect the core β-strands and that display a high degree of variation in length and sequence [80]. Indeed, although structural studies of LPMO-substrate interactions are rare [86-89] it has been shown that these loops accommodate residues that interact with substrates. Aromatic side-chains play an important role in binding carbohydrates through CH–π stacking interactions, and one or more aromatic residues are indeed observed in substrate-binding surfaces of LPMOs [80] (Fig. 9).

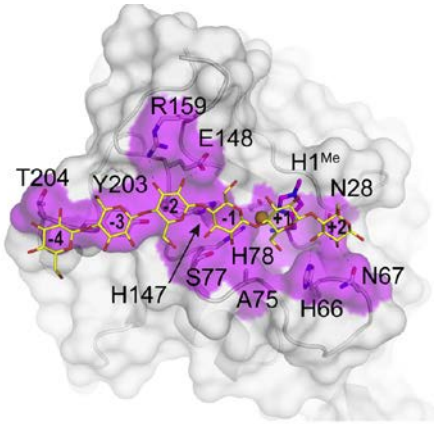

Figure 9. Substrate-binding interface of *Ls*LPMO9A. The figure shows the X-ray structure of *Ls*LPMO9A solved in the presence of cellohexaose (PDB: 5ACI). The residues interacting with the substrate are labeled and colored magenta. The figure was taken from [80].

Like many other carbohydrate-binding enzymes, LPMOs may be multi-domain proteins and the most common additional domain(s) are carbohydrate-binding modules (CBMs) [57,90,91]. Existing data suggest that CBMs are capable of much stronger binding to insoluble substrates, compared to LPMO catalytic domains [92,93]. As outlined below, substrate-binding, i.e., high affinity for the substrate and/or a high substrate concentration, is important for LPMO action since this prevents off-pathway reactions. Therefore, as discussed in more detail below, CBMs may have a profound impact on enzyme activity and stability [90,93].

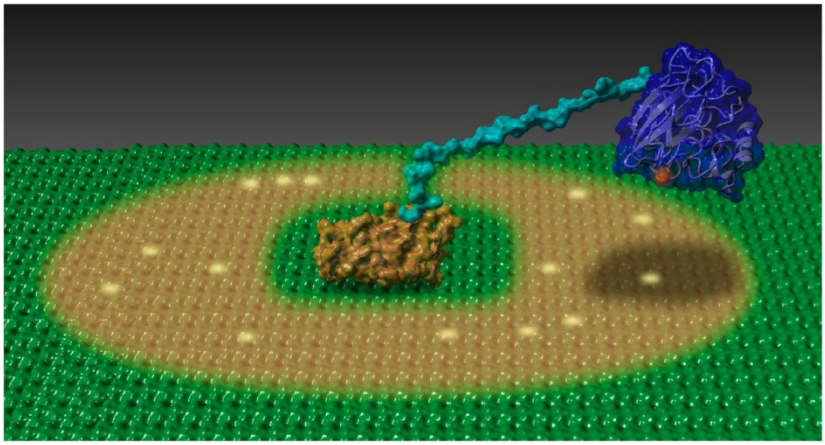

Figure 10. Cellulose oxidation by a two-domain LPMO. The figure shows *Sc*LPMO10C attached to a cellulose surface via carbohydrate-binding module (CBM; orange), which is connected to the family 10 catalytic core (AA10; blue) through a flexible linker (cyan). The brown circle indicates the theoretical area of ~1300 Å^2, corresponding to about 300 glucose residues, that the AA10 domain can sample. The figure was taken from [90].

In a recent study, Courtade et al. presented a structural model of a two-domain bacterial LPMO (*Sc*LPMO10C), which showed that the CBM and the catalytic domain are rather rigid entities that are connected by a highly flexible linker [90] (Fig. 10). The modeling data showed that, thanks to this linker, the cellulose-bound CBM would keep the catalytic domain close to the

substrate surface while at the same time allowing it to sample a large area where oxidative cleavage of glycosidic bonds could take place (Fig 10).

1.3.3 Reaction mechanism and nature of co-substrate

Despite many uncertainties regarding the detailed mechanism of LPMO-catalyzed reactions (discussed below), there are few fundamental facts that are well-established. It has long been known that LPMO-Cu(II) is the inactive resting state of these enzymes [35] and that initial reduction to LPMO-Cu(I) is essential for catalysis. It has been unambiguously demonstrated that in the presence of electron donors, LPMOs promote formation of reactive oxygen species that carry out oxidation (hydroxylation) of carbohydrate substrates at the C1 or C4 position resulting in destabilization and cleavage of glycosidic bonds [33,36]. Oxidation of the C1 carbon leads to formation of a lactone, whereas oxidation of the C4 carbon yields 4-ketoaldose. These oxidized products are unstable and exist in equilibrium with their hydrated forms (Fig. 11).

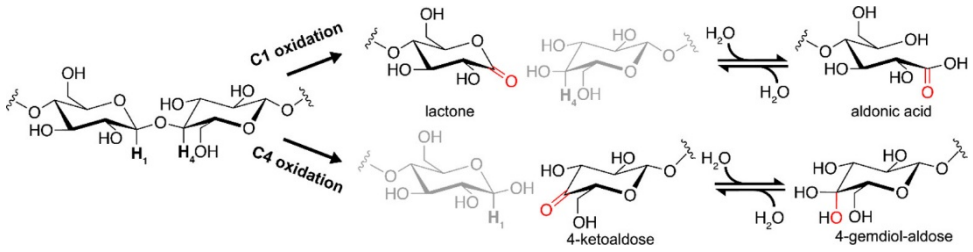

Figure 11. Oxidized LPMO products formed during cellulose depolymerization. The figure shows oxidized sugars generated by C1- or C4-oxidizing LPMOs. Some LPMOs are less regioselective and generate a mixture of C1-, C4- and double-oxidized products. The figure was taken from [94].

Some LPMOs lack regioselectivity and can act on both C1 and C4 carbons (e.g., [95,96]), releasing mixtures of C1-, C4- and double oxidized products.

Interestingly, there is recent data showing that these double oxidized products may not be oxidized at the C1 and C4 positions, as one would expect [63], but rather at the C4 and C6 positions [97].

Since reduced LPMOs cleave their substrates by introducing oxygen atoms into carbohydrate chains, the enzymes depend on a source of oxygen (i.e., a co-substrate), in addition to an electron donor. Being an essential aspect of the reaction mechanism, the nature of the LPMO co-substrate remains a matter of discussion and some controversy. Historically, LPMOs were thought to rely on molecular oxygen (hence, the name "monooxygenase"). This notion was based on experiments showing that isotopically labeled oxygen atoms are incorporated into reaction products when reactions were carried out with $^{18}O_2$ [33]. However, this apparent dependency of LPMO reactions on molecular oxygen does not exclude the possibility that LPMO catalysis can be fueled by reactive oxygen species that are generated from O_2 under reducing conditions. Indeed, in 2017, Bissaro and colleagues discovered that LPMOs can use H_2O_2 as a co-substrate and clearly prefer it over molecular oxygen in competition experiments [98]. Notably, H_2O_2-dependent (i.e., peroxygenase) LPMO reactions were shown to be fast [98-103] compared to monooxygenase reactions, which are typically two to three orders of magnitude slower.

Importantly, despite several studies done in the decade, detailed mechanisms for the monooxygenase and peroxygenase LPMO reactions are yet to be established. In particular, the nature of the reactive Cu-oxygen species that abstract a hydrogen atom from the polysaccharide substrate remains unknown. Fig. 12 shows possible scenarios for O_2- and H_2O_2-driven LPMO catalysis derived from computational studies [104,105] and involving a Cu(II)-oxyl active intermediate. Several alternative catalytic pathways have been proposed in literature that rely on other active species, such as Cu(II)-superoxide [106] and Cu(III)−OH [89,107].

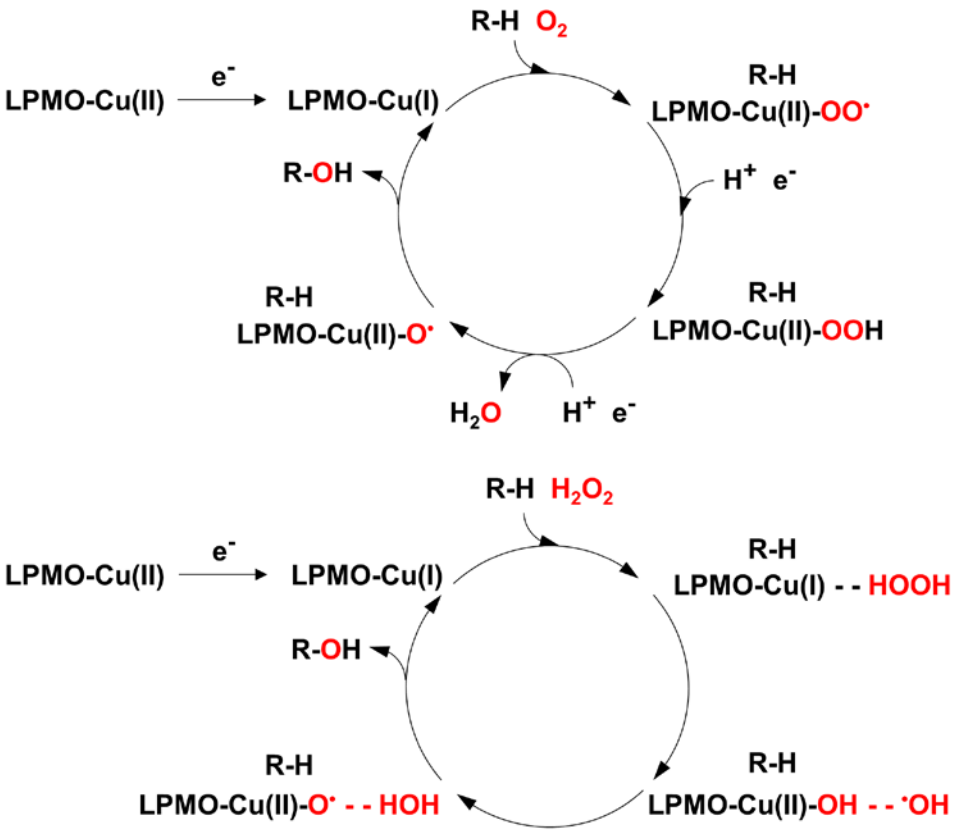

Figure 12. Monooxygenase (top) and peroxygenase (bottom) LPMO reactions. The figure shows possible mechanisms for O_2- and H_2O_2-driven oxidation of carbohydrates by LPMOs. Both catalytic pathways potentially involve LPMO-Cu(II)-O· active intermediate. Regardless of the nature of the oxygen co-substrate, initial reduction of Cu(II) to Cu(I) is required for the enzyme to enter the catalytic cycle. The figure was adapted from [94].

Regardless of the nature of the co-substrate, the LPMO catalytic cycle starts with reduction of active site copper resulting in the LPMO-Cu(I) state. Next, reduced LPMO binds both substrate and co-substrate. In case of a monooxygenase reaction (Fig. 12, top), it is plausible that a LPMO-Cu(I)-OO· superoxide complex is first formed [108] and further converted to LPMO-Cu(II)-O· (oxyl) intermediate via consecutive proton-coupled transfer of two electrons leading to elimination of water molecule [104]. The resulting,

hypothetical, Cu(II)-O· intermediate is thought to be responsible for abstraction of a hydrogen atom from C1 or C4 carbon of the scissile bond. This step is followed by rapid rebound of the resulting hydroxyl radical to the substrate [109] and recovery of the LPMO-Cu(I) state. The hydroxylation of the C1 or C4 carbons destabilizes the glycosidic linkage [36], leading to its cleavage and formation of the corresponding lactone or 4-ketoaldose, as shown in Fig. 11.

Several catalytic scenarios were proposed when the peroxygenase activity of LPMOs was discovered [98] and one of these, based on homolytic cleavage of H_2O_2, is currently prevailing [100]. The reaction pathway for H_2O_2-driven catalysis (Fig. 12, bottom) is likely based on the initial formation of LPMO-Cu(I)-OH complex together with a ·OH radical [98,100]. It is thought that the ·OH radical is stabilized by the enzyme [105,110] and, instead of directly reacting with the substrate, abstracts a proton from the LPMO-Cu(I)-OH complex, leading to elimination of water and formation of the LPMO-Cu(II)-O· intermediate that attacks the glycosidic bond in the same way it was described for monooxygenase reaction (Fig. 12).

As can be seen in Fig. 12, the essential difference between the monooxygenase and peroxygenase catalytic cycles is the amount of electrons that are channeled through the enzyme catalytic center. In the monooxygenase reaction, two electrons (and two protons) must be delivered to the active site to complete catalytic cycle after the reduced enzyme binds to O_2. By contrast, H_2O_2 carries both the protons and reducing equivalents that are necessary for LPMO activity and for regeneration of the LPMO-Cu(I) state. In other words, in case of the peroxygenase reaction, LPMOs only require an initial priming reduction after which the enzyme can catalyze multiple reactions if supplied with hydrogen peroxide and substrate. Indeed, experimental data suggest that LPMO reactions that are fueled by H_2O_2 consume sub-stoichiometric amounts of reductant. It has been shown that

under peroxygenase conditions a reduced enzyme can perform about 20 turnovers before returning to resting LPMO-Cu(II) state [101,111,112].

It is worth noting that consecutive delivery of two electrons and protons during the LPMO catalytic cycle, which is required according to the monooxygenase paradigm (Fig. 12, top), poses a serious theoretical problem. Computational studies show that binding to the substrate shields the LPMO active site from the solvent to a degree that will only allow O_2 and H_2O_2 (but not reducing compounds) to access the copper atom [113]. It is clear that the first electron can be "stored" in the reduced active site, whereas the potential route of the second electron towards the active site of the substrate-bound enzyme is enigmatic. Some researchers proposed that the additional electron may be delivered to the active site via a hypothetical electron transport chain [114,115], however these claims remain unsupported by experimental data.

Given the difficulty of solving this "second electron conundrum" and the clear preference of LPMOs for H_2O_2, one may wonder whether monooxygenase reactions can occur at all. It is well known that hydrogen peroxide can be produced *in situ* in aerobic LPMO reactions [116]. Therefore, distinguishing between monooxygenase and peroxygenase activity is problematic [117], as discussed in section 1.3.4 below, and in several of the research papers presented in this thesis.

On a side note, reduced LPMOs may occasionally undergo auto-catalytic oxidation. These "futile" reactions are one to three orders of magnitude slower than productive turnovers [99] [118] and can be prevented by binding to the substrate ([119] and Paper III of this thesis). Self-oxidation predominantly affects the histidine residues of the copper-binding center [98,119]. Interestingly, recent work has shown that multiple futile turnovers are possible prior to irreversible damage to LPMO [118]. In other words, it would seem that slow futile peroxidase reactions of LPMOs may very well leave the enzyme intact. Oxidative inactivation of LPMOs is often observed in

the presence of hydrogen peroxide, which has led some researchers to claim that H_2O_2 is not a biologically relevant co-substrate [65]. On the other hand, there is ample evidence showing that, when properly controlled, i.e., when keeping H_2O_2 concentrations low and substrate concentrations high, LPMO peroxygenase reactions are stable, with each enzyme molecule catalyzing thousands of turnovers [111]. Under "peroxygenase" conditions, productive binding to substrate becomes a key factor limiting the LPMO stability, since lack of productive binding increases the chances for off-pathway reactions and autocatalytic enzyme inactivation. As illustrated by Paper IV of this thesis, stoichiometric productive conversion of high amounts (600 μM) of H_2O_2 by LPMOs can be achieved when using a soluble rapidly diffusing low-molecular-weight substrate.

1.3.4 Electron sources and *in situ* H_2O_2 generation

As alluded to above, LPMO catalysis requires reduction of the active site copper. One of the most remarkable LPMO features is the ability to accept electrons from a diverse range of donors, which is likely due to the solvent-exposed topology of the copper site. LPMO reactions can be fueled by low molecular weight compounds such as ascorbic acid [33,90,95,98], gallic acid [35], dithiothreitol (DTT) [62], L-cysteine [120], reduced glutathione [33], plant or fungal phenols [121] and lignin derivatives [122,123]. Furthermore, it has been shown that LPMOs can be reduced by photocatalytic systems based on naturally occurring pigments [124,125] or on vanadium-doped titanium dioxide [126].

Interestingly, sugar dehydrogenases such as cellobiose dehydrogenase (CDH) [36,56,127], glucose dehydrogenase (GDH) [128] or pyrroloquinoline-quinone-dependent pyranose dehydrogenase (PDH) [129] can also serve as

electron donors for LPMOs. Sugar dehydrogenases occur in families AA3 and AA12 of the CAZy database and have a flavin adenine dinucleotide (FAD) or a pyrroloquinoline-quinone (PQQ) co-factor, respectively. The reductive half-reaction catalyzed by these enzymes entails substrate oxidation and two-electron reduction of the co-factor. In the subsequent oxidative half-reaction, the co-factor is re-oxidized and electrons are transferred to various acceptors. Sugar dehydrogenases were shown to be capable of reducing LPMO active site either directly [128] or via redox mediators, such as cytochrome domains or small molecules (e.g., benzoquinones) [121].

Notably, sugar dehydrogenases are often co-expressed and secreted with LPMOs [1] in biomass-degrading fungi, suggesting that reduction of LPMO copper sites by these enzymes can be biologically relevant. An overview of possible routes for LPMO reduction, involving low molecular weight reductants, light-activated pigments, lignin derivatives and/or partner enzymes is shown in Fig. 13.

The promiscuity of LPMOs with respect to the reductant may be taken to show that the reduction of the solvent-exposed copper, which has a higher redox potential than free copper [81,86], is relatively easy and does not require specific interactions between the LPMO and its redox partner. Indeed, it has been shown that one-electron reduction of LPMOs (in the absence of substrate) is very fast [110,121,127], relative to observed catalytic rates, and thus not likely to be rate-limiting. Paradoxically, nevertheless, LPMO catalytic rates depend strongly on the type of reductant (e.g., [121,130] and Papers I, II and IV of this thesis). This dependency could relate to the speed of the delivery of the second electron in a monooxygenase reaction (Fig. 12). Alternatively, and perhaps more likely in view of recent findings regarding the high peroxygenase activity of LPMOs, this observation could reflect the impact of the reductant on *in situ* generation of H_2O_2, which may be rate-

limiting for the LPMO reaction under commonly used laboratory conditions ("monooxygenase conditions"; see below for further discussion).

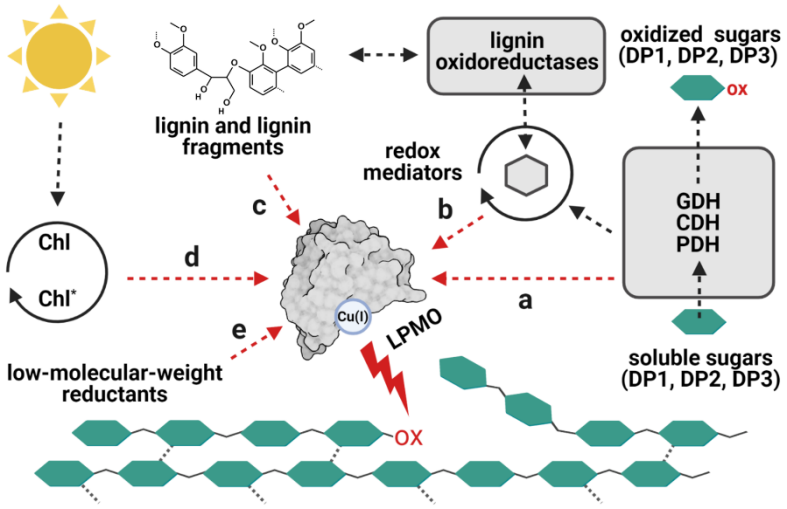

Figure 13. Reduction of LPMOs. The figure shows various electron sources for LPMOs, including redox enzymes (routes a,b), which may engage in direct transfer or use a redox mediator possibly derived from enzymatic lignin degradation, lignin itself (c), light-activated photosynthetic pigments (d) and various other low-molecular-weight reductants such as ascorbic acid (e). GDH, glucose dehydrogenase; CDH, cellobiose dehydrogenase; PDH, pyrroloquinoline-quinone-dependent pyranose dehydrogenase. The figure was taken from [1].

There are multiple potential sources of hydrogen peroxide in typical aerobic LPMO reactions. First of all, it has been known since 2012 that reduced LPMOs can interact with molecular oxygen in a manner that leads to generation of hydrogen peroxide. First observed by Kittl et al. [116], this oxidase activity is still not fully understood. It is possible that LPMOs catalyze single-electron reduction of molecular oxygen to superoxide [108] which leaves the active site to be further converted to H_2O_2 through reactions with reducing compounds or by spontaneous disproportionation. An alternative scenario implies two-electron reduction of O_2 to H_2O_2 by the LPMO without release of intermediates into the solution [131].

Historically, H_2O_2 generation by LPMOs was thought to represent a "futile" uncoupled reaction. However, in the light of recent findings regarding the peroxygenase activity of LPMOs, it is possible that enzymatic H_2O_2 generation can fuel LPMO catalysis in the absence of exogenous hydrogen peroxide, and should thus be considered part of productive LPMO action [98,117]. In any case, there is accumulating evidence, including results presented in several Chapters of this thesis, indicating that the slow apparent "monooxygenase" reactions observed in standard aerobic LPMO reactions may in fact be peroxygenase reactions that are limited by (low) *in situ* H_2O_2 production.

Reactions between reductants and molecular oxygen, sometimes called reductant auto-oxidation, provide another source of hydrogen peroxide in LPMO reactions. Commonly used low-molecular weight reducing agents, such as ascorbic acid [132], gallic acid [133], reduced glutathione [134] and L-cysteine [135] are known to be oxygen scavengers and can interact with dissolved O_2 in a manner that leads to formation of H_2O_2. Notably, the rates of these non-enzymatic reactions typically depend on many factors such as pH [132,136-138] and the concentration of free Cu(II) ions in solution [132,134,135,139,140]. There are recent data showing that enzyme-independent H_2O_2 generation plays a considerable role in driving LPMO activity under commonly used LPMO reaction conditions in the absence of exogenous hydrogen peroxide ([103] and Paper I of this thesis).

The idea that hydrogen peroxide is the only "true" LPMO co-substrate was proposed by Bissaro et al. [98,117]. This idea not only provides an explanation for the orders-of-magnitude gap between LPMO catalytic rates under "peroxygenase" and "monooxygenase" conditions, but also solves (or, rather, avoids) the "second electron conundrum". However, this concept has not been accepted by some researchers and has triggered a debate to which this thesis aims to contribute. The dispute stems in part from data showing

that enzymatic hydrogen peroxide production seems to not be taking place in the presence of LPMO substrates [63,65,116]. Some researchers claim that these observations show that H_2O_2 generation by LPMOs is suppressed by substrate binding, which could imply that LPMO activity observed under "monooxygenase conditions" (i.e., in aerobic set-ups without exogenously added H_2O_2) is due to a true monooxygenase reaction [65]. Yet, other researchers have pointed out that the apparent lack of hydrogen peroxide accumulation in these reactions is a result of the productive consumption of the generated H_2O_2 by LPMOs, which is to be expected given the high affinity (e.g., $K_M \approx 2$ μM [99]) of these enzymes for H_2O_2. As it was alluded to above, computational studies show that binding to the insoluble substrate may prevent reductants from accessing the LPMO active site [113] and, thus, may suppress enzyme-dependent H_2O_2 generation. Indeed, Filandr et al., have recently demonstrated that substrate-binding does decrease LPMO-dependent H_2O_2 generation [102]. Still, H_2O_2 will be generated in typical LPMO reactions with substrate, by non-substrate-bound LPMOs or by LPMO-independent reductant oxidation. Of note, there is experimental evidence that catalytic domains of LPMOs bind the substrate rather weakly [92,93]. As discussed in Paper III of this thesis, LPMO-dependent H_2O_2-generation will depend on the enzyme's affinity for the substrate (and the substrate concentration). These affinities will likely vary between different LPMOs and enzyme-substrate combinations, which could in part explain why the catalytic properties of LPMOs under "monooxygenase conditions" vary.

All in all, while monooxygenase reactions cannot be fully excluded, the availability of H_2O_2 produced *in situ* by the combination of enzyme-dependent and non-enzymatic factors (Fig. 14) will likely render this O_2-pathway kinetically irrelevant [98,102]. This is illustrated by inhibition experiments presented in Papers II and IV of this thesis, showing that the LPMO-catalyzed generation of oxidized products from both insoluble (microcrystalline

cellulose) and soluble (cellopentaose) substrates can be suppressed almost completely by competing H_2O_2-consuming enzymes (horseradish peroxidase or bovine liver catalase).

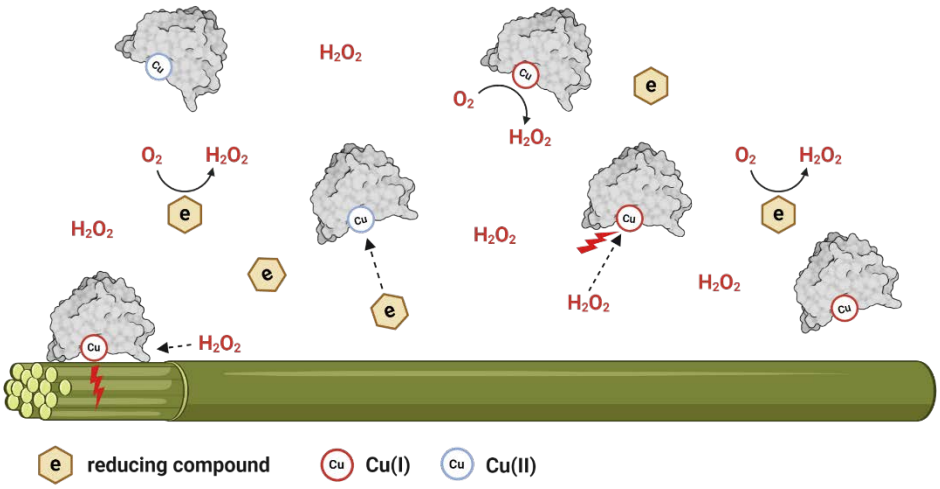

Figure 14. *In situ* H_2O_2 generation in typical LPMO reactions with an insoluble substrate. The figure shows a schematic representation of enzyme-dependent and non-enzymatic pathways leading to formation of hydrogen peroxide in reaction mixtures with a low-molecular-weight reductant (e.g., ascorbic acid or L-cysteine) and O_2. The accumulating H_2O_2 will drive productive peroxygenase reactions by substrate-bound enzymes or result in futile turnover by non-substrate-bound LPMOs, which may lead to the auto-catalytic damage to the active site. Note that two electrons are required to generate H_2O_2 from molecular oxygen.

2 Outline and purpose of the work described in this thesis

Despite intense research on LPMOs during the past decade and despite extensive use of these enzymes by industry for processing of lignocellulosic biomass, there are still many open questions regarding the mechanism and kinetics of LPMO-catalyzed reactions. In fact, it has been hypothesized that, due to this lack of understanding, the true power of LPMOs is currently not being harnessed in most reaction settings [141]. The discovery that these enzymes prefer H_2O_2 over O_2 and are capable of catalyzing fast peroxygenase reactions has provided new insights into LPMO functionality, but also raised debate and novel questions. For example, based on this new paradigm, it seems feasible that the slow apparent monooxygenase (i.e., O_2-dependent) LPMO activity observed in the absence of exogenously provided hydrogen peroxide is in fact a peroxygenase activity that is driven and limited by *in situ* H_2O_2 generation. This notion, which was not generally accepted at the start of the work described in this thesis, could shed new light on the role of reductants in LPMO reaction, since these would affect the potentially crucial rate of H_2O_2 generation in the system.

The overall goals of the work described in this thesis were to study enzymatic and abiotic H_2O_2-generating reactions that can occur under commonly used experimental conditions, and to address the potential impact of these reactions on LPMO catalytic rates and stability. In particular, experiments were performed to investigate whether the vast variation in

reported catalytic efficiencies of different LPMO-reductant combinations is related to differences in hydrogen peroxide production. The work presented in this thesis is described in four research papers.

Paper I proposes a modified version of the HRP/Amplex Red assay that allows for obtaining more reliable quantitative data for *in situ* H_2O_2 generation in reaction mixtures that contain reductants that interfere with the assay signal. This assay, and other methods, were then used to evaluate the relative contributions of enzymatic and enzyme-independent sources of hydrogen peroxide in typical reactions with a bacterial family AA10 LPMO that were driven by two commonly used reductants, ascorbic acid and gallic acid. Importantly, the impact of free copper, which is redox-active and which may occur in LPMO reactions, on hydrogen peroxide production was also assessed. By measuring both hydrogen peroxide production and cellulose oxidation, correlations between these two processes were revealed.

Papers II and IV build upon the methods described in **Paper I**, and further assess the correlation between LPMO catalytic rates and the rate of H_2O_2 generation in reaction mixtures containing various reducing compounds, such as ascorbic acid, gallic acid, L-cysteine, as well as, in **Paper II**, dehydroascorbic acid, which is not generally considered a reductant but which can drive LPMO reactions. Importantly, these papers include experiments showing that H_2O_2-consuming enzymes, catalase (**Paper II**) or HRP (**Paper IV**), inhibit LPMO reactions, thus shedding more light on the catalytic relevance of monooxygenase LPMO reactions, compared to peroxygenase LPMO reactions. **Paper II** addresses the impact of reductants on the activity of a novel bacterial (AA10) LPMO acting on an insoluble cellulosic substrate. **Paper IV** describes work with two fungal (AA9) LPMOs that oxidize soluble cello-oligosaccharide.

The findings described in **Papers I & II** generated new hypothesis as to how different LPMO types could act synergistically during cellulose

degradation. Specifically, it was hypothesized that such synergies could depend on variation in the H_2O_2-generating and H_2O_2-consuming abilities of LPMOs, as well as on LPMO substrate affinity. **Paper III** describes experiments done to investigate whether cellulose-degrading activity and enzyme stability in an LPMO reaction could be enhanced by combining LPMOs with different H_2O_2-generating and substrate-binding capacities.

The work described in this thesis was done within the framework of the OxyMod project, which is aimed at understanding and optimizing enzymatic redox systems for conversion of lignocellulosic biomass.

3 Main results and discussion

3.1 Paper I: Unraveling the roles of the reductant and free copper ions in LPMO kinetics

As alluded to above, LPMOs depend on an electron source to maintain their catalytic cycle and are known for their promiscuity towards reducing compounds. The reduction of enzyme-bound Cu(II) to Cu(I) was shown to be extremely fast compared to observed catalytic rates (e.g., [110,127]), and yet there is a remarkable variation in the reported efficiencies of various LPMO-reductant combinations at standard aerobic conditions [121,130]. This variation remains largely unexplained. Within the monooxygenase paradigm, this variation suggests that the reaction is limited by delivery of the second electron to the substrate-bound LPMO (Fig. 12). However, the discovery of LPMO peroxygenase activity provides an alternative explanation, because it is now conceivable that the apparent monooxygenase (i.e., O_2-dependent) activity observed in typical "monooxygenase" reaction set-ups is in fact peroxygenase activity fueled by H_2O_2 produced *in situ* [98]. Therefore, the dependency of LPMOs on the type of reductant may reflect variation in H_2O_2 production rates promoted by these compounds. Under standard reaction conditions, hydrogen peroxide can be formed via interaction of reducing compounds with molecular oxygen (so-called "auto-oxidation" of the reductant) or by reduced LPMOs engaging into oxidase reactions [116] (see Introduction for a detailed discussion).

To investigate the relative impact of both enzyme-dependent and non-enzymatic pathways for H_2O_2 generation, a novel bacterial LPMO comprising a catalytic domain and a CBM2 carbohydrate-binding module was used as a model. This enzyme, which is similar to well-studied *Sc*LPMO10C [34], was cloned from a marine Actinomycete and produced in *E. coli* (Paper I: Fig. 1). The enzyme was shown to be a C1-cellulose oxidizer and was named AA10_7 (Paper I: Fig. 2).

While studying *in situ* hydrogen peroxide generation in LPMO reactions, it is extremely important to consider the level of free Cu(II) ions in the reaction mixtures. Cu(II) is known to catalyze auto-oxidation of ascorbic acid and many other reductants by acting as redox mediator between the electron donor and O_2 [132,134-136,139]. Importantly, being copper-dependent enzymes, LPMOs are often saturated with Cu(II) by co-incubating with a slight molar surplus of free copper, followed by desalting. It is reasonable to assume that LPMO preparations may vary in terms of the amounts of free copper, due to variations in desalting protocols, and this will affect the rates of H_2O_2 generation in reaction mixtures. To account for such effects in Paper I, protein-free fractions were obtained from enzyme stock solutions by ultrafiltration and were tested for (copper-driven) hydrogen peroxide production in the presence of ascorbic acid (Paper I: Fig. 3). These protein-free control samples did not promote H_2O_2 production, whereas added $Cu(II)SO_4$ in concentrations as low as 0.2 μM did, indicating negligible levels of residual free copper in the LPMO preparations used in the study. This was further confirmed by ICP-MS analysis, showing the presence of 0.98 ± 0.18 μM and 0.90 ± 0.14 μM total copper in 1 μM enzyme solutions prepared from two batches of purified copper-saturated LPMO.

Next, Avicel degradation by 1 μM LPMO was assessed at standard aerobic conditions (i.e., in the absence of exogenously added hydrogen peroxide), using 1 mM ascorbic acid or 1 mM gallic acid to fuel the reaction. Both

reactions were remarkably slow (approximately 0.06 min^{-1} in the presence of ascorbic acid and 0.2 min^{-1} in the presence of gallic acid), but steady, with almost linear progress curves for the 24 h of the experiment (Paper I: Fig. 4A). Importantly, repeating the same experiments in the presence of 100 μM H_2O_2 led to two orders of magnitude faster substrate oxidation with no significant difference between ascorbic acid-driven and gallic acid-driven reactions (Paper I: Fig. 4B). These initial results indicated that the variation in reductant efficiency observed at standard aerobic conditions could relate to different levels of *in situ* H_2O_2 supply.

Digging deeper into this topic, the levels of *in situ* H_2O_2 generation in reaction mixtures containing 1 mM reductant and varying amounts of LPMO (1-8 μM) were assessed (Paper I: Fig. 6A) using the HRP/Amplex Red assay. It is worth noting that the typical reaction conditions for this standard assay involve very low reductant concentrations (e.g., 50 μM) [116,142] due to the well-described tendency of reducing compounds to repress the assay signal [110,143,144]. However, when using such low reductant concentrations in the HRP/Amplex Red experiments and 20-fold higher (1 mM) reductant concentrations in cellulose degradation experiments, it becomes difficult to compare the H_2O_2 generating ability of the reaction system with its cellulose-oxidizing ability. Therefore, the assay was modified by using 1 mM reductants, whereas at the same time, this amount of reductant was also added to the standard curves for H_2O_2, to correct for signal repression by ascorbic acid and gallic acid.

Comparison of H_2O_2 generation rates (Paper I: Fig. 6A) and substrate oxidation rates (Paper I: Fig. 4A) obtained with 1 μM LPMO at standard aerobic conditions revealed a correlation between the cellulose oxidation efficiency and the expected endogenous hydrogen peroxide supply: reactions with gallic acid gave more cellulose degradation and higher production of H_2O_2. Comparison of H_2O_2 generation rates obtained with and without LPMO

(Paper I: Fig. 6A) indicated that auto-oxidation of the reductant is the major source of hydrogen peroxide in reactions with gallic acid. On the other hand, in experiments with ascorbic acid LPMO-dependent hydrogen peroxide generation was pronounced (Paper I: Fig. 6A).

To further investigate the interplay between enzymatic and abiotic routes for H_2O_2 generation, a series of LPMO reactions with Avicel were carried out in the presence of 1 mM ascorbic acid or 1 mM gallic acid using increasing amounts of the enzyme (Paper I: Fig. 7). Surprisingly, regardless of the reductant used, these experiments showed that product formation was almost independent of the enzyme dose in a wide range of LPMO concentrations (0.1 – 4 μM), meaning that the enzyme contribution to H_2O_2 generation was low compared to non-enzymatic reactions (i.e., auto-oxidation of reductants). While this was expected for gallic acid (see above), one could have expected a larger effect of the enzyme dose in the case of ascorbic acid since, as shown above, the LPMO contributes significantly to H_2O_2 generation in reactions with this reductant. One explanation for these observations would be that binding of the LPMO to the substrate reduces the enzyme's ability to generate H_2O_2 [63,110,116]. Overall, the lack of dependency on the enzyme concentration supports the notion that the reaction is limited by *in situ* generation of the H_2O_2 co-substrate.

Importantly, control H_2O_2 production experiments with 1 μM free copper revealed that copper ions cause a massive increase in hydrogen peroxide generation in reactions with ascorbic acid, but hardly affect H_2O_2 production in reactions with gallic acid (Paper I: Fig. 5 & Fig. 6B). On the same note, introduction of varying amounts of Cu(II) to reaction mixtures containing LPMO, reductants and cellulose resulted in a copper dose-dependent boost in enzyme activity in reactions with ascorbic acid, but not in reactions with gallic acid (Paper I: Fig. 8A,B). This H_2O_2-mediated effect of free copper and ascorbic acid on the LPMO catalytic rate was remarkably strong: a 1 h reaction in the

presence of 1 μM Cu(II)SO_4 (Paper 1: Fig. 8A) yielded more oxidized products than a 24 h copper-free reaction with the same reductant (Paper 1: Fig. 4A). Taken together, these experiments indicate that, while being the most popular LPMO reductant, ascorbic acid may cause non-enzyme related variation in observed catalytic rates, due to varying amounts of Cu(II) in enzyme preparations and substrates.

Indeed, as summarized in Paper I, previously reported rates for ascorbic acid-driven cellulose-oxidation by the well-characterized model bacterial LPMO *Sc*LPMO10C display major (up to two orders of magnitude) variation, despite using seemingly comparable reaction conditions (Paper I: Table 1). Of note, the lowest catalytic rate reported for *Sc*LPMO10C is approximately 0.2 min^{-1}, which is comparable to the rate described for AA10_7 in Paper I, where the level of free copper in solution was controlled and negligible. Comparison of two in-house produced batches of *Sc*LPMO10C, one freshly prepared and one older batch, revealed large differences in product yields. The older, putatively less clean, enzyme batch showed much increased activity, which was reduced after this batch had been subjected to additional round of desalting (Paper I: Fig. S5). Overall, it is clear that free copper is a major factor determining the activity of ascorbic acid-driven LPMO reactions and that this should be taken into account when interpreting literature data on LPMOs.

All in all, the results of Paper I provide evidence that LPMO activity observed at standard aerobic conditions represents peroxygenase reactions that are fueled and limited by *in situ* hydrogen peroxide generation, which depends on the type of reductant and the presence of free transition metals. Under the standard conditions used in this study (1 μM enzyme, 1 mM reductant, no exogenous hydrogen peroxide, pH 6.0), auto-oxidation of ascorbic acid and gallic acid is a major source of H_2O_2, partly because enzyme-dependent hydrogen peroxide generation is suppressed by substrate binding. The auto-oxidation of ascorbic acid is increased many folds in the presence of

free Cu(II) ions, which makes LPMO reactions fueled by this commonly used reductant very sensible to copper contamination and hard to control.

Several elements of the above need further investigation, such as the impact of pH, which undoubtedly will affect redox properties of both the LPMO and the reductant [142]. Another question is whether the contribution of the LPMO itself to *in situ* H_2O_2 generation may vary between different LPMO types (e.g., bacterial AA10s versus fungal AA9s); this is addressed in Paper IV. The impact of substrate-binding on H_2O_2 production, and possible implications on how LPMOs perform and interact, are addressed in Paper III. Studies similar to those described in Paper I, but including two more reductants, are described in Paper II.

3.2 Paper II: The impact of reductants on the catalytic efficiency of a lytic polysaccharide monooxygenase and the special role of dehydroascorbic acid

Paper II of this thesis describes a biochemical characterization of *Ssc*LPMO10B, a novel LPMO from the phytopathogenic bacterium *Streptomyces scabies*, with particular focus on links between this enzyme's catalytic rate and *in situ* hydrogen peroxide production in the presence of various reducing compounds. This study included an assessment of dehydroascorbic acid (DHA), which is an oxidized form of ascorbic acid. The interest in DHA, which is not considered a reductant, was triggered by a study, published in 2021, showing that DHA is able to drive LPMO reactions on cellulose via largely unknown mechanism [145].

The *Ssc*LPMO10B gene sequence (GenBank accession number WP_173402964.1) was obtained from the publicly available *Streptomyces scabies* genome (strain 87.22, GenBank accession number NC_013929.1). The protein, comprising an AA10 catalytic domain and a CBM2 carbohydrate-binding module (Paper II: Fig. 2), was produced in *E. coli* and the presence of negligible levels of residual free copper in the resulting preparation of the copper-saturated LPMO was confirmed using the ultrafiltration-based assay, described in Paper I.

Screening of LPMO activity towards a large panel of soluble and insoluble carbohydrate substrates (including chitin and various hemicelluloses) revealed that *Ssc*LPMO10B is C1-oxidizing enzyme acting on amorphous and microcrystalline cellulose as well as on CMC, a soluble derivative of cellulose (Paper II: Figs. 3 & 4). Next, the capacity of various reductants (ascorbic acid, gallic acid, L-cysteine and DHA, at 1 mM concentration) to fuel Avicel solubilization by 0.5 μM *Ssc*LPMO10B was assessed (Paper II: Fig. 5). The use of ascorbic acid and gallic acid in reactions with *Ssc*LPMO10B and Avicel,

resulted in slow, but steady oxidation of cellulose over 24 h. The rates obtained with ascorbic acid and gallic acid amounted to approximately 0.12 min^{-1} and 0.25 min^{-1}, respectively. Such excessively low catalytic rates are comparable to the data reported in Paper I for another AA10 LPMO under the same reaction conditions. Notably, the reaction with L-cysteine displayed a much faster rate (≈1.3 min^{-1}), compared to gallic acid and ascorbic acid, but product formation diminished early on in the reaction, which is indicative of LPMO inactivation. Importantly, the experiment with DHA confirmed the recent report [145] by showing that this oxidized derivative of ascorbic acid can, indeed, drive LPMO reactions on cellulose. The rate of DHA-fueled substrate oxidation amounted to approximately 0.32 min^{-1}, meaning that, remarkably, the reaction with DHA outperformed the reactions with gallic acid and ascorbic acid.

Using the modified version of the HRP/Amplex Red assay described in Paper I, the H_2O_2 production capacity of LPMO reactions containing 1 mM reductant was tested, showing strong dependency of H_2O_2 production on the nature of electron donor. Taken together, the hydrogen peroxide production data (Paper II: Fig. 6) and the substrate oxidation data (Paper II: Fig. 5) show a strong correlation between the *Ssc*LPMO10B catalytic efficiency and *in situ* H_2O_2 generation for reactions with ascorbic acid, gallic acid and L-cysteine. Very fast accumulation of hydrogen peroxide was observed in reactions with L-cysteine, which likely explains why early enzyme inactivation occurred during L-cysteine-driven reactions with cellulose. All in all, the results obtained for reactions with ascorbic acid, gallic acid and L-cysteine confirm the notion that LPMO activity under standard aerobic conditions reflects an H_2O_2-limited peroxygenase reaction, rather than a monooxygenase (i.e., O_2-dependent) reaction.

On the other hand, the experiments with DHA seemingly pointed in a very different direction. While DHA-driven oxidation of cellulose by

*Ssc*LPMO10B was fast, compared to reactions with ascorbic acid and gallic acid, H_2O_2 production in the presence of DHA was negligible, potentially indicating that (H_2O_2-independent) monooxygenase LPMO reactions are fueled by this reductant.

To further investigate the role of H_2O_2 in DHA-driven *Ssc*LPMO10B activity, LPMO reactions with Avicel were carried out in the presence of 100 μM hydrogen peroxide (Paper II: Fig. 7A) and either DHA or ascorbic acid. As expected, the addition of H_2O_2 to the LPMO reaction with ascorbic acid resulted in a vast increase in the product release rate (≈5.6 min^{-1}) compared to the rate obtained at standard aerobic conditions (≈0.12 min^{-1}). At the same time, the effect of H_2O_2 on the DHA-driven *Ssc*LPMO10B reaction was minimal, showing a product release rate (≈0.86 min^{-1}) that was close to the rate observed at standard aerobic conditions (≈0.32 min^{-1}). Given these results, one may assume that DHA is a highly unusual reductant that cannot efficiently reduce the LPMO to support peroxygenase activity (Paper II: Fig. 7A) but works perfectly fine under "monooxygenase" conditions (Paper II: Fig. 5).

Looking for explanations, we first considered the possibility that DHA has very high reactivity with H_2O_2, thus removing the co-substrate from the reaction before it can be productively consumed by the enzyme. A control reaction with added H_2O_2 in the presence of both ascorbic acid and DHA (Paper II: Fig. 7B) yielded a progress curve almost equal to the curve obtained with ascorbic acid alone, showing that hydrogen peroxide scavenging by DHA was negligible.

Surprisingly, the rate of the DHA-driven *Ssc*LPMO10B reaction with Avicel and added H_2O_2 dramatically improved when DHA was pre-incubated in buffer for 6 hours prior to the addition of the enzyme and hydrogen peroxide. In this case, the reactions with ascorbic acid and (pre-incubated) DHA gave similar progress curves (Paper II: Fig. 7C). This experiment suggests that a slowly accumulating DHA derivative (or multiple derivatives)

rather than DHA itself is responsible for reducing the LPMO active site and for driving cellulose degradation. Indeed, slow generation of a redox-active DHA derivative can explain the apparent high efficiency of DHA in 24 h LPMO reactions at standard aerobic conditions (Paper 2: Fig. 5A), compared to the experiments with exogenously added H_2O_2 that were conducted in just 30 minutes (Paper 2: Fig. 7A). It is conceivable that an incubation time as short as 30 minutes does not allow for a significant amount of the LPMO-reducing DHA derivative to accumulate.

On the same note, the indirect and delayed effect of DHA is a likely reason why almost no H_2O_2 generation was observed in the HRP/Amplex Red assay (Paper II: Fig. 6). As described in Paper I, redox-active compounds may suppress the signal of the HRP/Amplex Red assay. This can to some extent be compensated for by introducing reductants into standard curves for H_2O_2, as was done in the studies described in Papers I and II. For unstable DHA, such a correction is problematic because the degree of signal repression will change over time. Therefore, another (slower) H_2O_2 assay, based on a selective fluorescent probe for H_2O_2, Peroxy Orange 1, was adopted. Importantly, co-incubation of LPMO and DHA, or just DHA, with Peroxy Orange 1 revealed both enzymatic and non-enzymatic hydrogen peroxide generation, which became detectible after 4 - 5 hours of experiment (Paper II: Fig. 8).

Additional proof for the role of H_2O_2 in DHA-driven LPMO reactions was obtained through experiments with an enzymatic H_2O_2 scavenger, bovine liver catalase. Addition of catalase to reactions with *Ssc*LPMO10B, DHA and Avicel resulted in almost complete inhibition of the LPMO reaction, confirming that H_2O_2 (and not O_2) is the kinetically relevant LPMO co-substrate under these conditions (Paper II: Fig. 9).

Instability of DHA in aqueous solutions has been observed previously and is described in biochemical literature. It has been shown that DHA can spontaneously convert to 2,3-diketo-l-gulonic acid (DKG), and that DKG can

then give rise to additional and not fully characterized compounds, some of which are thought to be redox-active [146-149]. Indeed, UV-VIS spectroscopy of reaction mixtures containing DHA and Avicel indicated that new UV-absorbing species are formed during incubation under the conditions used in this study and that these species are consumed upon addition of the LPMO (Paper II: Fig. 11). Attempts to identify the catalytically relevant DHA derivatives by NMR failed, but the NMR experiments did show that neither DHA nor DKG are consumed by the LPMO directly (Paper II: Fig. 12).

Taken together, the experiments with *Ssc*LPMO10B and four different reductants under standard aerobic conditions show that the depolymerization of cellulosic substrate is predominantly driven by peroxygenase reactions. While the results did not allow identification of the redox-active DHA derivative that is responsible for driving the LPMO reaction, it is clear that this transient compound is capable of promoting both enzyme-dependent and enzyme-independent H_2O_2 production *in situ*.

3.3 Paper III: Enhanced *in situ* H_2O_2 production explains synergy between an LPMO with a cellulose-binding domain and a single-domain LPMO

Paper III of this thesis builds on the idea that catalytic rates of LPMOs at standard aerobic conditions are limited by the supply of *in situ* generated hydrogen peroxide (see Papers I and II). The study of Paper III addressed the interplay between enzyme-dependent H_2O_2 production and substrate binding, which is an important but rather unexplored aspect of LPMO chemistry. As originally suggested by Kittl et al. [116], binding of LPMO to insoluble substrate suppresses enzyme-depended H_2O_2 generation, most likely due to preventing the access of reducing compounds to the active site [113]. The substrate affinities of LPMOs have not been systematically studied and may vary between enzymes. In many LPMOs, such as the well-characterized bacterial enzyme *Sc*LPMO10C, substrate affinity is potentiated by auxiliary carbohydrate-binding modules (CBMs), which bind to the polysaccharide substrate with higher affinity than the catalytic domains [92,93]. The goal of the study described in Paper III was to investigate the effect of the CBM on enzyme-dependent H_2O_2 generation using CBM-containing *Sc*LPMO10C and its truncated form comprising the catalytic domain only (*Sc*LPMO10C-AA10).

*Sc*LPMO10C and *Sc*LPMO10C-AA10 were produced in *E. coli* using previously described expression strains. Surprisingly, assessment of H_2O_2 generation by the full-length and truncated enzyme in the presence of ascorbic acid revealed a three-fold difference in the reaction rates under the conditions of HRP/Amplex Red assay (i.e., conditions that do not involve an LPMO substrate and where CBM effects are not expected). The truncated enzyme, *Sc*LPMO10C-AA10, produced more hydrogen peroxide (Paper III:

Fig. 2) and control experiments (Paper III: Fig. 2) showed that this was not due to variation in free Cu(II) levels, but relates to intrinsic enzyme properties (i.e., the oxidase activity of the LPMO variants). One can speculate that the higher H_2O_2 production rate of ScLPMO10C-AA10 in the absence of substrate is an artifact of LPMO truncation, which, in principle could affect the protein fold and make the reduced copper more prone to oxidation by O_2. However, this seems unlikely, given the fact that the truncation point is >35 Å away from the active site and that the X-ray structure of *Sc*LPMO10C-AA10 shows no perturbations of the active site (PDB: 4OY7) [95]. A possible, although speculative, explanation for the observed difference in oxidase activity between the full-length and truncated LPMO, suggested in Paper III, is that the CBM weakly interacts with the substrate-binding surface of the catalytic domain, which could reduce H_2O_2 generation by shielding the active site copper from interactions with reductant molecules.

The difference in H_2O_2 generation between the two enzyme variants was confirmed by control experiments in which the LPMOs were incubated with reductant in the absence of substrate after which residual activity was tested. One would expect that the enzyme with the strongest oxidase activity, i.e., the truncated enzyme, would be most prone to auto-catalytic inactivation and this was indeed observed (Paper III: Fig. 6). Of note, the difference in H_2O_2 generation between the two enzyme variants is probably larger in the presence of substrate, since H_2O_2 production by the better binding full length enzyme will be more inhibited by the substrate, compared to the truncated variant.

Next, Avicel oxidation experiments with *Sc*LPMO10C and *Sc*LPMO10C-AA10 were carried out in the presence of ascorbic acid (Paper III: Fig. 3). Cellulose depolymerization by 1 μM or 2 μM *Sc*LPMO10C resulted in a slow (≈0.05 min^{-1}) but steady release of oxidized products over 24 hours, with the reaction rate being comparable to the rates described for the *Sc*LPMO10C

homologues discussed in Papers I and II. The experiments with 1 μM or 2 μM *Sc*LPMO10C-AA10 displayed faster initial rates of product release, but product accumulation stopped after 3 hours of reaction, which is indicative of LPMO inactivation. As discussed in the Introduction to this thesis, auto-catalytic damage to the LPMO active site can be promoted by excess H_2O_2 and low substrate binding. Both these factors may be applicable when trying to understand the differences between the reactions with *Sc*LPMO10C-AA10 compared to *Sc*LPMO10C.

Importantly, combining 1 μM *Sc*LPMO10C and 1 μM *Sc*LPMO10C-AA10 in a single reaction (Paper III: Fig. 3) led to stable degradation of Avicel with no signs of inactivation whatsoever. Furthermore, the amount of oxidized products released after 24 hours was higher compared to the sum of the products generated by these enzymes in individual reactions, indicative of synergy between the truncated and full-length LPMO. In light of the H_2O_2 production data for the two enzymes, it is conceivable that this synergy relates to enhanced *in situ* hydrogen peroxide generation, driven by the truncated enzyme, and more efficient productive H_2O_2 consumption by the full-length enzyme. This would lead to higher LPMO activity and improved LPMO stability, as is observed. Recent studies have indicated that, in the presence of proper substrates, the damaging off-path reactions of LPMOs with hydrogen peroxide are one to three orders of magnitude slower compared to productive peroxygenase reactions [99,118]. Therefore, the (better binding) full-length enzyme is expected to be a faster H_2O_2 consumer, relative to *Sc*LPMO10C-AA10, thus channeling H_2O_2 to productive cellulose-degrading LPMO reactions rather than to LPMO-damaging off-pathway reactions.

To increase understanding of what is happening in these reactions, reductant consumption was monitored. Since it is well-known that auto-catalytic damage predominately affects copper-binding histidine residues of LPMOs [98,119], one may expect that copper ions can be released into

solution upon enzyme inactivation. Importantly, release of copper, even to levels considerably lower than the LPMO concentrations used in the reactions, would drastically increase ascorbic acid depletion rate (Paper III: Figs. 2 & 4A) and, thus, can be easily detected.

Analysis of ascorbic acid consumption during LPMO-catalyzed depolymerization of Avicel showed that reactions with 1 μM *Sc*LPMO10C, 2 μM *Sc*LPMO10C and 1 μM *Sc*LPMO10C + 1 μM *Sc*LPMO10C-AA10 resulted in a slow and steady reductant depletion over 24 hours (Paper III: Fig. 4B). In stark contrast, reactions with the truncated form of the LPMO led to full depletion of ascorbic acid within the first 3 – 6 hours of the experiment, and reductant consumption was not proportional to (i.e., much larger than) the amount of products released from cellulose. The observed rates of reductant depletion in these latter reactions were comparable to the depletion rates observed in control experiments with added free Cu(II) (Paper III: Fig. 4A). Taken together, these data point at the possibility that the fast consumption of ascorbic acid in experiments with the truncated LPMO may be predominantly driven by abiotic reactions involving the reductant and copper ions leaving the metal-binding center of damaged LPMO molecules.

Remarkably, and somewhat coincidently, the reaction with 1 μM ScLPMO10C + 2 μM ScLPMO10C-AA10 revealed an intermediate pattern of reductant depletion (Paper III: Figs. 4 & 5). An initial slow depletion phase (first 16 hours of the experiment) was followed by a rapid depletion phase, indicating that, after 16 hours, 1 μM ScLPMO10C was no longer able to consume the H_2O_2 generated by 2 μM ScLPMO10C-AA10, and that Cu(II) ions started to be released into the solution. This order of events is reflected in LPMO product formation, which was fast and steady during the first phase of the reaction, but which slowed down and eventually stopped as the reaction system collapsed due to a combination of LPMO inactivation and copper-mediated reductant depletion (Paper III: Fig. 5). In the light of these

observations, one may think of LPMO inactivation (in ascorbic acid-driven reactions) as a self-reinforcing process, where the oxidative damage caused by a surplus of H_2O_2 to a fraction of the enzyme molecules leads to even higher amounts of hydrogen peroxide due to the release of copper from the active site.

In conclusion, Paper III provides insight into the complex interplay between LPMOs with different H_2O_2 generating and consuming capabilities that, notably, are affected by substrate-affinity. Paper III shows how LPMOs can act in H_2O_2-mediated synergy and provides important insight into how LPMO reaction systems may collapse, in case hydrogen peroxide accumulation is not thoroughly controlled.

3.4 Paper IV: Fast and specific peroxygenase reactions catalyzed by fungal mono-copper enzymes

Paper IV of this thesis presents a detailed kinetic investigation of *Nc*LPMO9C, an enzyme of fungal origin capable of oxidizing soluble cello-oligosaccharides. While the biological relevance of this type of LPMO activity is unclear, the use of oligosaccharides allows to overcome technical hurdles that arise when studying the degradation of (insoluble) amorphous or crystalline cellulose. To begin with, the concentration of productive binding sites on insoluble substrates (i.e., the true substrate concentration) is difficult to assess, which complicates the interpretation of kinetic data. On top of that, in contrast to rapidly diffusing cello-oligosaccharides, insoluble cellulosic substrates may cause kinetic complications related to slow substrate association and/or dissociation, which may promote off-pathway LPMO reactions and auto-catalytic damage.

First, oxidation of 1 mM cellopentaose by *Nc*LPMO9C was studied in the absence of exogenously added hydrogen peroxide, using 1 mM ascorbic acid, gallic acid or L-cysteine, while the H_2O_2 generating capacity of these LPMO-reductant combinations was assessed using the modified version of the HRP/Amplex Red assay described in Paper I (Paper IV: Fig. 2, Table 1). The substrate conversion rates observed in the presence of ascorbic acid, gallic acid and L-cysteine amounted to approximately 0.05 s^{-1}, 0.01 s^{-1} and 0.06 s^{-1}, respectively. The relative performance of the various reducing compounds in H_2O_2 production experiments with *Nc*LPMO9C showed the same trend (L-cysteine > ascorbic acid > gallic acid). Quantitative comparison of the rates of substrate conversion and hydrogen peroxide accumulation revealed that the substrate conversion was three times faster than the H_2O_2 generation in the presence of ascorbic acid and L-cysteine. This observation is paradoxical if

one accepts the premise that *in situ* hydrogen peroxide production drives the LPMO reaction at standard aerobic conditions (see Papers I, II). However, the discrepancy between LPMO activity and H_2O_2 generation was explained by a control experiment showing that the commercially obtained cellopentaose preparation used in this study was contaminated with copper (or other transition metals), which would promote enzyme-independent H_2O_2 generation in the reactions with ascorbic acid (Paper I) or L-cysteine [135], but not in the reaction with gallic acid (Paper I; for the results, see Paper IV: Fig. 2C). Therefore, the true rates of hydrogen peroxide production in reactions containing substrate and ascorbic acid/L-cysteine were likely higher than the rates observed under the conditions of the HRP/Amplex Red assay (i.e., in the absence of contaminated cellopentaose).

Despite auto-oxidation of gallic acid not being sensitive to the presence of transition metals, the data obtained for reactions with this reductant revealed an even larger (5-fold) difference between the substrate conversion rate and the rate of H_2O_2 generation. This gap is caused by underestimation of hydrogen peroxide generation assessed with the HRP/Amplex Red assay for reactions in the presence of gallic acid and the LPMO. As can be seen from Table I in Paper IV, the addition of LPMO to reaction mixtures containing 1 mM gallic acid results in significant apparent decrease in H_2O_2 accumulation, indicating that the enzyme consumes hydrogen peroxide in a side-reaction with gallic acid. H_2O_2-dependent conversion of gallic acid by an LPMO, in the absence of carbohydrate substrate has, indeed, been reported before [150]. Due to this side-process, the true rate of the oxidase reaction catalyzed by *Nc*LPMO9C in the presence of gallic acid is difficult to assess, and it seems to be higher than the apparent rate, given the cellopentaose oxidation efficiency. Addition of HRP to a reaction with *Nc*LPMO9C, cellopentaose and gallic acid resulted in LPMO inhibition, proving that hydrogen peroxide is the catalytically relevant co-substrate under these conditions (Paper IV: Fig. 3).

The correlation between the relative performance of ascorbic acid, gallic acid and L-cysteine in H_2O_2 production assays and cellopentaose oxidation assays was confirmed in studies with another fungal LPMO capable of acting on soluble oligosaccharides, *Ls*LPMO9A (Paper IV: Fig. 6, Table 2).

In an attempt to explore the full peroxygenase potential of LPMOs, the capacity of *Nc*LPMO9C to catalyze cellopentaose oxidation in the presence of exogenous hydrogen peroxide was assessed. Reactions with 300 μM H_2O_2, 1 mM substrate and 100 μM reductant revealed apparent, and partly underestimated, catalytic rates of approximately 70 s^{-1} (ascorbic acid), 25 s^{-1} (gallic acid) and 6 s^{-1} (L-cysteine) (Paper IV: Fig. 4). It is worth noting that for the reactions with ascorbic acid and gallic acid these rates are some three orders of magnitude higher, compared to rates obtained at standard aerobic conditions, whereas the rate difference for reactions with cysteine was two orders of magnitude.

To investigate whether the reductant concentration may be limiting these fast peroxygenase reactions, the experiment was repeated with 1 mM reductants. For gallic acid and ascorbic acid the increase in the amount of reductant resulted in increased (up to two-fold) reaction rates, showing that the reductant to some extent limits these very fast peroxygenase reactions (Paper IV: Fig. 4). It is conceivable that occasional re-reduction of the LPMOs is needed, which could explain the impact of the reductant concentration. Increasing the L-cysteine concentration had no effect on the LPMO catalytic rate. While the data presented in Paper IV do not provide an explanation for the lower turnover numbers obtained with L-cysteine, literature data [151] suggest that the enzyme active site may engage in forming cuprous thiolate complexes, which may inhibit the LPMO reaction with H_2O_2.

Next, Michaelis-Menten analysis of the *Nc*LPMO9C peroxygenase activity on cellopentaose were carried out (Paper IV: Fig. 5A). For the reaction fueled with 600 μM of H_2O_2 and 0.1 mM ascorbic acid (and carried out at 4 °C), a K_m

for cellopentaose of 2.1 ± 0.3 mM was determined, which is in accordance with previously published data [152]. Most notably , the k_{cat} was found to be as high as 124 ± 27 s^{-1}. Such high reaction rates have never been reported for LPMOs before. Underpinning the efficiency and specificity of the *Nc*LPMO9C peroxygenase reactions, the data show that 600 µM H_2O_2 is stoichiometrically converted to oxidized cellopentaose (Fig. 5B). It is also worth noting that starting concentrations of H_2O_2 as high as 600 µM H_2O_2 would be expected to result in rapid enzyme inactivation in other types of LPMO reactions, such as reactions with cellulose [98] .

Taken together, the results described in Paper IV suggest that reductant- and LPMO-dependent *in situ* hydrogen peroxide formation limit the catalytic rates of fungal AA9 LPMOs acting on a soluble substrate at standard aerobic conditions. Most importantly, the results show that when provided with a rapidly diffusing substrate, fast stoichiometric conversion of very high amounts of H_2O_2 can be achieved through specific oxidation of the oligosaccharide substrate. These results not only underpin that hydrogen peroxide is, indeed, a relevant LPMO co-substrate, but also reveal that, under optimal conditions LPMOs are highly efficient enzymes.

4 Concluding remarks

The work presented in this thesis provides new insights into LPMO catalysis and reveal factors that affect the efficiency and stability of LPMOs under turnover conditions. The correlations between the rates of *in situ* hydrogen peroxide formation and substrate oxidation, observed for reactions with both AA9 and AA10 LPMOs in the presence of various reducing compounds show that peroxygenase reactions are predominant under what may be referred to as "monooxygenase" conditions (Papers I, II, IV). While data obtained in these studies do not allow to fully exclude monooxygenase reactions, the almost complete inhibition of LPMO activity by enzymatic H_2O_2 scavengers that was observed in reactions with both soluble and insoluble substrates shows that the hypothetical O_2-dependent reactions are kinetically irrelevant (Papers II, IV). Importantly, the reliance of LPMOs on *in situ* hydrogen peroxide supply at standard aerobic conditions explains the remarkable dependency of reported catalytic rates on the nature of the reducing compound used to drive the reactions.

The data presented in this thesis shed light on the interplay between enzymatic and non-enzymatic *in situ* sources of H_2O_2, which is complicated by the impact of substrate binding. While LPMO dose-response experiments with a CBM-containing AA10 enzyme (AA10_07) indicated that reductant auto-oxidation is the major source of hydrogen peroxide at standard aerobic conditions (Paper I), further work showed that this is not the case for a CBM-free AA10 LPMO (*Sc*LPMO10C-AA10) with lower affinity for cellulose (Paper III). The results described in Paper III show that enzyme-dependent H_2O_2 production by *Sc*LPMO10C-AA10 is high enough to have a pronounced

positive impact on the activity of another LPMO present in the same reaction mixture.

On another note, non-enzymatic pathways for H_2O_2 generation in LPMO reactions may strongly depend on experimental conditions in a combination with some reductants. As the studies presented in this thesis show, auto-oxidation of ascorbic acid and L-cysteine increases manyfold in the presence of free copper ions and, potentially, other transition metals. A metal-dependent boost in H_2O_2 production, which may occur at metal concentrations that are considerably lower than the LPMO concentrations typically used in the experiments, has great repercussions for LPMO activity and stability (Paper I). Possible sources of copper include the enzyme preparations (Paper I), the substrate (Paper IV), and, as discussed below, oxidatively damaged LPMOs that my release their bound copper into solution (Paper III).

Even when the free copper content of the enzyme and substrate preparations is negligible, free copper ions may be released into solution during LPMO reactions as a result of auto-catalytic oxidative damage to the copper-binding catalytic center (Paper III). This effect was never reported before and is expected to potentially have major impact on the efficiency and stability of an LPMO reaction that is fueled by copper-sensitive reductants, such as ascorbic acid [132], L-cysteine [135], reduced glutathione [134], DTT [139], catechol and caffeic acid [140]. Paper III shows that, in the presence of such copper-sensitive compounds, LPMO inactivation may become a self-reinforcing process, where copper release due to H_2O_2-mediated damage to the active site of a fraction of the enzymes will result in even higher amounts of H_2O_2 being produced and increased enzyme inactivation.

Paper IV of this thesis shows that, under the right conditions, a fungal LPMO can stoichiometrically convert high amounts of hydrogen peroxide (600 μM) to oxidized oligosaccharide products and do so at unprecedentedly

high rates. Apart from showing the true power of LPMOs, these results may be taken to indicate that the enzyme inactivation commonly observed in H_2O_2-fueled LPMO reactions is not caused by H_2O_2 *per se*, as some authors claim [65], but rather reflects limitations in substrate binding that make the LPMO susceptible to off-pathway reactions. The turnover rates reported in Paper IV add to an increasing body of data showing that kinetic parameters for well-controlled LPMO-catalyzed peroxygenase reactions are similar to those for other peroxygenases [99,103].

Some of the results described in this thesis cannot not be fully explained and call for further investigation. One example is the difference in performance between reducing compounds in reactions catalyzed by fungal LPMOs in the presence of high amounts of exogenous hydrogen peroxide (Paper IV). It is clear that the impact of *in situ* H_2O_2 generation is minimal under such conditions, and yet, considerable variation between different LPMO-reductant combinations was observed. Such variation is best illustrated by the reactions fueled by L-cysteine, which give substrate oxidation rates that are one order of magnitude lower, compared to identical reactions with ascorbic acid and gallic acid. One possible explanation for the lower efficiency of L-cysteine is formation of a relatively stable cuprous thiolate complex in the LPMO active site, which would limit the rate of the very fast peroxygenase reactions with exogenously provided H_2O_2 but would not have a pronounced impact on much slower reactions observed under "monooxygenase" conditions.

Another important (and unanswered) question is why LPMOs vary in H_2O_2-producting capacity. The data obtained in papers II and IV using ascorbic acid as a reductant show that the rate of LPMO-dependent H_2O_2 accumulation is approximately 7-fold higher in the presence of an AA9 LPMO (*Nc*LPMO9C) compared to an AA10 LPMO (*Ssc*LPMO10B). However, when the same oxidase reactions were fueled by L-cysteine, *Ssc*LPMO10B

outperformed *Nc*LPMO9C, resulting in ≈2.5 times faster hydrogen peroxide production. This reductant-dependent gap in oxidase activity is remarkable and may be driven by the difference in LPMO intrinsic properties, such as subtle variations in the copper coordination sphere, as well as by the difference in reaction conditions (e.g., pH 6.0 vs pH 6.5 in Papers II and IV, respectively).

Despite the work described in this thesis, the impact of the reductants on LPMO performance needs further investigation. For example, there is no doubt that reductant properties are strongly affected by pH [142,153,154] and this has not been addressed at all in the present study. Another aspect, already touched upon in the above, is the possibility of specific (binding) interactions between certain reductants and certain LPMOs. Such interactions may involve the copper, as discussed above for L-cysteine, but could also involve residues on the LPMO surface.

The observation, described in Paper III, that truncation of the CBM domain from a two-domain AA10 LPMO (*Sc*LPMO10C) results in a significant increase in enzyme-dependent hydrogen peroxide generation is intriguing. A possible (and highly speculative) explanation for this effect is that the catalytic and cellulose-binding domains of ScLPMO10C weakly interact in an inter-molecular or intra-molecular fashion. It is tempting to propose that the CBM may protect the LPMO from auto-catalytic damage in the absence of substrate by shielding the copper site, thus preventing reduction and keeping the fraction of H_2O_2-producing enzyme molecules low. Further studies are needed to explore this possible scenario, the biological relevance of which also may need further attention.

In conclusion, the work described in this thesis underpins the increasingly accepted notion that LPMOs are peroxygenases rather than monooxygenases and that, under the right conditions, these enzymes can be orders of magnitude faster than originally described. Studying, understanding

and optimizing LPMO catalysis raises numerous complications and the present results shed light on several of these (effects of free copper, reductants and substrate affinity). In this respect, the self-reinforcing LPMO inactivation scenario described in Paper III is of particular importance. Hopefully, the increased insight into LPMO catalysis that this thesis aims to provide will help harnessing the power of these unique enzymes in existing and novel applications.

5 References

1 Manavalan, T., Stepnov, A. A., Hegnar, O. A. & Eijsink, V. G. H. Sugar oxidoreductases and LPMOs - two sides of the same polysaccharide degradation story? *Carbohydr Res* **505**, 108350, doi:10.1016/j.carres.2021.108350 (2021).

2 Mariano, M., El Kissi, N. & Dufresne, A. Cellulose nanocrystals and related nanocomposites: Review of some properties and challenges. *Journal of Polymer Science Part B: Polymer Physics* **52**, 791-806, doi:10.1002/polb.23490 (2014).

3 Jonas, R. & Farah, L. F. Production and application of microbial cellulose. *Polymer Degradation and Stability* **59**, 101-106, doi:10.1016/s0141-3910(97)00197-3 (1998).

4 Zhao, Y. & Li, J. Excellent chemical and material cellulose from tunicates: diversity in cellulose production yield and chemical and morphological structures from different tunicate species. *Cellulose* **21**, 3427-3441, doi:10.1007/s10570-014-0348-6 (2014).

5 Heinze, T., El Seoud, O. A. & Koschella, A. in *Cellulose Derivatives Springer Series on Polymer and Composite Materials* Chapter 1, 1-38 (2018).

6 Himmel, M. E. *et al.* Biomass recalcitrance: engineering plants and enzymes for biofuels production. *Science* **315**, 804-807, doi:10.1126/science.1137016 (2007).

7 Hallac, B. B. & Ragauskas, A. J. Analyzing cellulose degree of polymerization and its relevancy to cellulosic ethanol. *Biofuels, Bioproducts and Biorefining* **5**, 215-225, doi:10.1002/bbb.269 (2011).

8 Pauly, M. & Keegstra, K. Cell-wall carbohydrates and their modification as a resource for biofuels. *Plant J* **54**, 559-568, doi:10.1111/j.1365-313X.2008.03463.x (2008).

9 Meier, K. K. *et al.* Oxygen activation by Cu LPMOs in recalcitrant carbohydrate polysaccharide conversion to monomer sugars. *Chem Rev* **118**, 2593-2635, doi:10.1021/acs.chemrev.7b00421 (2018).

10 Girio, F. M. *et al.* Hemicelluloses for fuel ethanol: A review. *Bioresour Technol* **101**, 4775-4800, doi:10.1016/j.biortech.2010.01.088 (2010).

11 Sun, R., Sun, X. F. & Tomkinson, J. in *Hemicelluloses: Science and Technology ACS Symposium Series* 2-22 (2003).

12 Ebringerová, A. Structural diversity and application potential of hemicelluloses. *Macromolecular Symposia* **232**, 1-12, doi:10.1002/masy.200551401 (2005).

13 Chio, C., Sain, M. & Qin, W. Lignin utilization: A review of lignin depolymerization from various aspects. *Renewable and Sustainable Energy Reviews* **107**, 232-249, doi:10.1016/j.rser.2019.03.008 (2019).

14 Lewis, N. G. A 20th century roller coaster ride: a short account of lignification. *Current Opinion in Plant Biology* **2**, 153-162, doi:10.1016/s1369-5266(99)80030-2 (1999).
15 Boerjan, W., Ralph, J. & Baucher, M. Lignin biosynthesis. *Annu Rev Plant Biol* **54**, 519-546, doi:10.1146/annurev.arplant.54.031902.134938 (2003).
16 Rinaldi, R. & Schuth, F. Acid hydrolysis of cellulose as the entry point into biorefinery schemes. *ChemSusChem* **2**, 1096-1107, doi:10.1002/cssc.200900188 (2009).
17 Cragg, S. M. *et al.* Lignocellulose degradation mechanisms across the Tree of Life. *Curr Opin Chem Biol* **29**, 108-119, doi:10.1016/j.cbpa.2015.10.018 (2015).
18 Mayer, W. E., Schuster, L. N., Bartelmes, G., Dieterich, C. & Sommer, R. J. Horizontal gene transfer of microbial cellulases into nematode genomes is associated with functional assimilation and gene turnover. *BMC Evol Biol* **11**, 13, doi:10.1186/1471-2148-11-13 (2011).
19 Fontes, C. M. & Gilbert, H. J. Cellulosomes: highly efficient nanomachines designed to deconstruct plant cell wall complex carbohydrates. *Annu Rev Biochem* **79**, 655-681, doi:10.1146/annurev-biochem-091208-085603 (2010).
20 Bayer, E. A., Belaich, J. P., Shoham, Y. & Lamed, R. The cellulosomes: multienzyme machines for degradation of plant cell wall polysaccharides. *Annu Rev Microbiol* **58**, 521-554, doi:10.1146/annurev.micro.57.030502.091022 (2004).
21 Divne, C., Stahlberg, J., Teeri, T. T. & Jones, T. A. High-resolution crystal structures reveal how a cellulose chain is bound in the 50 A long tunnel of cellobiohydrolase I from *Trichoderma reesei*. *J Mol Biol* **275**, 309-325, doi:10.1006/jmbi.1997.1437 (1998).
22 Larsson, A. M. *et al.* Crystal structure of *Thermobifida fusca* endoglucanase Cel6A in complex with substrate and inhibitor: the role of tyrosine Y73 in substrate ring distortion. *Biochemistry* **44**, 12915-12922, doi:10.1021/bi0506730 (2005).
23 Beenakker, T. J. M. *et al.* Carba-cyclophellitols are neutral retaining-glucosidase inhibitors. *J Am Chem Soc* **139**, 6534-6537, doi:10.1021/jacs.7b01773 (2017).
24 Davies, G. & Henrissat, B. Structures and mechanisms of glycosyl hydrolases. *Structure* **3**, 853-859, doi:10.1016/s0969-2126(01)00220-9 (1995).
25 Igarashi, K. *et al.* High speed atomic force microscopy visualizes processive movement of *Trichoderma reesei* cellobiohydrolase I on crystalline cellulose. *J Biol Chem* **284**, 36186-36190, doi:10.1074/jbc.M109.034611 (2009).
26 Juturu, V. & Wu, J. C. Microbial cellulases: Engineering, production and applications. *Renewable and Sustainable Energy Reviews* **33**, 188-203, doi:10.1016/j.rser.2014.01.077 (2014).
27 Obeng, E. M. *et al.* Lignocellulases: a review of emerging and developing enzymes, systems, and practices. *Bioresources and Bioprocessing* **4**, doi:10.1186/s40643-017-0146-8 (2017).

28 Teugjas, H. & Valjamae, P. Product inhibition of cellulases studied with 14C-labeled cellulose substrates. *Biotechnol Biofuels* **6**, 104, doi:10.1186/1754-6834-6-104 (2013).

29 Nam, K. H., Sung, M. W. & Hwang, K. Y. Structural insights into the substrate recognition properties of beta-glucosidase. *Biochem Biophys Res Commun* **391**, 1131-1135, doi:10.1016/j.bbrc.2009.12.038 (2010).

30 Gomez del Pulgar, E. M. & Saadeddin, A. The cellulolytic system of *Thermobifida fusca*. *Crit Rev Microbiol* **40**, 236-247, doi:10.3109/1040841X.2013.776512 (2014).

31 Wilson, D. B. Studies of *Thermobifida fusca* plant cell wall degrading enzymes. *Chem Rec* **4**, 72-82, doi:10.1002/tcr.20002 (2004).

32 Brigham, J. S., Adney, W. S. & Himmel, M. E. in *Handbook on Bioethanol* Chapter 7, 119-141 (2018).

33 Vaaje-Kolstad, G. *et al.* An oxidative enzyme boosting the enzymatic conversion of recalcitrant polysaccharides. *Science* **330**, 219-222, doi:10.1126/science.1192231 (2010).

34 Forsberg, Z. *et al.* Cleavage of cellulose by a CBM33 protein. *Protein Sci* **20**, 1479-1483, doi:10.1002/pro.689 (2011).

35 Quinlan, R. J. *et al.* Insights into the oxidative degradation of cellulose by a copper metalloenzyme that exploits biomass components. *Proc Natl Acad Sci U S A* **108**, 15079-15084, doi:10.1073/pnas.1105776108 (2011).

36 Phillips, C. M., Beeson, W. T., Cate, J. H. & Marletta, M. A. Cellobiose dehydrogenase and a copper-dependent polysaccharide monooxygenase potentiate cellulose degradation by *Neurospora crassa*. *ACS Chem Biol* **6**, 1399-1406, doi:10.1021/cb200351y (2011).

37 Horn, S. J., Vaaje-Kolstad, G., Westereng, B. & Eijsink, V. G. Novel enzymes for the degradation of cellulose. *Biotechnol Biofuels* **5**, 45, doi:10.1186/1754-6834-5-45 (2012).

38 Eibinger, M. *et al.* Cellulose surface degradation by a lytic polysaccharide monooxygenase and its effect on cellulase hydrolytic efficiency. *J Biol Chem* **289**, 35929-35938, doi:10.1074/jbc.M114.602227 (2014).

39 Vaaje-Kolstad, G., Horn, S. J., van Aalten, D. M., Synstad, B. & Eijsink, V. G. The non-catalytic chitin-binding protein CBP21 from *Serratia marcescens* is essential for chitin degradation. *J Biol Chem* **280**, 28492-28497, doi:10.1074/jbc.M504468200 (2005).

40 Harris, P. V. *et al.* Stimulation of lignocellulosic biomass hydrolysis by proteins of glycoside hydrolase family 61: structure and function of a large, enigmatic family. *Biochemistry* **49**, 3305-3316, doi:10.1021/bi100009p (2010).

41 Chylenski, P. *et al.* Enzymatic degradation of sulfite-pulped softwoods and the role of LPMOs. *Biotechnol Biofuels* **10**, 177, doi:10.1186/s13068-017-0862-5 (2017).

42 Cannella, D., Hsieh, C. W., Felby, C. & Jorgensen, H. Production and effect of aldonic acids during enzymatic hydrolysis of lignocellulose at high dry matter content. *Biotechnol Biofuels* **5**, 26, doi:10.1186/1754-6834-5-26 (2012).

43 Costa, T. H. F. *et al.* Demonstration-scale enzymatic saccharification of sulfite-pulped spruce with addition of hydrogen peroxide for LPMO activation. *Biofuels, Bioproducts and Biorefining* **14**, 734-745, doi:10.1002/bbb.2103 (2020).

44 Reese, E. T., Siu, R. G. & Levinson, H. S. The biological degradation of soluble cellulose derivatives and its relationship to the mechanism of cellulose hydrolysis. *J Bacteriol* **59**, 485-497, doi:10.1128/jb.59.4.485-497.1950 (1950).

45 Eriksson, K.-E., Pettersson, B. & Westermark, U. Oxidation: An important enzyme reaction in fungal degradation of cellulose. *FEBS Letters* **49**, 282-285, doi:10.1016/0014-5793(74)80531-4 (1974).

46 Westermark, U. *et al.* Cellobiose:Quinone oxidoreductase, a new wood-degrading enzyme from white-rot fungi. *Acta Chemica Scandinavica* **28b**, 209-214, doi:10.3891/acta.chem.scand.28b-0209 (1974).

47 Dumonceaux, T., Bartholomew, K., Valeanu, L., Charles, T. & Archibald, F. Cellobiose dehydrogenase is essential for wood invasion and nonessential for kraft pulp delignification by *Trametes versicolor*. *Enzyme and Microbial Technology* **29**, 478-489, doi:10.1016/s0141-0229(01)00407-0 (2001).

48 Schnellmann, J., Zeltins, A., Blaak, H. & Schrempf, H. The novel lectin-like protein CHB1 is encoded by a chitin-inducible *Streptomyces olivaceoviridis* gene and binds specifically to crystalline alpha-chitin of fungi and other organisms. *Mol Microbiol* **13**, 807-819, doi:10.1111/j.1365-2958.1994.tb00473.x (1994).

49 Suzuki, K., Suzuki, M., Taiyoji, M., Nikaidou, N. & Watanabe, T. Chitin binding protein (CBP21) in the culture supernatant of *Serratia marcescens* 2170. *Biosci Biotechnol Biochem* **62**, 128-135, doi:10.1271/bbb.62.128 (1998).

50 Cantarel, B. L. *et al.* The Carbohydrate-Active EnZymes database (CAZy): an expert resource for Glycogenomics. *Nucleic acids research* **37**, D233-238, doi:10.1093/nar/gkn663 (2009).

51 Saloheimo, M., Nakari-Setala, T., Tenkanen, M. & Penttila, M. cDNA cloning of a *Trichoderma reesei* cellulase and demonstration of endoglucanase activity by expression in yeast. *Eur J Biochem* **249**, 584-591, doi:10.1111/j.1432-1033.1997.00584.x (1997).

52 Vaaje-Kolstad, G., Houston, D. R., Riemen, A. H., Eijsink, V. G. & van Aalten, D. M. Crystal structure and binding properties of the *Serratia marcescens* chitin-binding protein CBP21. *J Biol Chem* **280**, 11313-11319, doi:10.1074/jbc.M407175200 (2005).

53 Karkehabadi, S. *et al.* The first structure of a glycoside hydrolase family 61 member, Cel61B from *Hypocrea jecorina*, at 1.6 A resolution. *J Mol Biol* **383**, 144-154, doi:10.1016/j.jmb.2008.08.016 (2008).

54 Merino, S. T. & Cherry, J. Progress and challenges in enzyme development for biomass utilization. *Adv Biochem Eng Biotechnol* **108**, 95-120, doi:10.1007/10_2007_066 (2007).

55 Westereng, B. *et al.* The putative endoglucanase PcGH61D from *Phanerochaete chrysosporium* is a metal-dependent oxidative enzyme that cleaves cellulose. *PLoS One* **6**, e27807, doi:10.1371/journal.pone.0027807 (2011).

56 Langston, J. A. *et al.* Oxidoreductive cellulose depolymerization by the enzymes cellobiose dehydrogenase and glycoside hydrolase 61. *Appl Environ Microbiol* **77**, 7007-7015, doi:10.1128/AEM.05815-11 (2011).

57 Levasseur, A., Drula, E., Lombard, V., Coutinho, P. M. & Henrissat, B. Expansion of the enzymatic repertoire of the CAZy database to integrate auxiliary redox enzymes. *Biotechnol Biofuels* **6**, 41, doi:10.1186/1754-6834-6-41 (2013).

58 Vandhana, T. M. *et al.* On the expansion of biological functions of lytic polysaccharide monooxygenases. *New Phytol*, doi:10.1111/nph.17921 (2021).

59 Frommhagen, M. *et al.* Discovery of the combined oxidative cleavage of plant xylan and cellulose by a new fungal polysaccharide monooxygenase. *Biotechnol Biofuels* **8**, 101, doi:10.1186/s13068-015-0284-1 (2015).

60 Hegnar, O. A. *et al.* Quantifying oxidation of cellulose-associated glucuronoxylan by two lytic polysaccharide monooxygenases from *Neurospora crassa*. *Appl Environ Microbiol* **87**, e0165221, doi:10.1128/AEM.01652-21 (2021).

61 Huttner, S. *et al.* Specific xylan activity revealed for AA9 lytic polysaccharide monooxygenases of the thermophilic fungus *Malbranchea cinnamomea* by functional characterization. *Appl Environ Microbiol* **85**, doi:10.1128/AEM.01408-19 (2019).

62 Kojima, Y. *et al.* A lytic polysaccharide monooxygenase with broad xyloglucan specificity from the brown-rot fungus *Gloeophyllum trabeum* and its action on cellulose-xyloglucan complexes. *Appl Environ Microbiol* **82**, 6557-6572, doi:10.1128/AEM.01768-16 (2016).

63 Isaksen, T. *et al.* A C4-oxidizing lytic polysaccharide monooxygenase cleaving both cellulose and cello-oligosaccharides. *J Biol Chem* **289**, 2632-2642, doi:10.1074/jbc.M113.530196 (2014).

64 Frandsen, K. E. H., Poulsen, J. N., Tandrup, T. & Lo Leggio, L. Unliganded and substrate bound structures of the cellooligosaccharide active lytic polysaccharide monooxygenase LsAA9A at low pH. *Carbohydr Res* **448**, 187-190, doi:10.1016/j.carres.2017.03.010 (2017).

65 Hangasky, J. A., Iavarone, A. T. & Marletta, M. A. Reactivity of O_2 versus H_2O_2 with polysaccharide monooxygenases. *Proc Natl Acad Sci U S A* **115**, 4915-4920, doi:10.1073/pnas.1801153115 (2018).

66 Yadav, S. K., Archana, Singh, R., Singh, P. K. & Vasudev, P. G. Insecticidal fern protein Tma12 is possibly a lytic polysaccharide monooxygenase. *Planta* **249**, 1987-1996, doi:10.1007/s00425-019-03135-0 (2019).

67 Chiu, E. *et al.* Structural basis for the enhancement of virulence by viral spindles and their *in vivo* crystallization. *Proc Natl Acad Sci U S A* **112**, 3973-3978, doi:10.1073/pnas.1418798112 (2015).

68 Hemsworth, G. R., Henrissat, B., Davies, G. J. & Walton, P. H. Discovery and characterization of a new family of lytic polysaccharide monooxygenases. *Nat Chem Biol* **10**, 122-126, doi:10.1038/nchembio.1417 (2014).

69 Rieder, L., Petrovic, D., Valjamae, P., Eijsink, V. G. H. & Sorlie, M. Kinetic characterization of a putatively chitin-active LPMO reveals a preference for soluble substrates and absence of monooxygenase activity. *ACS Catal* **11**, 11685-11695, doi:10.1021/acscatal.1c03344 (2021).

70 Wang, D. *et al.* Production of functionalised chitins assisted by fungal lytic polysaccharide monooxygenase. *Green Chemistry* **20**, 2091-2100, doi:10.1039/c8gc00422f (2018).

71 Stopamo, F. G. *et al.* Characterization of a lytic polysaccharide monooxygenase from *Aspergillus fumigatus* shows functional variation among family AA11 fungal LPMOs. *J Biol Chem* **297**, 101421, doi:10.1016/j.jbc.2021.101421 (2021).

72 Vu, V. V., Beeson, W. T., Span, E. A., Farquhar, E. R. & Marletta, M. A. A family of starch-active polysaccharide monooxygenases. *Proc Natl Acad Sci U S A* **111**, 13822-13827, doi:10.1073/pnas.1408090111 (2014).

73 Couturier, M. *et al.* Lytic xylan oxidases from wood-decay fungi unlock biomass degradation. *Nat Chem Biol* **14**, 306-310, doi:10.1038/nchembio.2558 (2018).

74 Sabbadin, F. *et al.* An ancient family of lytic polysaccharide monooxygenases with roles in arthropod development and biomass digestion. *Nat Commun* **9**, 756, doi:10.1038/s41467-018-03142-x (2018).

75 Filiatrault-Chastel, C. *et al.* AA16, a new lytic polysaccharide monooxygenase family identified in fungal secretomes. *Biotechnol Biofuels* **12**, 55, doi:10.1186/s13068-019-1394-y (2019).

76 Sabbadin, F. *et al.* Secreted pectin monooxygenases drive plant infection by pathogenic oomycetes. *Science* **373**, 774-779, doi:10.1126/science.abj1342 (2021).

77 Askarian, F. *et al.* The lytic polysaccharide monooxygenase CbpD promotes *Pseudomonas aeruginosa* virulence in systemic infection. *Nat Commun* **12**, 1230, doi:10.1038/s41467-021-21473-0 (2021).

78 Ipsen, J. O. *et al.* Copper binding and reactivity at the histidine brace motif: insights from mutational analysis of the *Pseudomonas fluorescens* copper chaperone CopC. *FEBS Lett* **595**, 1708-1720, doi:10.1002/1873-3468.14092 (2021).

79 Labourel, A. *et al.* A fungal family of lytic polysaccharide monooxygenase-like copper proteins. *Nat Chem Biol* **16**, 345-350, doi:10.1038/s41589-019-0438-8 (2020).

80 Vaaje-Kolstad, G., Forsberg, Z., Loose, J. S., Bissaro, B. & Eijsink, V. G. Structural diversity of lytic polysaccharide monooxygenases. *Curr Opin Struct Biol* **44**, 67-76, doi:10.1016/j.sbi.2016.12.012 (2017).

81 Petrovic, D. M. *et al.* Methylation of the N-terminal histidine protects a lytic polysaccharide monooxygenase from auto-oxidative inactivation. *Protein Sci* **27**, 1636-1650, doi:10.1002/pro.3451 (2018).

82 Gudmundsson, M. *et al.* Structural and electronic snapshots during the transition from a Cu(II) to Cu(I) metal center of a lytic polysaccharide monooxygenase by X-ray photoreduction. *J Biol Chem* **289**, 18782-18792, doi:10.1074/jbc.M114.563494 (2014).

83 Hemsworth, G. R. *et al.* The copper active site of CBM33 polysaccharide oxygenases. *J Am Chem Soc* **135**, 6069-6077, doi:10.1021/ja402106e (2013).

84 Tandrup, T., Frandsen, K. E. H., Johansen, K. S., Berrin, J. G. & Lo Leggio, L. Recent insights into lytic polysaccharide monooxygenases (LPMOs). *Biochem Soc Trans* **46**, 1431-1447, doi:10.1042/BST20170549 (2018).

85 Frandsen, K. E., Poulsen, J. C., Tovborg, M., Johansen, K. S. & Lo Leggio, L. Learning from oligosaccharide soaks of crystals of an AA13 lytic polysaccharide monooxygenase: crystal packing, ligand binding and active-site disorder. *Acta Crystallogr D Struct Biol* **73**, 64-76, doi:10.1107/S2059798316019641 (2017).

86 Aachmann, F. L., Sorlie, M., Skjak-Braek, G., Eijsink, V. G. & Vaaje-Kolstad, G. NMR structure of a lytic polysaccharide monooxygenase provides insight into copper binding, protein dynamics, and substrate interactions. *Proc Natl Acad Sci U S A* **109**, 18779-18784, doi:10.1073/pnas.1208822109 (2012).

87 Courtade, G. *et al.* Interactions of a fungal lytic polysaccharide monooxygenase with beta-glucan substrates and cellobiose dehydrogenase. *Proc Natl Acad Sci U S A* **113**, 5922-5927, doi:10.1073/pnas.1602566113 (2016).

88 Tandrup, T. *et al.* oligosaccharide binding and thermostability of two related AA9 lytic polysaccharide monooxygenases. *Biochemistry* **59**, 3347-3358, doi:10.1021/acs.biochem.0c00312 (2020).

89 Frandsen, K. E. *et al.* The molecular basis of polysaccharide cleavage by lytic polysaccharide monooxygenases. *Nat Chem Biol* **12**, 298-303, doi:10.1038/nchembio.2029 (2016).

90 Courtade, G., Forsberg, Z., Heggset, E. B., Eijsink, V. G. H. & Aachmann, F. L. The carbohydrate-binding module and linker of a modular lytic polysaccharide monooxygenase promote localized cellulose oxidation. *J Biol Chem* **293**, 13006-13015, doi:10.1074/jbc.RA118.004269 (2018).

91 Guillen, D., Sanchez, S. & Rodriguez-Sanoja, R. Carbohydrate-binding domains: multiplicity of biological roles. *Appl Microbiol Biotechnol* **85**, 1241-1249, doi:10.1007/s00253-009-2331-y (2010).

92 Forsberg, Z. *et al.* Comparative study of two chitin-active and two cellulose-active AA10-type lytic polysaccharide monooxygenases. *Biochemistry* **53**, 1647-1656, doi:10.1021/bi5000433 (2014).

93 Crouch, L. I., Labourel, A., Walton, P. H., Davies, G. J. & Gilbert, H. J. The contribution of non-catalytic carbohydrate binding modules to the activity of lytic polysaccharide monooxygenases. *J Biol Chem* **291**, 7439-7449, doi:10.1074/jbc.M115.702365 (2016).

94 Chylenski, P. *et al.* Lytic polysaccharide monooxygenases in enzymatic processing of lignocellulosic biomass. *ACS Catalysis* **9**, 4970-4991, doi:10.1021/acscatal.9b00246 (2019).

95 Forsberg, Z. *et al.* Structural and functional characterization of a conserved pair of bacterial cellulose-oxidizing lytic polysaccharide monooxygenases. *Proc Natl Acad Sci U S A* **111**, 8446-8451, doi:10.1073/pnas.1402771111 (2014).

96 Vu, V. V., Beeson, W. T., Phillips, C. M., Cate, J. H. & Marletta, M. A. Determinants of regioselective hydroxylation in the fungal polysaccharide monooxygenases. *J Am Chem Soc* **136**, 562-565, doi:10.1021/ja409384b (2014).

97 Sun, P. *et al.* Regioselective C4 and C6 double oxidation of cellulose by lytic polysaccharide monooxygenases. *ChemSusChem* **15**, e202102203, doi:10.1002/cssc.202102203 (2022).

98 Bissaro, B. *et al.* Oxidative cleavage of polysaccharides by monocopper enzymes depends on H_2O_2. *Nat Chem Biol* **13**, 1123-1128, doi:10.1038/nchembio.2470 (2017).
99 Kuusk, S. *et al.* Kinetics of H_2O_2-driven degradation of chitin by a bacterial lytic polysaccharide monooxygenase. *J Biol Chem* **293**, 523-531, doi:10.1074/jbc.M117.817593 (2018).
100 Jones, S. M., Transue, W. J., Meier, K. K., Kelemen, B. & Solomon, E. I. Kinetic analysis of amino acid radicals formed in H_2O_2-driven Cu(I) LPMO reoxidation implicates dominant homolytic reactivity. *Proc Natl Acad Sci U S A* **117**, 11916-11922, doi:10.1073/pnas.1922499117 (2020).
101 Hedison, T. M. *et al.* Insights into the H_2O_2-driven catalytic mechanism of fungal lytic polysaccharide monooxygenases. *FEBS J*, doi:10.1111/febs.15704 (2020).
102 Filandr, F. *et al.* The H_2O_2-dependent activity of a fungal lytic polysaccharide monooxygenase investigated with a turbidimetric assay. *Biotechnol Biofuels* **13**, 37, doi:10.1186/s13068-020-01673-4 (2020).
103 Kont, R., Bissaro, B., Eijsink, V. G. H. & Väljamäe, P. Kinetic insights into the peroxygenase activity of cellulose-active lytic polysaccharide monooxygenases (LPMOs). *Nature Communications* **11**, doi:10.1038/s41467-020-19561-8 (2020).
104 Bertini, L. *et al.* Catalytic mechanism of fungal lytic polysaccharide monooxygenases investigated by first-principles calculations. *Inorg Chem* **57**, 86-97, doi:10.1021/acs.inorgchem.7b02005 (2018).
105 Wang, B. *et al.* QM/MM Studies into the H_2O_2-dependent activity of lytic polysaccharide monooxygenases: evidence for the formation of a caged hydroxyl radical intermediate. *ACS Catalysis* **8**, 1346-1351, doi:10.1021/acscatal.7b03888 (2018).
106 Li, X., Beeson, W. T. t., Phillips, C. M., Marletta, M. A. & Cate, J. H. Structural basis for substrate targeting and catalysis by fungal polysaccharide monooxygenases. *Structure* **20**, 1051-1061, doi:10.1016/j.str.2012.04.002 (2012).
107 Hemsworth, G. R., Davies, G. J. & Walton, P. H. Recent insights into copper-containing lytic polysaccharide mono-oxygenases. *Curr Opin Struct Biol* **23**, 660-668, doi:10.1016/j.sbi.2013.05.006 (2013).
108 Kjaergaard, C. H. *et al.* Spectroscopic and computational insight into the activation of O_2 by the mononuclear Cu center in polysaccharide monooxygenases. *Proc Natl Acad Sci U S A* **111**, 8797-8802, doi:10.1073/pnas.1408115111 (2014).
109 Kim, S., Stahlberg, J., Sandgren, M., Paton, R. S. & Beckham, G. T. Quantum mechanical calculations suggest that lytic polysaccharide monooxygenases use a copper-oxyl, oxygen-rebound mechanism. *Proc Natl Acad Sci U S A* **111**, 149-154, doi:10.1073/pnas.1316609111 (2014).
110 Bissaro, B. *et al.* Molecular mechanism of the chitinolytic peroxygenase reaction. *Proc Natl Acad Sci U S A* **117**, 1504-1513, doi:10.1073/pnas.1904889117 (2020).

111 Muller, G., Chylenski, P., Bissaro, B., Eijsink, V. G. H. & Horn, S. J. The impact of hydrogen peroxide supply on LPMO activity and overall saccharification efficiency of a commercial cellulase cocktail. *Biotechnol Biofuels* **11**, 209, doi:10.1186/s13068-018-1199-4 (2018).

112 Kuusk, S. *et al.* Kinetic insights into the role of the reductant in H_2O_2-driven degradation of chitin by a bacterial lytic polysaccharide monooxygenase. *J Biol Chem* **294**, 1516-1528, doi:10.1074/jbc.RA118.006196 (2019).

113 Bissaro, B., Isaksen, I., Vaaje-Kolstad, G., Eijsink, V. G. H. & Rohr, A. K. How a lytic polysaccharide monooxygenase binds crystalline chitin. *Biochemistry* **57**, 1893-1906, doi:10.1021/acs.biochem.8b00138 (2018).

114 Walton, P. H. & Davies, G. J. On the catalytic mechanisms of lytic polysaccharide monooxygenases. *Curr Opin Chem Biol* **31**, 195-207, doi:10.1016/j.cbpa.2016.04.001 (2016).

115 Beeson, W. T., Vu, V. V., Span, E. A., Phillips, C. M. & Marletta, M. A. Cellulose degradation by polysaccharide monooxygenases. *Annu Rev Biochem* **84**, 923-946, doi:10.1146/annurev-biochem-060614-034439 (2015).

116 Kittl, R., Kracher, D., Burgstaller, D., Haltrich, D. & Ludwig, R. Production of four *Neurospora crassa* lytic polysaccharide monooxygenases in *Pichia pastoris* monitored by a fluorimetric assay. *Biotechnol Biofuels* **5**, 79, doi:10.1186/1754-6834-5-79 (2012).

117 Bissaro, B., Varnai, A., Rohr, A. K. & Eijsink, V. G. H. Oxidoreductases and reactive oxygen species in conversion of lignocellulosic biomass. *Microbiol Mol Biol Rev* **82**, doi:10.1128/MMBR.00029-18 (2018).

118 Kuusk, S. & Valjamae, P. Kinetics of H_2O_2-driven catalysis by a lytic polysaccharide monooxygenase from the fungus *Trichoderma reesei*. *J Biol Chem* **297**, 101256, doi:10.1016/j.jbc.2021.101256 (2021).

119 Loose, J. S. M. *et al.* Multipoint precision binding of substrate protects lytic polysaccharide monooxygenases from self-destructive off-pathway processes. *Biochemistry* **57**, 4114-4124, doi:10.1021/acs.biochem.8b00484 (2018).

120 Chalak, A. *et al.* Influence of the carbohydrate-binding module on the activity of a fungal AA9 lytic polysaccharide monooxygenase on cellulosic substrates. *Biotechnol Biofuels* **12**, 206, doi:10.1186/s13068-019-1548-y (2019).

121 Kracher, D. *et al.* Extracellular electron transfer systems fuel cellulose oxidative degradation. *Science* **352**, 1098-1101, doi:10.1126/science.aaf3165 (2016).

122 Westereng, B. *et al.* Enzymatic cellulose oxidation is linked to lignin by long-range electron transfer. *Sci Rep* **5**, 18561, doi:10.1038/srep18561 (2015).

123 Frommhagen, M. *et al.* Boosting LPMO-driven lignocellulose degradation by polyphenol oxidase-activated lignin building blocks. *Biotechnol Biofuels* **10**, 121, doi:10.1186/s13068-017-0810-4 (2017).

124 Bissaro, B., Kommedal, E., Rohr, A. K. & Eijsink, V. G. H. Controlled depolymerization of cellulose by light-driven lytic polysaccharide oxygenases. *Nat Commun* **11**, 890, doi:10.1038/s41467-020-14744-9 (2020).

125 Cannella, D. *et al.* Light-driven oxidation of polysaccharides by photosynthetic pigments and a metalloenzyme. *Nat Commun* **7**, 11134, doi:10.1038/ncomms11134 (2016).
126 Bissaro, B. *et al.* Fueling biomass-degrading oxidative enzymes by light-driven water oxidation. *Green Chemistry* **18**, 5357-5366, doi:10.1039/c6gc01666a (2016).
127 Loose, J. S. *et al.* Activation of bacterial lytic polysaccharide monooxygenases with cellobiose dehydrogenase. *Protein Sci* **25**, 2175-2186, doi:10.1002/pro.3043 (2016).
128 Garajova, S. *et al.* Single-domain flavoenzymes trigger lytic polysaccharide monooxygenases for oxidative degradation of cellulose. *Sci Rep* **6**, 28276, doi:10.1038/srep28276 (2016).
129 Varnai, A., Umezawa, K., Yoshida, M. & Eijsink, V. G. H. The pyrroloquinoline-quinone-dependent pyranose dehydrogenase from coprinopsis cinerea drives lytic polysaccharide monooxygenase action. *Appl Environ Microbiol* **84**, doi:10.1128/AEM.00156-18 (2018).
130 Frommhagen, M. *et al.* Lytic polysaccharide monooxygenases from *Myceliophthora thermophila* C1 differ in substrate preference and reducing agent specificity. *Biotechnol Biofuels* **9**, 186, doi:10.1186/s13068-016-0594-y (2016).
131 Span, E. A., Suess, D. L. M., Deller, M. C., Britt, R. D. & Marletta, M. A. The role of the secondary coordination sphere in a fungal polysaccharide monooxygenase. *ACS Chem Biol* **12**, 1095-1103, doi:10.1021/acschembio.7b00016 (2017).
132 Wilson, R. J., Beezer, A. E. & Mitchell, J. C. A kinetic study of the oxidation of L-ascorbic acid (vitamin C) in solution using an isothermal microcalorimeter. *Thermochimica Acta* **264**, 27-40, doi:10.1016/0040-6031(95)02373-a (1995).
133 Akagawa, M., Shigemitsu, T. & Suyama, K. Production of hydrogen peroxide by polyphenols and polyphenol-rich beverages under quasi-physiological conditions. *Biosci Biotechnol Biochem* **67**, 2632-2640, doi:10.1271/bbb.67.2632 (2003).
134 Kachur, A. V., Koch, C. J. & Biaglow, J. E. Mechanism of copper-catalyzed oxidation of glutathione. *Free Radic Res* **28**, 259-269, doi:10.3109/10715769809069278 (1998).
135 Kachur, A. V., Koch, C. J. & Biaglow, J. E. Mechanism of copper-catalyzed autoxidation of cysteine. *Free Radic Res* **31**, 23-34, doi:10.1080/10715769900300571 (1999).
136 Zhou, P. *et al.* Generation of hydrogen peroxide and hydroxyl radical resulting from oxygen-dependent oxidation of l-ascorbic acid via copper redox-catalyzed reactions. *RSC Advances* **6**, 38541-38547, doi:10.1039/C6RA02843H (2016).
137 Pant, A. F., Ozkasikci, D., Furtauer, S. & Reinelt, M. The effect of deprotonation on the reaction kinetics of an oxygen scavenger based on gallic acid. *Front Chem* **7**, 680, doi:10.3389/fchem.2019.00680 (2019).

138 Hanaki, A. & Kamide, H. The copper-catalyzed autoxidation of cysteine.the amount of hydrogen peroxide produced under various conditions and the stoichiometry of the reaction. *Bulletin of the Chemical Society of Japan* **56**, 2065-2068, doi:10.1246/bcsj.56.2065 (1983).

139 Kachur, A. V., Held, K. D., Koch, C. J. & Biaglow, J. E. Mechanism of production of hydroxyl radicals in the copper-catalyzed oxidation of dithiothreitol. *Radiation research* **147**, doi:10.2307/3579496 (1997).

140 Li, Y. & Trush, M. A. Reactive oxygen-dependent DNA damage resulting from the oxidation of phenolic compounds by a copper-redox cycle mechanism. *Cancer Res* **54**, 1895s-1898s (1994).

141 Eijsink, V. G. H. *et al.* On the functional characterization of lytic polysaccharide monooxygenases (LPMOs). *Biotechnol Biofuels* **12**, 58, doi:10.1186/s13068-019-1392-0 (2019).

142 Hegnar, O. A. *et al.* pH-dependent relationship between catalytic activity and hydrogen peroxide production shown via characterization of a lytic polysaccharide monooxygenase from *Gloeophyllum trabeum*. *Appl Environ Microbiol* **85**, doi:10.1128/AEM.02612-18 (2019).

143 Wang, N., Miller, C. J., Wang, P. & Waite, T. D. Quantitative determination of trace hydrogen peroxide in the presence of sulfide using the Amplex Red/horseradish peroxidase assay. *Anal Chim Acta* **963**, 61-67, doi:10.1016/j.aca.2017.02.033 (2017).

144 Jiang, S. & Penner, M. H. Overcoming reductant interference in peroxidase-based assays for hydrogen peroxide quantification. *J Agric Food Chem* **65**, 8213-8219, doi:10.1021/acs.jafc.7b02248 (2017).

145 Brander, S. *et al.* Colorimetric LPMO assay with direct implication for cellulolytic activity. *Biotechnol Biofuels* **14**, 51, doi:10.1186/s13068-021-01902-4 (2021).

146 Kimoto, E., Tanaka, H., Ohmoto, T. & Choami, M. Analysis of the transformation products of dehydro-L-ascorbic acid by ion-pairing high-performance liquid chromatography. *Anal Biochem* **214**, 38-44, doi:10.1006/abio.1993.1453 (1993).

147 Deutsch, J. C. & Santhosh-Kumar, C. R. Dehydroascorbic acid undergoes hydrolysis on solubilization which can be reversed with mercaptoethanol. *Journal of Chromatography A* **724**, 271-278, doi:10.1016/0021-9673(95)00968-x (1996).

148 Karkonen, A., Dewhirst, R. A., Mackay, C. L. & Fry, S. C. Metabolites of 2,3-diketogulonate delay peroxidase action and induce non-enzymic H_2O_2 generation: Potential roles in the plant cell wall. *Arch Biochem Biophys* **620**, 12-22, doi:10.1016/j.abb.2017.03.006 (2017).

149 Dewhirst, R. A., Murray, L., Mackay, C. L., Sadler, I. H. & Fry, S. C. Characterisation of the non-oxidative degradation pathway of dehydroascorbic acid in slightly acidic aqueous solution. *Arch Biochem Biophys* **681**, 108240, doi:10.1016/j.abb.2019.108240 (2020).

150 Breslmayr, E. *et al.* A fast and sensitive activity assay for lytic polysaccharide monooxygenase. *Biotechnol Biofuels* **11**, 79, doi:10.1186/s13068-018-1063-6 (2018).

151 Rigo, A. *et al.* Interaction of copper with cysteine: stability of cuprous complexes and catalytic role of cupric ions in anaerobic thiol oxidation. *J Inorg Biochem* **98**, 1495-1501, doi:10.1016/j.jinorgbio.2004.06.008 (2004).

152 Borisova, A. S. *et al.* Structural and functional characterization of a lytic polysaccharide monooxygenase with broad substrate specificity. *J Biol Chem* **290**, 22955-22969, doi:10.1074/jbc.M115.660183 (2015).

153 Isaacs, N. S. & van Eldik, R. A mechanistic study of the reduction of quinones by ascorbic acid. *Journal of the Chemical Society, Perkin Transactions 2*, 1465-1468, doi:10.1039/a701072i (1997).

154 Abdel-Hamid, R. & Newair, E. F. Electrochemical behavior of antioxidants: I. Mechanistic study on electrochemical oxidation of gallic acid in aqueous solutions at glassy-carbon electrode. *Journal of Electroanalytical Chemistry* **657**, 107-112, doi:10.1016/j.jelechem.2011.03.030 (2011).

6 Publications

Unraveling the roles of the reductant and free copper ions in LPMO kinetics

Stepnov AA, Forsberg Z, Sørlie M, Nguyen GS, Wentzel A, Røhr ÅK, Eijsink VG

Paper I

Stepnov et al. Biotechnol Biofuels (2021) 14:28
https://doi.org/10.1186/s13068-021-01879-0

Biotechnology for Biofuels

RESEARCH Open Access

Unraveling the roles of the reductant and free copper ions in LPMO kinetics

Anton A. Stepnov[1], Zarah Forsberg[1], Morten Sørlie[1], Giang-Son Nguyen[2], Alexander Wentzel[2], Åsmund K. Røhr[1] and Vincent G. H. Eijsink[1*]

Abstract

Background: Lytic polysaccharide monooxygenases (LPMOs) are monocopper enzymes that catalyze oxidative depolymerization of industrially relevant crystalline polysaccharides, such as cellulose, in a reaction that depends on an electron donor and O_2 or H_2O_2. While it is well known that LPMOs can utilize a wide variety of electron donors, the variation in reported efficiencies of various LPMO-reductant combinations remains largely unexplained.

Results: In this study, we describe a novel two-domain cellulose-active family AA10 LPMO from a marine actinomycete, which we have used to look more closely at the effects of the reductant and copper ions on the LPMO reaction. Our results show that ascorbate-driven LPMO reactions are extremely sensitive to very low amounts (micromolar concentrations) of free copper because reduction of free Cu(II) ions by ascorbic acid leads to formation of H_2O_2, which speeds up the LPMO reaction. In contrast, the use of gallic acid yields steady reactions that are almost insensitive to the presence of free copper ions. Various experiments, including dose–response studies with the enzyme, showed that under typically used reaction conditions, the rate of the reaction is limited by LPMO-independent formation of H_2O_2 resulting from oxidation of the reductant.

Conclusion: The strong impact of low amounts of free copper on LPMO reactions with ascorbic acid and O_2, i.e. the most commonly used conditions when assessing LPMO activity, likely explains reported variations in LPMO rates. The observed differences between ascorbic acid and gallic acid show a way of making LPMO reactions less copper-dependent and illustrate that reductant effects on LPMO action need to be interpreted with great caution. In clean reactions, with minimized generation of H_2O_2, the (O_2-driven) LPMO reaction is exceedingly slow, compared to the much faster peroxygenase reaction that occurs when adding H_2O_2.

Keywords: Lytic polysaccharide monooxygenase, AA10, Enzyme kinetics, Hydrogen peroxide, Copper, Ascorbic acid, Gallic acid

Background

Lytic polysaccharide monooxygenases (LPMOs) are monocopper enzymes that catalyze oxidative cleavage of polysaccharide substrates, such as chitin and cellulose [1–4]. The LPMO active site is formed by two conserved histidine residues coordinating a copper ion in a rare structural motif that is called the "histidine brace" [3, 5]. The histidine brace is part of a solvent-exposed substrate binding surface, which, for LPMOs acting on chitin and cellulose, is characteristically flat [5, 6]. This spatial configuration reflects the unparalleled ability of LPMOs to act on highly crystalline substrate surfaces, rather than on isolated polysaccharide chains within amorphous regions. By doing so, LPMOs provide a substantial boost to conventional hydrolytic enzymes both in nature and in commercial enzyme cocktails [7, 8]. Due to their intriguing capabilities and industrial applications, there

*Correspondence: vincent.eijsink@nmbu.no
[1] Faculty of Chemistry, Biotechnology and Food Science, NMBU-Norwegian University of Life Sciences, Ås, Norway
Full list of author information is available at the end of the article

is considerable interest in discovering new LPMOs and in understanding how to optimally harness the catalytic potential of these enzymes.

LPMOs rely on reducing power to enable the formation of reactive oxygen species that hydroxylate glycosidic bonds at the C1- or C4-position [1, 4, 9]. Interestingly, LPMOs can utilize a vast variety of electron donors, including small phenolic compounds and partner enzymes such as cellobiose dehydrogenase [10, 11]. Ascorbic acid is typically used as a reductant in most experimental setups. LPMO reactions were previously thought to involve molecular oxygen, hence the name monooxygenase, but recently, it has been shown that hydrogen peroxide is the preferred co-substrate [12]. H_2O_2-driven reactions are orders of magnitude faster than the reactions with oxygen, where the latter tend to be slow, with rates normally being around 1 min^{-1} or lower. Importantly, the supply of H_2O_2 needs to be controlled to avoid enzyme damage due to self-oxidation [12].

In the presence of oxygen, reduced LPMOs are capable of H_2O_2 production. This phenomenon was initially described as a futile reaction that occurs in the absence of a substrate [13]. Given the current insights into the role of H_2O_2 as the (preferred) co-substrate, it has been suggested that under commonly used standard aerobic conditions, i.e., in the presence of a reductant and with no exogenously added hydrogen peroxide, the rate and yield of the LPMO reaction are determined by the in situ generation of H_2O_2 that is produced by the enzyme or in reactions involving the reductant and molecular oxygen [12]. It is worth noting that there is an ongoing debate on whether truly O_2-driven LPMO reactions (i.e., reactions that are not coupled to in situ H_2O_2 production) can occur at all [14–17].

Importantly, enzyme-independent H_2O_2 production can take place in typical LPMO reaction setups, especially if the reaction, next to a reductant such as ascorbic acid, also contains free transition metal ions, such as Cu(II) [18, 19]. Such enzyme-independent generation of hydrogen peroxide could lead to a substantial boost of LPMO activity on polysaccharide substrates [20]. Due to the use of different enzyme preparation methods and/or reaction conditions, the free copper content of LPMO reactions may vary, which, considering the above, will have repercussions for the reliability and comparability of observed LPMO activities. For example, a significant amount of metal ions may enter the reaction if a contaminated substrate is used, or in case the target enzyme is not sufficiently purified after copper saturation [21].

In this paper, we describe a cellulose-active family 10 (AA10) LPMO, AA10_07, that was discovered by mining the genome of a marine Actinomycete, isolated from the Trondheim fjord, Norway and referred to as "strain P01-F09" below. Next to characterizing the activity of this LPMO, we have used this enzyme as a model to study how reductants and free copper affect LPMO activity on cellulose and to study if and how the observed catalytic activity can be linked to production of H_2O_2 in the reaction mixture. Our results demonstrate that ascorbate-driven LPMO reactions are extremely sensitive to free copper in micromolar concentrations, whereas use of gallic acid as reductant allows for steady and controllable reactions that are almost insensitive to the presence of free copper ions.

Results and discussion

Identification, sequence and domain structure of AA10_07

Actinomycete strain P01-F09 was isolated from a finger sponge harvested at 60 m depth near Tautra, an island located within the Trondheim fjord, Norway. In silico mining of the P01-F09 draft genome sequence using LPMO HMM profiles led to the identification of a 1083 bp gene encoding a hypothetical family 10 (AA10) LPMO. The candidate enzyme was named AA10_07 and its sequence was annotated using the Pfam domain prediction server [22]. AA10_07 is a 360-residue protein, comprising a 33-residue signal peptide, a catalytic AA10 domain and a C-terminal cellulose-binding module (CBM2) (Fig. 1). The two AA10_07 domains are connected through a linker rich in proline and threonine. BLAST analysis [23] identified *Sc*LPMO10C (CelS2) [2,

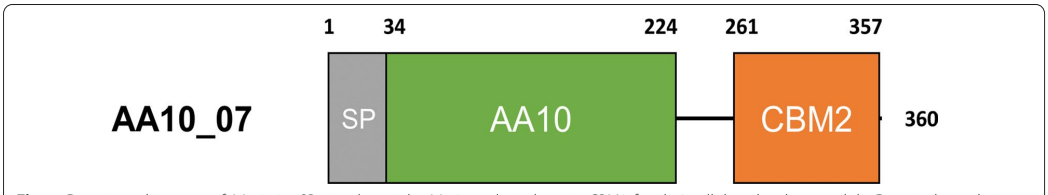

Fig. 1 Domain architecture of AA10_07. *SP*, signal peptide; *AA10*, catalytic domain; *CBM2*, family 2 cellulose-binding module. Domain boundaries were annotated using Pfam [22]. Note that the native signal peptide (shown in the figure) was substituted by the pelB signal peptide in the enzyme produced in this study, and that the signal peptide is cleaved off during secretion resulting in the mature enzyme that starts at position 34 (His34)

24] as the closest characterised AA10_07 homolog (85.6% sequence identity between catalytic domains).

Enzyme production and characterization of LPMO activity

The AA10_07 gene sequence was codon optimized for expression in *E. coli* and modified to encode the pelB periplasmic localization signal [25, 26] instead of the native signal peptide. The gene was cloned into the pET-26(b)+vector and the enzyme was produced in *E. coli* BL21(DE3) in a soluble form. Starting with a periplasmic extract, AA10_07 was purified to electrophoretic homogeneity by ion-exchange and size-exclusion chromatography. The final yield amounted to approximately 7 mg of purified LPMO per 500 ml of *E. coli* culture.

To assess AA10_07 activity, 1 µM copper-saturated enzyme was incubated with 1% (w/v) Avicel in 50 mM sodium phosphate buffer, pH 6.0, supplied with 1 mM ascorbic acid (30 °C, 24 h). The MS spectrum of the reaction mixture (Fig. 2a) shows a product profile that is typical for LPMOs that exclusively oxidize cellulose at C1. Such oxidation leads to the formation of aldonic acids that give characteristic MS signals due to the formation of sodium and potassium salts. We did not detect any signals that could indicated the formation of double oxidized products, which would appear, albeit at low intensities, if C4 oxidation would also have occurred [24]. This oxidative regioselectivity of the LPMO reaction was confirmed by chromatographic analysis of products

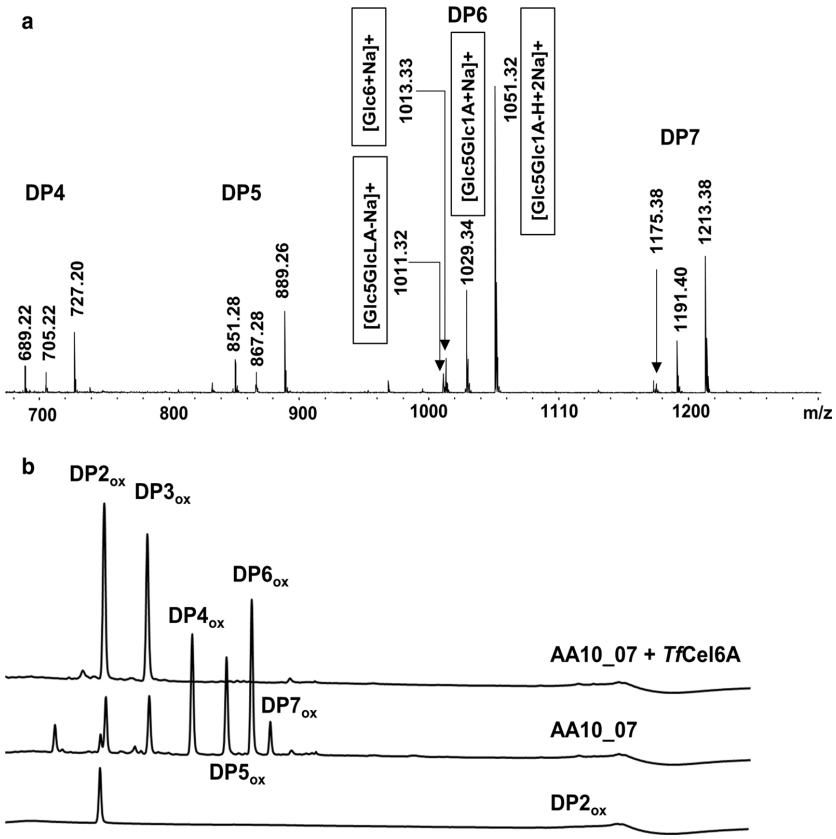

Fig. 2 Catalytic activity of AA10_07. **a** MALDI-TOF MS analysis of products released by 1 µM AA10_07 from 1% (w/v) Avicel in the presence of 1 mM ascorbic acid. The figure shows signals representing LPMO products within the DP4–DP7 range (*DP*, degree of polymerization). Oxidized and native products are observed as sodium adducts and/or as sodium adducts of sodium salts, as indicated (*Glc*, glucose; *Glc1A*, gluconic acid; *GlcLA*, lactone). Annotated product peaks were not detected in negative control reactions lacking the enzyme or lacking the reductant. **b** A chromatographic analysis of oxidized products generated by 1 µM AA10_07 from 1% (w/v) Avicel. The picture includes a chromatogram of a product mixture that had been treated with TfCel6A and a chromatogram showing the GlcGlc1A (DP2ox) standard

generated from Avicel, which only showed C1-oxidized products (Fig. 2b). Figure 2b also shows how the product profile changes after treating the products with *Tf*Cel6A endoglucanase; this approach was used for quantification of oxidized sites in the experiments described below.

The impact of the copper saturation protocol on the level of residual free copper in LPMO samples

Free copper ions will affect LPMO reactions since they promote enzyme-independent H_2O_2 production in the presence of ascorbic acid, even when present at sub-micromolar concentrations ([19–21]; see also Fig. 3). It is reasonable to assume that LPMO preparations vary in terms of the amounts of free copper, due to variations in protein preparation protocols, and this may affect the apparent activity of the LPMOs in certain reaction set-ups. Copper saturation of the purified LPMO likely is the most critical step, since during that stage a free copper is deliberately introduced into the system.

Here, and in several other studies, copper saturation was achieved by incubating the LPMO with a slight molar surplus of free copper, followed by desalting. We compared AA10_7 samples obtained by two alternative desalting techniques. In one case, unbound copper was removed by fast desalting using a small gravity-flow gel filtration column. In the other case, a high-resolution preparative SEC column was used instead. The resulting two different batches of copper saturated and desalted AA10_07 showed identical apparent rates of H_2O_2 production (Fig. 3) and identical abilities to degrade Avicel (Additional file 1: Fig S1), in reactions with ascorbic acid as the reductant. These observations indicate that both procedures worked equally well in terms of removing free copper.

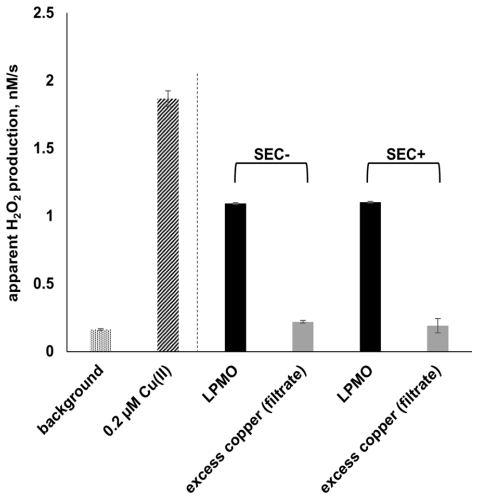

Fig. 3 Apparent hydrogen peroxide production by two batches of AA10_07. The figure shows apparent H_2O_2 production by 3 µM AA10_07 in 50 mM sodium phosphate buffer, pH 6.0 supplied with 50 µM ascorbic acid, 5 U/ml HRP, 100 µM Amplex Red and 1% (v/v) DMSO. SEC−/SEC+ labels indicate the procedure used to remove unbound copper from the LPMO sample after copper saturation. SEC−, gravity-flow desalting column; SEC+, high-resolution SEC chromatography. Excess copper control reactions (grey bars) were set up using protein-free samples, obtained by ultrafiltration. These samples contained the same amount of free copper as the LPMO preparation used in the experiment. The two reactions shown to the left are control reactions: "background", reaction without enzyme; "0.2 µM Cu(II)", reaction without enzyme and with addition of 0.2 µM Cu(II). Error bars indicate standard deviations between triplicates

The copper content of the resulting enzyme preparations was assessed in two manners. Protein-free fractions ("filtrates") produced from these LPMO samples by ultrafiltration did not promote H_2O_2 production in a reaction with ascorbic acid, whereas added copper in concentrations as low as 0.2 µM did (Fig. 3), indicating that the levels of residual copper were low in both enzyme samples. To confirm this conclusion, both LPMO samples were subjected to ICP-MS analysis. The results indicated the presence of 0.98 ± 0.18 µM and 0.90 ± 0.14 µM total copper in 1 µM solutions of gravity flow-desalted and SEC-treated LPMO, respectively. These ICP-MS results are compatible with the notion that the LPMOs were copper saturated, whereas the amounts of free copper were negligible. Finally, the copper content of Avicel was determined by ICP-MS showing that only negligible amounts of this metal were present (< 49 ng copper per 1 g of substrate, corresponding to less than 10 nM in reactions with 1% (w/v) Avicel).

Comparison of ascorbic acid and gallic acid in LPMO reactions with Avicel

Next, we assessed the capacity of gallic acid to drive the oxidation of cellulose by AA10_07. The LPMO reaction supplied with 1 mM gallic acid was more efficient than the reaction supplied with 1 mM ascorbic acid (Fig. 4a). Both reactions were remarkably slow (approximately 0.06 min^{-1} in the presence of ascorbic acid and 0.2 min^{-1} in the presence of gallic acid) with almost linear progress within the 24 h of the experiment.

To verify that the LPMO was catalytically competent and that H_2O_2 speeds up the reaction, a control experiment with externally added H_2O_2 was conducted, which showed an increase in the initial substrate oxidation rate by two orders of magnitude and, as expected under these conditions, rapid inactivation, regardless of whether the reductant was ascorbic acid or gallic acid (Fig. 4b; note that the *X*-axis has a minutes time scale).

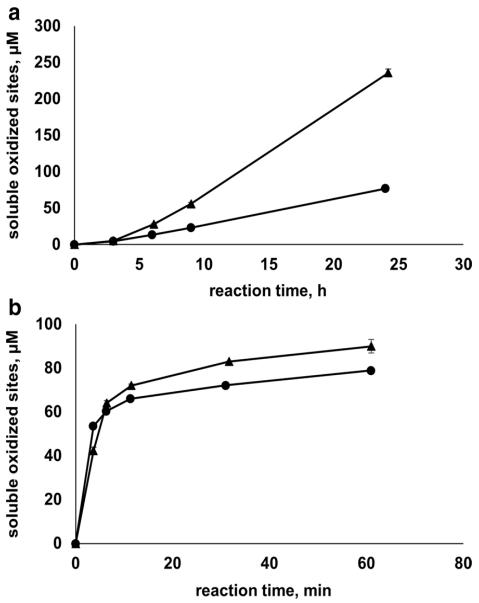

Fig. 4 Cellulose solubilisation by AA10_07 in the presence of ascorbic acid or gallic acid. The figure shows the release of oxidised products in LPMO reactions (1 µM AA10_07 in 50 mM sodium phosphate buffer, pH 6.0, 30 °C) with 1% (w/v) Avicel that were carried out in the absence of hydrogen peroxide (**a**) or in the presence of 200 µM H_2O_2 (**b**) using 1 mM ascorbic acid (circular markers) or 1 mM gallic acid (triangle markers) as a reductant. Error bars indicate standard deviations between triplicates. Note that **a**, **b** feature different time scales. Product accumulation was not observed in control reactions with substrate and reductant or in reactions with substrate, reductant and H_2O_2

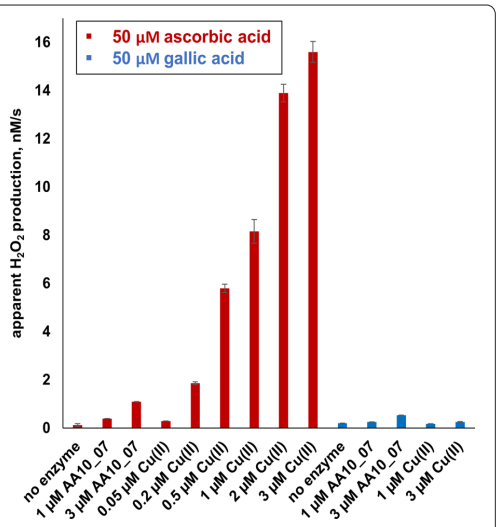

Fig. 5 Apparent H_2O_2 production in reactions with free copper and 50 µM ascorbic acid or gallic acid. All experiments were carried out in 50 mM sodium phosphate buffer, pH 6.0, at 30 °C. The rates of H_2O_2 production by AA10_07 in the presence of 50 µM ascorbic acid or 50 µM gallic acid are given for reference. The experiment with 0.2 µM Cu(II) is also shown in Fig. 3. Reaction mixtures contained 5 U/ml HRP, 100 µM Amplex Red and approximately 1% (v/v) DMSO. Error bars indicate standard deviations between triplicates

Apparent H_2O_2 production in reactions with LPMO, free copper and 50 µM reductant

To further investigate the effects of free copper, we assessed H_2O_2 production in a series of reactions with various amounts of Cu(II)SO_4 in the presence of two commonly used LPMO reductants, ascorbic acid and gallic acid. Of note, to reduce complications due to reactions between HRP and the reductant (see below), the reductant concentrations typically used in the HRP/Amplex Red H_2O_2 assay are much lower (e.g. 50 µM; [13, 27]) than those typically used in LPMO reactions with substrate (e.g. 1 mM). The results of the standard H_2O_2 assay (Fig. 5) show that sub-micromolar concentrations of free copper increased the apparent rate of H_2O_2 production in reactions with 50 µM ascorbic acid. Even the reaction with only 0.2 µM free copper gave a higher apparent H_2O_2 production rate than a reaction lacking free copper but containing 3 µM copper-loaded AA10_7. It is noteworthy that these results may be taken to suggest that the LPMO protects reduced copper from reacting with molecular oxygen. Similar experiments with 50 µM gallic acid showed different results. The apparent initial rate of H_2O_2 formation by 3 µM AA10_07 in the presence of 50 µM gallic acid amounted to 0.53 nM/s, which is two times lower compared to the reaction with ascorbic acid (Fig. 5). Strikingly, hydrogen peroxide accumulation in the presence of free copper and gallic acid was very low compared to similar reactions with ascorbate (Fig. 5). For example, in large contrast to the results obtained with ascorbic acid, the apparent H_2O_2 production rate in the reaction with 3 µM free copper and gallic acid was not higher than the one observed with LPMO and gallic acid under the same conditions. The observed low reactivity of free copper in the presence of gallic acid is in agreement with electron paramagnetic resonance data [28] showing that gallic acid is likely to form complexes with Cu(II) rather than reducing it.

Apparent H_2O_2 production in the presence of 1 mM reductant

The experiments with AA10_07 and gallic acid revealed lower apparent H_2O_2 production rates compared to the similar setups with ascorbate. However, the LPMO catalytic rate on Avicel was significantly higher in the

presence of gallic acid, which is surprising if one accepts the premise that generation of H_2O_2 limits the reaction.

In search of an explanation for this paradoxical finding, it is important to consider the limitations of the HRP/Amplex Red assay [29]. The assay is based on single electron oxidation of Amplex Red by HRP in the presence of H_2O_2 as a co-substrate [30]. This oxidation leads to the formation of two Amplex Red radicals, which then react to form one molecule of highly chromogenic resorufin and one molecule of Amplex Red. It was previously shown that addition of ascorbic acid leads to repression of the resorufin signal [15], likely due to reduction of Amplex Red radicals back to Amplex Red [30] and/or the ability of HRP to engage in a side-reaction with ascorbate that removes H_2O_2 from the system in a way that is uncoupled to resorufin formation [31]. There is evidence that other redox-active compounds may also influence the HRP/Amplex Red assay in a similar fashion [32, 33]. It is thus conceivable that the different apparent H_2O_2 production rates for ascorbic acid and gallic acid relate to varying degrees of signal repression. To test this hypothesis, we carried out the HRP/Amplex Red assay using different concentrations of H_2O_2 in the presence or absence of 50 µM ascorbic acid or gallic acid. This experiment indicated that gallic acid supresses the resorufin signal to approximately same extent as ascorbic acid (Additional file 1: Fig. S2).

We then asked the question whether the discrepancy between apparent H_2O_2 production rates and the observed LPMO activities in reactions with Avicel could be due to the largely different reductant concentrations in these two experiments. While low reductant concentrations are commonly used in the H_2O_2 production assay, for reasons discussed above, experiments with 1 mM reductant are rare [34]. Thus, we carried out the HRP/Amplex Red assay using various concentrations of hydrogen peroxide in the presence of 1 mM ascorbic acid or gallic acid, which showed that the resorufin signal repression increased only marginally compared to the previous measurement with 50 µM reductant (Additional file 1: Fig S2). Thus, measurements of H_2O_2 production in reactions with 1 mM reductant seemed feasible.

Therefore, the HRP/Amplex Red assay was performed again in the presence of 1 mM ascorbic acid or 1 mM gallic acid, together with various amounts of LPMO and free copper (Fig. 6a, b). Apparent hydrogen peroxide accumulation rates were corrected for resorufin signal repression using H_2O_2 standard curves obtained in the presence of reductants. In this setup, the H_2O_2 production rate by 1 µM AA10_07 was approximately 2.3 times higher with gallic acid compared to ascorbic acid. Assuming that generation of H_2O_2 limits the reaction, the higher H_2O_2 production level observed

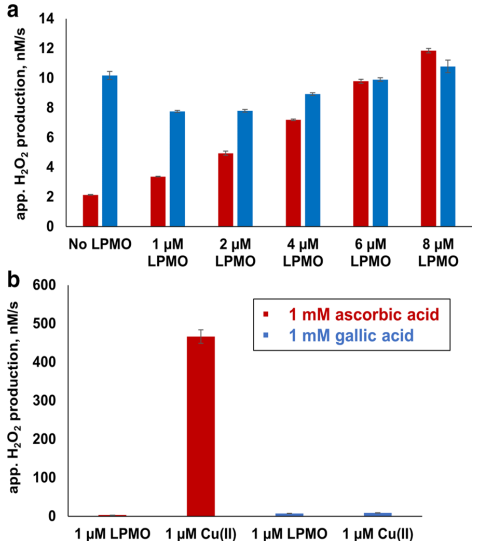

Fig. 6 Apparent H_2O_2 production in experiments with LPMO, free copper and 1 mM ascorbic acid or gallic acid. The figure shows hydrogen peroxide accumulation rates obtained in reactions with increasing amounts of LPMO (**a**) or with 1 µM free copper compared to 1 µM LPMO (**b**). All experiments were carried out in 50 mM sodium phosphate buffer, pH 6.0, at 30 °C. Reaction mixtures contained 5 U/ml HRP, 100 µM Amplex Red and 2% (v/v) DMSO. Error bars indicate standard deviations between triplicates. Note that plotted values were corrected for resorufin signal repression using H_2O_2 standard curves, obtained in the presence of 1 mM ascorbic acid or gallic acid. The "No LPMO" label indicates that the reaction contained only reductant, with no enzyme added (set up to monitor reactions between reductant and oxygen)

in the reaction with 1 mM gallic acid is in agreement with Avicel degradation data (Fig. 4a) showing that 1 µM AA10_07 was most efficient when using gallic acid as reductant. Quantitative comparison of the Avicel degradation data (Fig. 4a) and the H_2O_2 production data (Fig. 6a) indicates that the production rate of soluble oxidized products is roughly half of the H_2O_2 production rate, which makes sense considering that a considerable fraction of the oxidized sites will remain attached to the insoluble substrate.

Strikingly, when using 1 mM ascorbic acid concentration, H_2O_2 production by 1 µM free copper was two orders of magnitude higher compared to 1 µM LPMO, whereas H_2O_2 production in the reaction with free copper and gallic acid was minimal, also at this higher reductant concentration (Fig. 6b). Clearly, in standard LPMO reactions with 1 mM ascorbic acid, the effect of free copper may be considerable, whereas such a copper effect could be less or even absent in reactions with 1 mM gallic acid. This is addressed further below.

One key question is to what extent the enzyme plays a role in the generation of hydrogen peroxide in the LPMO reaction. Figure 6a shows that the H_2O_2 accumulation rates depended on the enzyme concentration, and that this dependency was stronger for ascorbic acid than for gallic acid. An eightfold increase in LPMO concentration (from 1 to 8 μM) resulted in 3.5 times higher H_2O_2 accumulation rates for ascorbic acid, whereas the increase was only a modest and 1.4-fold for gallic acid. In the case of ascorbic acid, the reaction with the lowest LPMO concentration (1 μM) generated more H_2O_2 than a reaction without enzyme. In contrast, for gallic acid, the experiment without enzyme gave higher hydrogen peroxide levels than the experiments with 1–6 μM enzyme, which may indicate that, in the absence of cellulose substrate, AA10_07 engages in side-reactions that consume H_2O_2 and involve gallic acid (or products of gallic acid oxidation). Such reactions are not entirely hypothetical, since it is well known that LPMOs can carry out peroxygenation reactions of small molecules. Breslmayr et al. have shown that after being reduced by 2,6-dimethoxyphenol, LPMOs can oxidize the hydrocoerulignone that is formed by dimerization of two 2,6-dimethoxyphenol radicals in an (H_2O_2-consuming) peroxygenation reaction [35]. Similar reactions could occur with dimers of gallic acid that are likely to emerge upon its oxidation [36].

Overall, our results suggest that the amount of hydrogen peroxide produced by 1 μM LPMO supplied with 1 mM gallic acid is low (Fig. 6a), compared to the amount of H_2O_2 generated by the enzyme-independent reaction between reductant and oxygen. In other words, the autooxidation of 1 mM gallic acid is likely to fuel LPMO reactions on Avicel in our setups. In the case of ascorbic acid, both the LPMO and the reductant contribute to generation of H_2O_2, at least in the absence of an LPMO substrate (see below).

Effect of the LPMO concentration on degradation of Avicel

To obtain further insight into factors that limit the LPMO reaction under typical LPMO assay conditions, without depending on the HRP/Amplex Red assay, we carried out a series of LPMO reactions with Avicel (Fig. 7, Additional file 1: Fig. S3) in the presence of 1 mM ascorbic acid or 1 mM gallic acid using a wide range of AA10_07 concentrations (0.01–8 μM). In light of the H_2O_2 accumulation data shown in Fig. 6a, and assuming that enzyme-independent generation of H_2O_2 limits the reaction, one could expect limited effects of the LPMO concentration on the cellulose degradation rate, in particular for reactions with gallic acid.

Such behaviour was indeed observed in the experiment with 1 mM gallic acid, (Fig. 7, Additional file 1: Fig. S3). Within the enzyme concentration range of 0.1 μM to 4 μM, the enzyme dose had almost no effect on the rate of cellulose degradation. Note that progress curves (Additional file 1: Fig. S3) obtained for the reactions with 0.1–4 μM LPMO were linear, showing that the amount of substrate was not limiting these reactions.

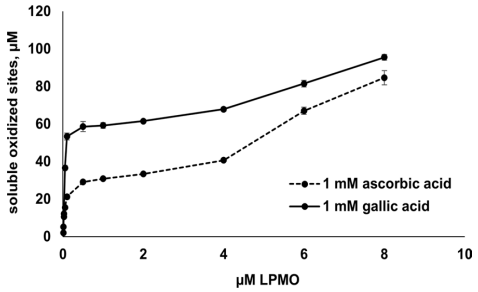

Fig. 7 Avicel solubilisation by increasing amounts of AA10_07 in the presence of ascorbic acid or gallic acid. The figure shows the release of oxidised products from 1% (w/v) Avicel in 9 h reactions with 0.01–8 μM AA10_07 in 50 mM sodium phosphate buffer, pH 6.0, 30 °C. The experiments were carried out using 1 mM ascorbic acid (dashed line) or 1 mM gallic acid (solid line) as a reductant. Error bars indicate standard deviations between triplicates. Note that the plotted data are derived from LPMO progress curves shown in Additional file 1: Fig. S3. All these reactions displayed linear behavior, except for experiments with 0.01 μM or 0.025 μM enzyme and gallic acid

Further increase of the LPMO dose resulted in a gradual increase in the rate of substrate oxidation, indicating that the enzyme's contribution to H_2O_2 production becomes significant at higher enzyme concentrations. At very low enzyme concentrations (<0.1 μM), there was a strong dose-dependency, most likely due to the fact that there was not enough enzyme to consume H_2O_2 effectively (i.e., the reaction was limited by the enzyme and not by hydrogen peroxide). The experiment with 1 mM ascorbic acid revealed the same low dependency of the cellulose oxidation rate on the LPMO concentration in the 0.1–4 μM range (Fig. 7, Additional file 1: Fig. S3). This observation was unexpected if one considers the H_2O_2 accumulation data (Fig. 6a), which suggest that, in reactions with ascorbic acid, the LPMO contribution to overall hydrogen peroxide generation is considerable. One obvious, but nevertheless speculative, explanation would be that binding of the LPMO to the substrate reduce the enzyme's ability to generate H_2O_2 [13, 15, 37]. Interestingly, at the higher LPMO concentrations, there was a dose–response effect that was more pronounced compared to the similar reactions with gallic acid, which is in agreement with the H_2O_2 accumulation data of Fig. 6a. Overall, our results indicate that under most commonly used reaction conditions, oxidation of the reductant by

O_2 is a major source of H_2O_2 that fuels cellulose degradation by AA10_07.

The effect of free copper on LPMO reactions with Avicel

Digging further into interactions between enzyme, free copper and electron donors, we carried out degradation reactions with Avicel using 1 mM ascorbic acid or 1 mM gallic acid as the reductant. Various amounts of free copper were added to the reactions to mimic copper contamination and to vary the rate of enzyme-independent production of H_2O_2. The addition of Cu(II) to reactions with ascorbic acid resulted in a copper dose-dependent increase in LPMO activity (Fig. 8a), which is to be expected considering the high rates of H_2O_2 production in reactions with free copper and 1 mM ascorbic acid (Fig. 6b). Comparison of Figs. 4a and 8a shows that a 1 h reaction in the presence of 1 μM $Cu(II)SO_4$ and ascorbic acid (Fig. 8a) yielded more oxidized products than a 24 h copper-free reaction with the same reductant (Fig. 4a). At 3 μM copper, the reaction is even faster, leading to high product concentrations at the first measuring point, but under these conditions, the enzyme becomes rapidly inactivated, as one would expect if (too) much H_2O_2 is produced [12, 20].

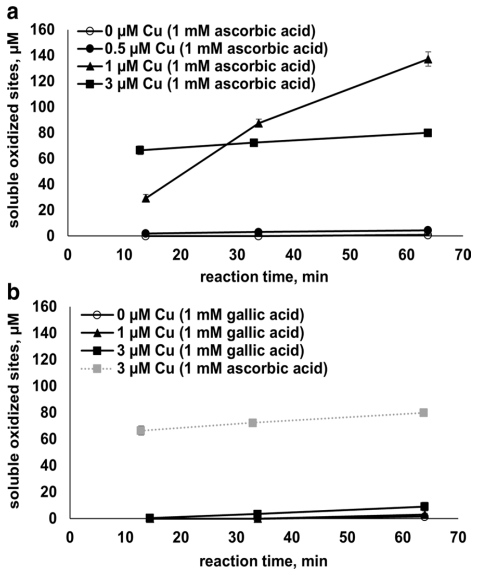

Fig. 8 The effect of free copper on AA10_07 reactions with cellulose in the presence of ascorbic acid or gallic acid. The figure shows progress curves obtained for AA10_07 reactions (1 μM LPMO in 50 mM sodium phosphate buffer, pH 6.0, 30 °C) with 1% (w/v) Avicel using 1 mM ascorbic acid (**a**) or 1 mM gallic acid (**b**) and various concentrations of free copper. Note that **b** also features the progress curve obtained with 3 μM free copper and 1 mM ascorbic acid, which is shown in **a**, for reference. Error bars indicate standard deviations between triplicates. Note the different time scale compared to Fig. 4a. Product accumulation was not observed in control reactions with no enzyme, containing substrate, free copper, and reductant

On the other hand, the LPMO reaction driven by gallic acid (Fig. 8b) turned out to be essentially insensitive to free copper (up to 3 μM $Cu(II)SO_4$), which is in agreement with the H_2O_2 production data (Figs. 5, 6) and with the notion that this reductant forms complexes with Cu(II), thus preventing Cu(II) from participating in redox reaction in solution [28].

Estimating catalytic rates from the progress curves of Figs. 4a, 8a shows that introduction of 1 μM Cu(II) to the LPMO reaction fuelled by ascorbate speeded up the reaction by some 50-fold, which is in the same order of magnitude as the effect of 1 μM Cu(II) on ascorbic acid-driven production of H_2O_2 (Fig. 6b). Nevertheless, the LPMO reaction fuelled by ascorbate and in the presence of 1 μM Cu(II) was still much slower and showed less rapid enzyme inactivation (Fig. 8a) compared to the reaction with initial addition of 200 μM hydrogen peroxide (Fig. 4b). This observation is not surprising, considering the hydrogen peroxide production data of Fig. 6b that show an approximate H_2O_2 production rate of 0.5 μM/s for the reaction with 1 μM Cu(II) and 1 mM ascorbic acid. Clearly, despite the effect of free copper, the H_2O_2 concentration in the reaction with exogenously added H_2O_2 was much higher.

The lack of an effect of low copper concentrations (< 1 μM) on the ascorbic acid-driven reaction was somewhat unexpected considering the H_2O_2 production curves shown in Fig. 5. It is conceivable that the Avicel used in the experiment possesses a weak copper-binding capacity that removes a fraction of free copper from the reaction. It is also possible that the LPMO has secondary (low affinity) copper-binding sites [38]. Finally, it is possible that under the conditions of the Avicel assay, copper and/or H_2O_2 engage in side-reactions that may reduce H_2O_2 production or increase futile H_2O_2 consumption, hiding the copper effect on LPMO activity at the lowest copper concentrations.

The sensitivity of the LPMO reaction to free copper in the presence of ascorbic acid must be taken into account when interpreting previously obtained dose–response curves for AA10_07 (Fig. 7). It is conceivable that the dependency of the product formation rate on the amount of LPMO observed at high enzyme concentrations (> 4 μM) is explained by increasing amounts of free copper that are introduced to the reaction together with the enzyme. A control experiment with protein-free ultrafiltrates of the enzyme stock solutions showed that this was not the case (Additional file 1: Fig. S4).

Copper bias in previously reported LPMO data

The Avicel degradation experiments with either ascorbic acid or gallic acid (in the absence of exogenous H_2O_2 and free copper) indicate that AA10_07 is a slow enzyme. Early in the reaction, i.e., within the first hour or so, the release of soluble products is close to negligible (Fig. 4a), which is likely due to the fact that in this early phase of the reaction, oxidized products are still polymeric and, thus, not soluble. Frommhagen et al. [39] have pointed out that it takes a while before the same cellulose chain has been cleaved sufficiently many times to generate short, soluble products that are released into solution. Later during the reaction (Fig. 4a), the release of oxidized products over time was close to linear, but very slow, with rates (estimated from Fig. 4a) in the range of 0.06–0.2 min^{-1}. Such rates are common among reported rate estimates for LPMOs [40], but these rates are really low and two orders of magnitude lower than rates obtained in reactions with Avicel that are supplied with exogenous H_2O_2, which are higher than 10 min^{-1} (Fig. 4b).

AA10_07 is a close homolog of the well-studied *Sc*LPMO10C (CelS2; 85.6% sequence identity between catalytic domains). In previous studies by our group, *Sc*LPMO10C displayed low cellulose oxidation rates (0.1–0.2 min^{-1}) in reactions fuelled by ascorbic acid [24, 41], which are comparable to the results obtained here for AA10_07. However, looking back on a larger set of (our own) data, we noted that much higher oxidation rates were observed in other studies while using seemingly comparable conditions, as shown in Table 1. Importantly, all *Sc*LPMO10C experiments quoted in Table 1 were based upon similar LPMO production, purification and copper saturation procedures.

Given the fact that all these studies involved ascorbic acid as the reductant, it is reasonable to assume that the observed variations in LPMO activity were caused by different levels of free copper in the reactions (as well as, in some cases, other factors such as pH and the type of substrate).

Comparison of two in-house produced batches of *Sc*LPMO10C, one freshly prepared and one older batch that had shown "high activity", in the same experiment indeed showed large differences in product yields (Additional file 1: Fig. S5). Most importantly, the difference between the two protein batches disappeared after the most active batch had been subjected to another round of desalting. Quantification of total copper by ICP-MS indicated the presence of 0.9 ± 0.139 µM and 1.7 ± 0.298 µM copper ions in 1 µM enzyme solutions of the freshly prepared and the older "active" enzyme batches, thus confirming that the observed activity differences indeed correlated with varying amounts of free copper.

It is worth noting that both *Sc*LPMO10C batches were prepared in the same manner. In both cases (as well as in the other studies featured in Table 1), a gravity-flow desalting column was used to remove excess copper after copper saturation. It is reasonable to assume that the efficiency of the desalting procedure may have varied. The desalting experiments described above show how LPMO preparations devoid of free copper can be prepared and the filtration experiment

Table 1 Cellulose oxidation rates derived from previously reported *Sc*LPMO10C reactions driven by ascorbic acid and molecular oxygen

Approximate cellulose oxidation rate	Product quantification routine[c]	Substrate and reaction conditions	References
0.2 min^{-1} [a]	DP2ox quantification (HPAEC-PAD) after treatment with *Tr*Cel7A cellobiohydrolase	0.2% (w/v) PASC, 20 mM ammonium acetate buffer, pH 6.0, 40 °C, 2 mM ascorbic acid	[24]: Fig. 2a
0.14 min^{-1} [a]	DP2ox quantification (HPAEC-PAD) after treatment with TfCel5A endogluconase	1% (w/v) Avicel, 50 mM sodium phosphate buffer, pH 6.0, 40 °C, 1 mM ascorbic acid	[41]: Fig. 2
6.7 min^{-1}	DP2ox + DP3ox quantification (HPAEC-PAD) after treatment with TfCel5A endogluconase	1% (w/v) Avicel, 50 mM sodium phosphate buffer, pH 7.0, 40 °C, 1 mM ascorbic acid	[42]: Fig. 4
3.4 min^{-1} [b]	DP2ox + DP3ox quantification (HPAEC-PAD) after treatment with TfCel5A endogluconase	1% (w/v) Avicel, 50 mM sodium phosphate buffer, pH 7.0, 40 °C, 1 mM ascorbic acid	[12]: Fig. 1f
2.5 min^{-1} [b]	DP2ox + DP3ox quantification (HPAEC-PAD) after treatment with TfCel5A endogluconase	0.5% (w/v) PASC, 50 mM sodium phosphate buffer, pH 6.0, 40 °C, 1 mM ascorbic acid	[43]: Fig. 8
7.9 min^{-1}	DP2ox + DP3ox quantification (HPAEC-PAD) after treatment with *Tf*Cel5A endoglucanase	1% (w/v) Avicel, 50 mM sodium phosphate buffer, pH 7.0, 40 °C, 1 mM ascorbic acid	[20]: Fig. 2a

[a] The reported rate is underestimated by approximately twofold due to limitations in product quantification. Only C1-oxidized cellobiose was quantified in the mixture of C1-oxidized cellobiose and C1-oxidized cellotriose. The molar ratio between these products is typically close to 1 in reactions with *Sc*LPMO10C [41]

[b] No progress curves were reported in the paper meaning that approximate oxidation rates were estimated using single time points

[c] DP2ox/DP3ox: C1-oxidized cellobiose/cellotriose

depicted in Fig. 3 provides a simple method to check for free copper that does not depend on the use of an ICP-MS.

Conclusions

Taken together, our results indicate that the use of ascorbic acid as a reductant in LPMO experiments is not optimal, if reproducibility of kinetic data is considered. Ascorbate-driven reactions are sensitive to micromolar concentrations of free copper due to high levels of copper-catalyzed enzyme-independent H_2O_2 production. On the other hand, when using gallic acid as an electron donor, the LPMO progress curves show no strong dependency on free copper in the system (at least up to a 3 µM concentration). This is most likely due to complexation of free Cu(II) by gallic acid, which prevents copper reduction.

Potential sources of free copper in LPMO reactions are numerous. LPMO samples may be contaminated as a result of a copper saturation procedure, in case excess Cu(II) ions are not completely removed from the system. Other components of typical LPMO reactions, such as the substrate, may also contain small amounts of copper. Notably, copper carry-over may be facilitated by secondary low affinity binding sites on the enzyme, as observed in some crystal structures [38], and by poly-histidine affinity tags, which are known to possess a high affinity for Cu(II) [44].

Given that ascorbic acid is the most commonly used reductant in the field, it is likely that published LPMO activity data to some extent are biased by the presence of varying and unknown amounts of free copper in the reactions that were conducted. As we illustrate above, this includes some of our own previous work on *Sc*LPMO10C for which we (implicitly) have reported different (higher) catalytic efficiencies which are due to variations in free copper.

The reported sensitivity to free copper is likely not exclusive to LPMO systems that are fuelled by ascorbate and may also apply to reactions with other reductants. For example, it has been established that autoxidation of both L-cysteine and glutathione, compounds that are regularly used as LPMO reductants [1, 11, 45–47], is catalysed by micromolar amounts of free Cu(II) ions in a manner that leads to the production of hydrogen peroxide [48, 49].

On another note, this study presents an illustration of the complex nature and limitations of the HRP/Amplex Red assay (see also [29]). We demonstrate that apparent H_2O_2 production rates obtained by this method using low concentrations of reductants (a rather common approach employed in many LPMO studies) may not necessarily describe trends that exist in reactions on cellulose at standard aerobic conditions (i.e., at ≥ 1 mM reductant concentration).

Our data provide insight into multiple mechanisms that may explain why LPMO activity is reductant-dependent. In this paper we show that, in the presence of substrate, hydrogen peroxide generation by 1 µM of a family AA10 LPMO is negligible compared to the amounts of H_2O_2 produced by the autoxidation of 1 mM ascorbic acid and, in particular, 1 mM gallic acid.

It is worth noting that LPMOs may significantly vary in hydrogen peroxide production and, thus, some enzymes, for example fungal AA9 type LPMOs, may show less dependency on reductant autoxidation. Furthermore, the oxidation of reductants by oxygen (both in the presence and in absence of free copper) is likely to be affected by pH (these effects are well-described for ascorbate, e.g. [18, 50]), hence the contribution of this process to overall H_2O_2 production may depend on reaction conditions.

All in all, this study sheds light on the complex impact of the reductant on LPMO catalysis. Under commonly used reaction conditions, the large surplus of reductant likely ensures that reduction of the LPMO is not rate-limiting, and the rate of the reaction is determined by the generation of H_2O_2, which, at least in the case of cellulose-active AA10s, is dominated by the oxidation of the reductant by oxygen.

Methods

Materials

Chemicals were obtained from Sigma-Aldrich (St. Louis, MO, USA) unless indicated otherwise. Microcrystalline cellulose used in this study was Avicel PH-101. Amplex Red was obtained from Thermo Fisher Scientific (Waltham, MA, USA). 10 mM Amplex Red stock solutions were prepared in DMSO and stored in light-protected tubes at − 20 °C. Ascorbic acid and gallic acid were stored at − 20 °C as 100 mM stock solutions in metal-free TraceSELECT water (Honeywell, Charlotte, NC, USA) and DMSO, respectively. Horseradish peroxidase type II (HRP) was stored in 50 mM sodium phosphate buffer, pH 6.0 at 4 °C (at 100 U/ml concentration). Tryptone and yeast extract were obtained from Thermo Fisher Scientific (Waltham, MA, USA).

Identification of the LPMO gene

Strain P01-F09 was isolated from a finger sponge harvested at 60 m depth near Tautra, an island located within the Trondheim fjord, Norway (063° 36′ 53″ N, 010° 31′ 22″ E) on September 22, 2005. Phylogenetic analysis (16 s rRNA) indicated the closest taxonomic neighbour being *Streptomyces griseolus* (98.8% sequence identity). Shotgun sequencing of the strain's genome was carried out at BaseClear BV (Leiden,

Netherlands) using Illumina HiSeq, revealing a genome size of 7,272,225 bp in 910 scaffolds.

Putative LPMO coding sequences within the obtained scaffolds were identified using the *hmmscan* tool from the HMMER software package version 3.1b2 (http://hmmer.org/) [51]. The Hidden Markov Model (HMM) profiles of all LMPO families were extracted from the dbCAN database [52] (version 7 at the time of the analysis), available from the dbCAN website (http://bcb.unl.edu/dbCAN2/). The analysis led to the identification of a seemingly complete gene putatively encoding an AA10 (family 10) LPMO, here referred to as AA10_07. The AA10_07 sequence has been submitted to Genbank under Accession number MT882343.

Protein expression

The AA10_07-encoding gene (GenBank accession number MT882343) was codon optimized for expression in *Escherichia coli* and synthesized by GenScript (Piscataway, NJ, USA). The resulting synthetic DNA contained a 66 bp leader sequence, encoding for the pelB signal peptide, followed by the *LPMO* gene (residue 34–360). The gene construct was cloned into the pET-26(b)+ expression vector (Merck, Darmstadt, Germany) using NdeI/XhoI restriction sites and sequenced (Sanger sequencing) by GenScript (Piscataway, NJ, USA).

An AA10_07 expression strain was established by heat-shock transformation of BL21 (DE3) competent cells (Invitrogen, Carlsbad, USA) with the expression vector, according to the supplier's protocol. The transformed cells were grown in LB medium at 37 °C for 1 h, and then plated on LB agar medium with 50 µg/ml kanamycin, followed by incubation overnight at the same temperature. A single colony was picked from the agar plate to inoculate 500 ml of Terrific Broth (TB) medium supplied with 50 µg/ml kanamycin. The resulting culture was incubated for 24 h at 30 °C in a LEX-24 Bioreactor (Harbinger Biotechnology & Engineering, Markham, Canada) using compressed air for aeration and mixing. Under the conditions used here, there was a considerable level of basal expression ("promotor leakage"), hence no IPTG induction was necessary.

The cells were harvested by centrifugation (6000×*g* for 10 min) at 4 °C, using a Beckman Coulter centrifuge (Brea, CA, USA), and then subjected to periplasmic extraction by osmotic shock as described previously [53]. The periplasmic extracts were sterilized by filtration through a sterile 0.22 µm syringe filter (Sarstedt, Nümbrecht, Germany) and stored at 4 °C prior to purification of the LPMO.

Protein purification

AA10_07 was purified from a periplasmic extract using ion-exchange chromatography with a HiTrap™ DEAE Sepharose FF 5 ml column (GE Healthcare, Chicago, USA). The enzyme was eluted using a linear gradient of NaCl (0–500 mM) in the starting buffer, which was 50 mM Tris-HCl, pH 7.5. Chromatography fractions were analysed by SDS-PAGE (Bio-Rad, Hercules, California, USA). Fractions containing purified enzyme were pooled and concentrated using Vivaspin ultrafiltration tubes with a molecular weight cut-off of 10 kDa (Sartorius, Göttingen, Germany). The concentrated preparations were subjected to size-exclusion chromatography using a HiLoad 16/60 Superdex 75 column (GE Healthcare, Chicago, USA), with 50 mM Tris-HCl, pH 7.5, containing 200 mM NaCl, which resulted in electrophoretically pure LPMO samples. Protein concentrations were determined by UV–Vis spectroscopy (A_{280}) using the theoretical extinction coefficient of AA10_07 (assuming that all pairs of Cys residues form disulphide bonds), as calculated with the ProtParam tool [54].

Copper-saturated enzyme was prepared by co-incubating the purified LPMO with Cu(II)SO_4 at a 1:3 molar ratio for 30 min, at room temperature in 50 mM Tris-HCl, pH 7.5, containing 200 mM NaCl. Excess copper was removed from the preparation by size-exclusion chromatography on a HiLoad 16/60 Superdex 75 column (as described above) or using a PD MidiTrap G-25 desalting column (GE Healthcare, Chicago, USA) equilibrated with 50 mM sodium phosphate buffer pH 6.0. To avoid contamination with free copper, the sample size in the desalting step with PD MidiTrap G-25 columns was only 350 µl and only the first 1 ml of the eluate (instead of 1.5 ml recommended by the manufacturer) was used in further experiments. In case a HiLoad 16/60 Superdex 75 column was used, subsequent to the gel filtration step, the buffer was exchanged to 50 mM sodium phosphate buffer pH 6.0 using a PD MidiTrap G-25 desalting column. The purified protein samples were stored at 4 °C until further use.

Assessment of copper content

The total copper content of selected protein and cellulose samples was determined by inductively coupled plasma mass spectrometry (ICP-MS) using a tandem quadrupole 8800 ICP-QQQ machine (Agilent Technologies), equipped with a collision/reaction cell. The samples were mixed with 70% ultrapure nitric acid and a multi-element internal ICP-MS standard (Inorganic Ventures, Christiansburg, VA, USA). All samples were then autoclaved at 121 °C in sealed tubes for 30 min using saturated steam under pressure. Tubes were allowed to cool,

and the solutions were diluted with deionized 18.2 MΩ water to 5% (v/v) nitric acid. The ICP-MS instrument was operated in single quadrupole mode using helium as a collision gas to minimize diatomic interferences from plasma or sample. A control standard (Inorganic Ventures, Christiansburg, VA, USA) was analysed in between the protein samples to check and compensate for instrument drift. Calibration curves were prepared prior to protein analysis and the copper concentration was determined according to these curves using Indium as internal standard.

As another method for assessing free copper in enzyme preparations (and its effect on the LPMO reaction), a small volume (≤ 200 µl) of LPMO stock solution was subjected to ultrafiltration using a 3 kDa MWCO 1.5 ml ultrafiltration tube (VWR International, Radnor, PA, USA) and centrifugation at 10,000*g* and room temperature for about 3 min. The protein-free filtrate will contain the same concentration of free copper as the LPMO containing retentate. Filtrates and retentates were collected and used in hydrogen peroxide production experiments (see below).

Hydrogen peroxide production

H_2O_2 production assays were based on the approach previously described by Kittl et al. [13]. 90 µl sample solutions containing LPMO, horse radish peroxidase (HRP) and Amplex Red in 50 mM sodium phosphate buffer pH 6.0 were pre-incubated in a 96-well microtiter plate for 5 min at 30 °C. The reactions were initiated by the addition of 10 µl of a reductant stock solution. The final concentrations of LPMO, HRP, Amplex Red and reductant were 3 µM, 5 U/ml, 100 µM and 50 µM (or 1 mM), respectively. For each experiment, control reactions were set up by substituting the LPMO with the same volume of water and/or with the same volume of a protein-free sample ("filtrate"), produced by ultrafiltration of the LPMO stock solution, as described above.

The formation of hydrogen peroxide was monitored by recording the optical absorbance of resorufin (the product generated from Amplex Red by HRP) at 563 nm over time, at 30 °C, using a Varioscan LUX plate reader (Thermo Fisher Scientific, Waltham, MA, USA). H_2O_2 standard solutions were prepared in 50 mM sodium phosphate buffer pH 6.0 and supplied with 5 U/ml HRP and 100 µM Amplex Red to generate a standard curve. Apparent H_2O_2 production rates were derived from the initial linear parts of the resorufin production curves.

Hydrogen peroxide production in reactions containing free copper and a reductant (gallic acid or ascorbic acid) was assessed in the same manner as described above, using various concentrations of $Cu(II)SO_4$.

LPMO reactions with Avicel

The LPMO activity on microcrystalline cellulose was studied by setting up reactions with varying amounts of enzyme (0.05–8 µM) and 1% (w/v) Avicel in 50 mM sodium phosphate buffer pH 6.0, supplied with 1 mM reductant (gallic acid or ascorbic acid) and varying amounts of $CuSO_4$ or H_2O_2. The reactions were carried out in a thermomixer (30 °C, 900 RPM). Note that LPMO reactions in the presence of gallic acid were set up using a 100 mM stock solution of gallic acid in DMSO. Thus, 1% (v/v) DMSO was introduced to the reaction mixtures. Control experiments were performed to confirm that 1% (v/v) DMSO does not have a significant impact on the LPMO reaction (Additional file 1: Fig S6).

100 µl aliquots were taken at various time points, and the reactions were stopped by immediately separating the enzyme and soluble products from the insoluble substrate by filtration using a 96-well filter plate (Millipore, Burlington, MA, USA), after which the filtrates were stored at − 20 °C. Note that the product profile of AA10_07 (see Fig. 2b) shows a range of shorter to longer oxidized products (DP2-7ox) with DP6ox being the most prominent product. If AA10_07 was capable of degrading soluble cello-oligosaccharides, accumulation of shorter products would be expected, but this is not the case. Thus, the reactions were considered quenched after filtration. For qualitative product analysis, the filtrates were subjected to analytical chromatography without any additional pre-treatment procedures. Prior to quantitative product analysis, the filtrates were incubated at 37 °C, overnight with 1 µM in-house produced recombinant *Thermobifida fusca* GH6 endoglucanase (*Tf*Cel6A; [55]) to convert oxidized cello-oligosaccharides to a mixture of oxidized dimers and trimers only.

Product analysis by HPAEC-PAD

Cellulose degradation products were analysed by high-performance anion-exchange chromatography with pulsed amperometric detection (HPAEC-PAD) using a Dionex ICS5000 system (Thermo Scientific, San Jose, CA, USA) equipped with a CarboPac PA200 analytical column. A stepwise gradient with an increasing amount of eluent B (eluent B: 0.1 M NaOH and 1 M NaOAc; eluent A: 0.1 M NaOH) was applied according to the following program: 0–5.5% B over 3 min, 5.5–15% B over 6 min, 15–100% B over 11 min, 100–0% B over 6 s, 0% B over 6 min. The flow rate was 0.5 ml/min. Chromeleon 7.0 software was used for data analysis. C1-oxidized cello-oligosaccharide standards with a degree of polymerization of two and three (DP2, DP3) were prepared in-house as described before [41, 56].

Product analysis by MALDI-ToF MS

Products of Avicel degradation were identified using a matrix-assisted laser desorption/ionization time-of-flight (MALDI-ToF) UltrafleXtreme mass spectrometer (Bruker Daltonics GmbH, Bremen, Germany). 1 µl of the LPMO reaction mixture was mixed with 2 µl of a matrix solution (9 mg/ml 2,5-dihydrooxybenzoic acid) on a MTP 384 ground steel target plate (Bruker Daltonics). The plate was air-dried, and the spectral data were acquired using Bruker flexControl software, as described previously [1].

Supplementary Information

The online version contains supplementary material available at https://doi.org/10.1186/s13068-021-01879-0.

Additional file 1: Fig S1. Cellulose solubilization by two batches of AA10_07. **Fig S2.** Underestimation of H_2O_2 in the presence of ascorbic acid or gallic acid. **Fig S3.** Cellulose solubilization by increasing amounts of AA10_07 in the presence of ascorbic acid or gallic acid. **Fig S4.** Cellulose solubilization by 1 µM AA10_07 in the presence of protein-free filtrates. **Fig S5.** Comparing the activity of two different batches of ScLPMO10C. **Fig S6.** The effect of DMSO on AA10_07 reactions with cellulose.

Acknowledgements

We thank Sven Andreas Högfeldt at the Norwegian University of Life Sciences for ICP-MS analysis of LPMO samples.

Author contributions

AAS did most of the experimental work, analysed data and drafted the manuscript. ZF contributed to designing the study, performed data analysis and edited the manuscript. MS contributed to data interpretation and edited the manuscript. GSN collected and analysed genomic data. AW supervised the project, collected and analysed genomic data and edited the manuscript. ÅKR and VGHE conceptualized the work, contributed to data interpretation and edited the manuscript. VGHE acquired funding, conceived and supervised the project. All authors read and approved the final manuscript.

Funding

This work was supported by the Research Council of Norway under Grant no. 269408 (Centre for Digital Life Norway, project OXYMOD).

Availability of data and materials

Data supporting the findings of this work are available within the paper and its Additional information file and from the corresponding author upon reasonable request.

Ethics approval and consent to participate

Non applicable.

Consent for publication

Non applicable.

Competing interests

The authors declare that they have no competing interests.

Author details

[1] Faculty of Chemistry, Biotechnology and Food Science, NMBU-Norwegian University of Life Sciences, Ås, Norway. [2] Department of Biotechnology and Nanomedicine, SINTEF Industry, Trondheim, Norway.

Received: 15 November 2020 Accepted: 7 January 2021
Published online: 21 January 2021

References

1. Vaaje-Kolstad G, et al. An oxidative enzyme boosting the enzymatic conversion of recalcitrant polysaccharides. Science. 2010;330(6001):219–22.
2. Forsberg Z, et al. Cleavage of cellulose by a CBM33 protein. Protein Sci. 2011;20(9):1479–83.
3. Quinlan RJ, et al. Insights into the oxidative degradation of cellulose by a copper metalloenzyme that exploits biomass components. Proc Natl Acad Sci USA. 2011;108(37):15079–84.
4. Phillips CM, et al. Cellobiose dehydrogenase and a copper-dependent polysaccharide monooxygenase potentiate cellulose degradation by Neurospora crassa. ACS Chem Biol. 2011;6(12):1399–406.
5. Vaaje-Kolstad G, et al. Structural diversity of lytic polysaccharide monooxygenases. Curr Opin Struct Biol. 2017;44:67–76.
6. Frandsen KE, Lo Leggio L. Lytic polysaccharide monooxygenases: a crystallographer's view on a new class of biomass-degrading enzymes. IUCrJ. 2016;3(6):448–67.
7. Johansen KS. Lytic polysaccharide monooxygenases: the microbial power tool for lignocellulose degradation. Trends Plant Sci. 2016;21(11):926–36.
8. Vaaje-Kolstad G, et al. The non-catalytic chitin-binding protein CBP21 from *Serratia marcescens* is essential for chitin degradation. J Biol Chem. 2005;280(31):28492–7.
9. Danneels B, Tanghe M, Desmet T. Structural features on the substrate-binding surface of fungal lytic polysaccharide monooxygenases determine their oxidative regioselectivity. Biotechnol J. 2019;14(3):e1800211.
10. Kracher D, et al. Extracellular electron transfer systems fuel cellulose oxidative degradation. Science. 2016;352(6289):1098–101.
11. Frommhagen M, et al. Lytic polysaccharide monooxygenases from *Myceliophthora thermophila* C1 differ in substrate preference and reducing agent specificity. Biotechnol Biofuels. 2016;9(1):186.
12. Bissaro B, et al. Oxidative cleavage of polysaccharides by monocopper enzymes depends on H_2O_2. Nat Chem Biol. 2017;13(10):1123–8.
13. Kittl R, et al. Production of four *Neurospora crassa* lytic polysaccharide monooxygenases in *Pichia pastoris* monitored by a fluorimetric assay. Biotechnol Biofuels. 2012;5(1):79.
14. Hangasky JA, Iavarone AT, Marletta MA. Reactivity of O_2 versus H_2O_2 with polysaccharide monooxygenases. Proc Natl Acad Sci USA. 2018;115(19):4915–20.
15. Bissaro B, et al. Molecular mechanism of the chitinolytic peroxygenase reaction. Proc Natl Acad Sci USA. 2020;117(3):1504–13.
16. Wang B, et al. Activation of O_2 and H_2O_2 by lytic polysaccharide monooxygenases. ACS Catal. 2020;10(21):12760–9.
17. Courtade G, et al. Mechanistic basis of substrate-O_2 coupling within a chitin-active lytic polysaccharide monooxygenase: an integrated NMR/EPR study. Proc Natl Acad Sci USA. 2020;117(32):19178–89.
18. Zhou P, et al. Generation of hydrogen peroxide and hydroxyl radical resulting from oxygen-dependent oxidation of l-ascorbic acid via copper redox-catalyzed reactions. RSC Adv. 2016;6(45):38541–7.
19. Buettner GR, Jurkiewicz BA. Catalytic metals, ascorbate and free radicals: combinations to avoid. Radiat Res. 1996;145(5):532–41.
20. Bissaro B, et al. Controlled depolymerization of cellulose by light-driven lytic polysaccharide oxygenases. Nat Commun. 2020;11(1):890.
21. Eijsink VGH, et al. On the functional characterization of lytic polysaccharide monooxygenases (LPMOs). Biotechnol Biofuels. 2019;12:58.
22. Sonnhammer ELL, Eddy SR, Durbin R. Pfam: a comprehensive database of protein domain families based on seed alignments. Proteins. 1997;28(3):405–20.
23. Altschul SF, et al. Gapped BLAST and PSI-BLAST: a new generation of protein database search programs. Nucleic Acids Res. 1997;25(17):3389–402.
24. Forsberg Z, et al. Structural and functional characterization of a conserved pair of bacterial cellulose-oxidizing lytic polysaccharide monooxygenases. Proc Natl Acad Sci USA. 2014;111(23):8446–51.
25. Lei SP, et al. Characterization of the *Erwinia carotovora* pelB gene and its product pectate lyase. J Bacteriol. 1987;169(9):4379–83.
26. Zhang W, et al. Development an effective system to expression recombinant protein in *E. coli* via comparison and optimization of signal peptides: expression of *Pseudomonas fluorescens* BJ-10 thermostable lipase as case study. Microb Cell Fact. 2018;17(1):50.
27. Hegnar OA, et al. pH-dependent relationship between catalytic activity and hydrogen peroxide production shown via characterization of a lytic polysaccharide monooxygenase from *Gloeophyllum trabeum*. Appl Environ Microbiol. 2019; 85(5):e02612–18.

28. Severino JF, et al. Is there a redox reaction between Cu(II) and gallic acid? Free Radic Res. 2011;45(2):115–24.
29. Kont R, et al. Kinetic insights into the peroxygenase activity of cellulose-active lytic polysaccharide monooxygenases (LPMOs). Nat Commun. 2020;11(1):5786.
30. Rodrigues JV, Gomes CM. Enhanced superoxide and hydrogen peroxide detection in biological assays. Free Radic Biol Med. 2010;49(1):61–6.
31. Mehlhorn H, et al. Ascorbate is the natural substrate for plant peroxidases. FEBS Lett. 1996;378(3):203–6.
32. Wang N, et al. Quantitative determination of trace hydrogen peroxide in the presence of sulfide using the Amplex Red/horseradish peroxidase assay. Anal Chim Acta. 2017;963:61–7.
33. Jiang S, Penner MH. Overcoming reductant interference in peroxidase-based assays for hydrogen peroxide quantification. J Agric Food Chem. 2017;65(37):8213–9.
34. Loose JS, et al. Activation of bacterial lytic polysaccharide monooxygenases with cellobiose dehydrogenase. Protein Sci. 2016;25(12):2175–86.
35. Breslmayr E, et al. A fast and sensitive activity assay for lytic polysaccharide monooxygenase. Biotechnol Biofuels. 2018;11:79.
36. Tulyathan V, Boulton RB, Singleton VL. Oxygen uptake by gallic acid as a model for similar reactions in wines. J Agric Food Chem. 1989;37(4):844–9.
37. Isaksen T, et al. A C4-oxidizing lytic polysaccharide monooxygenase cleaving both cellulose and cello-oligosaccharides. J Biol Chem. 2014;289(5):2632–42.
38. Borisova AS, et al. Structural and functional characterization of a lytic polysaccharide monooxygenase with broad substrate specificity. J Biol Chem. 2015;290(38):22955–69.
39. Frommhagen M, et al. Quantification of the catalytic performance of C1-cellulose-specific lytic polysaccharide monooxygenases. Appl Microbiol Biotechnol. 2018;102(3):1281–95.
40. Bissaro B, et al. Oxidoreductases and reactive oxygen species in conversion of lignocellulosic biomass. Microbiol Mol Biol Rev. 2018;82(4).
41. Bissaro B, et al. Fueling biomass-degrading oxidative enzymes by light-driven water oxidation. Green Chem. 2016;18(19):5357–66.
42. Courtade G, et al. The carbohydrate-binding module and linker of a modular lytic polysaccharide monooxygenase promote localized cellulose oxidation. J Biol Chem. 2018;293(34):13006–15.
43. Jensen MS, et al. Engineering chitinolytic activity into a cellulose-active lytic polysaccharide monooxygenase provides insights into substrate specificity. J Biol Chem. 2019;294(50):19349–64.
44. Wijekoon CJK, et al. Evaluation of employing poly-lysine tags versus poly-histidine tags for purification and characterization of recombinant copper-binding proteins. J Inorg Biochem. 2016;162:286–94.
45. Frandsen KEH, et al. Identification of the molecular determinants driving the substrate specificity of fungal lytic polysaccharide monooxygenases (LPMOs). J Biol Chem. 2020;Nov 16:jbc.RA120.015545.
46. Chalak A, et al. Influence of the carbohydrate-binding module on the activity of a fungal AA9 lytic polysaccharide monooxygenase on cellulosic substrates. Biotechnol Biofuels. 2019;12:206.
47. Sabbadin F, et al. An ancient family of lytic polysaccharide monooxygenases with roles in arthropod development and biomass digestion. Nat Commun. 2018;9(1):756.
48. Kachur AV, Koch CJ, Biaglow JE. Mechanism of copper-catalyzed autoxidation of cysteine. Free Radic Res. 1999;31(1):23–34.
49. Kachur AV, Koch CJ, Biaglow JE. Mechanism of copper-catalyzed oxidation of glutathione. Free Radic Res. 1998;28(3):259–69.
50. Wilson RJ, Beezer AE, Mitchell JC. A kinetic study of the oxidation of L-ascorbic acid (vitamin C) in solution using an isothermal microcalorimeter. Thermochim Acta. 1995;264:27–40.
51. Finn RD, Clements J, Eddy SR. HMMER web server: interactive sequence similarity searching. Nucleic Acids Res. 2011;39(Web server issue):W29-37.
52. Yin Y, et al. dbCAN: a web resource for automated carbohydrate-active enzyme annotation. Nucleic Acids Res. 2012;40(Web server issue):W445–51.
53. Manoil C, Beckwith J. A genetic approach to analyzing membrane protein topology. Science. 1986;233(4771):1403–8.
54. Gasteiger E, et al. Protein identification and analysis tools on the ExPASy Server. In: The proteomics protocols handbook. 2005. p. 571–607.
55. Spezio M, Wilson DB, Karplus PA. Crystal structure of the catalytic domain of a thermophilic endocellulase. Biochemistry. 1993;32(38):9906–16.
56. Forsberg Z, et al. Structural determinants of bacterial lytic polysaccharide monooxygenase functionality. J Biol Chem. 2018;293(4):1397–412.

Publisher's Note

Unraveling the roles of the reductant and free copper ions in LPMO kinetics

Anton A. Stepnov[1], Zarah Forsberg[1], Morten Sørlie[1], Giang-Son Nguyen[2], Alexander Wentzel[2], Åsmund K. Røhr[1] and Vincent G.H. Eijsink[1*]

[1] Faculty of Chemistry, Biotechnology and Food Science, NMBU - Norwegian University of Life Sciences, Ås, Norway

[2]Department of Biotechnology and Nanomedicine, SINTEF Industry, Trondheim, Norway

[*] corresponding author, vincent.eijsink@nmbu.no

Additional file 1

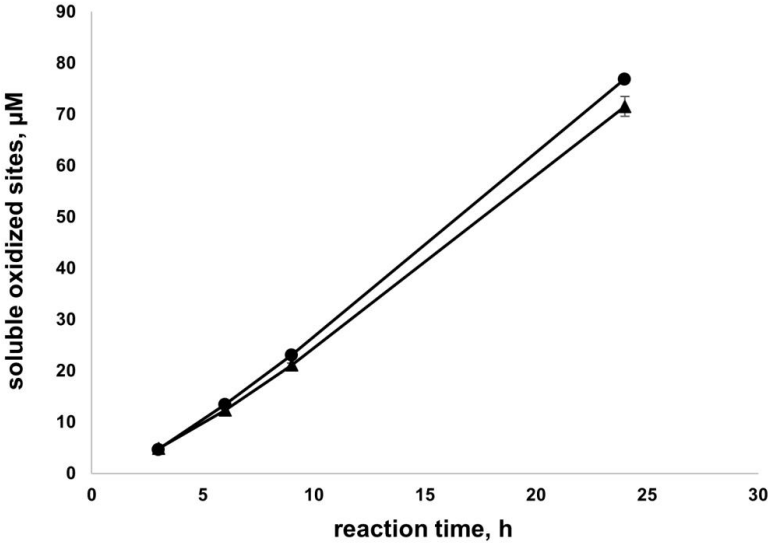

Fig S1. Cellulose solubilization by two batches of AA10_07. The figure shows progress curves obtained in LPMO reactions (1 µM AA10_07 in 50 mM sodium phosphate buffer, pH 6.0, 30 °C) with 1% (w/v) Avicel using desalted (circular markers) and SEC-treated (triangular markers) batches of AA10_07. For reduction, 1 mM ascorbic acid was present in the reaction mixtures. Error bars indicate standard deviations between triplicates. Prior to quantification of oxidized sites, soluble LPMO products of varying lengths were converted to a mixture of oxidized dimers and trimers by treatment with a cellulase.

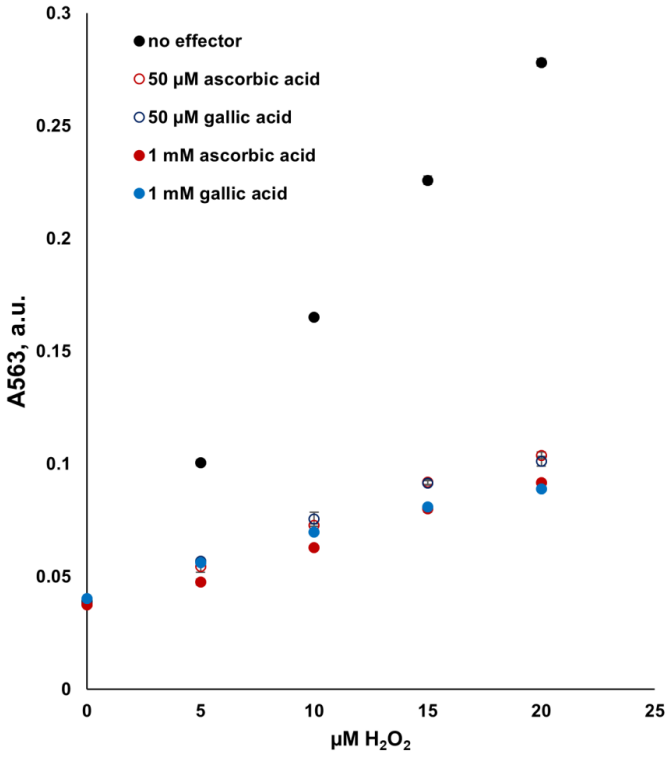

Fig S2. Underestimation of H_2O_2 in the presence of ascorbic acid or gallic acid. The figure shows HRP/Amplex Red results, obtained using various amounts of hydrogen peroxide in the presence and in the absence of 50 µM or 1 mM reductants. Note that both ascorbic acid and gallic acid supress the signal, i.e., the H_2O_2-fueled conversion of Amplex Red to the red-fluorescent oxidation product, resorufin, to a similar extent. Error bars indicate standard deviations between triplicates.

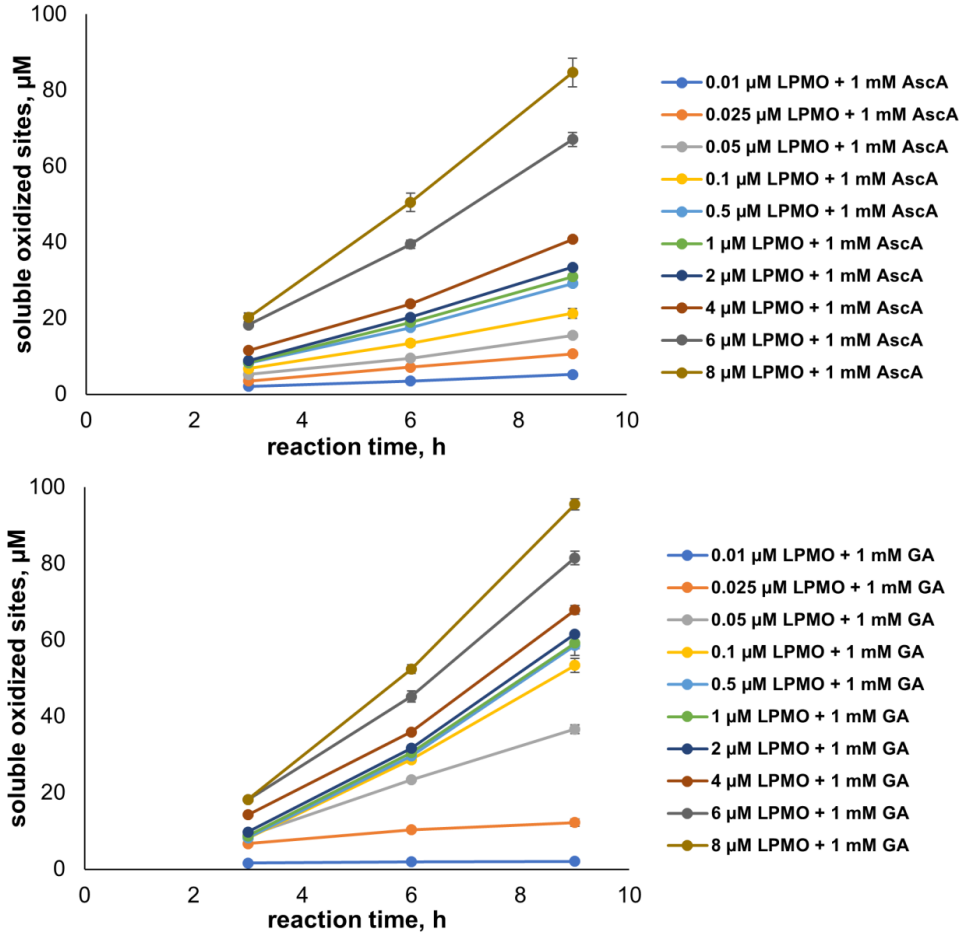

Fig S3. Cellulose solubilization by increasing amounts of AA10_07 in the presence of ascorbic acid or gallic acid. The figure shows progress curves obtained in LPMO reactions (in 50 mM sodium phosphate buffer, pH 6.0, 30 °C) with 1% (w/v) Avicel using 0.01 µM – 8 µM AA10_07. For reduction, 1 mM ascorbic acid or gallic acid was present in the reaction mixtures. AscA, ascorbic acid; GA, gallic acid. Error bars indicate standard deviations between triplicates. Product accumulation was not observed in control reactions with 1% (w/v) Avicel and no enzyme present. The 9 h end points were used to generate Fig. 7 in the main manuscript.

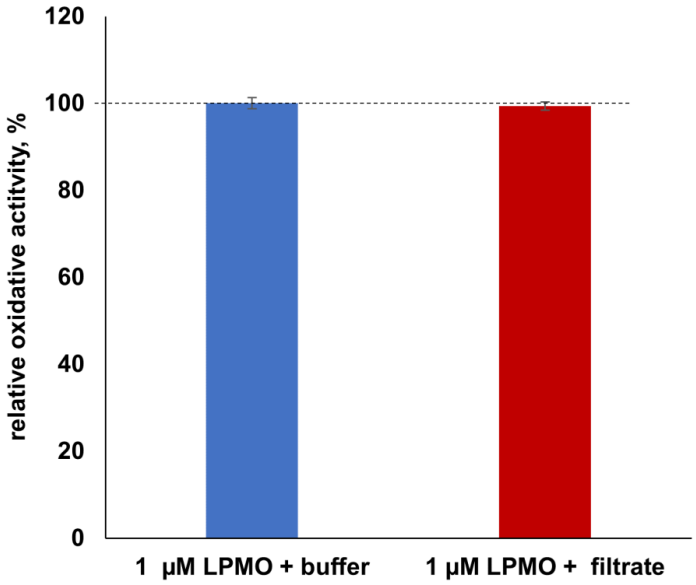

Fig S4. Cellulose solubilization by 1 µM AA10_07 in the presence of protein-free filtrates. The figure shows the activity of 1 µM AA10_07 in 6 hours reactions with 1% (w/v) Avicel in the absence or presence of protein-free solution obtained by ultra-filtration of the enzyme preparation. This control solution contained the same amount of free (unbound) copper as the LPMO stock solution used in this study. The control reaction (red bar) was started by mixing 5.2 µL of the enzyme stock solution with 41.6 µL (8 times more volume) of protein-free filtrate. In the reference reaction (blue bar), the protein-free filtrate was substituted by the same volume of 50 mM sodium phosphate buffer, pH 6.0. Note that due to addition of the filtrate, the control reaction with 1 µM LPMO (red bar) will contain the same concentration of free copper as a reaction with 9 µM LPMO. The graph shows that, despite the nine-fold increase in the (potentially very low) free copper concentration, the experiment with the filtrate did not show any boost to LPMO activity, compared to the reference reaction (blue bar; 100 %). This result indicates that free copper levels in the AA10_07 preparation were too low to bias the results of the LPMO dose-response experiments shown in Fig. 7 & S3. Reaction conditions: 57 mM sodium phosphate buffer, pH 6.0, 30 °C. 1 mM ascorbic acid was used as a reductant. Error bars indicate standard deviations between triplicates.

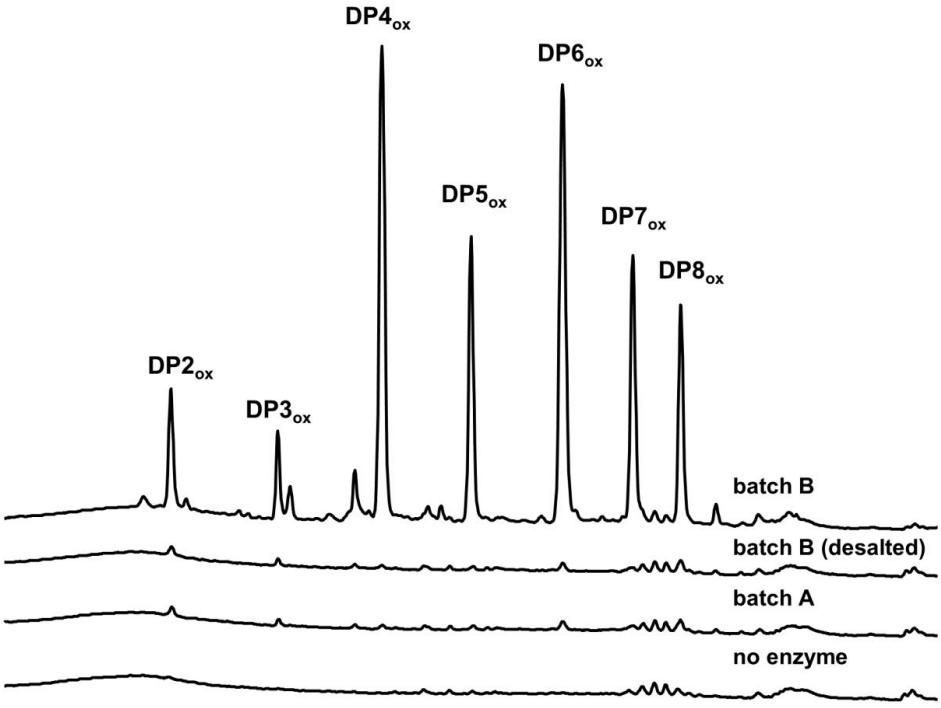

Fig S5. Comparing the activity of two different batches of *Sc*LPMO10C. The figure shows HPAEC-PAD chromatograms of products released by 1 µM *Sc*LPMO10C in 1 hour reactions (50 mM sodium phosphate buffer, pH 6.0, 30 °C) with 1 % (w/v) Avicel, supplied with 1 mM ascorbic acid. Batch A, *Sc*LPMO10C preparation obtained in this study; batch B, previously produced *Sc*LPMO10C sample, without or with an additional desalting step, as indicated. Oxidized product peaks were annotated based on previously published product profiles for *Sc*LPMO10C [2, 12, 42].

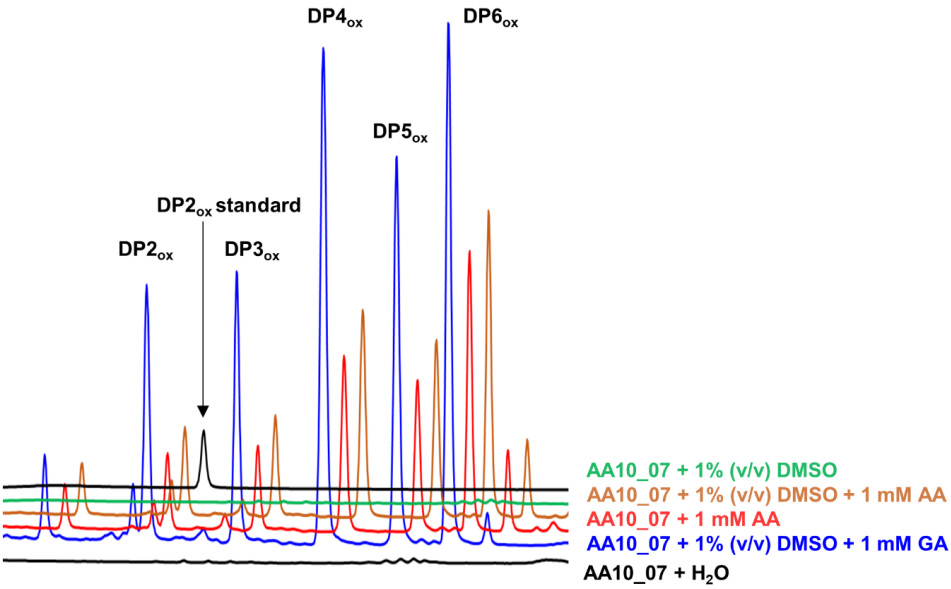

Fig S6. The effect of DMSO on AA10_07 reactions with cellulose. The figure shows HPAEC-PAD chromatograms of oxidized products released by AA10_07 in 24 hour reactions (1 µM LPMO in 50 mM sodium phosphate buffer, pH 6.0, 30 °C) with 1 % (w/v) Avicel in the presence of 1 mM reductant and/or 1% (v/v) DMSO. Note that the control experiment, performed at the same conditions, indicates that 1% (v/v) DMSO alone is not able to act as LPMO reductant. The oxidized products peaks are annotated based on retention times relative to the GlcGlc1A ($DP2_{ox}$) standard.

The impact of reductants on the catalytic efficiency of a lytic polysaccharide monooxygenase and the special role of dehydroascorbic acid

Stepnov AA, Christensen IA, Forsberg Z, Aachmann FL, Courtade G, Eijsink VG

Paper II

FEBS Letters

FEBS PRESS science publishing by scientists

RESEARCH ARTICLE

The impact of reductants on the catalytic efficiency of a lytic polysaccharide monooxygenase and the special role of dehydroascorbic acid

Anton A. Stepnov[1], Idd A. Christensen[2], Zarah Forsberg[1], Finn L. Aachmann[2], Gaston Courtade[2] and Vincent G. H. Eijsink[1]

1 Faculty of Chemistry, Biotechnology and Food Science, NMBU - Norwegian University of Life Sciences, Ås, Norway
2 NOBIPOL, Department of Biotechnology and Food Science, NTNU Norwegian University of Science and Technology, Trondheim, Norway

Correspondence
Vincent G. H. Eijsink, Faculty of Chemistry, Biotechnology and Food Science, NMBU - Norwegian University of Life Sciences, 1432 Ås, Norway.
Tel: +47 67232463
E-mail: vincent.eijsink@nmbu.no

(Received 2 September 2021, revised 21 November 2021, accepted 23 November 2021, available online 12 December 2021)

doi:10.1002/1873-3468.14246

Edited by Peter Brzezinski

Monocopper lytic polysaccharide monooxygenases (LPMOs) catalyse oxidative cleavage of glycosidic bonds in a reductant-dependent reaction. Recent studies indicate that LPMOs, rather than being O_2-dependent monooxygenases, are H_2O_2-dependent peroxygenases. Here, we describe *Ssc*LPMO10B, a novel LPMO from the phytopathogenic bacterium *Streptomyces scabies* and address links between this enzyme's catalytic rate and in situ hydrogen peroxide production in the presence of ascorbic acid, gallic acid and L-cysteine. Studies of Avicel degradation showed a clear correlation between the catalytic rate of *Ssc*LPMO10B and the rate of H_2O_2 generation in the reaction mixture. We also assessed the impact of oxidised ascorbic acid, dehydroascorbic acid (DHA), on LPMO activity, since DHA, which is not considered a reductant, was recently reported to drive LPMO reactions. Kinetic studies, combined with NMR analysis, showed that DHA is unstable and converts into multiple derivatives, some of which are redox active and can fuel the LPMO reaction by reducing the active site copper and promoting H_2O_2 production. These results show that the apparent monooxygenase activity observed in *Ssc*LPMO10B reactions without exogenously added H_2O_2 reflects a peroxygenase reaction.

Keywords: dehydroascorbic acid; enzyme kinetics; hydrogen peroxide; LPMO; NMR

Lytic polysaccharide monooxygenases (LPMOs) are monocopper enzymes that are involved in depolymerisation of polysaccharides such as cellulose, other glycans, xylan, chitin, pectin and starch [1–8]. LPMO catalysis relies on the controlled generation of a reactive oxygen species that is powerful enough to hydroxylate glycosidic bonds in crystalline and otherwise inaccessible substrates. The hydroxylation occurs at the C1 or C4 position and results in cleavage of the glycosidic bond, yielding a 1,5-δ-lactone (C1-oxidizing LPMOs) or a 4-ketoaldose (C4-oxidizing LPMOs) [9–11]. Some enzymes generate mixtures of C1- and C4-oxidised products [12]. In nature and in industrial applications, LPMOs provide an essential support to hydrolases whose activity is promoted upon LPMO-catalysed de-crystallisation of recalcitrant polysaccharide substrates [13–15].

Lytic polysaccharide monooxygenases depend on an electron source for their catalytic activity. Most likely due to their solvent-exposed active sites [16,17], these

Abbreviations
DHA, dehydroascorbic acid; HPAEC-PAD, high-performance anion-exchange chromatography with pulsed amperometric detection; HRP, horseradish peroxidase; LPMO, lytic polysaccharide monooxygenase.

enzymes can accept a remarkable variety of reductants, ranging from small organic molecules, such as ascorbic acid [1,18], gallic acid [3,19] or L-cysteine [20], to protein partners such as cellobiose dehydrogenase [11,21] and pyrroloquinoline quinone-dependent pyranose dehydrogenase [22].

Historically, LPMOs were thought to be strict monooxygenases (Figure 1A) and involve molecular oxygen as a co-substrate [1,23]. Subsequent studies showed that hydrogen peroxide is able to drive LPMO reactions (Figure 1B), suggesting that these enzymes can operate as peroxygenases [24]. Importantly, peroxygenase LPMO reactions are fast [25–30] compared to monooxygenase LPMO reactions, which are typically two to three orders of magnitude slower. Furthermore, the enzymes clearly prefer H_2O_2 over O_2 in competition experiments [24].

It is well established that, provided with electron donors, LPMOs are able to reduce molecular oxygen and generate hydrogen peroxide [31,32]. This activity was initially considered as a 'futile' uncoupled reaction. However, in light of recent findings on H_2O_2 being a preferred LPMO co-substrate, hydrogen peroxide production by these enzymes can no longer be considered an irrelevant side process. The notion that standard set-ups for aerobic LPMO reactions (LPMO, 1 mM reductant, substrate, O_2) likely lead to generation of H_2O_2 has led some to suggest that the apparent O_2-dependent monooxygenase reactions in fact are peroxygenase reactions that are limited by in situ production of H_2O_2 [24,26]. The question whether 'true' monooxygenase LPMO reactions occur at all is a subject of current debate [28,33,34].

This debate stems in part from data showing that hydrogen peroxide accumulation is not taking place in LPMO reactions with substrates [28,31,33,35]. Some researchers have interpreted these data to show that H_2O_2 generation by LPMOs is suppressed by substrate binding, which would imply that the observed LPMO activity is due to a true monooxygenase reaction [33]. Other authors have pointed out that the absence of hydrogen peroxide accumulation in LPMO reactions with substrates shows that in situ produced H_2O_2 is rapidly consumed in a productive peroxygenase reaction [26]. Substrate binding shields the copper site from the solvent, and it is, indeed, conceivable that this prevents LPMOs from generating hydrogen peroxide. Recent experimental work by Filandr et al. [28] lends support to this idea. However, the amount of non-substrate-bound LPMO will vary between different LPMO-substrate combinations. Based on observations that LPMO catalytic domains bind their substrates rather weakly (e.g. [36]), one would expect that typical LPMO reactions contain a significant fraction of free enzymes capable of generating H_2O_2. Furthermore, commonly used low-molecular-weight reductants react with dissolved oxygen leading to LPMO-independent formation of hydrogen peroxide [37–40]. Several recent studies suggest that these non-enzymatic reactions (sometimes referred to as reductant 'auto-oxidation') indeed may be rate-limiting in typical aerobic experiments with AA9 and AA10 LPMOs [28,29,41].

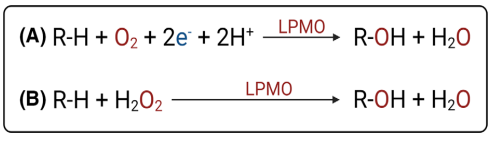

Fig. 1. Monooxygenase (A) and peroxygenase (B) LPMO reaction pathways. For both routes, initial reduction of Cu(II) to Cu(I) is required for the enzyme to enter the catalytic cycle. The figure was created with BioRender (www.biorender.com).

All in all, there is a growing amount of evidence suggesting that LPMO substrate oxidation rates obtained in the absence of exogenously provided H_2O_2 correlate with the rates of hydrogen peroxide production in the reaction [19,29,41,42]. Despite this growing insight, the factors that limit LPMO activity in standard aerobic reactions remain partly unresolved. For example, while it is well known that LPMO activity depends on the type of reductant [43,44], it remains to be established why this is so. Interpretation of existing literature data is complicated by the fact that researchers use quite different reaction conditions, for example strongly varying reductant concentrations and reaction time scales.

Recently, it became clear that LPMOs can play a role in host-pathogen interactions, and may promote microbial infection in both mammals [45] and plants [8]. Thus, characterisation of LPMOs from microbial pathogens is of significant interest. In this paper, we describe *Ssc*LPMO10B, a cellulose-active LPMO from *Streptomyces scabies*, a bacterium that is known for causing damage to potato crops [46]. Next to characterising this enzyme, we used it as a model to study the link between in situ hydrogen peroxide production and substrate oxidation in the presence of three commonly used reductants (ascorbic acid, gallic acid and L-cysteine). The results show a strong dependency of the LPMO catalytic rate on the level of H_2O_2 generation in the system. We have also studied *Ssc*LPMO10B activity in the presence of dehydroascorbic acid (DHA), which is an oxidised derivative of the most commonly used LPMO reductant, ascorbic acid. Since ascorbic acid plays a role in many natural redox

processes, further insight into the fate and functionalities of its oxidised derivatives is of general interest [47]. DHA was recently reported to be able to fuel cellulose oxidation by *Ta*LPMO9A [48], but the mechanism behind this remarkable observation remains unknown. To gain further insight into these matters, we carried out kinetic studies of LPMO reactions and used NMR spectroscopy to analyse the fate of DHA. We show that spontaneous degradation of DHA produces a complex set of redox-active derivatives that promote generation of hydrogen peroxide and fuel enzymatic oxidation of cellulose.

Results and discussion

Identification and cloning of putative LPMO genes

The *S. scabies* genome (strain 87.22, GenBank accession number NC_013929.1) was submitted to the dbCAN2 server for automated annotation of hypothetical LPMO genes. The in silico mining revealed four open reading frames encoding for putative LPMOs, all belonging to AA10 family (Figure 2) and referred to as *Ssc* LPMO10A, *Ssc*LPMO10B, *Ssc*LPMO10C and *Ssc*LP MO10D below (GenBank accession numbers WP_106437244.1, WP_173402964.1, WP_013003332.1 and WP_013006341.1, correspondingly). MMseqs2 searches [49] against the PDB database [50] identified *Sc*LPMO10C (cellulose-active C1-oxidizing LPMO) [2], *Sli*LPMO10E (chitin-active C1-oxidizing LPMO) [51] and *Kp*LPMO10A (cellulose- and chitin-active C1/C4-oxidising LPMO) [52] as the closest structurally characterised homologues of *Ssc*LPMO10B, *Ssc*LPMO10C and *Ssc*LPMO10D (56%, 79% and 58% sequence identity between catalytic domains), respectively. The closest structurally characterised homologue of *Ssc*LPMO10A is Tma12, an unusual (i.e. non-bacterial) AA10 chitinolytic LPMO from the fern *Tectaria macrodonta* (47% sequence identity between catalytic domains) [53]. *Ssc*LPMO10A lacks a signal peptide, which, considering the crucial role of Histidine 1 in correctly processed LPMOs, is remarkable. This protein also contains a predicted transmembrane segment, localised within an extensive C-terminal region of unknown function (Figure 2).

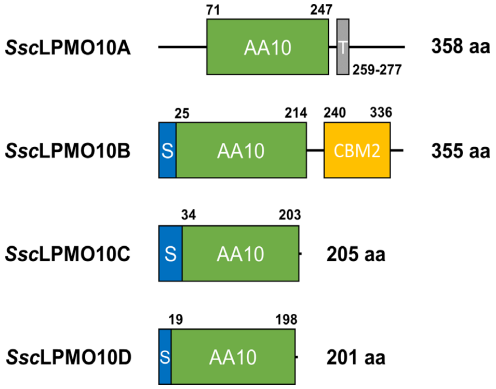

Fig. 2. Domain architecture of putative family 10 LPMOs encoded in the *Streptomyces scabies* genome. S, signal peptide; AA10, catalytic domain; T, transmembrane segment; CBM2, family 2 cellulose-binding module. Note that the native signal peptides (shown in the figure) were substituted by the *Sm*LPMO10A (CBP21) signal peptide in the enzymes produced in this study.

On the other hand, *Ssc*LPMO10B, *Ssc*LPMO10C and *Ssc*LPMO10D have domain architectures (Figure 2) that are common for secreted bacterial LPMOs. The three corresponding sequences were codon optimised for expression in *Escherichia coli* and modified to encode for the *Sm*LPMO10A signal peptide instead of native periplasmic localisation signals, after which the genes were synthesised and cloned into the pET-26(b)+ expression vector.

Production of *Ssc*LPMO10B and characterisation of LPMO activity

SDS-PAGE analysis of periplasmic extracts and whole-cell samples obtained from *E. coli* strains expressing LPMO candidate genes revealed that *Ssc*LPMO10C and *Ssc*LPMO10D accumulated in the cytoplasm in an insoluble form, while *Ssc*LPMO10B was soluble and exported. The latter enzyme was purified from a periplasmic extract by ion-exchange and size-exclusion chromatography (Figure S1) and subjected to copper saturation and desalting. The removal of free copper by desalting was confirmed using a previously described procedure [41] (Figure S2).

The substrate specificity of *Ssc*LPMO10B was assessed by setting up 24-h reactions containing 0.5 μM copper-loaded LPMO, 1 mM ascorbic acid and various carbohydrates, including 1% (w/v) Avicel, 0.5% (w/v) PASC, 1% (w/v) CMC, 1% (w/v) β-chitin, 0.5% (w/v) beechwood xylan, 0.5% (w/v) konjac glucomannan, 0.5% (w/v) tamarind xyloglucan, 0.5% (w/v) wheat arabinoxylan and 500 μM D-(+)-cellohexaose. HPAEC-PAD analysis of reaction mixtures showed product formation in the reactions with cellulosic substrates only (Avicel, PASC and the soluble cellulose derivative CMC; Figure 3). The chromatograms showed multiple C1-oxidised products, whereas signals corresponding to C4-oxidised products were not observed.

MALDI-TOF MS analysis of products generated from Avicel (Figure 4) gave a spectrum that is typical

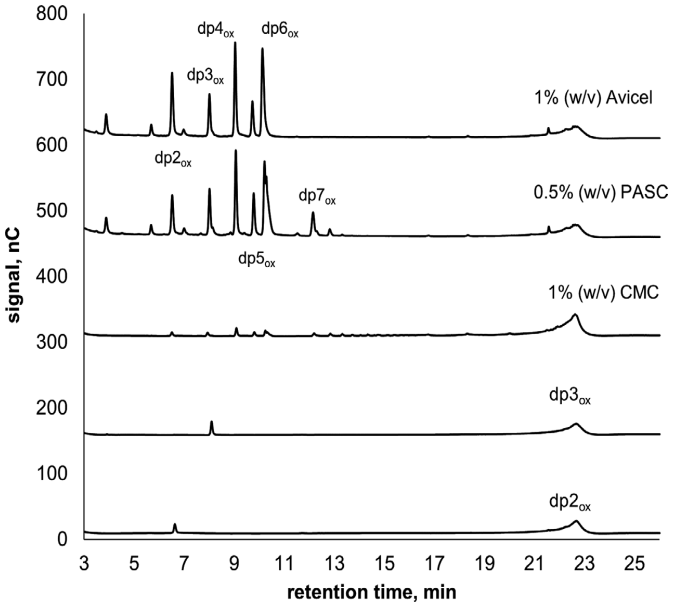

Fig. 3. Activity of *Ssc*LPMO10B on cellulosic substrates. The figure shows chromatograms of soluble oxidised products released by 0.5 μM *Ssc*LPMO10B from 1% (w/v) Avicel, 0.5% (w/v) PASC or 1% (w/v) CMC after 24 h of incubation at 30°C in 50 mM sodium phosphate buffer, pH 6.0 containing 1 mM ascorbic acid. C1-oxidised cello-oligosaccharides with various degrees of polymerisation (2-7) are designated as $dp2_{ox}$-$dp7_{ox}$. Product formation was not observed in control reactions lacking the enzyme or lacking the reductant. Products from the reaction with CMC could not be identified due to unavailability of carboxymethylated standards.

for strictly C1-oxidising LPMOs, with a clear signal for the sodium salt of the aldonic acid and absence of signals for double oxidised products, which could have emerged if the enzyme had been C1/C4-oxidising.

Avicel oxidation by *Ssc*LPMO10B in the presence of various reductants

Next, we compared the capacity of various reducing compounds to fuel Avicel solubilisation by *Ssc* LPMO10B. The experiment featured three commonly used LPMO reductants (ascorbic acid, gallic acid and L-cysteine) as well as DHA – an oxidised derivative of ascorbic acid, recently reported to drive cellulose oxidation by a AA9 LPMO [48].

The use of ascorbic acid and gallic acid in reactions with *Ssc*LPMO10B and Avicel, resulted in slow, but steady oxidation of cellulose over 24 h (Figure 5A). The rates obtained with 1 mM ascorbic acid and 1 mM gallic acid amounted to approximately 0.12 min^{-1} and 0.25 min^{-1}, respectively. Such excessively low catalytic rates are common among AA10 bacterial LPMOs operating under 'monooxygenase conditions' [26,41] and it has been claimed that they reflect the rate of hydrogen peroxide production in the reaction mixture [41].

The reaction with 1 mM L-cysteine displayed a much faster rate (≈1.3 min^{-1}), compared to the experiments with gallic acid and ascorbic acid, but product formation diminished early on in the reaction (after approximately 1 h; Figure 5B). The observed decrease in reaction rate over time can be explained by low reductant stability or by LPMO inactivation, which may occur if too much hydrogen peroxide is being generated in the reaction mixture [24,54] (see below).

Importantly, the experiment with 1 mM DHA confirmed that this oxidised derivative of ascorbic acid can, indeed, drive LPMO reactions with cellulose, not only for fungal AA9s [48] but also for bacterial AA10s (Figure 5A). The rate of DHA-fuelled substrate oxidation amounted to approximately 0.32 min^{-1}, meaning that the reaction with DHA outperformed the reactions with gallic acid and ascorbic acid. The variation in reductant efficiency is addressed further below.

Hydrogen peroxide production in the presence of various reductants

Our next goal was to test whether the reductant-dependent differences in catalytic rates on Avicel could be correlated to variation in the rate of in situ hydrogen peroxide production in the reactions. The results of HRP/Amplex Red experiments (Figure 6) revealed that the H_2O_2 production capacity of LPMO reactions indeed strongly depends on the nature of the reducing compound used to sustain the reactions. The highest hydrogen peroxide generation rate was observed in the presence of L-cysteine, whereas the experiment with DHA resulted in the lowest H_2O_2 accumulation rate.

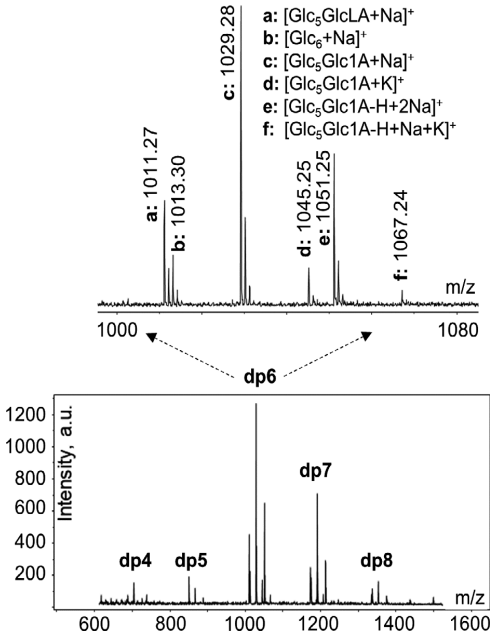

Fig. 4. MALDI-TOF analysis of Avicel depolymerisation by *Ssc*LPMO10B. The figure shows MS signals corresponding to LPMO products within the dp4–dp8 range, released after a 24-h reaction with 1% (v/w) Avicel, 0.5 μM enzyme and 1 mM ascorbic acid. Dp, degree of polymerization. Oxidised and native products were observed as sodium or potassium adducts and/or as sodium adducts of sodium and potassium salts, as indicated (Glc, glucose; Glc1A, gluconic acid; GlcLA, lactone). Substrate degradation did not occur in control reactions lacking the enzyme or lacking the reductant. The experiments were conducted at 30°C in 50 mM Bis-Tris, pH 6.0.

As alluded to above, hydrogen peroxide production in these reactions is a result of both LPMO-dependent and LPMO-independent oxidation of the reductant. Figure 6 shows that the LPMO contribution to the overall hydrogen peroxide production was considerable in the reactions with ascorbic acid and, particularly, L-cysteine. On the other hand, the LPMO did not promote apparent H_2O_2 production in the reactions with gallic acid and DHA. In the case of gallic acid, the LPMO even, seemingly, inhibited H_2O_2 production, which is likely due to a previously observed side reaction in which the LPMO oxidises gallic acid (or gallic acid derivatives) using H_2O_2 [41,55]. Such side reactions are likely to become pronounced in the absence of proper LPMO substrates (i.e. the conditions of HRP/Amplex Red assay).

Taken together, the hydrogen peroxide production data (Figure 6) and the substrate oxidation data (Figure 5) obtained with ascorbic acid, gallic acid and L-cysteine indicate that the *Ssc*LPMO10B catalytic rate correlates with the rate of H_2O_2 production in the reaction mixture. Very fast generation of H_2O_2 in the reaction with L-cysteine may explain why the LPMO reaction was so fast and why enzyme inactivation was observed (Figure 5B). Comparison of the rates estimated from the datasets depicted in Figures 5 and 6 shows that the product release rate (Figure 5) is 2–2.5 times lower than the hydrogen peroxide generation rate (Figure 6). This lack of stoichiometry is not surprising, considering that the presence of substrate will reduce the degree of LPMO-dependent H_2O_2 generation ([28,31]; see below for more discussion). Furthermore, only solubilised oxidised products were

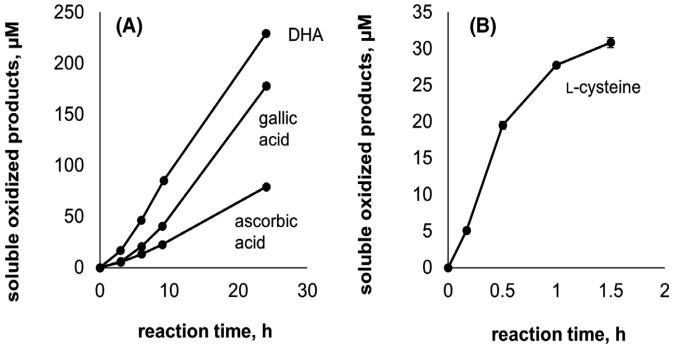

Fig. 5. Time course of Avicel solubilisation by *Ssc*LPMO10B in the presence of various reductants. The figure shows the release of oxidised products in LPMO reactions (0.5 μM *Ssc*LPMO10B in 50 mM sodium phosphate buffer, pH 6.0, 30°C) with 1% (w/v) Avicel that were carried out using 1 mM varying reductants. Error bars indicate standard deviations between triplicates and are in most cases hidden by the markers. Product accumulation was not observed in control reactions with only substrate and reductants. Note that the reaction mixtures with gallic acid and DHA contained 1% (v/v) DMSO.

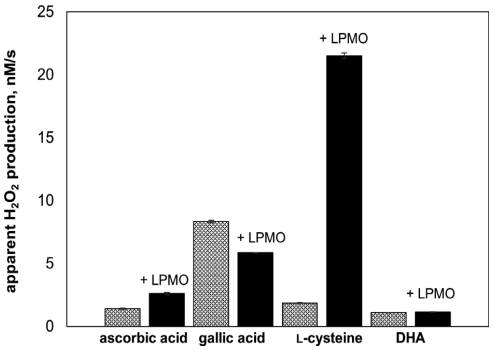

Fig. 6. Hydrogen peroxide production by *Ssc*LPMO10B in the presence of various reductants. The figure shows apparent hydrogen peroxide accumulation rates obtained in reactions with 0.5 μM LPMO and 1 mM reductant (black bars) or in reactions lacking the enzyme (grey bars). All experiments were carried out in 50 mM sodium phosphate buffer, pH 6.0, at 30°C. Reaction mixtures contained 5 U/ml HRP, 100 μM Amplex Red and 1% (v/v) DMSO (experiments with ascorbic acid and L-cysteine) or 5 U/ml HRP, 100 μM Amplex Red and 2% (v/v) DMSO (experiments with gallic acid and DHA). The rates were derived from linear progress curves. Error bars indicate standard deviations between triplicates.

quantified, while oxidised sites on the remaining insoluble substrate were not assessed. Of note, previous studies with *Sc*LPMO10C, which has a similar two-domain structure as *Ssc*LPMO10B (Figure 2), suggest that under the assay conditions used here, the majority of the oxidised products will be soluble [18].

Strikingly, while the experiments with the other reductants support the idea that LPMO activity under 'monooxygenase conditions' reflects an H_2O_2-limited peroxygenase reaction, the results obtained with DHA point in a different direction. The DHA-fuelled LPMO reaction with Avicel resulted in a fast product release (second only to the reaction with L-cysteine; Figure 5A), while the amount of hydrogen peroxide produced in the presence of DHA was the lowest among the reducing compounds used in this study (Figure 6). The impact of DHA on LPMO activity is addressed in the detail below.

Avicel oxidation by *Ssc*LPMO10B in the presence of exogenous hydrogen peroxide and DHA

To investigate the role of hydrogen peroxide in DHA-driven LPMO reactions, we analysed Avicel depolymerisation by *Ssc*LPMO10B in the presence of exogenously supplied H_2O_2 and either DHA or ascorbic acid (Figure 7A). The addition of hydrogen peroxide to the LPMO reaction with ascorbic acid resulted in an (expected) drastic increase in the product formation rate (≈5.6 min^{-1}) compared to the rate obtained at standard aerobic conditions (≈0.12 min^{-1}). The progress curve shows that product formation diminished after a fast and linear initial phase. This is indicative of enzyme inactivation, which is to be expected in experiments with high amounts of added H_2O_2 [24,56,57].

Strikingly, the impact of adding H_2O_2 to a reaction with DHA was minimal, leading to a substrate oxidation rate (≈0.86 min^{-1}) that was only a little higher than the rate observed in the absence of H_2O_2 (≈0.32 min^{-1}) and much lower than the rate observed in the reaction with H_2O_2 and ascorbic acid (Figure 7A). This observation suggests that, in contrast to ascorbic acid, DHA is not an efficient reductant for the LPMO, which is a prerequisite for the peroxygenase reaction to happen. This conclusion, however, is in stark contrast with the observation that DHA outperforms ascorbic acid under 'monooxygenase conditions'(Figure 5A). One might even wonder whether the results with DHA indicate that *Ssc*LPMO10B is a true monooxygenase (so, not dependent on H_2O_2 formation) or whether DHA perhaps facilitates another, hitherto unresolved catalytic mechanism. Interestingly, Brander et al. [48] recently showed that DHA is able to promote the oxidation of reduced phenolphthalein by an AA9 LPMO in the absence of both oxygen and hydrogen peroxide, which could be taken to suggest that LPMOs catalyse a hitherto unknown reaction.

Looking for possible explanations, we first considered the possibility that DHA may engage in a rapid side reaction with H_2O_2, thus scavenging the co-substrate. A control reaction with added H_2O_2 in the presence of both ascorbic acid and DHA (Figure 7B) yielded a progress curve very similar to that obtained in the experiment with H_2O_2 and only ascorbic acid, which shows that hydrogen peroxide scavenging by DHA was negligible.

We then considered whether an unknown DHA derivative (e.g. a product resulting from spontaneous hydrolysis), rather than DHA itself, could reduce the LPMO and fuel the LPMO reaction. If this would be the case and if the hypothetical DHA derivative would accumulate in LPMO reactions at a relatively slow rate, then one could expect DHA to not work well in the experiments with H_2O_2 (Figure 7A) due to a short overall incubation time. On the other hand, the *Ssc*LPMO10B reactions carried out at standard aerobic conditions (Figure 5A) were incubated for 24 h, potentially allowing for significant amounts of a hypothetical DHA derivative to be formed.

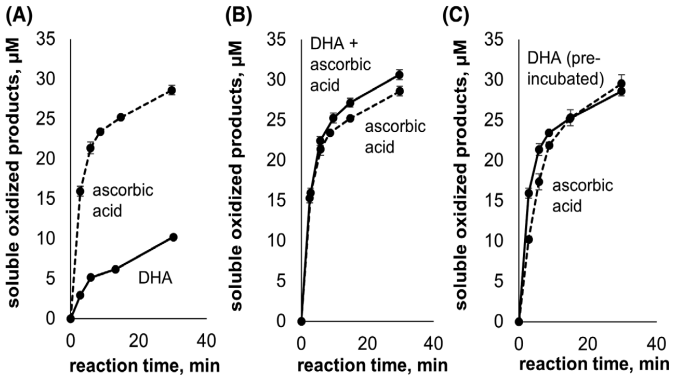

Fig. 7. Time course of Avicel solubilisation by *Ssc*LPMO10B in the presence of various reductants and hydrogen peroxide. The figure shows the accumulation of soluble oxidized products in LPMO reactions (1 μM *Ssc*LPMO10B in 50 mM sodium phosphate buffer, pH 6.0, 30°C, supplied with 100 μM H_2O_2) with 1% (w/v) Avicel. Panel A shows reactions fuelled by 1 mM ascorbic acid or 1 mM DHA, whereas panels B and C show LPMO activity in the presence of a mixture of 1 mM ascorbic acid and 1 mM DHA (B) or in the presence of 1 mM DHA that had been pre-incubated for 6 h prior to addition of the enzyme and hydrogen peroxide (C). Error bars indicate standard deviations between triplicates. The progress curves for the reaction with 1 mM ascorbic acid (dotted lines in panels A, B and C) represent the same experiment. Product accumulation was not observed in control reactions with substrate, reductant and H_2O_2. The reaction mixtures featuring DHA contained 1% (v/v) DMSO.

To test this simple but speculative explanation, the Avicel degradation experiment was conducted again, this time using 1 mM DHA that had been pre-incubated with Avicel in reaction buffer at 30°C for 6 h, prior to addition of the enzyme and hydrogen peroxide. Surprisingly, the rate of the DHA-fuelled peroxygenase reaction dramatically increased when using the pre-incubated reductant (Figure 7C), matching the rate obtained in the reaction with H_2O_2 and ascorbic acid. This observation suggests that, indeed, an unidentified slowly accumulating DHA derivative (or multiple derivatives) can reduce the LPMO. This may explain why DHA works well in the 24-h standard reactions depicted in Figure 5A, whereas DHA performs poorly in the 30-min reactions depicted in Figure 7A.

Importantly, these observations regarding DHA stability can also explain the discrepancy between the very low apparent rates of H_2O_2 production observed in the presence of DHA (Figure 6) and the efficiency of DHA under 'monooxygenase conditions' (Figure 5A). Next to the difference in time scale, complications of the HRP/Amplex Red assay may play a role. It is well established that reductants may, to varying extents, interfere with the HRP/Amplex Red assay signal, leading to underestimation of hydrogen peroxide levels [29,41,58]. This can to some extent be handled by adding reductants to the standard curves for H_2O_2, as we did in this study. For unstable DHA, the situation is problematic because signal repression will change over time and the compounds involved are unknown (and possibly transient; see below). It is thus possible that the H_2O_2 production levels observed in the presence of DHA are underestimated.

Monitoring H_2O_2 production by *Ssc*LPMO10B in the presence of DHA using selective fluorescent probe

Given the limitations of the standard HRP/Amplex Red assay discussed above, we evaluated Peroxy Orange 1 (PO1, a boron-based fluorescent H_2O_2 probe [59]) as a new tool to monitor the hydrogen peroxide production in LPMO reactions. PO1 is irreversibly activated by the nucleophilic addition of hydrogen peroxide to the boron atom, resulting in formation of unstable borate ester, which undergoes spontaneous hydrolysis to yield a highly fluorescent stable product [60]. This approach allowed monitoring of H_2O_2 production over a time scale that is comparable to that of the reactions with cellulose. First, we carried out a simple reaction with 25 μM PO1 and 25 μM H_2O_2, confirming that the probe can be used to detect hydrogen peroxide under LPMO reaction conditions (Figure S3). Note that relatively low PO1 concentration was used to avoid a precipitation of the probe, which has limited solubility in water [60]. Next, 25 μM PO1 was introduced to the reaction mixture containing 1 mM DHA (Figure 8), leading to a significant increase of the fluorescence over time, compared to a

control reaction with only PO1. Importantly, when 1 μM *Ssc*LPMO10B was added to the system alongside DHA, the fluorescence increased even further (Figure 8).

To confirm that the observed PO1-derived fluorescence was indeed due to the accumulation of hydrogen peroxide, a control experiment was carried out using catalase, which can compete with LPMOs for H_2O_2 when applied at sufficiently high concentrations [28]. As expected, addition of catalase repressed H_2O_2 generation both in reactions with DHA alone and in reactions with LPMO and DHA (Figure 8). Quantitative interpretation of fluorescence data obtained with PO1 is complicated by the fact that the probe activation is exceedingly slow (Figure S3), meaning that the assay signal will be affected by potential side reactions that can occur with H_2O_2 in the presence of DHA and LPMO. Nevertheless, Figure 8 clearly shows that hydrogen peroxide is produced in a DHA-dependent manner.

Finally, to prove that DHA-fuelled reactions of *Ssc*LPMO10B with cellulose depend on in situ produced H_2O_2 under standard aerobic conditions, an inhibition experiment was performed in the presence of Avicel and catalase. As shown in Figure 9, catalase inhibited *Ssc*LPMO10B activity, confirming that the apparent monooxygenase reaction in the presence of DHA indeed is an H_2O_2-dependent peroxygenase reaction.

The accumulation of DHA derivatives in the presence and absence of LPMO

It has previously been demonstrated that DHA spontaneously converts to 2,3-diketo-L-gulonic acid (DKG) [61–63] in aqueous solutions. DKG is known to undergo additional transformations in solution giving rise to various compounds, some of which are known to be redox-active [64,65]. Importantly, one such DKG derivative (called 'compound 1') has been isolated by HPLC and shown to be capable of inducing non-enzymatic hydrogen peroxide production, which is a relevant feature in the context of LPMO catalysis [64]. Based on characterisation of compound 1 by electrospray mass spectrometry, Kärkönen et al. proposed the formula $C_6H_6O_5$, suggesting that compound 1 has a higher reduction state than DKG ($C_6H_8O_7$) [64]. While the mechanism by which compound 1 is generated remains unclear, its formation likely results from a redox reaction involving DKG and one of the multiple potential products of spontaneous DHA hydrolysis. Interestingly, a hypothetical chemical structure of compound 1 proposed by Kärkönen et al. [64] shows some resemblance to ascorbic acid ($C_6H_8O_6$; Figure 10). The structural similarity between these two molecules is supported by the fact that ascorbate oxidase is able to recognise compound 1 as a substrate [64]. In view of these data, it seems feasible that, like ascorbic acid [66], compound 1 can interact with the LPMO active site and reduce it.

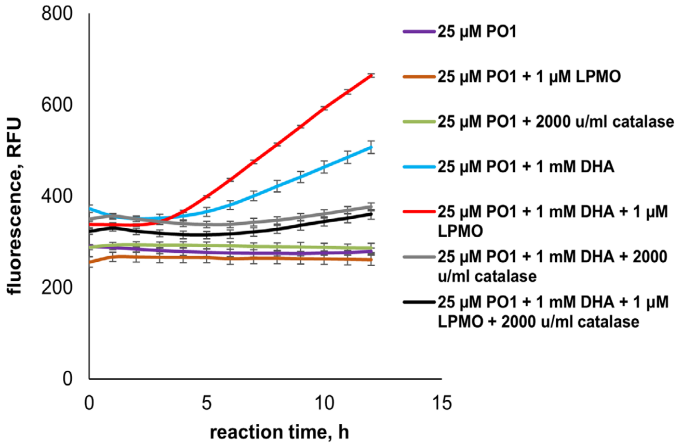

Fig. 8. H_2O_2 production by *Ssc*LPMO10B in the presence of DHA. The figure shows the generation of hydrogen peroxide in reactions containing 1 mM DHA and 1 μM SscLPMO10B or 1 mM DHA alone. Note that the addition of LPMO to DHA solution significantly promoted H_2O_2 formation. The experiments were carried out using 25 μM PO1 (Ex/Em = 540/560 nm) in 50 mM sodium phosphate buffer, pH 6.0, at 30°C. Reaction mixtures supplied with DHA contained 1.5% (v/v) DMSO, whereas reaction mixtures lacking DHA contained 0.5% (v/v) DMSO. Error bars indicate standard deviation between triplicates.

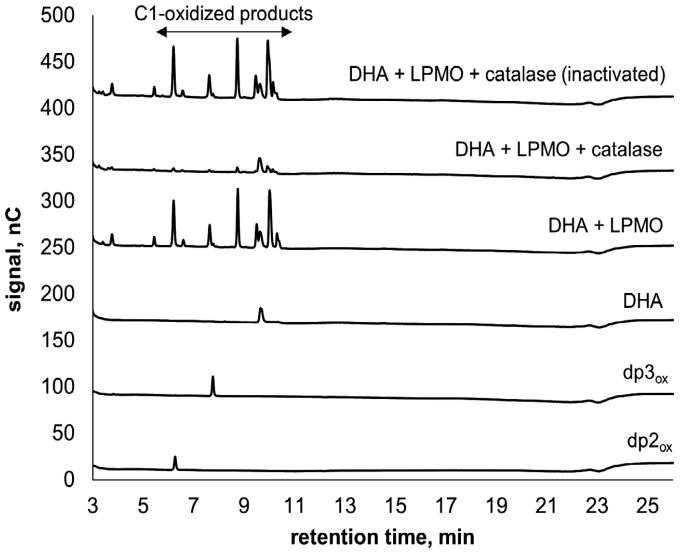

Fig. 9. Inhibition of *Ssc*LPMO10B by catalase in reactions with DHA. The figure shows HPAEC-PAD chromatograms of reaction mixtures containing 1 mM DHA, 1% (w/v) Avicel and 0.5 μM LPMO, with or without catalase. The reactions were carried out using 50 mM sodium phosphate buffer, pH 6.0, and were incubated at 30°C for 9 h. The graphs show that the addition of 2000 U/ml catalase resulted in almost complete suppression of *Ssc*LPMO10B activity, whereas the addition of the same amount of heat-inactivated catalase (20 min pre-incubation at + 100°C) did not affect the LPMO reaction. The figure includes chromatograms for a control reaction mixture containing Avicel and DHA and lacking LPMO and catalase (marked 'DHA'), and chromatograms of GlcGlc1A ($dp2_{ox}$) and GlcGlcGlc1A ($dp3_{ox}$) standards.

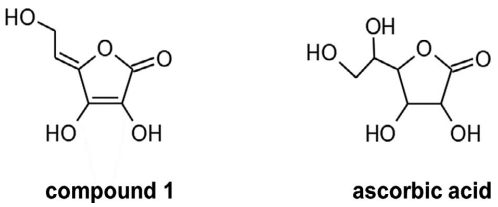

Fig. 10. Hypothetical structure of compound 1 [64].

UV-VIS spectroscopy of DHA under standard aerobic LPMO reaction conditions (1 mM DHA, 1% Avicel, no LPMO, pH 6.0) revealed the formation of a pronounced new peak with an absorbance maximum at 268 nm (Figure 11A). This value is very close to the λ_{max} (271–272 nm) previously reported for compound 1 at mildly acid conditions (pH 5.6) [64]. The peak area increased over time with a concomitant shift in the λ_{max} (from 268 nm to 285 nm). This notable shift in λ_{max} over time suggests the formation of additional DHA derivatives. To rule out the possibility that the observed accumulation of DHA derivatives was driven by Avicel or potential contaminations in the Avicel, a control UV-VIS experiment was carried out in the absence of cellulose, showing that the cellulose did not affect the formation of UV-absorbing species and did not affect the shift in λ_{max} over time (Figure S4). A similar reaction conducted in the presence of both Avicel and LPMO (Figure 11B) gave remarkably lower UV absorption signals after 24 h, lending support to the notion that DHA-derived compounds (or their hypothetical precursors) are involved in LPMO catalysis.

Somewhat surprisingly, a control experiment with DHA and LPMO in the absence of substrate showed even lower UV signals (Figure 11B). While we cannot explain why this is the case, there are plausible explanations, one being that in the absence of a bona fide substrate the LPMO may catalyse H_2O_2-dependent oxidation of one or more of the DHA-derived compounds, analogous to findings by Breslmayr et al. [55]. It is also possible that in the absence of substrate, H_2O_2 production is elevated [28] and that the produced H_2O_2 reacts directly with DHA-derived redox active compounds. Overall, the results described above support the idea that DHA decomposition involves the formation of reducing species that can drive LPMO action on cellulosic substrates.

To get more insight in the chemistry of DHA and ascorbic acid conversion, we monitored the transformation of these compounds by NMR spectroscopy. Using

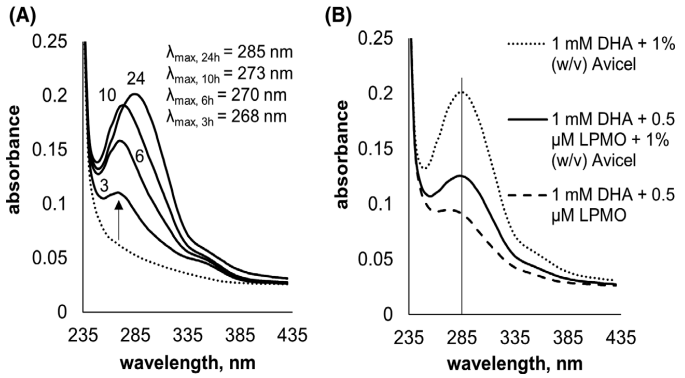

Fig. 11. UV-VIS spectroscopy of reaction mixtures containing DHA. Panel A shows UV-VIS spectra of 1 mM DHA incubated with 1% (w/v) Avicel for 3, 6, 10 and 24 h at standard LPMO reaction conditions (50 mM sodium phosphate buffer, pH 6.0, 30°C). The dotted line is the spectrum of DHA solution at the beginning of experiment. Panel B shows UV-VIS spectra of the same type of reaction mixtures containing the indicated combinations of DHA, LPMO and substrate, after incubation for 24 h. All experiments were carried out in triplicates; the figure shows average absorbance values.

NMR allowed direct observation of the main compounds generated in situ, with high temporal resolution. This contrasts with previous studies on the fate of ascorbic acid and DHA, which were largely based on electrophoretic separation of compounds prior to analysis [64,67]. Firstly, partial assignment of ascorbic acid, DHA and DKG was performed using 10 mM ascorbic acid and DHA solutions. C-H spin pairs were assigned using ^{13}C-HSQC spectra (Figure S5), and ^{13}C-HSQC-[^{1}H-^{1}H]-TOCSY correlations were used to establish connectivity. Attempts to assign the quaternary carbons using HMBC correlations were not successful. Nevertheless, the assignment for ascorbic acid fits previously published assignments (Biological Magnetic Resonance Data Bank entry bmse000182; www.bmrb.io), whereas the assignments for DHA and DKG fit the chemical shifts predicted by an empirical neural-network algorithm provided by the NMRShiftDB server (https://nmrshiftdb.nmr.uni-koeln.de/nmrshiftdb/). DHA is known to exist as a single ring or in a bicyclic form. The high chemical shift for the methylene C6 (78.7 ppm) indicates that the bicyclic form of DHA is the only one visible in our NMR experiments. This is an expected observation, as bicyclic DHA is known to be the dominant DHA form [67]. For the single ring form of DHA, a lower chemical shift (around 62 ppm) for the methylene C6 is to be expected.

Next, based on the assigned chemical shifts, we recorded and analysed NMR spectra of 1 mM DHA solution in 50 mM sodium phosphate buffer, pH 6.0 supplied with 1% (w/v) Avicel in the presence or absence of 0.5 µM LPMO. The NMR analysis clearly showed that the conversion of DHA to DKG was not affected by the presence of the enzyme (Figure 12A,B), indicating that both DHA and DKG are not directly involved in LPMO reduction. Although the UV-VIS data (Figure 11A) clearly showed that further conversion of DKG takes place under these conditions, we did not detect NMR signals corresponding to compound 1 or other DHA derivatives in any of the reactions. This is likely due to the low sensitivity of NMR, which implies that compounds would only be visible at concentrations above ~0.1 mM.

For comparison, the NMR experiment was repeated using ascorbic acid as an electron donor. In contrast to the observations with DHA, the rate of ascorbate consumption increased upon the addition of LPMO (Figure 12C), which is to be expected, considering that this compound can reduce the LPMO directly [66]. The experiment further showed that, as expected, ascorbic acid oxidation resulted in the generation of DHA and DKG (Figure 12D,E). It is not clear from our data to what extent DHA derivatives contribute to enzyme reduction and H_2O_2 production in typical LPMO reactions containing ascorbic acid at high (≥1 mM) concentration. However, it seems reasonable to assume that DHA-related effects could have noticeable impact in certain experiments, for example experiments that involve low amounts of ascorbic acid that will become depleted during prolonged incubation times.

Concluding remarks

Taken together, our experiments with *Ssc*LPMO10B and four different reductants under conditions referred

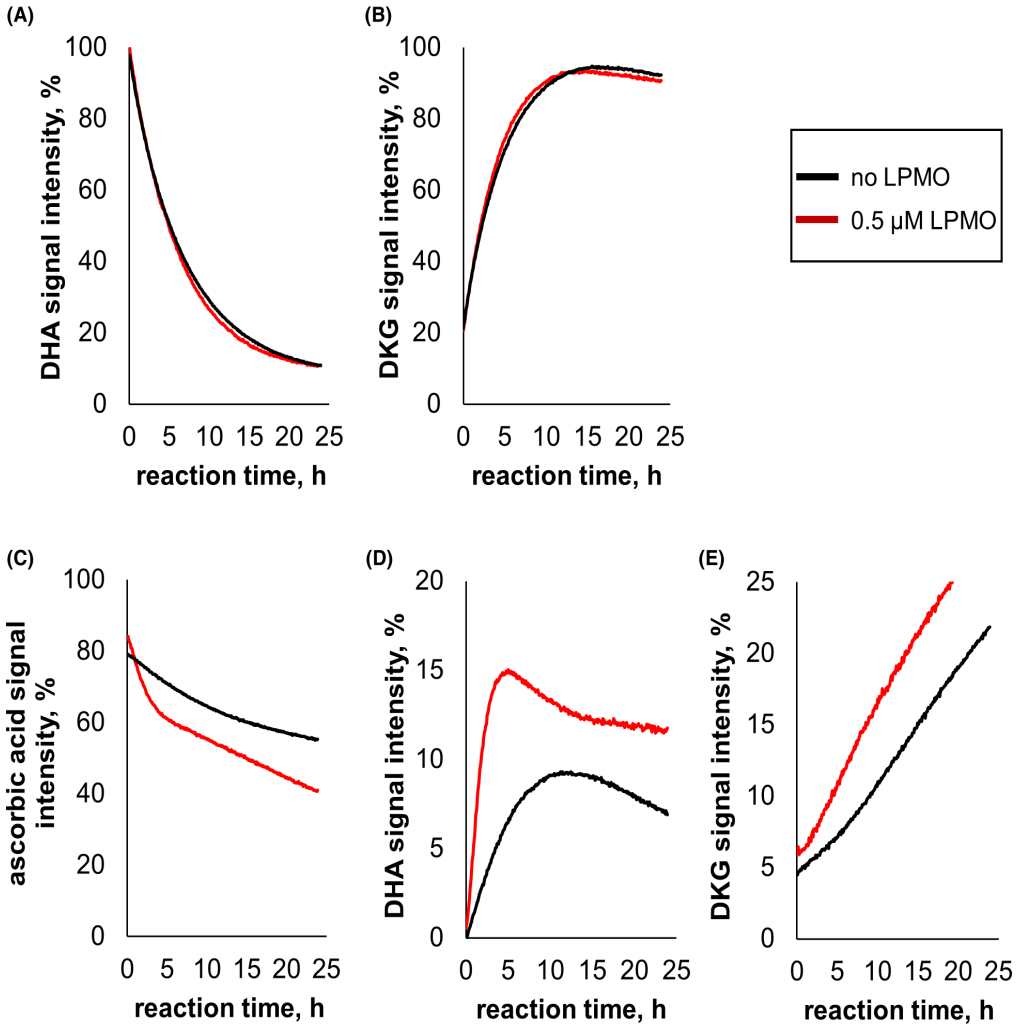

Fig. 12. Time courses of (A) DHA conversion to (B) DKG, and (C) ascorbic acid conversion to (D) DHA and (E) DKG. All experiments were carried out at 30°C in 50 mM sodium phosphate buffer, pH 6.0 prepared in D_2O (D, 99.9%) and supplied with 1% (w/v) Avicel. The reactions containing 0.5 μM LPMO are marked with red colour, whereas the reactions lacking the enzyme are marked with black colour. The signal intensity % in the plots corresponds to integrals in pseudo-2D NMR spectra recorded over 24 h. To facilitate comparison across experiments, all signals were normalised to the DHA signal at the beginning of the reaction for the sample with 0.5 μM SscLPMO10B and 1% (w/v) Avicel (red curve in panel A).

to here as 'standard aerobic reactions' or 'monooxygenase conditions' show that the LPMO catalytic rate depends on the level of in situ hydrogen peroxide production. This study adds to a growing amount of evidence in support of the notion that slow apparent monooxygenase LPMO reactions in fact are peroxygenase reactions, limited by endogenous H_2O_2 supply. It seems clear by now that the impact of the reductant on LPMO activity, which is as such remarkable since reduction of LPMOs is much faster than the apparent monooxygenase reaction [24,43], relates to H_2O_2 production and not to LPMO reduction.

The results of the hydrogen peroxide assays should be interpreted with caution. It is well established that reductants interfere with the HRP/Amplex Red assay signal, for example by reducing Amplex Red radicals back to Amplex Red, leading to reduced resorufin formation and, thus, underestimation of hydrogen

peroxide levels [29,41,58]. While the reductant-mediated repression of the HRP/Amplex Red assay signal can be accounted for when using a well-defined reductant, this cannot be applied to reactions containing DHA, which, as a result of spontaneous DHA conversion, contain unknown amounts of unknown reductants that change over time. When it comes to quantitatively correlating H_2O_2 production levels to LPMO activity, another complication comes from the fact that the presence of substrate at LPMO turnover conditions will reduce LPMO-dependent H_2O_2 production [28,31,35,58]. Indeed, recent data indicate that the substrate oxidation rates of bacterial LPMOs show a surprisingly low dependency on the LPMO concentration [28,29,41], which supports the notion that the reaction is limited by the co-substrate and that LPMO-dependent in situ generation of the co-substrate is hampered by substrate binding. While we are not able to quantitatively link H_2O_2 production levels by a particular LPMO-reductant combination to the rate of cellulose degradation, the results depicted in Figures 5 and 6 show a clear correlation between the two.

Ascorbic acid is an abundant compound in nature that has been studied in multiple contexts [68,69]. In that sense, our findings with DHA not only shed light on an unusual LPMO-activating compound but may also have implications for other redox processes involving ascorbic acid. Our LPMO studies show that, rather than reducing the enzyme directly, DHA is spontaneously converted into a variety of derivatives including at least one that can act as an electron donor for LPMOs and that can promote H_2O_2 production. We were not able to quantitatively assess the H_2O_2 production potential of this mixture due to the limitations of the HRP/Amplex red assay that are discussed above; however, our experiments with the PO1 probe confirm that hydrogen peroxide generation is taking place in the presence of DHA. Furthermore, it is clear that the LPMO catalytic rate in reactions with DHA is limited by H_2O_2 produced in situ, as demonstrated by the catalase inhibition experiment. There is no reason to assume that a DHA-driven reaction is mechanistically different from, for example an ascorbic acid-driven reaction.

Methods

Materials

Chemicals were purchased from Sigma-Aldrich (St. Louis, MO, USA) unless stated otherwise. Amplex Red was obtained from Thermo Fisher Scientific (Waltham, MA, USA). A stock solution containing 10 mM Amplex Red was prepared in DMSO and stored at −20°C in light-protected tubes. Ascorbic acid was stored at −20°C as filter-sterilised (0.22-μm syringe filter) 100 mM stock solution in metal-free TraceSELECT water (Honeywell, Charlotte, NC, USA). Gallic acid and DHA were stored at −20°C as filter-sterilised (0.22-μm syringe filter) 100 mM stock solutions in DMSO. The reductant solutions were aliquoted and used only once. Fresh L-cysteine stock solutions were prepared immediately prior to experiments by dissolving the compound in metal-free TraceSELECT water at 100 mM concentration. These solutions were filtered through a 0.22-μm syringe filter and used only once. Horseradish peroxidase type II (HRP; Sigma-Aldrich, St. Louis, MO, USA) was stored in 50 mM sodium phosphate buffer, pH 6.0 at 4°C (at 100 U/ml concentration). Bovine liver catalase (Sigma-Aldrich, St. Louis, MO, USA) was stored in 50 mM sodium phosphate buffer, pH 6.0 at 4°C (at 9500 U/ml concentration). Peroxy Orange 1 (PO1) was stored at −20°C as 5 mM stock solution in DMSO. Tryptone and yeast extract were from Thermo Fisher Scientific (Waltham, MA, USA). The model microcrystalline cellulose used in the study was Avicel PH-101. Phosphoric acid swollen cellulose (PASC) was produced from Avicel as described before [70]. Carboxymethyl cellulose (CMC) was stored as 2% (w/v) solution in 50 mM sodium phosphate buffer, pH 6.0. Beechwood xylan, konjac glucomannan, tamarind xyloglucan and wheat arabinoxylan were obtained from Megazymes (Bray, Ireland). β-Chitin extracted from squid pen was purchased from France Chitin (Orange, France).

Identification and cloning of LPMO genes

The publicly available *S. scabies* genome (strain 87.22, GenBank accession number NC_013929.1) was mined for hypothetical LPMO encoding sequences using the dbCAN2 server (http://bcb.unl.edu/dbCAN2/) [71]. Putative signal peptides and transmembrane helixes were predicted using the SignalP-5.0 (http://www.cbs.dtu.dk/services/SignalP/) [72] and TMpred (https://embnet.vital-it.ch/software/TMPRED_form.html) servers, respectively. Four open reading frames were found to encode hypothetical AA10 LPMOs (GenBank accession numbers WP_106437244.1, WP_173402964.1, WP_013003332.1 and WP_013006341.1) that are referred to as *Ssc*LPMO10A, *Ssc*LPMO10B, *Ssc*LPMO10C and *Ssc*LPMO10D, respectively.

The *Ssc*LPMO10B, *Ssc*LPMO10C and *Ssc*LPMO10D full-length sequences (including stop codons) were codon optimised for expression in *E. coli* and modified to encode for the *Sm*LPMO10A (CBP21) [1] periplasmic localisation signal ('MNKTSRTLLSLGLLSAAMFGVSQQANA') instead of native signal peptides. Due to this set-up the C-terminal His-tag encoded by the vector was not included in the expressed proteins. The corresponding genes were

synthesised and cloned into the pET-26(b)+ expression vector (Merck, Darmstadt, Germany) by GenScript (Piscataway, NJ, USA) using *Nde*I/*Xho*I restriction sites. Correct synthesis and cloning of the target inserts were confirmed by Sanger sequencing (GenScript, Piscataway, NJ, USA).

Protein expression and purification

*Ssc*LPMO10B, *Ssc*LPMO10C and *Ssc*LPMO10D expression strains were established by heat-shock transformation of BL21 (DE3) competent cells (Invitrogen, Carlsbad, USA) with the LPMO gene-containing pET-26(b)+ plasmids according to the supplier's protocol. The transformants were incubated in LB medium at 37°C for 1 h, and then plated on LB agar medium with 50 μg/ml kanamycin, followed by overnight incubation at the same temperature. A single colony was picked from the plate and used to inoculate 500 ml of Terrific Broth (TB) medium supplied with 50 μg/ml kanamycin. The culture was incubated for 24 h at 30°C in a LEX-24 Bioreactor (Harbinger Biotechnology & Engineering, Markham, Canada) using compressed air for mixing and aeration. Considerable levels of basal expression were observed when using these conditions; hence, IPTG induction of the T7 promoter was not required.

The cells were collected by centrifugation (6000 × g for 10 min at 4°C) using a Beckman Coulter centrifuge (Brea, CA, USA). Periplasmic extracts were produced by osmotic shocking as described previously [73] and filter-sterilised through 0.22-μm syringe filters (Sarstedt, Nümbrecht, Germany).

The periplasmic extract containing soluble *Ssc*LPMO10B was subjected to ion-exchange chromatography with a HiTrap™ Q FF (Q Sepharose) 5-ml column (GE Healthcare, Chicago, USA). Protein elution was achieved by applying a linear gradient of NaCl (0–500 mM, 250 ml) in the starting buffer (25 mM Tris-HCl, pH 8.0). Chromatographic fractions containing LPMO were pooled, concentrated (Vivaspin ultrafiltration tubes, Sartorius, Göttingen, Germany) and further purified by size-exclusion chromatography using a HiLoad 16/60 Superdex 75 column (GE Healthcare, Chicago, USA) equilibrated with 50 mM Tris-HCl, pH 7.5, containing 200 mM NaCl.

Enzyme purity was confirmed by SDS-PAGE (Bio-Rad, Hercules, CA, USA) and the concentration of *Ssc*LPMO10B was determined by UV spectroscopy at 280 nm using the theoretical extinction coefficient predicted with the ProtParam tool, assuming that all pairs of cysteine residues are involved in the formation of disulphide bridges [74].

The resulting LPMO sample was co-incubated with a three-fold molar surplus of $Cu(II)SO_4$ for 30 min at room temperature to ensure complete active site loading. Copper saturation was performed in 50 mM Tris-HCl, pH 7.5, containing 200 mM NaCl. Excess copper was removed from the enzyme preparation by desalting using a PD MidiTrap G-25 gravity flow column (GE Healthcare, Chicago, USA), equilibrated with 50 mM sodium phosphate buffer, pH 6.0, using previously described protocol [41].

HRP/Amplex Red hydrogen peroxide production assay

Hydrogen peroxide production by *Ssc*LPMO10B in the presence of various reducing compounds was studied using the HRP/Amplex Red assay, previously described by Kittl et al. [31]. In brief, 90 μl of LPMO solution in 50 mM sodium phosphate buffer, pH 6.0, containing HRP and Amplex Red, was pre-incubated for 5 min at 30°C in a 96-well microtiter plate. To start the reactions, 10 μl of reductant solution was added, followed by 10 s of mixing (600 RPM) in a Varioscan LUX plate reader (Thermo Fisher Scientific, Waltham, MA, USA). The final concentrations of LPMO, HRP, Amplex Red and reductant were 0.5 μM, 5 U/ml, 100 μM and 1 mM, respectively. Hydrogen peroxide production was detected by following the formation of resorufin, which is the product of Amplex Red oxidation that has strong absorbance at 563 nm.

Control reactions containing no LPMO were carried out to assess the level of hydrogen peroxide production in the presence of reductants and oxygen.

Hydrogen peroxide standard solutions were prepared in 50 mM sodium phosphate buffer, pH 6.0, and were supplied with reductant, immediately followed by HRP and Amplex Red, to produce calibration curves. The final concentrations of HRP, Amplex Red and reductants in the calibration samples were the same as in experimental samples (see above). The apparent hydrogen peroxide production rates were calculated from the linear part of the resorufin accumulation curves.

Hydrogen peroxide detection using Peroxy Orange 1

Hydrogen peroxide generation was also studied using Peroxy Orange 1 (PO1), a H_2O_2-selective fluorescent probe. Reaction mixtures containing 1 μM LPMO, 1 mM DHA and/or 2000 u/ml catalase were supplied with 25 μM PO1, loaded into a 96-well non-transparent microtiter plate and incubated at 30°C for 12 h. Fluorescence signals were recorded every hour using 540/560 nm excitation/emission wavelengths. Samples containing 25 μM PO1 or 25 μM PO1 and 25 μM H_2O_2 were used as negative and positive controls, respectively.

LPMO reactions with polysaccharide and oligosaccharide substrates

Lytic polysaccharide monooxygenase reactions with various soluble and insoluble substrates [1% (w/v) Avicel, 0.5%

(w/v) PASC, 1% (w/v) CMC, 500 μM cellohexaose, 0.5% (w/v) beechwood xylan, 0.5% (w/v) konjac glucomannan, 0.5% (w/v) tamarind xyloglucan, 0.5% (w/v) wheat arabinoxylan and 1% (w/v) β-chitin] were carried out in 50 mM sodium phosphate buffer, pH 6.0 using an Eppendorf thermomixer (Eppendorf, Hamburg, Germany) set to 30°C and 900 RPM. Experiments with Avicel were set up in the absence and in the presence of 100 μM H_2O_2, whereas reactions with other substrates were performed at standard aerobic conditions only (i.e. no exogenous hydrogen peroxide). The reaction mixtures were supplied with 1 mM reductant (ascorbic acid, gallic acid, L-cysteine or DHA). Note that the reaction mixtures featuring gallic acid and DHA contained 1% (v/v) DMSO, introduced from the reductant stock solutions. It has previously been shown that 1% (v/v) DMSO does not affect LPMO activity [41].

Aliquots were taken at various time points and the reactions were quenched either by filtering out insoluble substrates using a 96-well filter plate (Millipore, Burlington, MA, USA) or by adding NaOH (0.1 M final concentration) to samples containing soluble substrates.

Filtered samples obtained from reactions with Avicel were treated with in-house produced recombinant *Thermobifida fusca* GH6 endoglucanase (*Tf*Cel6A, [75]; 2 μM final concentration) to convert oxidized LPMO products to a simple, quantifiable mixture of dimers and trimers.

Product analysis by HPAEC-PAD

The LPMO products were detected and quantified by high-performance anion-exchange chromatography with pulsed amperometric detection (HPAEC-PAD) using a Dionex ICS5000 system (Thermo Scientific, San Jose, CA, USA) equipped with a CarboPac PA200 analytical column, as previously described [41]. Data were collected and processed using Chromeleon 7.0 software. C1-oxidised cellobiose and cellotriose standards were prepared in-house according to a previously published protocol [76].

Product analysis by MALDI-TOF MS

Products generated by *Ssc*LPMO10B in the reaction with 1% (w/v) Avicel were analysed using a matrix-assisted laser desorption/ionization time-of-flight (MALDI-ToF) UltrafleXtreme mass spectrometer (Bruker Daltonics GmbH, Bremen, Germany). In this experiment, 50 mM Bis-Tris, pH 6.0, was used instead of 50 mM sodium phosphate buffer, pH 6.0, to achieve optimal co-crystallisation of the sample with matrix solution. One microlitre of the LPMO reaction samples was mixed with 2 μl of a matrix solution (9 mg/ml 2,5-dihydrooxybenzoic acid in 30% acetonitrile) on an MTP 384-ground steel target plate (Bruker Daltonics). The target plate was air-dried, and the MS data were acquired using Bruker flexControl software, as described previously [1].

UV-VIS spectroscopy of LPMO reaction mixtures featuring Avicel and DHA

Samples were taken from LPMO reactions at various time points and reactions were quenched by removing the insoluble substrate as described above. Hundred microlitres of filtered reaction samples were transferred to a UV-transparent 96-well microtiter plate. UV-VIS absorbance spectra were recorded in the 230–900 nm range using 1-nm scanning steps in a Varioscan LUX plate reader (Thermo Fisher Scientific, Waltham, MA, USA).

NMR spectroscopy

The following samples (500 μL) were prepared in 5-mm LabScape Stream NMR tubes (Bruker BioSpin AG, Fällanden, Switzerland) to monitor the kinetics of ascorbic acid and DHA degradation by NMR spectroscopy: (a) 0.5 μM *Ssc*LPMO10B and 1% (w/v) Avicel with 1 mM ascorbic acid in 50 mM sodium phosphate buffer (pH 6.0) prepared in D_2O (D, 99.9%), (b) 1% (w/v) Avicel with 1 mM ascorbic acid in 50 mM sodium phosphate buffer (pH 6.0) prepared in D_2O, (c) 0.5 μM *Ssc*LPMO10B and 1% (w/v) Avicel with 1 mM DHA and 1% (v/v) DMSO (D, 99.9%; Merck) in 50 mM sodium phosphate buffer (pH 6.0) prepared in D_2O, (d) 1% (w/v) Avicel with 1 mM DHA and 1% (v/v) DMSO (D, 99.9%; Merck, Darmstadt, Germany) in 50 mM sodium phosphate buffer (pH 6.0) prepared in D_2O, (e) 10 mM ascorbic acid in 50 mM sodium phosphate buffer (pH 6.0) prepared in D_2O and (f) 10 mM DHA and 1% (v/v) DMSO (D, 99.9%; Merck, Darmstadt, Germany) in 50 mM sodium phosphate buffer (pH 6.0) prepared in D_2O.

All NMR experiments were recorded at 30°C on a Bruker Ascend 800 MHz spectrometer with an Avance III HD console and equipped with a 5-mm Z-gradient CP-TCI (H/C/N) cryogenic probe at the NV-NMR-Centre/Norwegian NMR Platform (NNP) at the Norwegian University of Science and Technology (NTNU). ^{1}H chemical shifts were internally referenced to the water signal, while ^{15}N and ^{13}C chemical shifts were indirectly referenced to the water signal, based on absolute frequency ratios [77]. The spectra were recorded, processed and analysed using TopSpin 3.6pl7 and TopSpin 4.0.7 software (Bruker BioSpin AG, Fällanden, Switzerland).

Time-course kinetics of the above-mentioned samples were followed using a series of 1D Nuclear Overhauser Effect Spectroscopy (NOESY) spectra with a 10-ms mixing time being recorded every 12 min for 24 h, resulting in pseudo-2D spectra with time as the second dimension. The 1D NOESY experiment was selected because it provides excellent water suppression without causing artefacts and signal reduction around the water resonance [78,79]. To assign the chemical shifts of the compounds present in the solutions, we recorded 1D-NOESY, 2D ^{13}C-Heteronuclear

Single Quantum Coherence (HSQC) with multiplicity editing, 2D ^{13}C-HSQC-[^{1}H,^{1}H]-Total Correlation Spectroscopy (TOCSY) with 90-ms mixing time, and two-dimensional Heteronuclear Multibond Correlation (HMBC) with three-fold low-pass J-filter for suppression of one-bond correlations, using samples (5) and (6). The signals were recorded immediately after preparation of these solutions and once again after a 24-hour incubation.

Acknowledgements

This work was supported by the Research Council of Norway under Grant no. 269408 (Centre for Digital Life Norway, project OXYMOD) and by Novo Nordisk Foundation Grant no. NNF18OC0032242 (NMR work).

Conflict of interests

The authors declare no conflicts of interest.

Data accessibility

The data that support the findings of this study are available in Figure 1-12 and the supplementary material of this article.

Author contributions

Anton A. Stepnov designed experiments, did most of the experimental work, analysed data and drafted the manuscript. Idd A. Christensen performed NMR experiments, analysed data and edited the manuscript. Zarah Forsberg, Finn L. Aachmann and Gaston Courtade contributed to designing the study, performed data analysis and edited the manuscript. Vincent G. H. Eijsink conceived and supervised the project, contributed to data interpretation and edited the manuscript. All authors read and approved the final manuscript.

References

1 Vaaje-Kolstad G, Westereng B, Horn SJ, Liu Z, Zhai H, Sorlie M et al., An oxidative enzyme boosting the enzymatic conversion of recalcitrant polysaccharides. *Science*. 2010;**330**:219–22.
2 Forsberg Z, Vaaje-Kolstad G, Westereng B, Bunaes AC, Stenstrom Y, MacKenzie A et al., Cleavage of cellulose by a CBM33 protein. *Protein Sci*. 2011;**20**:1479–83.
3 Quinlan RJ, Sweeney MD, Lo Leggio L, Otten H, Poulsen JC, Johansen KS et al., Insights into the oxidative degradation of cellulose by a copper metalloenzyme that exploits biomass components. *Proc Natl Acad Sci USA*. 2011;**108**:15079–84.
4 Vu VV, Beeson WT, Span EA, Farquhar ER, Marletta MA. A family of starch-active polysaccharide monooxygenases. *Proc Natl Acad Sci USA*. 2014;**111**:13822–7.
5 Couturier M, Ladeveze S, Sulzenbacher G, Ciano L, Fanuel M, Moreau C et al., Lytic xylan oxidases from wood-decay fungi unlock biomass degradation. *Nat Chem Biol*. 2018;**14**:306–10.
6 Frommhagen M, Sforza S, Westphal AH, Visser J, Hinz SW, Koetsier MJ et al., Discovery of the combined oxidative cleavage of plant xylan and cellulose by a new fungal polysaccharide monooxygenase. *Biotechnol Biofuels*. 2015;**8**:101.
7 Agger JW, Isaksen T, Varnai A, Vidal-Melgosa S, Willats WG, Ludwig R et al., Discovery of LPMO activity on hemicelluloses shows the importance of oxidative processes in plant cell wall degradation. *Proc Natl Acad Sci USA*. 2014;**111**:6287–92.
8 Sabbadin F, Urresti S, Henrissat B, Avrova AO, Welsh LRJ, Lindley PJ et al., Secreted pectin monooxygenases drive plant infection by pathogenic oomycetes. *Science*. 2021;**373**:774–9.
9 Forsberg Z, Mackenzie AK, Sorlie M, Rohr AK, Helland R, Arvai AS et al., Structural and functional characterization of a conserved pair of bacterial cellulose-oxidizing lytic polysaccharide monooxygenases. *Proc Natl Acad Sci USA*. 2014;**111**:8446–51.
10 Danneels B, Tanghe M, Desmet T. Structural features on the substrate-binding surface of fungal lytic polysaccharide monooxygenases determine their oxidative regioselectivity. *Biotechnol J*. 2019;**14**: e1800211.
11 Phillips CM, Beeson WT, Cate JH, Marletta MA. Cellobiose dehydrogenase and a copper-dependent polysaccharide monooxygenase potentiate cellulose degradation by *Neurospora crassa*. *ACS Chem Biol*. 2011;**6**:1399–406.
12 Tanghe M, Danneels B, Camattari A, Glieder A, Vandenberghe I, Devreese B et al., Recombinant Expression of *Trichoderma reesei* Cel61A in *Pichia pastoris*: optimizing yield and N-terminal processing. *Mol Biotechnol*. 2015;**57**:1010–7.
13 Vaaje-Kolstad G, Horn SJ, van Aalten DM, Synstad B, Eijsink VG. The non-catalytic chitin-binding protein CBP21 from *Serratia marcescens* is essential for chitin degradation. *J Biol Chem*. 2005;**280**:28492–7.
14 Johansen KS. Lytic polysaccharide monooxygenases: the microbial power tool for lignocellulose degradation. *Trends Plant Sci*. 2016;**21**:926–36.
15 Eibinger M, Ganner T, Bubner P, Rosker S, Kracher D, Haltrich D et al., Cellulose surface degradation by a lytic polysaccharide monooxygenase and its effect on

cellulase hydrolytic efficiency. *J Biol Chem*. 2014;**289**:35929–38.
16 Vaaje-Kolstad G, Forsberg Z, Loose JS, Bissaro B, Eijsink VG. Structural diversity of lytic polysaccharide monooxygenases. *Curr Opin Struct Biol*. 2017;**44**:67–76.
17 Tandrup T, Frandsen KEH, Johansen KS, Berrin JG, Lo Leggio L. Recent insights into lytic polysaccharide monooxygenases (LPMOs). *Biochem Soc Trans*. 2018;**46**:1431–7.
18 Courtade G, Forsberg Z, Heggset EB, Eijsink VGH, Aachmann FL. The carbohydrate-binding module and linker of a modular lytic polysaccharide monooxygenase promote localized cellulose oxidation. *J Biol Chem*. 2018;**293**:13006–15.
19 Hegnar OA, Petrovic DM, Bissaro B, Alfredsen G, Varnai A, Eijsink VGH. pH-dependent relationship between catalytic activity and hydrogen peroxide production shown via characterization of a lytic polysaccharide monooxygenase from *Gloeophyllum trabeum*. *Appl Environ Microbiol*. 2019;**85**:e02612–8.
20 Chalak A, Villares A, Moreau C, Haon M, Grisel S, d'Orlando A et al., Influence of the carbohydrate-binding module on the activity of a fungal AA9 lytic polysaccharide monooxygenase on cellulosic substrates. *Biotechnol Biofuels*. 2019;**12**:206.
21 Loose JS, Forsberg Z, Kracher D, Scheiblbrandner S, Ludwig R, Eijsink VG et al., Activation of bacterial lytic polysaccharide monooxygenases with cellobiose dehydrogenase. *Protein Sci*. 2016;**25**:2175–86.
22 Varnai A, Umezawa K, Yoshida M, Eijsink VGH. The pyrroloquinoline-quinone-dependent pyranose dehydrogenase from Coprinopsis cinerea drives lytic polysaccharide monooxygenase action. *Appl Environ Microbiol*. 2018;**84**:e00156-18.
23 Beeson WT, Phillips CM, Cate JH, Marletta MA. Oxidative cleavage of cellulose by fungal copper-dependent polysaccharide monooxygenases. *J Am Chem Soc*. 2012;**134**:890–2.
24 Bissaro B, Rohr AK, Muller G, Chylenski P, Skaugen M, Forsberg Z et al., Oxidative cleavage of polysaccharides by monocopper enzymes depends on H_2O_2. *Nat Chem Biol*. 2017;**13**:1123–8.
25 Jones SM, Transue WJ, Meier KK, Kelemen B, Solomon EI. Kinetic analysis of amino acid radicals formed in H_2O_2-driven Cu(I) LPMO reoxidation implicates dominant homolytic reactivity. *Proc Natl Acad Sci U S A*. 2020;**117**:11916–22.
26 Bissaro B, Varnai A, Rohr AK, Eijsink VGH. Oxidoreductases and reactive oxygen species in conversion of lignocellulosic biomass. *Microbiol Mol Biol Rev*. 2018;**82**.
27 Hedison TM, Breslmayr E, Shanmugam M, Karnpakdee K, Heyes DJ, Green AP et al., Insights into the H_2O_2 -driven catalytic mechanism of fungal lytic polysaccharide monooxygenases. *FEBS J*. 2020;**288**:4115–28.
28 Filandr F, Man P, Halada P, Chang H, Ludwig R, Kracher D. The H_2O_2-dependent activity of a fungal lytic polysaccharide monooxygenase investigated with a turbidimetric assay. *Biotechnol Biofuels*. 2020;**13**:37.
29 Kont R, Bissaro B, Eijsink VGH, Väljamäe P. Kinetic insights into the peroxygenase activity of cellulose-active lytic polysaccharide monooxygenases (LPMOs). *Nat Commun*. 2020;**11**:1–10.
30 Kuusk S, Bissaro B, Kuusk P, Forsberg Z, Eijsink VGH, Sorlie M et al., Kinetics of H_2O_2-driven degradation of chitin by a bacterial lytic polysaccharide monooxygenase. *J Biol Chem*. 2018;**293**:523–31.
31 Kittl R, Kracher D, Burgstaller D, Haltrich D, Ludwig R. Production of four *Neurospora crassa* lytic polysaccharide monooxygenases in Pichia pastoris monitored by a fluorimetric assay. *Biotechnol Biofuels*. 2012;**5**:79.
32 Kjaergaard CH, Qayyum MF, Wong SD, Xu F, Hemsworth GR, Walton DJ et al., Spectroscopic and computational insight into the activation of O_2 by the mononuclear Cu center in polysaccharide monooxygenases. *Proc Natl Acad Sci USA*. 2014;**111**:8797–802.
33 Hangasky JA, Iavarone AT, Marletta MA. Reactivity of O_2 versus H_2O_2 with polysaccharide monooxygenases. *Proc Natl Acad Sci USA*. 2018;**115**:4915–20.
34 Courtade G, Ciano L, Paradisi A, Lindley PJ, Forsberg Z, Sorlie M et al., Mechanistic basis of substrate-O_2 coupling within a chitin-active lytic polysaccharide monooxygenase: AN integrated NMR/EPR study. *Proc Natl Acad Sci USA*. 2020;**117**:19178–89.
35 Isaksen T, Westereng B, Aachmann FL, Agger JW, Kracher D, Kittl R et al., A C4-oxidizing lytic polysaccharide monooxygenase cleaving both cellulose and cello-oligosaccharides. *J Biol Chem*. 2014;**289**:2632–42.
36 Forsberg Z, Rohr AK, Mekasha S, Andersson KK, Eijsink VG, Vaaje-Kolstad G et al., Comparative study of two chitin-active and two cellulose-active AA10-type lytic polysaccharide monooxygenases. *Biochemistry*. 2014;**53**:1647–56.
37 Wilson RJ, Beezer AE, Mitchell JC. A kinetic study of the oxidation of L-ascorbic acid (vitamin C) in solution using an isothermal microcalorimeter. *Thermochim Acta*. 1995;**264**:27–40.
38 Tulyathan V, Boulton RB, Singleton VL. Oxygen uptake by gallic acid as a model for similar reactions in wines. *J Agric Food Chem*. 1989;**37**:844–9.
39 Kachur AV, Koch CJ, Biaglow JE. Mechanism of copper-catalyzed oxidation of glutathione. *Free Radic Res*. 1998;**28**:259–69.

40 Kachur AV, Koch CJ, Biaglow JE. Mechanism of copper-catalyzed autoxidation of cysteine. *Free Radic Res*. 1999;**31**:23–34.
41 Stepnov AA, Forsberg Z, Sorlie M, Nguyen GS, Wentzel A, Rohr AK et al., Unraveling the roles of the reductant and free copper ions in LPMO kinetics. *Biotechnol Biofuels*. 2021;**14**:28.
42 Petrovic DM, Varnai A, Dimarogona M, Mathiesen G, Sandgren M, Westereng B et al., Comparison of three seemingly similar lytic polysaccharide monooxygenases from *Neurospora crassa* suggests different roles in plant biomass degradation. *J Biol Chem*. 2019;**294**:15068–81.
43 Kracher D, Scheiblbrandner S, Felice AK, Breslmayr E, Preims M, Ludwicka K et al., Extracellular electron transfer systems fuel cellulose oxidative degradation. *Science*. 2016;**352**:1098–101.
44 Frommhagen M, Koetsier MJ, Westphal AH, Visser J, Hinz SW, Vincken JP et al., Lytic polysaccharide monooxygenases from *Myceliophthora thermophila* C1 differ in substrate preference and reducing agent specificity. *Biotechnol Biofuels*. 2016;**9**:186.
45 Askarian F, Uchiyama S, Masson H, Sorensen HV, Golten O, Bunaes AC et al., The lytic polysaccharide monooxygenase CbpD promotes *Pseudomonas aeruginosa* virulence in systemic infection. *Nat Commun*. 2021;**12**:1230.
46 Lerat S, Simao-Beaunoir AM, Beaulieu C. Genetic and physiological determinants of *Streptomyces scabies* pathogenicity. *Mol Plant Pathol*. 2009;**10**:579–85.
47 Conklin PL, Barth C. Ascorbic acid, a familiar small molecule intertwined in the response of plants to ozone, pathogens, and the onset of senescence. *Plant Cell Environ*. 2004;**27**:959–70.
48 Brander S, Lausten S, Ipsen JO, Falkenberg KB, Bertelsen AB, Norholm MHH et al., Colorimetric LPMO assay with direct implication for cellulolytic activity. *Biotechnol Biofuels*. 2021;**14**:51.
49 Steinegger M, Soding J. MMseqs2 enables sensitive protein sequence searching for the analysis of massive data sets. *Nat Biotechnol*. 2017;**35**:1026–8.
50 Burley SK, Berman HM, Kleywegt GJ, Markley JL, Nakamura H, Velankar S. Protein Data Bank: the single global archive for 3D macromolecular structure data. *Nucleic Acids Res*. 2019;**47**:D520–8.
51 Chaplin AK, Wilson MT, Hough MA, Svistunenko DA, Hemsworth GR, Walton PH et al., Heterogeneity in the histidine-brace copper coordination sphere in auxiliary activity family 10 (AA10) lytic polysaccharide monooxygenases. *J Biol Chem*. 2016;**291**:12838–50.
52 Correa TLR, Junior AT, Wolf LD, Buckeridge MS, Dos Santos LV, Murakami MT. An actinobacteria lytic polysaccharide monooxygenase acts on both cellulose and xylan to boost biomass saccharification. *Biotechnol Biofuels*. 2019;**12**:117.
53 Yadav SK, Archana, Singh R, Singh PK, Vasudev PG. Insecticidal fern protein Tma12 is possibly a lytic polysaccharide monooxygenase. *Planta*. 2019;**249**:1987–96.
54 Eijsink VGH, Petrovic D, Forsberg Z, Mekasha S, Rohr AK, Varnai A et al., On the functional characterization of lytic polysaccharide monooxygenases (LPMOs). *Biotechnol Biofuels*. 2019;**12**:58.
55 Breslmayr E, Hanzek M, Hanrahan A, Leitner C, Kittl R, Santek B et al., A fast and sensitive activity assay for lytic polysaccharide monooxygenase. *Biotechnol Biofuels*. 2018;**11**:79.
56 Kadic A, Varnai A, Eijsink VGH, Horn SJ, Liden G. In situ measurements of oxidation-reduction potential and hydrogen peroxide concentration as tools for revealing LPMO inactivation during enzymatic saccharification of cellulose. *Biotechnol Biofuels*. 2021;**14**:46.
57 Muller G, Chylenski P, Bissaro B, Eijsink VGH, Horn SJ. The impact of hydrogen peroxide supply on LPMO activity and overall saccharification efficiency of a commercial cellulase cocktail. *Biotechnol Biofuels*. 2018;**11**:209.
58 Bissaro B, Streit B, Isaksen I, Eijsink VGH, Beckham GT, DuBois JL et al., Molecular mechanism of the chitinolytic peroxygenase reaction. *Proc Natl Acad Sci USA*. 2020;**117**:1504–13.
59 Dickinson BC, Huynh C, Chang CJ. A palette of fluorescent probes with varying emission colors for imaging hydrogen peroxide signaling in living cells. *J Am Chem Soc*. 2010;**132**:5906–15.
60 Lin VS, Dickinson BC, Chang CJ. Boronate-based fluorescent probes: imaging hydrogen peroxide in living systems. *Methods Enzymol*. 2013;**526**:19–43.
61 Kimoto E, Tanaka H, Ohmoto T, Choami M. Analysis of the transformation products of dehydro-L-ascorbic acid by ion-pairing high-performance liquid chromatography. *Anal Biochem*. 1993;**214**:38–44.
62 Deutsch JC, Santhosh-Kumar CR. Dehydroascorbic acid undergoes hydrolysis on solubilization which can be reversed with mercaptoethanol. *J Chromatogr A*. 1996;**724**:271–8.
63 Deutsch JC. Dehydroascorbic acid. *J Chromatogr A*. 2000;**881**:299–307.
64 Karkonen A, Dewhirst RA, Mackay CL, Fry SC. Metabolites of 2,3-diketogulonate delay peroxidase action and induce non-enzymic H_2O_2 generation: potential roles in the plant cell wall. *Arch Biochem Biophys*. 2017;**620**:12–22.
65 Dewhirst RA, Murray L, Mackay CL, Sadler IH, Fry SC. Characterisation of the non-oxidative degradation pathway of dehydroascorbic acid in slightly acidic aqueous solution. *Arch Biochem Biophys*. 2020;**681**:108240.

66 Wang B, Walton PH, Rovira C. Molecular mechanisms of oxygen activation and hydrogen peroxide formation in lytic polysaccharide monooxygenases. *ACS Catal*. 2019;**9**:4958–69.
67 Dewhirst RA, Fry SC. The oxidation of dehydroascorbic acid and 2,3-diketogulonate by distinct reactive oxygen species. *Biochem J*. 2018;**475**:3451–70.
68 Pohanka M, Pejchal J, Snopkova S, Havlickova K, Karasova JZ, Bostik P et al., Ascorbic acid: an old player with a broad impact on body physiology including oxidative stress suppression and immunomodulation: a review. *Mini Rev Med Chem*. 2012;**12**:35–43.
69 Gallie DR. The role of L-ascorbic acid recycling in responding to environmental stress and in promoting plant growth. *J Exp Bot*. 2013;**64**:433–43.
70 Wood TM Wood, TM. Preparation of crystalline, amorphous, and dyed cellulase substrates. Methods Enzymol. 1988;**160**:19-25.
71 Yin Y, Mao X, Yang J, Chen X, Mao F, Xu Y. dbCAN: a web resource for automated carbohydrate-active enzyme annotation. *Nucleic Acids Res*. 2012;**40**: W445–51.
72 Almagro Armenteros JJ, Tsirigos KD, Sonderby CK, Petersen TN, Winther O, Brunak S et al., SignalP 5.0 improves signal peptide predictions using deep neural networks. *Nat Biotechnol*. 2019;**37**:420–3.
73 Manoil C, Beckwith J. A genetic approach to analyzing membrane protein topology. *Science*. 1986;**233**:1403–8.
74 Gasteiger E, Hoogland C, Gattiker A, Duvaud SE, Wilkins MR, Appel RD et al., (2005) Protein identification and analysis tools on the ExPASy server in *The Proteomics Protocols Handbook*. pp. 571–607.
75 Spezio M, Wilson DB, Karplus PA. (1993) Crystal structure of the catalytic domain of a thermophilic endocellulase. *Biochemistry*. **32**:9906–16.
76 Bissaro B, Forsberg Z, Ni Y, Hollmann F, Vaaje-Kolstad G, Eijsink VGH. (2016) Fueling biomass-degrading oxidative enzymes by light-driven water oxidation. *Green Chem* **18**, 5357–66.
77 Zhang H, Neal S, Wishart DS. RefDB: a database of uniformly referenced protein chemical shifts. *J Biomol NMR*. 2003;**25**:173–95.
78 McKay RT. How the 1D-NOESY suppresses solvent signal in metabonomics NMR spectroscopy: an examination of the pulse sequence components and evolution. *Concepts in Magnetic Resonance Part A*. 2011;**38A**:197–220.
79 Sokolenko S, McKay R, Blondeel EJM, Lewis MJ, Chang D, George B et al., Understanding the variability of compound quantification from targeted profiling metabolomics of 1D–1H-NMR spectra in synthetic mixtures and urine with additional insights on choice of pulse sequences and robotic sampling. *Metabolomics*. 2013;**9**:887–903.

Supporting information

Additional supporting information may be found online in the Supporting Information section at the end of the article.

Figure S1. SDS-PAGE of *Ssc*LPMO10B after purification.

Figure S2. Hydrogen peroxide production by *Ssc*LPMO10B and by protein-free ultrafiltrates.

Figure S3. H_2O_2 detection using Peroxy Orange 1.

Figure S4. UV-VIS spectroscopy of DHA solutions in the presence or absence of Avicel.

Figure S5. Annotated ^{13}C-HSQC spectra of (A) 10 mM ascorbate and (B) 10 mM DHA and 1% (v/v) d-DMSO after 24 hours of incubation.

On the impact of reductants on LPMO efficiency and the special role of dehydroascorbic acid

Anton A. Stepnov[1], Idd A. Christensen[2], Zarah Forsberg[1], Finn L. Aachmann[2], Gaston Courtade[2], Vincent G. H. Eijsink[1*]

[1] - Faculty of Chemistry, Biotechnology and Food Science, NMBU - Norwegian University of Life Sciences, 1432 Ås, Norway

[2] - NOBIPOL, Department of Biotechnology and Food Science, NTNU Norwegian University of Science and Technology, Sem Sælands vei 6/8, 7491 Trondheim, Norway

[*] - corresponding author, vincent.eijsink@nmbu.no

Supporting information

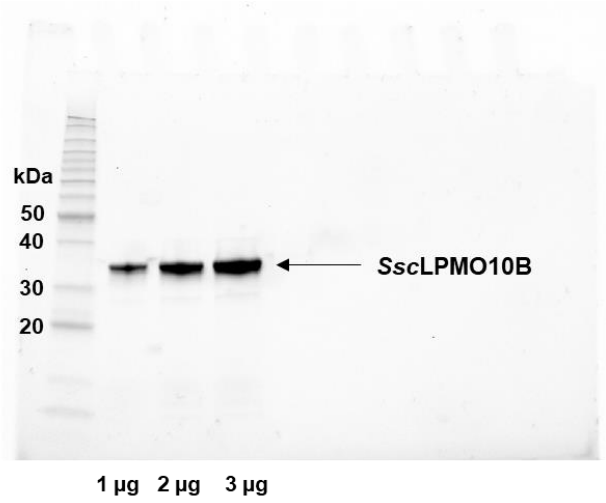

Figure S1. SDS-PAGE of *Ssc*LPMO10B after purification. The predicted molecular weight of mature LPMO (lacking the signal peptide) is 33.7 kDa. The gel was loaded with 1, 2 and 3 µg of the enzyme.

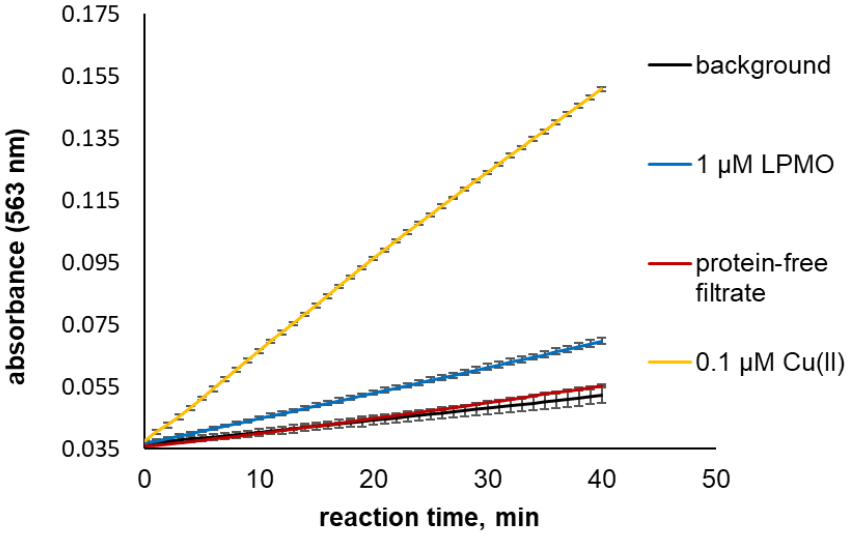

Figure S2. Hydrogen peroxide production by *Ssc*LPMO10B and by protein-free ultrafiltrates. The figure shows the HRP/Amplex Red assay signal (reflecting H_2O_2 production) recorded in the presence of 1 µM LPMO (blue curve) or in the presence of the same amounts of protein-free control samples (red curve) obtained by ultrafiltration of the enzyme stock solution using a 3 kDa MWCO 1.5 ml ultrafiltration tubes (VWR International, Radnor, PA, USA). These control samples contained the same amount of free copper as the LPMO preparation used in this study. The experiment indicates negligible level of free copper in *Ssc*LPMO10B stock solution, since even small amounts would lead to a massive enzyme independent H_2O_2 generation (yellow curve). All the experiments were carried out at 30 °C in 50 mM sodium phosphate buffer, pH 6.0, containing 1 mM ascorbic acid, 5 U/ml HRP, 100 µM Amplex Red and 1% (v/v) DMSO. The black ("background") curve denotes the reference reaction, containing the reductant but lacking the LPMO. Error bars indicate standard deviations between triplicates.

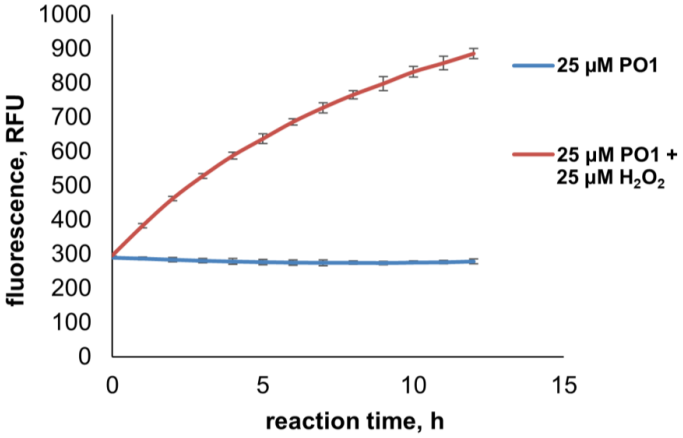

Figure S3. H_2O_2 detection using Peroxy Orange 1. The figure shows the fluorescence signal of the H_2O_2-selective probe Peroxy Orange 1 (PO1; Ex/Em = 540/560 nm) observed in the presence of 25 µM H_2O_2 at 30 °C in 50 mM sodium phosphate buffer, pH 6.0. The error bars indicate standard deviations between triplicates.

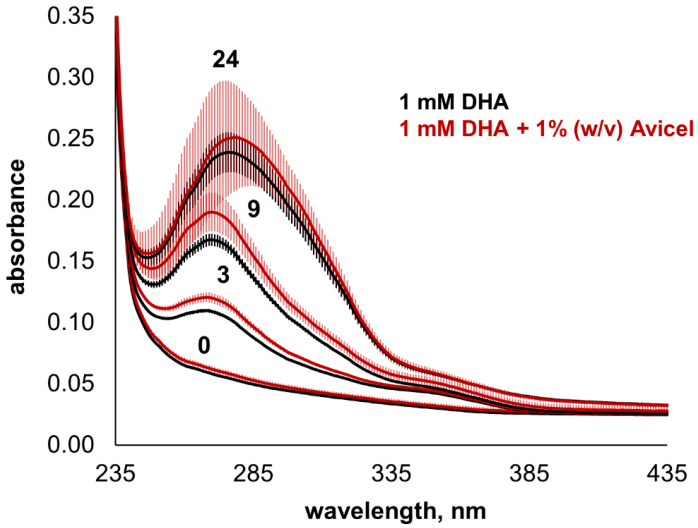

Figure S4. UV-VIS spectroscopy of DHA solutions in the presence or absence of Avicel. The figure shows UV-VIS spectra of 1 mM DHA incubated for 3, 9 and 24 hours at standard LPMO reaction conditions (50 mM sodium phosphate buffer, pH 6.0, 30 °C), in the presence (red curves) or absence (black curves) of 1% (w/v) Avicel. Error bars indicate standard deviations between triplicates. The experiment shows no significant effect of Avicel on the shift in λ_{max} over time.

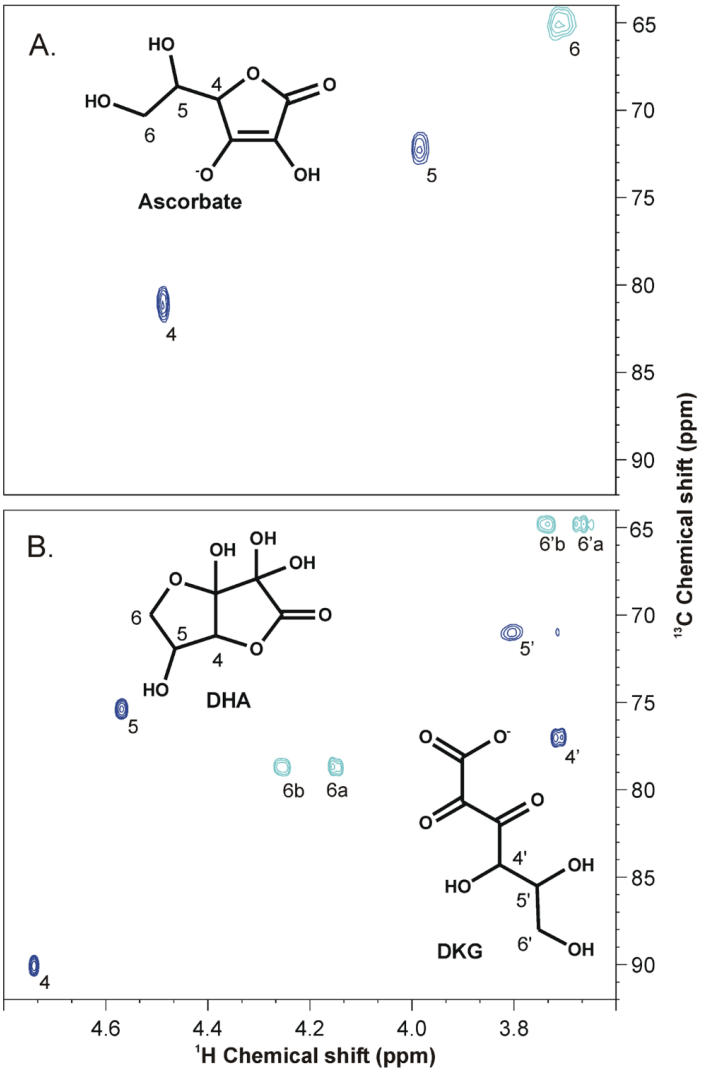

Figure S5. Annotated ^{13}C-HSQC spectra of (A) 10 mM ascorbate and (B) 10 mM DHA and 1% (v/v) d-DMSO after 24 hours of incubation. The spectra show the partial assignments of ascorbic acid, DHA and DKG. Blue peaks (positive) indicate C-H single bond correlations for methyl (CH_3) and methine (CH) groups, while cyan peaks (negative) indicate C-H single bond correlations for methylene (CH_2) groups. Carbon numbers are shown for the compounds and the corresponding assigned signals; # indicate the carbon number for the compound, #a and #b indicate the protons in the methylene groups. Signal labels marked with ‘ indicate DKG signals on panel B. Chemical shift assignments for the compounds are the following: **Ascorbate** (panel A) C4 (H4): 81.2 (4.49), C5 (H5): 72.5 (3.98), C6 (H6a, H6b): 65.4 (3.70, 3.73); **DHA** (panel B) C4 (H4): 90.1 (4.74), C5 (H5): 75.4 (4.57), C6 (H6a, H6b): 78.7 (4.15, 4.25); **DKG** (panel B) C4’ (H4’): 77.0 (3.71), C5’ (H5’): 71.0 (3.80), C6’ (H6’a, H6’b): 64.8 (3.74, 3.66). Note that the spectral data shown in panel A were obtained using a fresh ascorbic acid solution, whereas the signals in panel B were recorded after 24 hours of incubation of the DHA sample at 30 °C.

Enhanced *in situ* H_2O_2 production explains synergy between an LPMO with a cellulose-binding domain and a single-domain LPMO

Stepnov AA, Eijsink VG, Forsberg Z

Paper III

Enhanced in situ H_2O_2 production explains synergy between an LPMO with a cellulose-binding domain and a single-domain LPMO

Anton A. Stepnov[1], Vincent G. H. Eijsink[1*], Zarah Forsberg[1*]

[1] - Faculty of Chemistry, Biotechnology and Food Science, NMBU - Norwegian University of Life Sciences, 1432 Ås, Norway

[*] corresponding authors; vincent.eijsink@nmbu.no, zarah.forsberg@nmbu.no

Abstract

Lytic polysaccharide monooxygenases (LPMOs) are mono-copper enzymes that catalyze oxidative depolymerization of recalcitrant substrates such as chitin or cellulose. Recent work has shown that LPMOs catalyze fast peroxygenase reactions and that, under commonly used reaction set-ups, access to in situ generated H_2O_2 likely limits catalysis. Based on a hypothesis that the impact of a cellulose-binding module (CBM) on LPMO activity could relate to changes in in situ H_2O_2 production, we have assessed the interplay between CBM-containing *Sc*LPMO10C and its truncated form comprising the catalytic domain only (*Sc*LPMO10C-AA10). The results show that truncation of the linker and CBM leads to elevated H_2O_2 production and decreased enzyme stability. Most interestingly, combining the two enzyme forms yields strong synergistic effects, which are due to the combination of high H_2O_2 generation by *Sc*LPMO10C-AA10 and efficient productive use of H_2O_2 by the full-length enzyme. Thus, cellulose degradation becomes faster, while enzyme inactivation due to off-pathway reactions with excess H_2O_2 is reduced. These results underpin the complexity of ascorbic acid-driven LPMO reactions and reveal a potential mechanism for how LPMOs may interact synergistically during cellulose degradation.

Introduction

Lytic polysaccharide monooxygenases (LPMOs) are monocopper enzymes that catalyze oxidative depolymerization of polysaccharide substrates, such as chitin [1], cellulose [2-4] and xylan [5-7]. LPMOs depend on an electron source to maintain their catalytic cycle and possess a unique ability to act on crystalline surfaces of recalcitrant polysaccharides, making their targets prone to further degradation by classical hydrolytic enzymes [8]. The synergy between LPMOs, chitinases and cellulases has attracted significant attention not only in academia but also in industry [1, 9-14]. Modern commercial cellulolytic cocktails, such as Cellic CTec2 and CTec3, benefit from the inclusion of LPMOs in their formulations [10, 15].

LPMOs were previously thought to use molecular oxygen as a co-substrate, but it has recently been shown that these enzymes prefer hydrogen peroxide, thus operating as peroxygenases rather than strict monooxygenases [16]. Importantly, due to the preference for H_2O_2, the rates of LPMO reactions that are carried out in the absence of exogenously added hydrogen peroxide are limited by the in situ H_2O_2 generation [16-18] and are low compared to reactions with controlled addition of H_2O_2 [17, 19, 20].

Both non-enzymatic and enzyme-dependent pathways lead to hydrogen peroxide generation in typical LPMO reactions. Firstly, commonly used low-molecular-weight LPMO reductants, such as ascorbic acid, gallic acid and cysteine, are known to engage into direct reactions with dissolved molecular oxygen, yielding H_2O_2 [21-23]. Secondly, it is well established that reduced LPMOs have oxidase activity, which leads to hydrogen peroxide production [24] with rates that depend on the nature of the reductant that is being oxidized [17, 18, 25]. It is worth noting that, besides driving LPMO activity on carbohydrates, H_2O_2 may promote auto-catalytic damage to the active site of the LPMO, especially when substrate

concentrations are low [16, 26]. All in all, a detailed understanding of the factors determining the rate of in situ H_2O_2 generation in LPMO reactions is essential for unlocking the full potential of these enzymes.

One important but rather unexplored aspect of LPMO chemistry is the interplay between enzyme-dependent H_2O_2 production and substrate binding. A few recent studies involving fungal (family AA9) and bacterial (family AA10) LPMOs have confirmed early suggestions by Kittl et al. [24] by showing that hydrogen peroxide generation by these enzymes is repressed in the presence of insoluble substrate [27, 28]. Such observations make sense considering the fact that binding to a crystalline surface will shield the active site from the solvent to a degree that will prevent the interaction of low-molecular reductants with the copper atom [29]. In Nature, binding of LPMOs to insoluble polysaccharides is often guided by carbohydrate-binding modules (CBMs) [30]. Compared to LPMO catalytic domains, CBMs are capable of stronger binding to substrates [31, 32], and it has been shown that CBMs have pronounced impact on LPMO activity and stability because they contribute to keeping the active site closer to the substrate [32-34].

Considering the above, it is reasonable to assume that the presence or absence of a CBM will affect hydrogen peroxide production by LPMOs in reactions with insoluble polysaccharide substrates, with potential repercussions on (H_2O_2-driven) LPMO activity. To study these issues, we have used CBM-containing *Sc*LPMO10C and its truncated form lacking the CBM and the linker (*Sc*LPMO10C-AA10) as model enzymes and studied the interplay and possible synergy between these. We show that the two enzyme forms act synergistically during cellulose degradation and, by studying H_2O_2 production and reductant depletion in various reaction set-ups, we show that this synergy relates to redox processes in the reaction mixture that affect co-substrate availability and oxidative enzyme inactivation. Next to

shedding light on the possible interplay between CBM-containing and CBM-free LPMOs, our results provide fundamental insights into the complexity of LPMO reactions that are fueled by ascorbic acid, the most commonly used reductant in LPMO research.

Results and discussion

Protein production

To investigate the impact of cellulose-binding module (CBM) on LPMO performance in reactions with insoluble substrate, a well-characterized bacterial enzyme, *Sc*LPMO10C, was selected as the model. The LPMO and its truncated form lacking the linker and the CBM2, *Sc*LPMO10C-AA10 (Fig. 1A), were produced using previously described *E. coli* expression strains [35]. Both enzymes were isolated from the periplasm in soluble form and purified by ion-exchange and size-exclusion chromatography (Fig. 1B). The final yield amounted to approximately 60 mg of *Sc*LPMO10C and 20 mg of *Sc*LPMO10C-AA10 per liter of culture.

Hydrogen peroxide generation by *Sc*LPMO10C and *Sc*LPMO10C-AA10 and assessment of free copper levels in the enzyme preparations

In a recent study by our group, we showed that some of the previously published activity data for *Sc*LPMO10C likely were affected by the presence of free copper in the reaction mixture, probably as a result of incomplete desalting of the enzyme preparations after copper-saturation [28]. It is well established that the combination of free Cu(II) ions and ascorbic acid will promote enzyme-independent H_2O_2 generation [21], sometimes referred to as reductant autooxidation, which will boost LPMO activity and affect enzyme stability [28, 36]. To ensure that the residual free copper levels in *Sc*LPMO10C and *Sc*LPMO10C-AA10 preparations used in the present study were minimal, protein-free samples were obtained

from enzyme stock solutions by ultrafiltration through 3 kDa MWCO membranes. Analysis of these control samples with the HRP/Amplex Red assay, using 1 mM ascorbic acid as reductant, showed very low hydrogen peroxide production rates, compared to reactions with the LPMO (Fig. 2A), which demonstrates that the enzyme preparations contained negligible amounts of free copper.

Surprisingly, despite a comparable very low level of free copper in both enzyme preparations, as shown by the control reactions with the ultrafiltrates, the two enzyme variants (at 3 μM) showed a three-fold difference in the hydrogen peroxide generation rate (Fig. 2A). While it is reasonable to assume that these two enzymes generate different amounts of H_2O_2 in the presence of cellulose, due to variation in substrate binding affinity (as discussed in detail below), we expected to see equal performance of both LPMOs under the conditions of the HRP/Amplex Red assay (i.e., in the absence of any polysaccharide substrate).

Given the fact that even very low amounts of free copper will lead to significant H_2O_2 generation in this reaction set-up (Fig. 2B), one has to be extremely careful when interpreting the observed difference in H_2O_2 production between *Sc*LPMO10C and *Sc*LPMO10C-AA10. Looking for explanations, we first considered the possibility that the difference is caused by differences in the rate by which trace amounts of free copper (e.g., 0.1 μM copper, see Fig. 2B) are released from the active site of the LPMOs due to different rates of auto-catalytic damage. Release of copper from the LPMO active site under reducing conditions is conceivable since it is known that auto-catalytic oxidation predominately affects copper-binding histidine residues [16]. However, this scenario is incompatible with the linear shape of the H_2O_2-accumulation curves obtained for both LPMO variants (Fig. 2C) and thus seems not applicable.

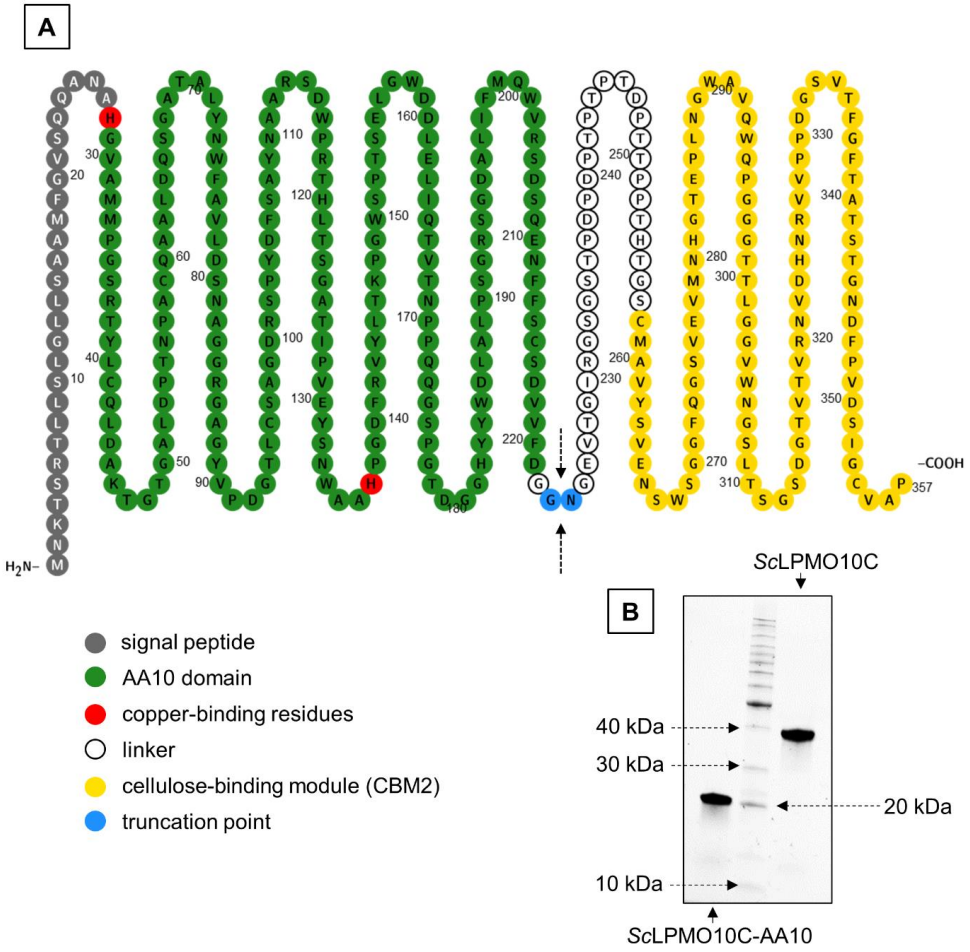

117

118 **Figure 1. Domain architecture of *Sc*LPMO10C (panel A) and SDS-PAGE of purified**
119 ***Sc*LPMO10C and *Sc*LPMO10C-AA10 (panel B).** *Sc*LPMO10C-AA10 is a modified form of
120 *Sc*LPMO10C produced by truncation of the cellulose-binding module as indicated by the blue
121 color and the arrows. For expression, the native signal peptide was replaced by the signal
122 peptide of *Sm*LPMO10A (CBP21), which is shown in the figure. Domain boundaries were
123 annotated using Pfam (http://pfam.xfam.org/), with minor manual adjustments based on
124 inspection of the crystal structure of the catalytic domain (PDB: 4OY7) and the NMR structure
125 of the cellulose-binding domain (PDB: 6F7E). The schematic representation of *Sc*LPMO10C
126 was created with the Protter protein visualization tool (http://wlab.ethz.ch/protter).

127

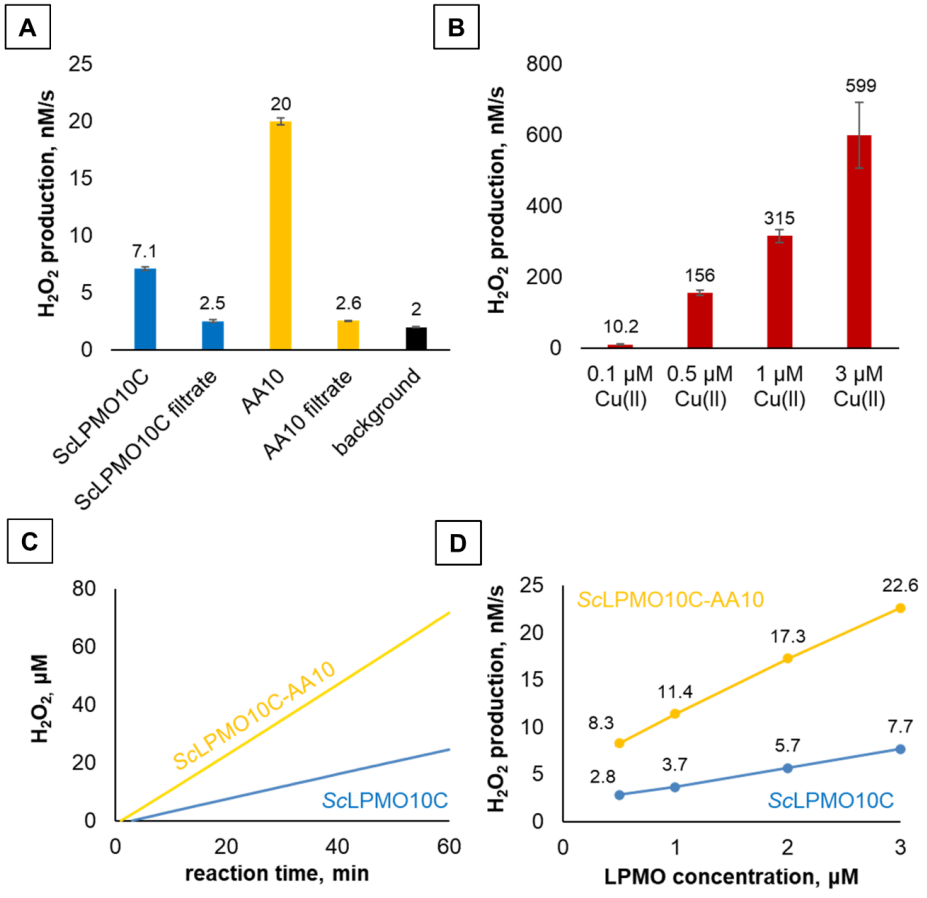

Figure 2. Apparent hydrogen peroxide production in reactions containing *Sc*LPMO10C and *Sc*LPMO10C-AA10 (panels A,C,D) or Cu(II)SO_4 (panel B). All experiments were carried out using 1 mM ascorbic acid in 50 mM sodium phosphate buffer, pH 6.0, at 30°C. Reaction mixtures contained 5 U/ml HRP, 100 µM Amplex Red, 1% (v/v) DMSO and varying concentrations of LPMOs and Cu(II)SO_4. The data shown in panels A and C are for LPMO concentrations of 3 µM. H_2O_2 production rates were derived from linear progress curves (such as shown in panel C). Free copper control experiments designated as "*Sc*LPMO10C filtrate" and "AA10 filtrate" in panel A were carried our using protein-free samples obtained from enzyme stock solutions by ultrafiltration. Such filtrates will contain the same amount of free copper ions as the LPMO preparations. The black bar in panel A denotes the background rate of hydrogen peroxide accumulation in the reaction containing reductant but lacking LPMO. Error bars indicate standard deviations between triplicates. The rates shown in panels A and D were obtained in independent experiments. Error bars in panel D are hidden behind the markers.

An additional control experiment with varying amounts of both LPMOs (0.5 – 3 μM) showed that the gap between the H_2O_2-generation rates is constant across all tested concentrations (Fig. 2D), which would not be the case if free copper is indeed released under the assay conditions at rates that differ between the two enzymes. Thus, it would seem that the observed difference in H_2O_2 production between *Sc*LPMO10C and *Sc*LPMO10C-AA10 relates to an intrinsic enzyme property, i.e., a difference in oxidase activity. A possible, although highly speculative, explanation is that the CBM weakly interacts with the substrate-binding surface of the catalytic domain, which could reduce oxidase activity by shielding the active site Cu(II) from the solvent and the reductant.

Cellulose solubilization by *Sc*LPMO10C and *Sc*LPMO10C-AA10

Our next goal was to compare the performance of *Sc*LPMO10C and *Sc*LPMO10C-AA10 during Avicel depolymerization. The hydrogen peroxide production gap between the full-length and truncated LPMO observed in the HRP/Amplex Red assay is likely to become more pronounced in the presence of cellulose. As alluded to above, existing data indicate that binding to polysaccharide substrates prevents LPMOs from producing hydrogen peroxide [27, 28]. Furthermore, it is well established that the cellulose-binding module of *Sc*LPMO10C is capable of much stronger interaction with substrate than the catalytic domain of the enzyme, and is thus important for keeping the enzyme active site closer to its substrate [31, 33]. Hence, it is sensible to expect enhanced in situ hydrogen peroxide generation by weak-binding *Sc*LPMO10C-AA10 compared to the stronger binding full-length LPMO during Avicel degradation.

Interestingly, if one accepts the premise that LPMO action is limited by access to H_2O_2, and if the above considerations about expected H_2O_2 production levels in the presence of

substrate are true, it is conceivable that weak binding *Sc*LPMO10C-AA10 and stronger binding full-length *Sc*LPMO10C may act synergistically during Avicel degradation. The truncated LPMO will spent most of its time in solution, generating hydrogen peroxide to boost the oxidative activity of the wild-type enzyme that is anchored on a crystalline surface by its CBM. On the other hand, the truncated enzyme, which is prone to damaging off-pathway reactions [33], may be protected by the full-length enzyme that removes H_2O_2 from the solution in productive reactions. To test this hypothesis, we carried out Avicel degradation experiments with *Sc*LPMO10C, *Sc*LPMO10C-AA10 or a combination of both LPMOs in the presence of ascorbic acid (Fig. 3).

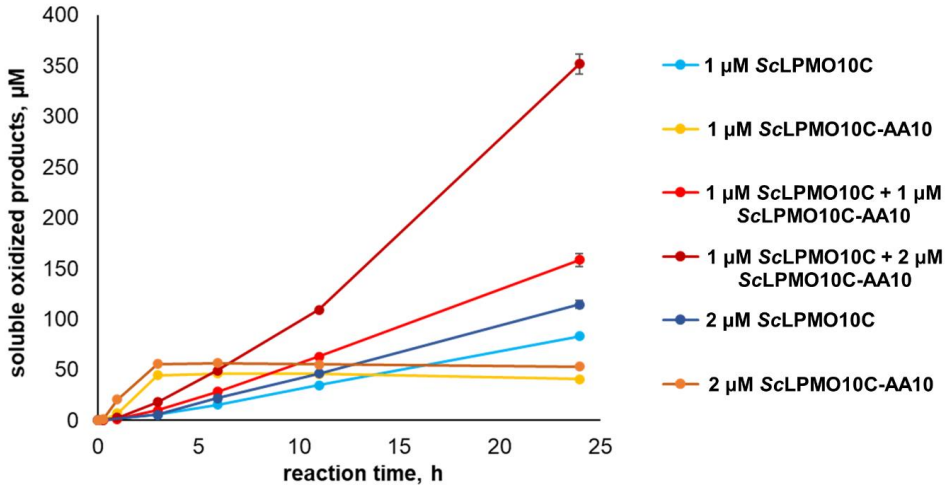

Figure 3. Cellulose oxidation by *Sc*LPMO10C and *Sc*LPMO10C-AA10. The graph shows soluble oxidized products released from 1% (w/v) Avicel by *Sc*LPMO10C, *Sc*LPMO10C-AA10 or mixtures of these LPMOs in the presence of 1 mM ascorbic acid. The reactions were carried out in 50 mM sodium phosphate buffer, pH 6.0, supplied with 1 mM ascorbic acid, at 30°C. Error bars indicate standard deviations between triplicates.

Cellulose depolymerization by 1 µM or 2 µM *Sc*LPMO10C resulted in a slow (0.05 min^{-1}) but steady release of oxidized products over 24 hours. Such low catalytic rates are common among bacterial LPMOs operating in the absence of exogenously added hydrogen peroxide [1, 18, 28]. In contrast to the full-length enzyme, the reactions with 1 µM or 2 µM *Sc*LPMO10C-AA10 were much (approximately 4-fold) faster. In these reactions, product release diminished early during the course of the experiment. This is indicative of LPMO auto-catalytic inactivation. It is well known that LPMO instability is promoted by reduced binding to the substrate [37] and high levels of H_2O_2 [16], and both apply to *Sc*LPMO10C-AA10 relative to the full-length enzyme.

Strikingly, reactions with 1 µM *Sc*LPMO10C + 1 µM *Sc*LPMO10C-AA10 or 1 µM *Sc*LPMO10C + 2 µM *Sc*LPMO10C-AA10 did not show signs of enzyme inactivation and generated higher product levels compared to reactions with the individual LPMOs (Fig. 3). The amount of oxidized products released after 24 hours was 1.3-fold (1 µM *Sc*LPMO10C + 1 µM *Sc*LPMO10C-AA10) and 2.6-fold (1 µM *Sc*LPMO10C + 2 µM *Sc*LPMO10C-AA10) higher compared to the sum of the products generated by these enzymes in individual reactions, indicative of strong synergistic action. The reaction with 1 µM *Sc*LPMO10C + 2 µM *Sc*LPMO10C-AA10 is remarkable, showing a much higher rate than *Sc*LPMO10C alone, no signs of enzyme inactivation and high product levels. Considering the observed (Fig. 2) and expected H_2O_2 production levels, the increased rate of the reaction may be explained by increased levels of available H_2O_2, which is produced by the truncated enzyme. At the same time, the truncated enzyme is protected from damaging off-pathway reactions with H_2O_2 because the oxidant is used in productive reactions by the full-length enzyme. There are indications, from modelling [38] and experiments [39], that binding of H_2O_2 by an LPMO is promoted by the presence of substrate. Thus, it is plausible that the full-length enzyme, with

high substrate affinity, outcompetes the truncated enzyme, with low substrate affinity, for binding (and reacting with) H_2O_2.

Paradoxically, the initial rate of the most efficient reaction (1 µM *Sc*LPMO10C + 2 µM *Sc*LPMO10C-AA10) was still considerably lower than the initial rate of the reaction with 1 µM or 2 µM *Sc*LPMO10C-AA10 alone (Fig. 3, first three hours). Looking for possible explanations, it is important to take into account the expected instability of *Sc*LPMO10C-AA10, which may lead to gradual release of copper into solution, which will boost the activity of still intact LPMOs because free copper promotes LPMO-independent H_2O_2 generation in the presence of ascorbic acid (Fig. 2B). In other words, the decreased initial rate of product release observed upon adding *Sc*LPMO10C to a reaction with *Sc*LPMO10C-AA10, may be a direct consequence of the above-mentioned stabilization of the truncated enzyme. This complicated scenario is further explained and experimentally verified below.

Reductant consumption in reactions with *Sc*LPMO10C and *Sc*LPMO10C-AA10

If copper is indeed released from the active site of unstable LPMOs then this effect should be carefully accounted for while interpreting the data shown on Fig. 3. Thus, our next goal was to evaluate whether spectroscopic quantification of ascorbic acid in LPMO reactions can be used as a tool to detect a leakage of copper ions from the oxidatively damaged histidine brace. At standard aerobic conditions, the depletion of reductant is driven by LPMO-dependent H_2O_2 production (oxidase activity), LPMO-dependent substrate oxidation (peroxygenase activity), reactions between hydrogen peroxide and ascorbic acid [25] and enzyme-independent H_2O_2 generation (i.e., oxidation of the reductant by O_2). For some reductants, including ascorbic acid, the latter reaction is strongly promoted by free copper [28]. Indeed, under the reaction conditions used here, major effects of free copper will occur

233 at concentrations (e.g., 0.1 μM; (Fig. 2B) that are well below the LPMO concentrations (1-3
234 μM) used in this study. Thus, copper release caused by oxidative damage to the active site of
235 only a fraction of the LPMOs could strongly affect the activity (and exposure to H_2O_2) of the
236 remaining intact enzymes.

237 Fig. 4A shows the impact of free copper on reductant depletion under the conditions
238 used for the reactions shown in Figs 2 & 3. In accordance with Fig. 2B, showing increased H_2O_2
239 production upon addition of 0.1 μM Cu(II), Fig. 4A shows that the presence of 0.1 μM Cu(II)
240 drastically speeds up the turnover of ascorbic acid. Thus, there is no doubt that under the
241 conditions used here, which are often applied in the field, release of copper from damaged
242 LPMOs will lead to increased H_2O_2 production and, thus, fueling of the remaining intact
243 LPMOs.

244 Quantification of ascorbic acid in reactions with substrate (i.e., the reactions displayed
245 in Fig. 3) revealed slow and steady reductant depletion in the reactions with 1 μM
246 *Sc*LPMO10C, 2 μM *Sc*LPMO10C or 1 μM *Sc*LPMO10C + *Sc*LPMO10C-AA10 (Fig. 4B), which
247 coincides with the close to linear product formation progress curves of Fig. 3. In stark contrast,
248 the reactions with 1 μM or 2 μM *Sc*LPMO10C-AA10 showed rapid and complete ascorbic acid
249 consumption within first 6 or 3 hours of the experiment, respectively (Fig. 4B). Notably, this
250 high consumption is nowhere near to being proportional to the low amounts of oxidized
251 LPMO products released in these reactions (Fig. 3), showing that reducing power is used in
252 another process, for example reduction of O_2 to H_2O_2. The reductant depletion rates observed
253 with 1 μM or 2 μM *Sc*LPMO10C-AA10 are comparable to the results of the control
254 experiments with free Cu(II) (Fig. 4A) and strongly suggest that copper indeed leaves the
255 LPMO active site, which will increase H_2O_2 production in the presence of ascorbic acid.

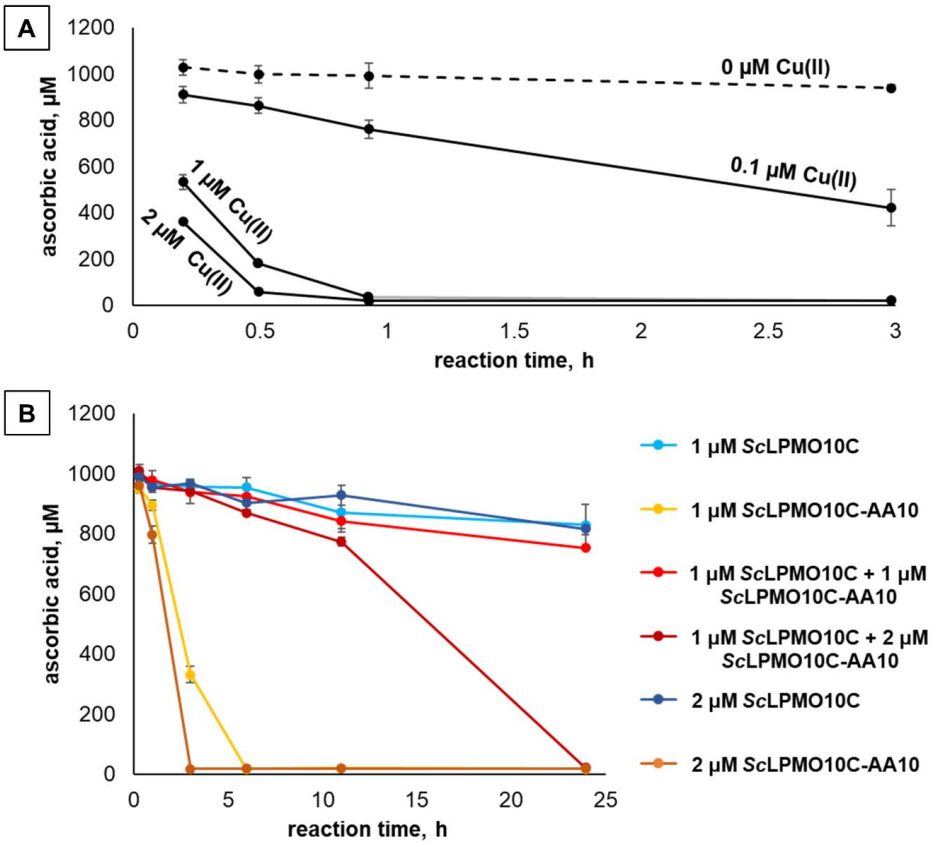

Figure 4. Ascorbic acid consumption in reactions containing Cu(II)SO_4 (panel A) or LPMOs (panel B). The reactions were carried out at 30 °C in 50 mM sodium phosphate buffer, pH 6.0, supplied with 1% (w/v) Avicel, and were initiated by the addition of 1 mM ascorbic acid at t = 0. The reductant concentration was determined by UV spectroscopy immediately after removing the insoluble LPMO substrate by filtration. Note that the reductant depletion curves in panel B were obtained using the same samples as shown in Fig. 3. Error bars indicate standard deviations between triplicates.

Thus, we propose, that the high initial rate and fast enzyme inactivation observed in reactions with 1 µM or 2 µM *Sc*LPMO10C-AA10 (Fig. 3) are the result of a self-reinforcing process: The LPMO binds weakly to the substrate and produces lots of H_2O_2; this leads to higher LPMO activity and higher LPMO inactivation, where the latter leads to the release of free copper, which, by promoting H_2O_2 production, further increases LPMO activity and LPMO

inactivation. The result is a high initial rate of reaction and fast cessation of the reaction, in accordance with the progress curves shown in Fig. 3. This self-reinforcing process will be hindered upon addition of the full-length LPMO that uses the H_2O_2 in productive LPMO reactions, which explains the paradox drawn up in the previous section.

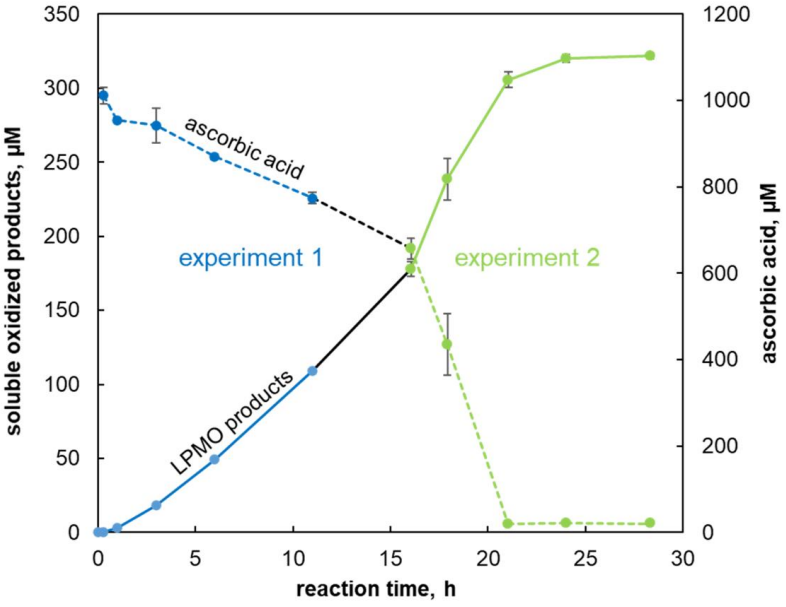

Figure 5. Release of oxidized products and reductant depletion in the reaction with 1 µM ScLPMO10C + 2 µM ScLPMO10C-AA10. The reactions were carried out at 30 °C in 50 mM sodium phosphate buffer, pH 6.0, supplied with 1% (w/v) Avicel and were initiated by adding 1 mM ascorbic acid. The data shown in blue and green color represent two independent experiments. The blue progress curves ("experiment 1") are the same as shown in Fig. 3 and Fig. 4B. In the second identical experiment (green) only later time points were monitored. The black lines connect the blue curves with the green curves. Error bars indicate standard deviations for triplicates.

Importantly, while cessation of product formation in LPMO reactions is usually ascribed to enzyme inactivation, the data in Fig. 4 illustrate, that, due to the self-reinforcing nature of the LPMO inactivation process, fast depletion of ascorbic acid may occur, which will

also stop the LPMO reaction. In the reactions shown here, both factors may have played a role. However, the progress curves for the reaction with 1 µM *Sc*LPMO10C-AA10 indicate that product formation stopped at or before 3 h (Fig. 3), while the reductant had not yet been completely depleted (Fig. 4B). Hence, in this experiment, oxidative inactivation of the LPMO was the dominating process leading to cessation of the reaction.

More insight into this matter may be derived from the ascorbic acid depletion curve for the reaction with 1 µM *Sc*LPMO10C + 2 µM *Sc*LPMO10C-AA10, which displayed an apparent biphasic behavior (Fig. 4B). A slow (i.e., enzyme-dependent) reductant consumption phase was followed by a phase with a faster decrease in the ascorbic acid concentration. Expansion of the progress curves shown in Fig. 3 and Fig. 4 with additional data points confirmed the biphasic nature of the process. Fig. 5 shows that the phase with steady ascorbic acid consumption was followed by a phase of rapid reductant consumption and cessation of product formation that reflects a collapse of the reaction system, similar to what was seen for the reactions with *Sc*LPMO10C-AA10 only, where this collapse happened earlier during the reaction due to the absence of the H_2O_2-consuming full-length enzyme (Fig. 4B).

The only plausible explanation for the collapse observed in this biphasic reaction is the release of copper by damaged LPMOs. Under turnover conditions gradual LPMO inactivation and copper-release from damaged LPMOs are to be expected due to off-pathway reactions, even though, in well controlled reaction systems, off-pathway reactions may be infrequent and not necessarily always destructive for the LPMO [40]. It is conceivable that at about 15 h in the biphasic reaction accumulated copper reached levels that triggered the self-reinforcing enzyme inactivation process described above. This process could initially speed up the reaction rate (as is visible in Fig. 5, showing a vaguely sigmoidal curve for product formation) but will lead to system collapse and rapid ascorbic acid depletion. Product formation (Fig. 3)

and ascorbic acid depletion (Fig. 4B) remained constant for the full 24 h of the reaction containing 50 % less of the truncated LPMO (1 µM *Sc*LPMO10C + 1 µM *Sc*LPMO10C-AA10 reaction). So, in this reaction, where one would expect less H_2O_2 production and less enzyme inactivation, the turning point leading to rapid ascorbic acid depletion and biphasic behavior was never reached because there was less release of free copper into solution.

Stability of *Sc*LPMO10C and *Sc*LPMO10C-AA10 in the absence of substrate

In line with previously published data, the above is based on the assumption that inactivation of an LPMO in the absence of substrate will relate to the oxidase activity of that LPMO (i.e., H_2O_2 production). To verify this assumption, we assessed the stability of the full-length and truncated enzymes under reducing conditions in the absence of substrate. 2 µM *Sc*LPMO10C or 2 µM *Sc*LPMO10C-AA10 were pre-incubated with 1 mM ascorbic acid for 2 hours to promote inactivation. Aliquots were taken at various time points and then supplied with Avicel and another (the same) dose of ascorbic acid to assess the residual activity. This approach is not without limitations because free copper ions that have left the histidine brace as a result of enzyme inactivation will affect the subsequent LPMO reaction with Avicel where free copper will affect both activity and stability. Nevertheless, the results, depicted in Fig. 6, show a clear difference: the full-length LPMO retained most of its catalytic potential during the pre-incubation, whereas the truncated enzyme was rapidly inactivated. This difference is expected in light of the difference in H_2O_2 production by the two enzymes (Fig. 2A). Taken together, the results shown in Fig. 2 and Fig. 6 suggest that truncation of the CBM significantly impairs the oxidative stability of *Sc*LPMO10C in the absence of substrate, which is remarkable.

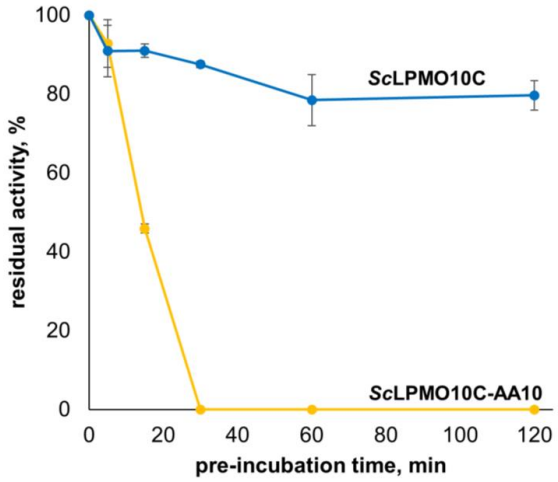

Figure 6. Oxidative stability of *Sc*LPMO10C and *Sc*LPMO10C-AA10. The figure shows the residual activity of 1 µM *Sc*LPMO10C and 1 µM *Sc*LPMO10C-AA10 in a reaction with 1% (w/v) Avicel after various periods of pre-incubation with 1 mM ascorbic acid in the absence of substrate (i.e., under conditions that promote auto-catalytic inactivation). The cellulose degradation reaction was carried out for 24 hours at 30 °C in 50 mM sodium phosphate buffer, pH 6.0, supplied with fresh 1 mM ascorbic acid. Error bars indicate standard deviations between triplicates.

Concluding remarks

This study provides insight into the interplay between LPMOs with different H_2O_2 generation and consumption capabilities. Being a much better hydrogen peroxide producer, *Sc*LPMO10C-AA10 is able to enhance cellulose oxidation by *Sc*LPMO10C. At the same time, *Sc*LPMO10C protects *Sc*LPMO10C-AA10 from fast auto-catalytic inactivation by removing excessive H_2O_2. The synergistic action of the two LPMOs allowed for steady cellulose depolymerization over 24 hours, with an efficiency that clearly surpassed the efficiencies of the individual enzymes.

While these results shed light on the complexity of LPMO reactions, especially when using “copper-sensitive” reductants, it remains to be seen whether the synergy observed here

also occurs in Nature. LPMOs are abundant and many organisms contain multiple LPMOs, some with and some without CBMs. These CBM-free LPMOs could help fueling other LPMOs with H_2O_2 as shown above, and could also fuel other H_2O_2-dependent enzymes such as lignin peroxidases [41]. On the other hand, in contrast to the catalytic domain of CBM-containing *Sc*LPMO10C, these natural single domain LPMOs may very well have evolved to bind their substrates strongly, as observed for, e.g., the archetypal single domain LPMO *Sm*LPMO10A (or CBP21; [39]), and may thus be less efficient H_2O_2-producers.

While we expected relatively fast H_2O_2 generation by *Sc*LPMO10C-AA10 in reactions with cellulose because of low binding, the truncated LPMO was found to produce more hydrogen peroxide than the full-length enzyme even in the absence of substrate. As we show and discuss above, this surprising result is not driven by free copper and thus seems related to hitherto unknown effects of the CBM on LPMO oxidase activity. It is possible that the higher H_2O_2 production rate of *Sc*LPMO10C-AA10 in the absence of substrate is an artifact of LPMO truncation, which, in principle could lead to minor changes in the enzyme structure that could make the reduced copper more prone to oxidation by O_2. However, this seems unlikely, given the fact that the truncation point is >35 Å away from the active site and that the X-ray structure of *Sc*LPMO10C-AA10 shows no anomalies [35] (PDB: 4OY7). Another possible explanation is that the catalytic and cellulose-binding domains of *Sc*LPMO10C interact in an inter-molecular or intra-molecular fashion. It is tempting, although highly speculative, to propose that the CBM may protect the LPMO from auto-catalytic damage in the absence of substrate by shielding the active site from the reductant (preventing reduction), or from reacting with O_2, thus keeping the fraction of H_2O_2-producing enzyme molecules low. Further studies are needed to explore this scenario.

In addition to providing insights into the possible impact of CBMs on LPMO functionality and generating more insight into the crucial role of H_2O_2 in LPMO catalysis, the present data shed light on the complexity of interpreting ascorbic acid-driven LPMO reactions. Ascorbic acid was, somewhat fortuitously, used in research leading to the discovery of LPMO activity [1] and has been used by many researchers since. This "copper-sensitive" reductant may engage in multiple reactions that are difficult to control and assess. One of these reactions, the scavenging of excess H_2O_2 (i.e., further reduction to water) was not considered in the above because there is ample data showing that this reaction is slow relative to the other possible reactions [17, 40].

Progress curves for LPMO reactions with ascorbic acid often show apparent enzyme inactivation and the present study reveals, to the best of our knowledge for the first time, a plausible underlying mechanism. We show that release of copper ions as a consequence of (well known; [16, 37]) oxidative damage to the LPMO active site triggers a self-reinforcing chain reaction leading to increased enzyme-independent H_2O_2 generation, rapid enzyme inactivation and reductant depletion. Similar processes may occur in reactions with other reductants whose ability to reduce O_2 is copper-dependent, such as L-cysteine [23] and reduced glutathione [42]. While fully controlling and understanding all these processes remains challenging, the present study underpins that optimization of LPMO activity and stability requires control of H_2O_2 levels and that, in many commonly used experimental settings, these levels are affected not only by LPMO oxidase activity but also by LPMO inactivation. Since oxidase activity varies between LPMOs [17, 43] optimal conditions for LPMO reactions, and the relative impact of free copper, will vary.

Methods

Materials

Chemicals were obtained from Sigma-Aldrich (St. Louis, MO, USA) unless specified otherwise. The model microcrystalline cellulose substrate used in the study was Avicel PH-101 with particle size of approximately 50 µm. 100 mM ascorbic acid stock solutions were prepared in metal-free TraceSELECT water (Honeywell, Charlotte, NC, USA) and then filter-sterilized using 0.22 µm syringe filters. Amplex Red was purchased from Thermo Fisher Scientific (Waltham, MA, USA) and dissolved in DMSO at 10 mM final concentration. The reductant and Amplex Red solutions were aliquoted, stored at -20 °C in light-protected tubes and used only once after thawing. Horseradish peroxidase type II (HRP; Sigma-Aldrich, St. Louis, MO, USA) was kept at 100 U/ml concentration in 50 mM sodium phosphate buffer, pH 6.0 at 4°C. Tryptone and yeast extract were obtained from Thermo Fisher Scientific.

Protein production and purification

Previously generated *Sc*LPMO10C and *Sc*LPMO10C-AA10 expressing *E. coli* BL21 DE3 strains [35] were used to inoculate Terrific Broth (TB) medium supplied with 100 µg/ml ampicillin. The cultures (2 × 500 ml for each LPMO-expressing strain) were incubated for 24 h at 30°C in a LEX-24 Bioreactor (Harbinger Biotechnology & Engineering, Markham, Canada) using compressed air for aeration. The cells were harvested by centrifugation (6000 × g for 10 min at 4°C) using a Beckman Coulter centrifuge (Brea, CA, USA). Periplasmic extracts were produced by applying osmotic shock as described previously [44] and were filter-sterilized through 0.22-µm syringe filters prior to further purification. These extracts were then subjected to ion-exchange chromatography using HiTrap Q FF (Q Sepharose) 5-ml columns

(GE Healthcare, Chicago, USA). Proteins were eluted at 2.5 ml/min flow rate with a linear gradient of NaCl (0–500 mM, 250 ml) in the starting buffer (50 mM Tris-HCl, pH 7.5). LPMO-containing fractions were pooled, concentrated to approximately 1 ml volume (Vivaspin ultrafiltration tubes, 10 kDa MWCO, Sartorius, Göttingen, Germany) and loaded onto a ProteoSEC Dynamic 16/60 3-70 HR preparative size-exclusion column (Protein Ark, Sheffield, UK) operating at 1 ml/min flow rate and equilibrated with 50 mM Tris-HCl, pH 7.5, containing 200 mM NaCl. Purity of resulting *Sc*LPMO10C and *Sc*LPMO10C-AA10 preparations was confirmed by SDS-PAGE. The LPMO concertation was determined using UV spectroscopy at 280 nm. The theoretical extinction coefficients were predicted using the Expasy ProtParam tool [45].

Copper saturation

Purified LPMO solutions were concentrated to 0.5 ml volume using Vivaspin ultrafiltration tubes (10 kDa MWCO, Sartorius, Göttingen, Germany) and incubated with two-fold molar surplus of $Cu(II)SO_4$ at room temperature for 30 minutes. The excess (unbound) copper was removed by desalting with a PD MidiTrap G-25 gravity flow column (GE Healthcare, Chicago, USA), equilibrated with 50 mM sodium phosphate buffer, pH 6.0. To ensure effective free copper removal, the *Sc*LPMO10C and *Sc*LPMO10C-AA10 samples were then subjected to multiple consecutive rounds of dilution and concertation using 50 mM sodium phosphate buffer, pH 6.0 and Vivaspin ultrafiltration tubes. The resulting total dilution factors for solutions of copper-saturated LPMOs amounted to at least 160 000.

Hydrogen peroxide detection

In situ hydrogen peroxide generation in LPMO reactions was assessed using a modified HRP/Amplex Red assay protocol [18], originally proposed by Kittl et al. [24]. In brief, 90 µl of LPMO solution in 50 mM sodium phosphate buffer, pH 6.0, supplied with HRP and Amplex Red, was pre-incubated for 5 min at 30°C in a 96-well microtiter plate. Next, 10 µl of 10 mM ascorbic acid was added to start the reaction, followed by 10 s of mixing at 600 RPM inside a Varioscan LUX plate reader (Thermo Fisher Scientific, Waltham, MA, USA). Hydrogen peroxide was detected by monitoring the formation of resorufin at 563 nm. The final concentrations of LPMOs, HRP, Amplex Red and ascorbic acid were 0.5-3 µM, 5 U/ml, 100 µM and 1 mM, respectively. H_2O_2 standard solutions were prepared in 50 mM sodium phosphate buffer, pH 6.0, and supplied with 1 mM ascorbic acid prior to the addition of HRP and Amplex Red. The background non-enzymatic H_2O_2 production was assessed in a control experiment with 1 mM ascorbic acid and no LPMO.

To ensure that the observed LPMO-dependent hydrogen peroxide generation is not biased by residual free copper ions in enzyme preparations, protein-free samples were obtained from the LPMO stock solutions using 3 kDa MWCO 1.5 ml ultrafiltration tubes (VWR International, Radnor, PA, USA) and were used to set up control experiments by substituting LPMOs with the same amount of filtrates, as previously described [28].

LPMO reactions with microcrystalline cellulose

LPMO reactions with insoluble substrate (1% w/v Avicel) were carried out in 50 mM sodium-phosphate buffer, pH 6.0 using an Eppendorf thermomixer (Eppendorf, Hamburg, Germany) set to 30°C and 950 RPM. The reactions were started by supplying 1 mM ascorbic acid (final concentration).

Aliquots were taken at various time points, and the reactions were quenched by removing the insoluble substrate using a 96-well filter plate (Millipore, Burlington, MA, USA). The concentration of ascorbic acid in filtered solutions was determined by UV spectrometry at 255 nm wavelength. Standard solutions of the reductant were prepared in metal-free TraceSELECT water. The samples were then treated with 2 µM of recombinant *Thermobifida fusca* GH6 endoglucanase (*Tf*Cel6A; produced in-house) [46] at 37°C overnight to convert soluble C1-oxidized oligosaccharides to a simple mixture of oxidized dimers and trimers (i.e. GlcGlc1A and Glc_2Glc1A).

LPMO oxidative stability assay

The oxidative stability of *Sc*LPMO10C and *Sc*LPMO10C-AA10 was assessed by pre-incubating 2 µM enzyme in 50 mM sodium phosphate buffer, pH 6.0, containing 1 mM ascorbic acid, for two hours at 30°C. Aliquots were taken at various time points and supplied with 1% (w/v) Avicel and another (the same) dose of ascorbic acid. LPMO reactions with Avicel were carried out for 24 hours and then stopped by filtering out the insoluble substrate. These samples were treated with *Tf*Cel6A as described above and used to quantify the residual LPMO activity. The final concentration of both LPMOs in the reactions with Avicel was 1 µM.

Quantification of LPMO products

C1-oxidized soluble LPMO products were detected and quantified by high-performance anion-exchange chromatography with pulsed amperometric detection (HPAEC-PAD) using a Dionex ICS6000 system (Thermo Scientific, San Jose, CA, USA) equipped with a CarboPac PA200 analytical column, as recently described [47]. In brief, a concave gradient from 1 mM to 100 mM potassium methanesulfonate (KMSA) was applied over 14 min with

63 µl/min flow rate to separate native and C1-oxidized oligosaccharides, followed by a 3 min washing step (100 mM KMSA) and a 9 min column reconditioning step (1 mM KMSA). LPMO products were quantified using standard mixtures of C1-oxidized cellobiose and cellotriose, which were produced in-house using cellobiose dehydrogenase [48], according to a previously published protocol [49].

References

1. Vaaje-Kolstad, G. *et al.* An oxidative enzyme boosting the enzymatic conversion of recalcitrant polysaccharides. *Science.* **330**, 219-22 (2010).
2. Forsberg, Z. *et al.* Cleavage of cellulose by a CBM33 protein. *Protein Sci.* **20**, 1479-83 (2011).
3. Quinlan, R. J. *et al.* Insights into the oxidative degradation of cellulose by a copper metalloenzyme that exploits biomass components. *Proc. Natl. Acad. Sci. U.S.A.* **108**, 15079-84 (2011).
4. Phillips, C. M., Beeson, W. T., Cate, J. H. & Marletta, M. A. Cellobiose dehydrogenase and a copper-dependent polysaccharide monooxygenase potentiate cellulose degradation by *Neurospora crassa*. *ACS Chem. Biol.* **6**, 1399-406 (2011).
5. Couturier, M. *et al.* Lytic xylan oxidases from wood-decay fungi unlock biomass degradation. *Nat Chem. Biol.* **14**, 306-310 (2018).
6. Frommhagen, M. *et al.* Discovery of the combined oxidative cleavage of plant xylan and cellulose by a new fungal polysaccharide monooxygenase. *Biotechnol. Biofuels.* **8**, 101 (2015).
7. Hegnar, O. A. *et al.* Quantifying oxidation of cellulose-associated glucuronoxylan by two lytic polysaccharide monooxygenases from *Neurospora crassa*. *Appl. Environ. Microbiol.* **87**, e0165221 (2021).
8. Eibinger, M. *et al.* Cellulose surface degradation by a lytic polysaccharide monooxygenase and its effect on cellulase hydrolytic efficiency. *J. Biol. Chem.* **289**, 35929-38 (2014).
9. Dimarogona, M., Topakas, E., Olsson, L. & Christakopoulos, P. Lignin boosts the cellulase performance of a GH-61 enzyme from *Sporotrichum thermophile. Bioresour. Technol.* **110**, 480-7 (2012).
10. Chylenski, P. *et al.* Enzymatic degradation of sulfite-pulped softwoods and the role of LPMOs. *Biotechnol. Biofuels.* **10**, 177 (2017).
11. Sanhueza, C., Carvajal, G., Soto-Aguilar, J., Lienqueo, M. E. & Salazar, O. The effect of a lytic polysaccharide monooxygenase and a xylanase from *Gloeophyllum trabeum* on the enzymatic hydrolysis of lignocellulosic residues using a commercial cellulase. *Enzyme Microb. Technol.* **113**, 75-82 (2018).
12. Vermaas, J. V., Crowley, M. F., Beckham, G. T. & Payne, C. M. Effects of lytic polysaccharide monooxygenase oxidation on cellulose structure and binding of oxidized cellulose oligomers to cellulases. *J. Phys. Chem. B.* **119**, 6129-43 (2015).
13. Eibinger, M., Sattelkow, J., Ganner, T., Plank, H. & Nidetzky, B. Single-molecule study of oxidative enzymatic deconstruction of cellulose. *Nat. Commun.* **8**, 894 (2017).
14. Harris, P. V., Xu, F., Kreel, N. E., Kang, C. & Fukuyama, S. New enzyme insights drive advances in commercial ethanol production. *Curr. Opin. Chem. Biol.* **19**, 162-70 (2014).
15. Cannella, D., Hsieh, C. W., Felby, C. & Jorgensen, H. Production and effect of aldonic acids during enzymatic hydrolysis of lignocellulose at high dry matter content. *Biotechnol. Biofuels.* **5**, 26 (2012).
16. Bissaro, B. *et al.* Oxidative cleavage of polysaccharides by monocopper enzymes depends on H_2O_2. *Nat. Chem. Biol.* **13**, 1123-1128 (2017).
17. Rieder, L., Stepnov, A. A., Sørlie, M. & Eijsink, V. G. H. Fast and specific peroxygenase reactions catalyzed by fungal mono-copper enzymes. *Biochemistry.* **60**, 3633-3643 (2021).
18. Stepnov, A. A. *et al.* The impact of reductants on the catalytic efficiency of a lytic polysaccharide monooxygenase and the special role of dehydroascorbic acid. *FEBS Lett.* **596**, 53-70 (2022).
19. Kuusk, S. *et al.* Kinetics of H_2O_2-driven degradation of chitin by a bacterial lytic polysaccharide monooxygenase. *J. Biol. Chem.* **293**, 523-531 (2018).
20. Jones, S. M., Transue, W. J., Meier, K. K., Kelemen, B. & Solomon, E. I. Kinetic analysis of amino acid radicals formed in H_2O_2-driven Cu(I) LPMO reoxidation implicates dominant homolytic reactivity. *Proc. Natl. Acad. Sci. U.S.A.* **117**, 11916-11922 (2020).
21. Wilson, R. J., Beezer, A. E. & Mitchell, J. C. A kinetic study of the oxidation of L-ascorbic acid (vitamin C) in solution using an isothermal microcalorimeter. *Thermochimica Acta.* **264**, 27-40 (1995).

22. Tulyathan, V., Boulton, R. B. & Singleton, V. L. Oxygen uptake by gallic acid as a model for similar reactions in wines. *J. Agric.Food Chem.* **37**, 844-849 (1989).
23. Kachur, A. V., Koch, C. J. & Biaglow, J. E. Mechanism of copper-catalyzed autoxidation of cysteine. *Free Radic. Res.* **31**, 23-34 (1999).
24. Kittl, R., Kracher, D., Burgstaller, D., Haltrich, D. & Ludwig, R. Production of four *Neurospora crassa* lytic polysaccharide monooxygenases in *Pichia pastoris* monitored by a fluorimetric assay. *Biotechnol. Biofuels.* **5**, 79 (2012).
25. Hegnar, O. A. *et al.* pH-dependent relationship between catalytic activity and hydrogen peroxide production shown via characterization of a lytic polysaccharide monooxygenase from *Gloeophyllum trabeum*. *Appl. Environ. Microbiol.* **85** (2019).
26. Eijsink, V. G. H. *et al.* On the functional characterization of lytic polysaccharide monooxygenases (LPMOs). *Biotechnol. Biofuels.* **12**, 58 (2019).
27. Filandr, F. *et al.* The H_2O_2-dependent activity of a fungal lytic polysaccharide monooxygenase investigated with a turbidimetric assay. *Biotechnol. Biofuels.* **13**, 37 (2020).
28. Stepnov, A. A. *et al.* Unraveling the roles of the reductant and free copper ions in LPMO kinetics. *Biotechnol. Biofuels.* **14**, 28 (2021).
29. Bissaro, B., Isaksen, I., Vaaje-Kolstad, G., Eijsink, V. G. H. & Røhr, Å. K. How a lytic polysaccharide monooxygenase binds crystalline chitin. *Biochemistry.* **57**, 1893-1906 (2018).
30. Guillen, D., Sanchez, S. & Rodriguez-Sanoja, R. Carbohydrate-binding domains: multiplicity of biological roles. *Appl. Microbiol. Biotechnol.* **85**, 1241-9 (2010).
31. Forsberg, Z. *et al.* Comparative study of two chitin-active and two cellulose-active AA10-type lytic polysaccharide monooxygenases. *Biochemistry.* **53**, 1647-56 (2014).
32. Crouch, L. I., Labourel, A., Walton, P. H., Davies, G. J. & Gilbert, H. J. The contribution of non-catalytic carbohydrate binding modules to the activity of lytic polysaccharide monooxygenases. *J. Biol. Chem.* **291**, 7439-49 (2016).
33. Courtade, G., Forsberg, Z., Heggset, E. B., Eijsink, V. G. H. & Aachmann, F. L. The carbohydrate-binding module and linker of a modular lytic polysaccharide monooxygenase promote localized cellulose oxidation. *J. Biol. Chem.* **293**, 13006-13015 (2018).
34. Chalak, A. *et al.* Influence of the carbohydrate-binding module on the activity of a fungal AA9 lytic polysaccharide monooxygenase on cellulosic substrates. *Biotechnol. Biofuels.* **12**, 206 (2019).
35. Forsberg, Z. *et al.* Structural and functional characterization of a conserved pair of bacterial cellulose-oxidizing lytic polysaccharide monooxygenases. *Proc. Natl. Acad. Sci. U.S.A.* **111**, 8446-51 (2014).
36. Bissaro, B., Kommedal, E., Røhr, Å. K. & Eijsink, V. G. H. Controlled depolymerization of cellulose by light-driven lytic polysaccharide oxygenases. *Nat. Commun.* **11**, 890 (2020).
37. Loose, J. S. M. *et al.* Multipoint precision binding of substrate protects lytic polysaccharide monooxygenases from self-destructive off-pathway processes. *Biochemistry.* **57**, 4114-4124 (2018).
38. Wang, B., Wang, Z., Davies, G. J., Walton, P. H. & Rovira, C. Activation of O_2 and H_2O_2 by lytic polysaccharide monooxygenases. *ACS Catalysis.* **10**, 12760-12769 (2020).
39. Bissaro, B. *et al.* Molecular mechanism of the chitinolytic peroxygenase reaction. *Proc. Natl. Acad. Sci. U.S.A.* **117**, 1504-1513 (2020).
40. Kuusk, S. & Väljamäe, P. Kinetics of H_2O_2-driven catalysis by a lytic polysaccharide monooxygenase from the fungus *Trichoderma reesei*. *J. Biol. Chem.* **297**, 101256 (2021).
41. Li, F. *et al.* A lytic polysaccharide monooxygenase from a white-rot fungus drives the degradation of lignin by a versatile peroxidase. *Appl. Environ. Microbiol.* **85** (2019).
42. Kachur, A. V., Koch, C. J. & Biaglow, J. E. Mechanism of copper-catalyzed oxidation of glutathione, *Free Radic. Res.* **28**, 259-69 (1998).
43. Petrović, D. M. *et al.* Comparison of three seemingly similar lytic polysaccharide monooxygenases from *Neurospora crassa* suggests different roles in plant biomass degradation. *J. Biol. Chem.* **294**, 15068-15081 (2019).

598 44. Manoil, C. & Beckwith, J. A genetic approach to analyzing membrane protein topology. *Science.*
599 **233**, 1403-8 (1986).
600 45. Gasteiger, E. *et al.* Protein Identification and analysis tools on the ExPASy Server in *The Proteomics*
601 *Protocols Handbook* pp. 571-607 (2005).
602 46. Spezio, M., Wilson, D. B. & Karplus, P. A. Crystal structure of the catalytic domain of a thermophilic
603 endocellulase. *Biochemistry.* **32**, 9906-16 (1993).
604 47. Østby, H., Jameson, J. K., Costa, T., Eijsink, V. G. H. & Arntzen, M. Ø. Chromatographic analysis of
605 oxidized cello-oligomers generated by lytic polysaccharide monooxygenases using dual electrolytic
606 eluent generation. *J. Chromatogr. A.* **1662**, 462691 (2022).
607 48. Zamocky, M. *et al.* Cloning, sequence analysis and heterologous expression in *Pichia pastoris* of a
608 gene encoding a thermostable cellobiose dehydrogenase from *Myriococcum thermophilum. Protein*
609 *Expr. Purif.* **59**, 258-65 (2008).
610 49. Bissaro, B., Forsberg, Z., Ni, Y., Hollmann, F., Vaaje-Kolstad, G. & Eijsink, V. G. H. Fueling biomass-
611 degrading oxidative enzymes by light-driven water oxidation. *Green Chemistry.* **18**, 5357-5366 (2016).

612

613 Acknowledgements

614 This work was supported by the Research Council of Norway through the OxyMod project
615 (269408) and by the Novo Nordisk Foundation through grant NNF18OC0055736 to Z.F.

616

617 Author contributions

618 AAS designed experiments, did most of the experimental work, analyzed data and drafted the
619 manuscript. VGHE and ZF provided funding, initiated the research, carried out supervision,
620 helped to design and conduct experiments, interpreted results, and contributed to writing
621 and editing the manuscript.

622

623 Competing interests

624 The authors declare no competing interests.

625

626

Data availability

The data that support the findings of this study are available in Figures 1-6.

Fast and specific peroxygenase reactions catalyzed by fungal mono-copper enzymes

Rieder L, Stepnov AA, Sørlie M, Eijsink VG

Paper IV

Biochemistry

pubs.acs.org/biochemistry Article

Fast and Specific Peroxygenase Reactions Catalyzed by Fungal Mono-Copper Enzymes

Lukas Rieder, Anton A. Stepnov, Morten Sørlie, and Vincent G.H. Eijsink*

Cite This: *Biochemistry* 2021, 60, 3633−3643 Read Online

ACCESS | Metrics & More | Article Recommendations | Supporting Information

ABSTRACT: The copper-dependent lytic polysaccharide monooxygenases (LPMOs) are receiving attention because of their role in the degradation of recalcitrant biomass and their intriguing catalytic properties. The fundamentals of LPMO catalysis remain somewhat enigmatic as the LPMO reaction is affected by a multitude of LPMO- and co-substrate-mediated (side) reactions that result in a complex reaction network. We have performed kinetic studies with two LPMOs that are active on soluble substrates, *Nc*AA9C and *Ls*AA9A, using various reductants typically employed for LPMO activation. Studies with *Nc*AA9C under "monooxygenase" conditions showed that the impact of the reductant on catalytic activity is correlated with the hydrogen peroxide-generating ability of the LPMO-reductant combination, supporting the idea that a peroxygenase reaction is taking place. Indeed, the apparent monooxygenase reaction could be inhibited by a competing H_2O_2-consuming enzyme. Interestingly, these fungal AA9-type LPMOs were found to have higher oxidase activity than bacterial AA10-type LPMOs. Kinetic analysis of the peroxygenase activity of *Nc*AA9C on cellopentaose revealed a fast stoichiometric conversion of high amounts of H_2O_2 to oxidized carbohydrate products. A k_{cat} value of 124 ± 27 s^{-1} at 4 °C is 20 times higher than a previously described k_{cat} for peroxygenase activity on an insoluble substrate (at 25 °C) and some 4 orders of magnitude higher than typical "monooxygenase" rates. Similar studies with *Ls*AA9A revealed differences between the two enzymes but confirmed fast and specific peroxygenase activity. These results show that the catalytic site arrangement of LPMOs provides a unique scaffold for highly efficient copper redox catalysis.

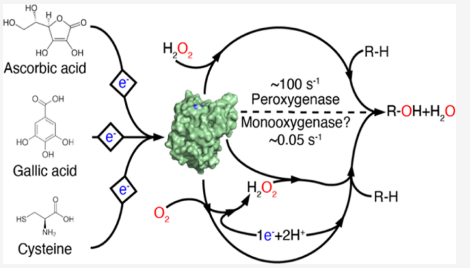

INTRODUCTION

Enzymes currently known as lytic polysaccharide monooxygenases (LPMOs) catalyze the oxidative scission of glycosidic bonds and by doing so they boost the activity of classical polysaccharide-degrading hydrolytic enzymes such as chitinases and cellulases.[1−10] LPMO catalytic sites contain a single copper-ion cofactor[11,12] that upon reduction reacts with either O_2 or H_2O_2 to generate oxygen species that is capable of abstracting a hydrogen atom from the C1 or the C4 carbon atom in glycosidic bonds.[9,13−16]

Initially, LPMOs were thought to be monooxygenases[3] (Figure 1A), but recent studies have shown that LPMOs can also act as peroxygenases[15] (Figure 1B) and that this reaction is faster than the monooxygenase reaction.[15−20] The peroxygenase reaction tends to lead to more enzyme damage compared to the monooxygenase reaction and may also lead to reduced catalytic specificity.[21] Relatively rapid enzyme inactivation under peroxygenase conditions may be taken to indicate that the peroxygenase reaction is not a true LPMO reaction[21] but could also have other explanations, such as subsaturating substrate concentrations that leave the enzyme prone to damaging off pathway reactions with H_2O_2.[16,20,22] Importantly, under the conditions typically used in LPMO "monooxygenase" reactions, H_2O_2 will be generated *in situ* and

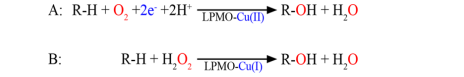

Figure 1. Reaction schemes for monooxygenase (A) and peroxygenase (B) reaction. The substrate is indicated by R. Hydroxylation of one of the carbons destabilizes the glycosidic bond, which, once oxidized, undergoes an elimination reaction leading to bond breakage.[12] Note the potential difference in reductant consumption between the two reaction schemes. In the peroxygenase scheme, a once reduced LPMO can carry out multiple reactions,[20,36,37] meaning that reductant consumption will be low if H_2O_2 is provided externally. If, however, H_2O_2 is generated *in situ* through the reduction of O_2, also the peroxygenase reaction will require two electrons per cycle ($O_2 + 2e^- + 2H^+ \rightarrow H_2O_2$).

there are indications that the observed reaction rates in such reactions, typically in the range of a few per minute,[17] reflect

Received: June 16, 2021
Revised: October 27, 2021
Published: November 5, 2021

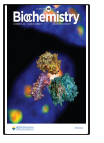

https://doi.org/10.1021/acs.biochem.1c00407
Biochemistry 2021, 60, 3633−3643

the rate of *in situ* generation of H_2O_2, rather than the rate of a true monooxygenase reaction.[23−25] *In situ* generation of H_2O_2 may result from LPMO-independent oxidation of the reductant by O_2 and may also involve the LPMO because LPMOs have oxidase activity.[26−28] These two routes toward H_2O_2 generation are intertwined in a manner that depends on both the reductant and the LPMO, whereas the impact of substrate binding on O_2 activation[28−30] adds an additional level of complexity. For example, Stepnov *et al.*[24] showed that the generation of H_2O_2 in standard reactions with an AA10 type (bacterial) LPMO (*i.e.*, LPMO + 1 mM reductant) was almost independent of the LPMO in reactions with gallic acid (GA), whereas the LPMO increased H_2O_2 production in reactions with ascorbic acid (AscA). It is not known whether the same would apply for the AA9 LPMOs that are abundant in biomass-degrading fungi.

Understanding LPMOs, which requires the robust assessment of LPMO kinetics, is complicated due to the many interconnected redox phenomena and catalytic pathways. In the presence of the substrate, LPMOs catalyze the oxidation of glycosidic bonds using O_2 or H_2O_2 [mono-oxygenase or peroxygenase reaction; Figure 1].[9,14,15,30] In the absence of a carbohydrate substrate, LPMOs catalyze the formation of H_2O_2 from molecular oxygen (oxidase reaction)[24,26] and may also catalyze reactions of H_2O_2 with the reducing agent.[24,31] The inhibitory effect of the substrate on H_2O_2 accumulation may reflect the inhibition of the oxidase reaction,[25] as originally proposed by Kittl *et al.*,[26] but may also reflect the consumption of the generated H_2O_2 in a productive LPMO reaction.[15] Next to engaging in oxidase reactions, reduced LPMOs may act as an H_2O_2 scavenger in peroxidase-like reactions.[31] Both these non-productive (per)oxidase reactions may lead to auto-catalytic enzyme inactivation.[15,20,22,32]

The substrate of most LPMOs is polymeric and insoluble, which complicates the determination of true substrate concentrations (*i.e.*, the concentration of productive binding sites) and generates kinetic complications related to potentially slow substrate association/dissociation. Slow substrate association is of particular importance because a reduced LPMO that is not bound to the substrate is prone to side reactions that may consume reactants and lead to enzyme damage, as outlined above.[15,32,33] Interestingly, Hangasky *et al.*[21] showed that H_2O_2-consuming horse radish peroxidase (HRP), which has a soluble substrate, inhibited an LPMO acting on an insoluble substrate, while having only a minor inhibitory effect on an LPMO acting on a soluble substrate. This observation underpins the impact of the substrate on LPMO behavior, likely including impact on the activation of O_2 and/or H_2O_2.[25,28−30]

In recent years, fungal AA9-type LPMOs active on soluble substrates have been discovered, including *Nc*AA9C from *Neurospora crassa*[34,35] and *Ls*AA9A from *Lentinus similis*.[29] These enzymes, acting on a diffusible and easy to analyze substrate, provide a unique opportunity to kinetically assess the various LPMO reactions. Here, we present an in-depth kinetic analysis of *Nc*AA9C acting on cellopentaose, showing that this enzyme is a fast and specific peroxygenase, capable of reaching unprecedented high catalytic rates. Similar studies with *Ls*AA9A revealed differences between the two enzymes but confirmed that these AA9 type LPMOs are indeed competent peroxygenases. These results demonstrate the catalytic potential of the LPMO scaffold, which is higher than what could be anticipated when the first slow LPMO reactions were described.

MATERIALS AND METHODS

Chemicals. All chemicals were, if not stated otherwise, purchased from Sigma-Aldrich, Thermo Fisher Scientific or VWR.

Expression, Purification and Copper Saturation. Recombinant LPMO expression was done as previously described by Rieder *et al.*[38] In summary: the genes encoding *Ls*AA9A (UniProtKB: A0A0S2GKZ1) and *Nc*AA9C (UniProtKB: Q7SHI8) were codon optimized for *Pichia pastoris*, using the online tool provided by Thermo Fisher Scientific and cloned into the $pBSYP_{GCW14}Z$ plasmid, which facilitates constitutive expression and employs the native LPMO signal peptides for secretion. After *Smi*I linearization, the $pBSYP_{GCW14}Z$-*LPMO* constructs were used for the transformation of killer plasmid-free *P. pastoris* BSYBG11 (Δ*AOX1*, Mut^S) one-shot ready competent cells (Bisy GmbH, Hofstätten a.d. Raab, Austria) following the manual provided by the supplier.

For enzyme production, a single yeast colony was used to inoculate 500 mL of YPD [1% (w/v) Bacto yeast extract (BD Bioscience, San Jose, CA, USA), 2% (w/v) peptone from casein (tryptone) (Merck Millipore, Burlington, MA, USA) and 2% (w/v) glucose]. Incubation was performed over 60 h in a 2 l baffled shake flask at 120 rpm and 28 °C. The LPMO-containing supernatant was separated from the cells by centrifugation at 10,000*g* for 15 min at 4 °C and filtered using a 0.22 μm Steritop bottle-top filter (Merck Millipore, Burlington, MA, USA) prior to the concentration using a VivaFlow 200 tangential crossflow concentrator (molecular weight cutoff, MWCO, 10 kDa, Sartorius Stedim Biotech Gmbh, Germany) and Amicon Ultra centrifugal filters (MWCO 10 kDa, Merck Millipore, Burlington, MA, USA).

The LPMOs were purified using an Äkta purifier system (GE Healthcare Life Sciences, Uppsala, Sweden) equipped with a HiLoad 16/60 Superdex 75 size exclusion column (GE Healthcare Life Sciences, Uppsala, Sweden) that was equilibrated in 50 mM BisTris-HCl (pH 6.5), 150 mM NaCl. The single step size exclusion purification was performed at a flow rate of 1 mL/min. The protein content of the fractions was assessed by sodium dodecyl sulfate-polyacrylamide gel electrophoresis and fractions containing pure LPMO were pooled.

To ensure the copper saturation of the active site, the enzyme preparation was incubated for 1 h with a 3-fold molar excess of $CuSO_4$ at 4 °C in 50 mM BisTris-HCl (pH 6.5) with 150 mM NaCl. Unbound copper was removed by three repetitions of buffer exchange to 50 mM BisTris-HCl (pH 6.5) using Amicon Ultra centrifugal filters (MWCO 10 kDa, Merck Millipore, Burlington, MA, USA). LPMO concentrations were determined using the Bradford protein assay with a bovine serum albumin as the standard. The copper saturated and purified proteins were stored in 50 mM BisTris-HCl (pH 6.5) at 4 °C until use.

*Af*AA11B, a chitin-active LPMO from *Aspergillus fumigatus* (UniProtKB: Q4WEH3), which will be described in detail elsewhere, was produced, purified, and copper saturated as described above for *Ls*AA9A and *Nc*AA9C.[38] Copper-saturated chitin-active bacterial *Sm*AA10A (CBP21) was prepared as described previously.[39]

https://doi.org/10.1021/acs.biochem.1c00407
Biochemistry 2021, 60, 3633−3643

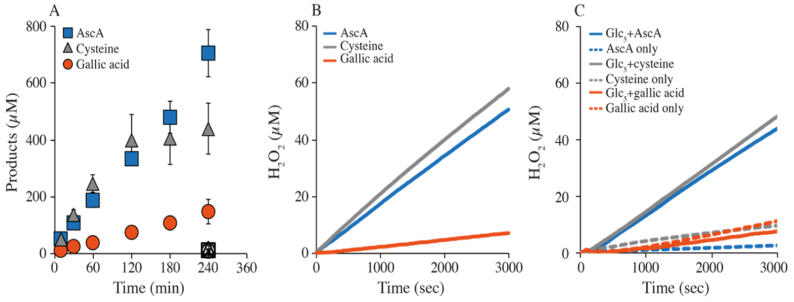

Figure 2. Progress curves showing the apparent monooxygenase (A) and oxidase (B) activity of *Nc*AA9C. Reactions were performed with 1 μM enzyme and 1 mM of either AscA (blue), cysteine (gray), or GA (orange) in the presence (A) or absence (B) of 1 mM Glc_5. The empty symbols in A (at 240 min only) show the product levels (~10 μM) found in the control reactions without a reductant. Panel (C) shows control reactions, that is, LPMO-independent H_2O_2 accumulation, in reactions with only reductant (dashed lines), or with reductant and 1 mM Glc_5 (solid lines).

LPMO Reactions with Soluble Substrates. All solutions used in activity assays were normal air-saturated solutions. LPMO reactions typically had a volume of 200 μL and were prepared in a 1.5 mL reaction tube with a conical bottom. Standard reactions contained 1 μL LPMO, 1 mM reductant, and 1 mM cellopentaose (95% purity; Megazyme, Wicklow, Ireland) in 50 mM BisTris-HCl (pH 6.5). Reactions supplemented with H_2O_2 contained typically 0.25 μM enzyme, 300 μM H_2O_2, 100 μM reductant, and 1 mM of the soluble substrate. Deviations from standard conditions were required for some experiments, as indicated in the appropriate figure legends. Stock solutions of 50 mM AscA (L-ascorbic acid, 99%, Simga-Aldrich), 10 mM GA (GA monohydrate ≥99%, Sigma-Aldrich), and 100 mM cysteine (L-cysteine ≥98%, Sigma-Aldrich) were prepared in ddH_2O, aliquoted, and stored at −20 °C until use. 10 mM stock solutions of H_2O_2 (37% Merck) were prepared in pure water (TraceSELECT, Fluka) and stored at −20 °C until use. The H_2O_2 concentration was assessed by measuring the absorbance at 240 nm and using a molar extinction coefficient of 43.6 M^{-1} cm^{-1}.

Because the order of mixing the various components of LPMO reactions matters, we started by mixing H_2O, buffer stock solution, and the substrate followed by the LPMO. After incubation for 1 min at the desired temperature and rpm, the reaction was initiated by the addition of the reductant (time point zero). In case the reaction was supplemented with H_2O_2 or HRP (Sigma-Aldrich), these were added after the LPMO but before the pre-incubation step and before the addition of the reductant. Reactions were incubated either at 37 or 4 °C and at 750 rpm (ThermoMixer C, Eppendorf, Hamburg, Germany). For sampling, 25 μL of aliquots were withdrawn from the main reaction at regular time points. To quench the reaction and to achieve an appropriate dilution factor for subsequent HPAEC-PAD analysis of products (see below), 175 μL of 200 mM NaOH were added to each sample. For quantification with the Dionex ICS6000 system, the dilution factor was 1:40, due to a higher sensitivity of this system. Reactions with mannopentaose and xylopentaose (95% purity; Megazyme, Wicklow, Ireland) were set up and sampled in the same manner but were diluted 1:4 prior to HPAEC-PAD analysis.

The presented data points are the average values of at least three individual replicates and include the standard deviation, which is shown as a vertical line. Negative control reactions were performed by leaving out the reductant.

Product Detection and Quantification. Reaction products were detected using high-performance anion exchange chromatography with pulsed amperometric detection (HPAEC-PAD). HPAEC was performed on a Dionex ICS5000 or ICS6000 system. The ICS5000 was equipped with a 3 × 250 mm CarboPac PA200 analytical column and a CarboPac PA200 guard column, and cello-oligomer containing samples were analyzed using a 26 min gradient, as described previously.[24] For analysis with the ICS6000, we used a 1 × 250 mm CarboPac PA200 analytical column and a guard column of the same type. The flow rate during analysis was 63 μL*min^{-1} and the applied gradient was as follows: 1−14 min, from 1 to 100 mM potassium methanesulfonate (KMSA), concave; 14−17 min, washing step at 100 mM KMSA; 17−26 min, re-conditioning at 1 mM KMSA.

To assess the LPMO activity on cellopentaose, the generation of native cellobiose and cellotriose, which would proportionally increase with the C4-oxidized products, was quantified. Products from reactions with mannopentaose and xylopentaose were analyzed using a Dionex ICS5000 system in the configuration described above. For analysis of manno-pentaose-containing samples, we used a 26 min gradient for the cellopentaose-containing samples. In case the reactions were set up with xylopentaose, we used a 39 min gradient as described elsewhere.[40] Chromatograms were recorded and analyzed with Chromeleon 7, and plots were made using Microsoft Excel.

H_2O_2 Production Assay. Hydrogen peroxide formation assays were performed as previously described by Kittl *et al.*[26] The reactions were performed in 96-well microplates with 100 μL of 50 mM BisTris/HCl buffer (pH 6.5) containing 1 μM LPMO, 100 μM Amplex Red (AR), 1% (v/v) DMSO, and 0.025 mg/mL HRP (final concentrations). After 5 min pre-incubation at 30 °C, the reactions were started by the addition of the 1 mM reductant (final concentration). The formation of resorufin was monitored over 30 min at 540 nm using a Multiskan FC microplate photometer (Thermo Fisher Scientific, Bremen Germany). Standard solutions for H_2O_2 quantification were supplemented with the reductant and if appropriate with 1 mM Glc_5 to capture potential side reactions, as recently explained.[19,24] The reductant and Glc_5 were added prior the addition of HRP.

https://doi.org/10.1021/acs.biochem.1c00407
Biochemistry 2021, 60, 3633−3643

Table 1. Apparent Rate Constants (s^{-1}) for Reactions Catalyzed by *Nc*AA9C, with Three Different Reductants[a]

	mono-oxygenase (Figure 2A; 1 mM reductant, 1 mM Glc_5, O_2)	oxidase (Figure 2B; 1 mM reductant, O_2, no substrate)	O_2 reduction, reductant only, with substrate (Figure 2C; 1 mM reductant, 1 mM Glc_5, O_2, no LPMO)	O_2 reduction, reductant only (Figure 2C; 1 mM reductant, O_2, no LPMO)	peroxygenase (Figure 4A; 0.1 mM reductant, 1 mM Glc_5, 300 μM H_2O_2, O2)
AscA	0.05 ± 0.01	0.017 ± 0.001	0.016 ± 0.000	0.0004 ± 0.0001	~70[b]
GA	0.011 ± 0.002	0.002 ± 0.001	0.004 ± 0.000	0.0040 ± 0.0009	~25[b]
cysteine	0.06 ± 0.01	0.019 ± 0.000	0.017 ± 0.000	0.0026 ± 0.0002	~6

[a]The values presented are derived from the progress curves shown in Figures 2 and 4 and are either estimates based on the first time point (peroxygenase reaction) or represent the average of three individual replicates (mono-oxygenase and oxidase reaction). [b]The shape of the progress curve in Figure 4A shows that this rate is underestimated.

RESULTS AND DISCUSSION

Reductant Influences the Apparent Monooxygenase Reaction. It is well known from earlier works that the reductant has a large impact on the efficiency of O_2-driven LPMO reactions.[23,24,41,42] In keeping with the monooxygenase paradigm, this dependency has been attributed to variation in the reductant's ability to deliver electrons to the LPMO. As outlined above, considering the peroxygenase activity of LPMOs, it is conceivable that the observed variation also, or even primarily, reflects the reductant-dependent variation in the *in situ* synthesis of H_2O_2 during the reaction.[23,24] Here, we addressed the impact of the reductant on *Nc*AA9C by studying the degradation of cellopentaose in the presence of AscA, cysteine, or GA. The reactions were performed using classical aerobic "monooxygenase" conditions with 1 μM enzyme, 1 mM Glc_5, and 1 mM reductant.

Figure 2A shows that stable reaction rates were obtained with AscA and GA, with apparent rate constants (k_{obs}), derived from the linear part of the progress curves, of 0.05 ± 0.01 and 0.011 ± 0.02 s^{-1}, respectively (Table 1). It is worth noting that the reaction with 1 mM AscA gave a linear progress curve up to at least the 800 μM oxidized product, which shows that the reaction was not O_2 limited. The reaction with cysteine showed the highest initial rate (k_{obs} = 0.06 ± 0.01 s^{-1}), but in this case product formation halted after approximately half of the substrate had been degraded. This is not surprising because, while AscA and GA can donate two electrons per molecule, cysteine can donate only one, meaning that two molecules of cysteine are needed per LPMO reaction and that 1 mM of cysteine can only fuel cleavage of 0.5 mM (*i.e.*, half) of the substrate.

To gain insights into the oxidase activity of *Nc*AA9C and a possible connection between this activity and the enzyme's apparent mono-oxygenase activity, we measured H_2O_2 production in the absence of the substrate using the AR/HRP assay, as described previously.[24,26] Of note, while this assay is very useful, it suffers from multiple complications (discussed in, *e.g.*, refs 19 and 24) that prevent extrapolation of apparent H_2O_2 production levels in a reaction without the substrate (Figure 2B) with expected H_2O_2 production levels in a reaction with the substrate (Figure 2A). First, the reductant suppresses the signal of the HRP assay and this will vary between reductants. Although the reductant is included in the standard curve for H_2O_2, this effect cannot be fully compensated for.[19,24] Second, H_2O_2 may react with the reductant (meaning that H_2O_2 levels will be underestimated) and this reaction may be promoted by HRP to an extent that differs between the reductants; this situation will be entirely different in a reaction with the substrate, where the productive LPMO reaction will outcompete slower background reactions with the reductant. Finally, as alluded to above, the presence of the substrate inhibits the oxidase activity of the LPMO.[25,26,34]

Figure 2B and the derived reaction rates (Table 1) show that apparent H_2O_2-production rates vary between the reductants, showing trends that align well with apparent mono-oxygenase reaction rates (Figure 2A; Table 1). The apparent mono-oxygenase activity is about 5 times higher with AscA and cysteine than with GA. The variation in the apparent oxidase rates shows a similar trend, but in this case, the rate difference between AscA/cysteine and GA is about 10-fold. For all reductants, the apparent mono-oxygenase activity is 3 to 5 times higher than the apparent oxidase activity, which could indicate that we indeed are observing mono-oxygenase activity in a reaction that is not limited by the generation of H_2O_2. However, this phenomenon could also be due to the underestimation of H_2O_2 production for reasons described above, and addressed further below, or be caused by an additional source of H_2O_2 in reactions with the substrate, Glc_5, as discussed below.

Intrigued by the difference between the apparent mono-oxygenase and oxidase activities, we investigated a possible effect of 1 mM Glc_5 on H_2O_2 production in reactions with standard amounts of all three reductants. The obtained results show that, for reactions with AscA and cysteine, incubation of Glc_5 with the reductant led to strongly increased H_2O_2 production, relative to reactions with only reductant (Figure 2C). The apparent H_2O_2 production rates in these reactions were not unlike the rates obtained in reactions with the reductant and LPMO (Figure 2B) and are thus quite significant (Table 1). This unexpected effect of Glc_5 could be due to the presence of transition metals, likely copper, which would enhance H_2O_2 production through the oxidation of AscA[24,43] and cysteine,[44] but not necessarily of GA[24] because GA is more likely to form complexes with Cu(II) rather than reducing it.[45] This additional source of H_2O_2 helps to close the gap observed between the rates of the apparent mono-oxygenase and oxidase activities.

Of note, the results depicted in Figure 2 show that the combination of *Nc*AA9C and GA is not suitable for the assessment of LPMO oxidase activity by the AR/HRP assay as the apparent rate of H_2O_2 production in reactions with GA alone (Figure 2C, Table 1) is higher that the apparent oxidase activity in reactions with GA and the LPMO (Figure 2B; Table 1). In this case, the assay is flawed due to the ability of *Nc*AA9C to engage in a H_2O_2-consuming side reaction with GA, as described by Breslmayr *et al.*[31] Of note, in a LPMO reaction mixture containing Glc_5, side reactions with GA will be outcompeted by the peroxygenase reaction with Glc_5, which is faster, as shown below.

A recent study on a cellulose-active AA10-type LPMO with AscA and GA as reductants showed that the LPMO had little

https://doi.org/10.1021/acs.biochem.1c00407
Biochemistry 2021, 60, 3633−3643

effect on H_2O_2 production, which was dominated by the LPMO-independent oxidation of the reductant.[24] Table 1 shows that the situation for *Nc*AA9C is different. In this case, the LPMO may contribute considerably to apparent H_2O_2 production in reactions with cysteine and AscA (compare "oxidase" with "O_2 reduction, reductant only"). In the case of AscA, the LPMO speeds up the H_2O_2 production rate by some 40-fold, whereas the increase is some 7-fold for cysteine. Similar comparisons for GA could not be made due to the technical issues discussed above.

If it is the *in situ* generation of H_2O_2 that is limiting the apparent mono-oxygenase reaction in the presence of GA, it should be possible to inhibit the LPMO reaction with another H_2O_2-consuming enzyme. Indeed, both Bissaro *et al.*[15] and Hangasky *et al.*[21] have shown that LPMO reactions with insoluble substrates under "mono-oxygenase conditions" are inhibited when adding HRP and its substrate, AR. While Hangasky *et al.* did not observe similarly strong inhibition in a reaction with a soluble substrate, Figure 3 shows that HRP

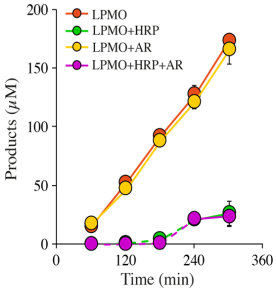

Figure 3. HRP inhibition for reactions with *Nc*AA9C and GA. Progress curves showing product formation by 1 μM LPMO in the presence of 1 mM GA and 1 mM Glc_5 with no supplementation (orange) or supplemented with 100 μM AR (yellow) or 2 μM HRP (green) or both (purple). Note that the HRP reaction does not depend on AR because GA is a substrate for HRP (see text). Dashed lines connect points with values that were close to the limit of detection.

strongly inhibits the GA-driven activity of *Nc*AA9C on Glc_5. A similar degree of inhibition was observed in the reaction-containing HRP but lacking AR, indicating that HRP can oxidize GA, which is not surprising considering the literature data.[46] Of note, it is highly unlikely that the LPMO inhibition in the presence of HRP is driven by reductant depletion rather than by competition for H_2O_2, given the high (1 mM) reductant concentration used in the experiment. Note that the observed side reaction between HRP and GA will also occur in the AR/HRP assay, contributing to the underestimation of the apparent H_2O_2 production rates derived from Figure 2.

Peroxygenase Reaction Is Dependent on the Reductant. To assess the influence of AscA, GA, and cysteine on the peroxygenase activity of *Nc*AA9C, we monitored the consumption of Glc_5 in reactions that contained 300 μM H_2O_2 (Figure 4A). In the presence of the 100 μM reductant, we observed apparent rate constants of ~70, ~25, and ~6 s^{-1} for AscA, GA, and cysteine, respectively, where the first and the second values are underestimated as a major part of H_2O_2 was consumed at the first time point. These rates are 100−2300 times higher than the apparent monooxygenase rates (Table 1). The progress curve for the reaction with AscA shows that

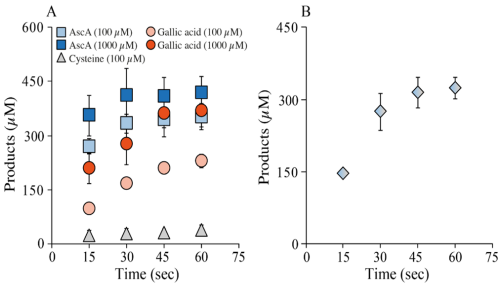

Figure 4. Peroxygenase reactions with *Nc*AA9C. (A) Time course experiments showing the impact of AscA (blue), cysteine (gray), and GA (orange) on the peroxygenase reaction catalyzed by *Nc*AA9C. Reaction mixtures containing 0.25 μM enzyme, 300 μM H_2O_2, 100 or 1000 μM reductant and 1 mM Glc_5 were incubated at 37 °C and reactions were started by adding the reductant. No products were detected in control reactions without an added reductant. (B) Product formation in a reaction with 0.25 μM *Nc*AA9C, 300 μM H_2O_2, 1 mM Glc_5, 0.1 mM AscA, and 0.1 mM cysteine. Note that this reaction was incubated at 4 °C, hence the slower rate compared to panel A.

the reaction is limited by the availability of H_2O_2 as product formation levels of at about 300 μM of the product, reflecting a 1:1 ratio with the added H_2O_2. It is worth noting that these reactions were monitored by measuring the generation of cellobiose and cellotriose, which means that uncertainties related to the instability of C4-oxidized products[40] were avoided. It is also worth noting that reactions with a starting concentration of 300 μM H_2O_2 would lead to rapid LPMO inactivation in reactions with an insoluble substrate[15] but that in the present case, with a rapidly diffusing soluble substrate, stoichiometric catalytic conversion of the H_2O_2 was achieved.

To investigate if the availability of the reductant is rate limiting, the experiments depicted in Figure 4A are redone with 1 mM (*i.e.*, 10-fold more) reductant concentrations. By doing so, the already high and most certainly underestimated rate for the reaction with AscA increased slightly, whereas the reaction with GA became approximately twice as fast. While this clearly shows that the reductant to some extent limits, the very high rates of these peroxygenase reactions (note the difference in time scale with the mono-oxygenase reactions of Figure 2), increasing the amount of the reductant had no effect on the (lower) rate of the reaction with cysteine (results not shown). The lower activity with cysteine was not due to H_2O_2 scavenging by the reductant, as an addition of 0.1 mM cysteine to a reaction with 0.1 mM AscA did not affect product formation (Figure 4B), which shows that all the added H_2O_2 was used by the LPMO. This result is in line with the literature data showing that, while cysteine can react with H_2O_2, the rate of this reaction is orders of magnitude lower[47] than the rate of the peroxygenase reaction of *Nc*AA9C. Possibly, the reduction of copper by cysteine leads to the formation of a relatively stable cuprous thiolate complex[48] that limits LPMO reactivity under "fast" peroxygenase conditions, whereas this inhibitory effect could remain unnoticed under much slower mono-oxygenase conditions. Of note, even with cysteine, a k_{obs} of ~6 s^{-1} is still much higher than typical k_{obs} values for mono-oxygenase reactions.

These results show that the peroxygenase reaction of *Nc*AA9C is much faster than the apparent mono-oxygenase reaction (Table 1), which implies that minor variations in the

https://doi.org/10.1021/acs.biochem.1c00407
Biochemistry 2021, 60, 3633−3643

levels of *in situ* H_2O_2 generation will have dramatic effects on the low rates of the latter reaction. Within the time scale of the peroxygenase reaction, the main contribution of the reductant is to keep the LPMO reduced (*i.e.*, catalytically competent) and our data reveal differences between the reductants in this respect. While the experiments with polymeric substrates have shown that once reduced LPMOs may catalyze 15−20 peroxygenase reactions before being re-oxidized,[20,36,37] the re-oxidation frequency, and, thus, the reductant dependency may be higher in the case of a soluble substrate, which will bind less strongly and, upon binding, create less confinement of the copper site, thus increasing the chances for side reactions that involve copper reoxidation and the loss of electrons.

Kinetics of the LPMO-Catalyzed Peroxygenase Reaction. To gain more insights into the peroxygenase reaction, we performed Michaelis−Menten kinetics (Figure 5A). The underlying linear progress curves covered Glc_5 concentrations ranging from 75 to 2500 μM and reactions were run at 4 °C to obtain manageable product formation rates. This setup resulted in a hyperbolic curve, yielding a K_m (for Glc_5) of 2.1 ± 0.3 mM, a k_{cat} of 124 ± 27 s^{-1}, and a k_{cat}/K_m of 5.9*10^4 M^{-1} s^{-1} (Figure 5A). This k_{cat} value, determined at 4 °C, is 2.5 × 10^3-fold higher than the k_{obs} value for the apparent mono-oxygenase reaction with AscA described above (37 °C), 1.1 × 10^3-fold higher than the k_{cat} value reported for *Ls*AA9A acting on an analogue of Glc_4 in a mono-oxygenase setup with AscA (37 °C),[29] and 19-fold higher than the k_{cat} reported for a peroxygenase action on chitin nanowhiskers by a bacterial AA10-type LPMO at 25 °C.[18] The K_m measured for *Nc*AA9C of ∼2 mM is comparable to a K_d of 0.81 ± 0.08 mM that Borisova *et al.*[35] measured for the same enzyme binding to Glc_6 under non-turnover conditions.

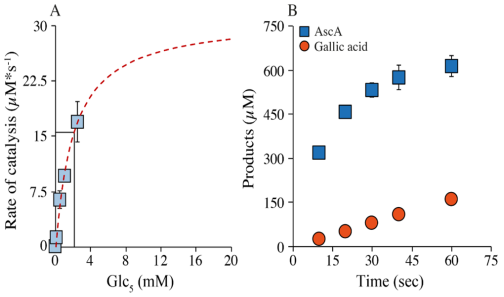

Figure 5. Kinetics of the *Nc*AA9C-catalyzed peroxygenase reaction with Glc_5. (A) Michealis−Menten kinetics showing the dependency of the catalytic activity on the Glc_5 concentration. The rates were derived from linear progress curves and the dashed line shows the fit to the Michalis−Menten equation. Reactions were set up with a 0.25 μM enzyme and 600 μM H_2O_2 at 4 °C and were started by adding 0.1 mM AscA (note that the K_m for H_2O_2 is expected to be below 10 μM[18]). (B) Progress curves for the peroxygenase reaction at 4 °C. The data points show product formation in a reaction with 0.25 μM *Nc*AA9C, 600 μM H_2O_2, 1 mM Glc_5, and either 1 mM AscA (blue) or GA (orange) that was incubated at 4 °C.

To further substantiate the strikingly high catalytic rate of *Nc*AA9C, we then conducted additional initial rate measurements to obtain k_{obs} values that would be more reliable than those obtained from the non-linear progress curves shown in Figure 4A. To do so, we decreased the reaction temperature to 4 °C and increased the H_2O_2 concentration to 600 μM to ensure that the oxygen-donating substrate would not become limiting within seconds. The resulting progress curve for the reaction with AscA (Figure 5B) showed the formation of 600 μM products within 30 s showing that the reaction was limited by the availability of H_2O_2. Based on the first 20 s of the experiment (R^2 = 0.95), we calculated a k_{obs} of 90.8 ± 3.6 s^{-1}. As expected, based on Figure 4A, the reaction with GA was slower. This reaction showed a linear increase in the product level and gave a k_{obs} of 10.7 ± 0.3 s^{-1} (Figure 5B). Of note, these rates were obtained using sub-saturating substrate conditions as the used Glc_5 concentration was just about 50% of the measured K_m. Still the obtained k_{obs} of ∼90 and ∼11 s^{-1} for *Nc*AA9C in combination with AscA and GA, respectively, represent the two highest rates ever measured for the LPMO-catalyzed oxidation of a carbohydrate substrate.

AA9 LPMOs Acting on Soluble Substrates Have Different Properties. One of the other AA9 LPMOs known to act on soluble substrates is *Ls*AA9A.[29] A previous kinetic characterization of this enzyme using a Förster-resonance energy-transfer (FRET) substrate analogue of Glc_4 as a substrate and mono-oxygenase conditions (5 mM AscA,

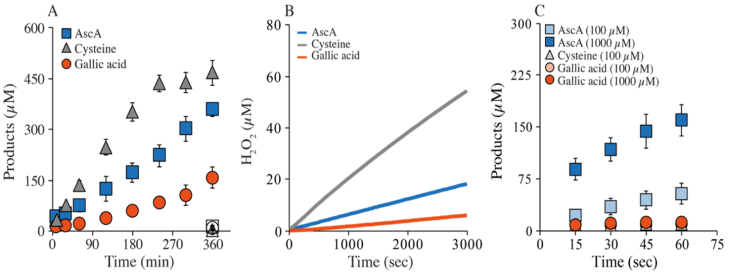

Figure 6. Mono-oxygenase, peroxygenase, and oxidase activity for *Ls*AA9A. Mono-oxygenase (A) and oxidase (B) reactions were performed with 1 μM LPMO and either 1 mM AscA (blue), cysteine (gray), or GA (orange) in presence (A) and absence (B) of 1 mM Glc_5. The empty symbols in A (at 360 min only) show the product levels found in the control reactions without a reductant. For the peroxygenase reactions shown in panel (C), we lowered the enzyme concentration to 0.25 μM and added 300 μM H_2O_2 with the same reductants as used for the mono-oxygenase reaction at concentrations of either 100 or 1000 μM at 37 °C. In panel C, the points for the reaction with 100 μM GA and cysteine, respectively, are hidden by the points for the reaction with 1000 μM GA; the reaction with 1000 μM cysteine yielded the same curve as the reaction with 100 μM and is not shown, for clarity.

https://doi.org/10.1021/acs.biochem.1c00407
Biochemistry 2021, 60, 3633−3643

Table 2. Apparent Rate Constants (s^{-1}) for the Oxidation of 1 mM Glc_5 by *Ls*AA9A under Various Conditions[a]

	mono-oxygenase (Figure 6A; 1 mM reductant, 1 mM Glc_5, O_2)	oxidase (Figure 6B; 1 mM reductant, O_2, no substrate)	O_2 reduction, reductant only (Figure 2C; 1 mMreductant, O_2, no LPMO)	peroxygenase (Figure 6C; 0.1 mM reductant, 1 mM Glc_5, 300 μM H_2O_2, O_2)	peroxygenase (Figure 6C; 1 mM reductant, 1 mM Glc_5, 300 μM H_2O_2, O_2)
AscA	0.014 ± 0.002	0.006 ± 0.000 (35%)	0.0004 ± 0.0001	5.8 ± 2.3	23.4 ± 4.2
GA	0.006 ± 0.001	0.002 ± 0.000 (100%)	0.0040 ± 0.0009	0.1 ± 0.0	0.4 ± 0.1
cysteine	0.029 ± 0.001	0.018 ± 0.000 (95%)	0.0026 ± 0.0002	0.3 ± 0.1	0.2 ± 0.1

[a]The values presented are estimates derived from the progress curves shown in Figure 6. The oxidase values are also expressed as a percentage of the oxidase value observed for *Nc*AA9C (Table 1). Other quantitative comparisons between the two LPMOs are not straightforward due to the occurrence of substrate inhibition in the reactions with *Ls*AA9A.

no added H_2O_2) yielded a k_{cat} = 0.11 ± 0.01 s^{-1}, that is, a typical value for LPMOs acting in the "mono-oxygenase mode", and in the same range as apparent oxidase and mono-oxygenase rates reported here for reactions with AscA (Table 1). The obtained K_m value of 43 ± 9 μM is remarkably low, compared to, for example, the K_m for Glc_5 cleavage by *Nc*AA9C reported above and suggests high substrate affinity, which could perhaps be due in part to the presence of aromatic groups that appear at the reducing and non-reducing ends of the FRET substrate analogue.

Our studies confirmed high substrate affinity, albeit not necessarily specific, as we observed increasing substrate inhibition (*i.e.*, an increasing reduction of LPMO activity) at Glc_5 concentrations above 0.1 mM (results not shown). Due to this substrate inhibition, a quantitative comparison of the catalytic properties of the two LPMOs is not straightforward. Assays identical to those described above for *Nc*AA9C showed apparent mono-oxygenase and oxidase rates in the same order of magnitude and confirmed the considerable impact of the reductant of LPMO activity (Figure 6; Table 2). The most notable difference is that H_2O_2 production by *Ls*AA9A in the presence of AscA is less efficient compared to *Nc*AA9C (Figures 2B and 6B). Accordingly, the AscA-driven apparent mono-oxygenase reaction is slower, making cysteine the clearly most efficient reductant for this LPMO in a "mono-oxygenase" setup (Figure 6A).

The peroxygenase reactions were slower than for *Nc*AA9C, possibly due to substrate inhibition (Figure 6C). Still, the apparent rates recorded for reactions with two concentrations of AscA (Table 2) are 35−141 times higher than the previously determined k_{cat} for an apparent mono-oxygenase reaction[29] and 280−1100 times higher than the apparent mono-oxygenase reaction rates determined here. For this LPMO, peroxygenase reactions with both cysteine and GA were relatively slow and not or hardly dependent on the reductant concentration. Still, these rates were some 10 and 100 times higher than the determined apparent mono-oxygenase rates (Table 2).

It is interesting to note that the efficient peroxygenase reaction catalyzed by *Ls*AA9A in the presence of AscA was much more dependent on the reductant concentration (Figure 6C; Table 2) compared to *Nc*AA9C (Figure 2). This reflects that, compared to *Nc*AA9C, *Ls*AA9A is more prone to oxidation and a subsequent need for re-reduction. Substrate binding and the resulting confinement of the reduced catalytic copper form a major determinant of the degree of non-productive LPMO oxidation. The data could thus indicate that *Ls*AA9A binds the substrate less for firmy or less precisely, where the first option is in conflict with the previously reported low K_m value. A more oxidation-prone copper site in the enzyme−substrate complex would also translate into decreased enzyme stability at higher H_2O_2 concentrations, as non-productive reactions between the reduced enzyme and H_2O_2 may lead to oxidative damage.[15] Indeed, Figure 7 shows that

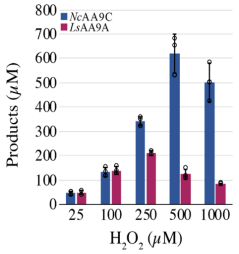

Figure 7. Sensitivity of *Nc*AA9C and *Ls*AA9A for oxidative damage. The graph shows product levels obtained after a 2 min reaction containing 1 mM AscA and various amounts of H_2O_2. Reaction mixtures containing 1 μM *Ls*AA9A (purple) or 1 μM *Nc*AA9C (blue), 1 mM Glc_5, and varying H_2O_2 concentrations (25−1000 μM) were pre-incubated for 1 min, after which the reaction was started by adding the reductant. In reactions not showing signs of enzyme inactivation, product levels were slightly higher than the amount of added H_2O_2 due to the combination of AscA-mediated H_2O_2 generation and a small systematic error in the concentration of the H_2O_2 stock solution.

*Ls*AA9A is more sensitive to H_2O_2-induced damage than *Nc*AA9C. While product formation by *Nc*AA9C first started decreasing at 1000 μM, the highest tested H_2O_2 concentration, *Ls*AA9A, showed signs of enzyme inactivation already at 250 μM (Figure 7).

As a cautionary note, we cannot exclude that the non-natural glycosylation of the *Pichia*-produced LPMOs may affect their properties. Considering the predicted location of glycosylation sites and the crystal structure of the *Pichia*-produced protein,[35] such an effect of glycosylation can be excluded for *Nc*AA9C. Based on the predicted glycosylation sites, glycosylation effects on the interaction between *Ls*AA9A and Glc_5 seem unlikely but cannot be excluded. Assuming that glycosylation effects do not play a role, the comparison of the results obtained for *Nc*AA9C and *Ls*AA9A show two important things. First, the data reveal functional differences between these two C4-oxidizing cellulose-active LPMOs, which are reductant dependent. Because soluble cello-oligomers can easily be degraded by hydrolytic enzymes, it is not likely that nature has evolved LPMOs for the purpose of cleaving these compounds (as also suggested by the high K_m value for *Nc*AA9C). Therefore, we hypothesize that the functional differences between *Nc*AA9C and *Ls*AA9A should be considered as a proxy for hitherto undescribed differences in substrate preferences that relate to the structural and compositional complexity of the true biomass. Second, while our studies show quite different peroxygenase reaction rates and reductant dependencies for

https://doi.org/10.1021/acs.biochem.1c00407
Biochemistry 2021, 60, 3633−3643

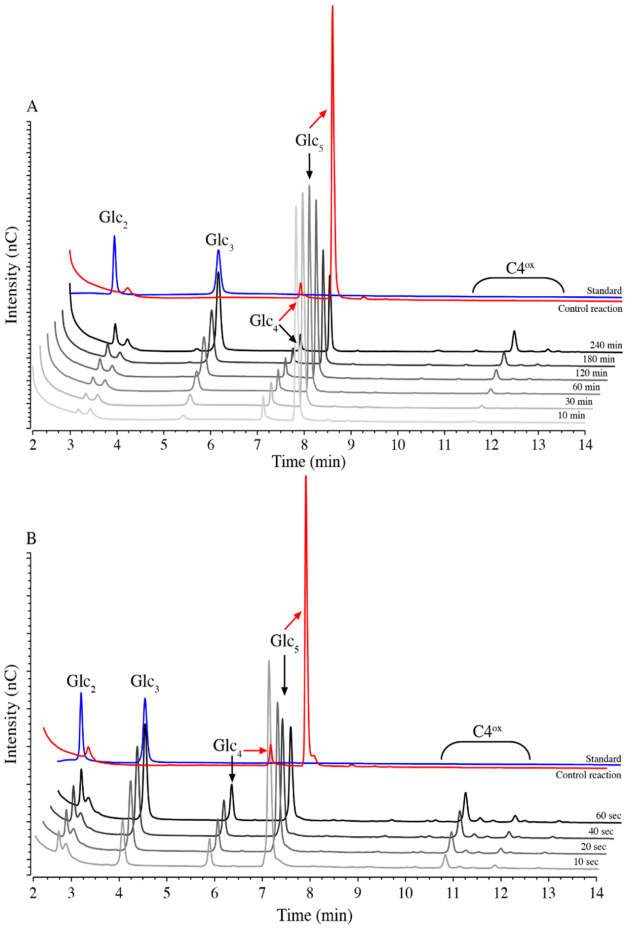

Figure 8. HPAEC-PAD chromatograms showing product formation in reactions with *Nc*AA9C and Glc_5, using mono-oxygenase (A) or peroxygenase (B) setup. Chromatograms for the mono-oxygenase reaction (1 μM LPMO, 1 mM AscA, and 1 mM Glc_5 at 37 °C) and peroxygenase reaction (0.25 μM LPMO, 600 μM H_2O_2, 1 mM AscA, and 1 mM Glc_5 at 4 °C) are shown as lines in gradations of gray and black. The chromatograms correspond to the time course experiments shown in Figures 2A and 5B, respectively. The red lines show the chromatograms of the appropriate control reaction without a reductant, after incubation for 240 min (A) or 60 s (B). The blue chromatograms show the Glc_2 + Glc_3 standard.

*Nc*AA9C and *Ls*AA9A and they suggest that Glc_5 is not an optimal substrate for *Ls*AA9A, all the observed peroxygenase rates are much higher than any reported apparent rate for apparent mono-oxygenase reactions.

LPMO-Catalyzed Peroxygenase Reaction Is Specific. Previously, it has been claimed that the addition of H_2O_2 to LPMO reactions results in a loss in specificity[21] and some argue that this shows that H_2O_2 is not a bonafide co-substrate for LPMOs and that, thus, LPMOs are not bonafide peroxygenases. In the present study, we used high H_2O_2 amounts that were stoichiometrically used to convert cellopentaose to cellobiose and cellotriose. This shows that there is little, if any, random oxidation of the substrate and that the reaction is specific (Figure 8).

To further assess specificity, we set up aerobic reactions with 1 μM *Ls*AA9A or 1 μM *Nc*AA9C with either 1 mM xylopentaose (Xyl_5) or 1 mM mannopentaose (Man_5) as a substrate (Figure S1; Figure S2). The conditions used were as follows: (i) 1 mM AscA ("mono-oxygenase" conditions), (ii) 20 μM H_2O_2 and 20 μM AscA, or (iii) 300 μM H_2O_2 and 100 μM AscA. Note that the latter reaction conditions would lead to very fast (within < 1 min) conversion of Glc_5 by *Nc*AA9C (Figure 4A). Additionally, we tested well-characterized chitin-active *Sm*AA10A[3] and a recently described chitin-active AA11, called *Af*AA11B[38] for their ability to oxidize 1 mM Glc_5 using the same reaction conditions (Figure S3).

None of these reactions yielded a detectable turnover of the substrate, except the positive control reactions with *Nc*AA9C or *Ls*AA9A and Glc_5 (Figure S3). We were not able to detect any degradation products by MALDI-TOF MS, whereas the HPAEC-PAD chromatograms only showed a few minimal signals that could indicate a low level of an oxidative cleavage of xylopentaose, which, for *Ls*AA9A, would be in accordance with a previously observed weak xylan-degrading ability.[49] Crystallographic studies have shown that xylopentaose binds atypically to *Ls*AA9A, leaving a not properly confined copper

https://doi.org/10.1021/acs.biochem.1c00407
Biochemistry 2021, 60, 3633−3643

site prone to engaging in potentially enzyme-inactivating side reactions.[10,49] One would thus expect rapid enzyme inactivation in reactions with large amounts of H_2O_2, which could explain why, if at all present, only trace amounts of LPMO products were observed.

The main take home message of these experiments is that the addition of H_2O_2 at low or high concentration, in combination with different concentrations of AscA, does not result in a loss of substrate specificity. The chromatograms and mass spectra for the peroxygenase reactions did not show any conspicuous features compared to the negative controls or the chromatograms for the apparent mono-oxygenase reactions.

CONCLUDING REMARKS

The experiments described above show two important aspects of LPMO enzymology. First, they illustrate that it is complicated to properly assess LPMO catalysis experimentally, due to the plethora of interconnected (side) reactions. Many of these complications emerged in our experiments and by studying multiple reductants, each with its own peculiarities, we were able to overcome most of these complications and generate insights into LPMO catalysis. Second, we show that LPMOs, when acting on rapidly diffusing soluble substrates and provided with H_2O_2, indeed are very efficient peroxygenases. We observed a stoichiometric conversion of high starting amounts of H_2O_2 that would lead to rapid LPMO inactivation in reactions with an insoluble substrate. Our data for reactions with soluble substrates show that the peroxygenase reaction is stable and specific.

We observed a correlation between the H_2O_2-producing potential of an LPMO-reductant combination and the observed apparent monooxygenase activity, which supports the idea that, under these conditions, the rate of the apparent monooxygenase reaction may reflect the rate of an H_2O_2-limited peroxygenase reaction, as originally suggested by Bissaro *et al.*[15] This is supported by the strong inhibitory effect of HRP on the LPMO reaction. We cannot exclude that a monooxygenase reaction also occurs, and it is well known that reduced LPMOs react with O_2.[13,26] It is also known that this reaction may be influenced by substrate binding.[29,30] The rates of the two reactions vary a lot for both soluble and insoluble substrates (refs 16−19; this study) and here, we show that peroxygenase reactions with a soluble substrate may reach rates in an order of 100 s^{-1}.

Notably, our data indicate that the oxidase activity of the AA9 type LPMOs studied here is higher that the oxidase activity of a previously studied AA10 type LPMO.[24] This could imply that, compared to AA10 LPMOs, the AA9 LPMOs are more active under monooxygenase conditions than AA10 LPMOs because they generate more H_2O_2. However, the extrapolation of oxidase activities measured in the absence of the substrate to oxidase activities under turnover conditions is not straightforward because of the impact of substrate binding on oxidase activity.[25] Further studies are warranted to study whether the observed difference in oxidase activity is general and to identify its structural determinants. It is also worth noting that in systems where the LPMO peroxygenase reaction is driven by the oxidase activity of the LPMO itself, the nature of the reductant will have a decisive impact on LPMO efficiency.

Our study revealed differences between *Nc*AA9C and *Ls*AA9A, which suggests that these enzymes have different substrate specificities and biological roles. It is important to realize that laboratory experiments with substrates such as Glc_5 or pure cellulose only give limited insights into the true role of an LPMO during fungal biomass conversion.

The most important and novel findings of the present study is that the unique LPMO scaffold enables highly efficient copper-catalyzed peroxygenase reactions with a soluble substrate. This high efficiency may in part be due to the copper site being exposed and rather rigid, with an open coordination position for co-substrate binding.[50] Thus, as originally pointed out by Kjaergaard *et al.*,[13] catalysis requires little reorganization energy, which may contribute to efficiency. It is encouraging that high specificity and high catalytic rates were achieved with what seems to be a low affinity substrate. It may be possible to engineer similar or better affinities for other, perhaps non-carbohydrate, substrates, which eventually could endow these powerful enzymes with the ability to catalyze efficient peroxygenation of such substrates. Furthermore, the unique peroxygenase chemistry of these mono-copper enzymes may open new avenues for the future design of enzyme-inspired synthetic copper catalysts.

ASSOCIATED CONTENT

Supporting Information

The Supporting Information is available free of charge at https://pubs.acs.org/doi/10.1021/acs.biochem.1c00407.

HPLC product profiles for reactions of *Nc*AA9C or *Ls*AA9A with xylopentaose; HPLC product profiles for reactions of *Nc*AA9C or *Ls*AA9A with mannopentaose; and HPLC product profiles for reactions of *Af*AA11B or *Sm*AA10A with cellopentaose (PDF)

Accession Codes

*Nc*AA9C, a family AA9 LPMO from *Neurospora crassa*, UniProt Q7SHI8; *Ls*AA9A, a family (AA) LPMO from *Lentinus similis*, UniProt A0A0S2GKZ1; *Af*AA11B, a family AA11 LPMO from *Aspergillus fumigatus*, UniProt Q4WEH3; *Sm*AA10A, a family AA10 LPMO from *Serratia marcescens*, UniProt O83009.

AUTHOR INFORMATION

Corresponding Author

Vincent G.H. Eijsink − *Faculty of Chemistry, Biotechnology, and Food Sciences, Norwegian University of Life Sciences (NMBU), 1432 Ås, Norway;* orcid.org/0000-0002-9220-8743; Phone: +47 67232463; Email: vincent.eijsink@nmbu.no

Authors

Lukas Rieder − *Faculty of Chemistry, Biotechnology, and Food Sciences, Norwegian University of Life Sciences (NMBU), 1432 Ås, Norway;* orcid.org/0000-0002-3632-2007

Anton A. Stepnov − *Faculty of Chemistry, Biotechnology, and Food Sciences, Norwegian University of Life Sciences (NMBU), 1432 Ås, Norway*

Morten Sørlie − *Faculty of Chemistry, Biotechnology, and Food Sciences, Norwegian University of Life Sciences (NMBU), 1432 Ås, Norway;* orcid.org/0000-0001-7259-6710

Complete contact information is available at: https://pubs.acs.org/10.1021/acs.biochem.1c00407

Author Contributions

L.R. designed the experiments, performed research, and wrote the first draft of the manuscript. A.A.S. designed experiments, performed research, and contributed to writing the manuscript. M.S. and V.G.H.E. provided funding, initiated the research, carried out supervision, helped to design experiments, interpreted results, and contributed to writing the manuscript.

Funding

The research for this work has received funding from the European Union's Horizon 2020 research and innovation program under the Marie Skłodowska-Curie grant agreement no. 722390. Additional support was obtained from the Research Council of Norway through projects 269408, 270038, and 262853.

Notes

The authors declare no competing financial interest.

■ ACKNOWLEDGMENTS

This work was performed as part of OXYTRAIN, a project under the EU's Horizon 2020 program; grant number 722390.

■ REFERENCES

(1) Vaaje-Kolstad, G.; Horn, S. J.; Van Aalten, D. M. F.; Synstad, B.; Eijsink, V. G. H. The non-catalytic chitin-binding protein CBP21 from Serratia marcescens is essential for chitin degradation. *J. Biol. Chem.* **2005**, *280*, 28492−28497.

(2) Harris, P. V.; Welner, D.; McFarland, K. C.; Re, E.; Navarro Poulsen, J.-C.; Brown, K.; Salbo, R.; Ding, H.; Vlasenko, E.; Merino, S.; Xu, F.; Cherry, J.; Larsen, S.; Lo Leggio, L. Stimulation of lignocellulosic biomass hydrolysis by proteins of glycoside hydrolase family 61: Structure and function of a large, enigmatic family. *Biochemistry* **2010**, *49*, 3305−3316.

(3) Vaaje-Kolstad, G.; Westereng, B.; Horn, S. J.; Liu, Z.; Zhai, H.; Sørlie, M.; Eijsink, V. G. H. An oxidative enzyme boosting the enzymatic conversion of recalcitrant polysaccharides. *Science* **2010**, *330*, 219−222.

(4) Forsberg, Z.; Vaaje-kolstad, G.; Westereng, B.; Bunaes, A. C.; Stenstrøm, Y.; Mackenzie, A.; Sørlie, M.; Horn, S. J.; Eijsink, V. G. H. Cleavage of cellulose by a cbm33 protein. *Protein Sci.* **2011**, *20*, 1479−1483.

(5) Horn, S. J.; Vaaje-Kolstad, G.; Westereng, B.; Eijsink, V. Novel enzymes for the degradation of cellulose. *Biotechnol. Biofuels* **2012**, *5*, 45.

(6) Hemsworth, G. R.; Johnston, E. M.; Davies, G. J.; Walton, P. H. Lytic polysaccharide monooxygenases in biomass conversion. *Trends Biotechnol.* **2015**, *33*, 747−761.

(7) Beeson, W. T.; Vu, V. V.; Span, E. A.; Phillips, C. M.; Marletta, M. A. Cellulose degradation by polysaccharide monooxygenases. *Annu. Rev. Biochem.* **2015**, *84*, 923−946.

(8) Johansen, K. S. Discovery and industrial applications of lytic polysaccharide mono-oxygenases. *Biochem. Soc. Trans.* **2016**, *44*, 143−149.

(9) Chylenski, P.; Bissaro, B.; Sørlie, M.; Røhr, Å. K.; Várnai, A.; Horn, S. J.; Eijsink, V. G. H. Lytic polysaccharide monooxygenases in enzymatic processing of lignocellulosic biomass. *ACS Catal.* **2019**, *9*, 4970−4991.

(10) Forsberg, Z.; Sørlie, M.; Petrović, D.; Courtade, G.; Aachmann, F. L.; Vaaje-Kolstad, G.; Bissaro, B.; Røhr, Å. K.; Eijsink, V. G. Polysaccharide degradation by lytic polysaccharide monooxygenases. *Curr. Opin. Struct. Biol.* **2019**, *59*, 54−64.

(11) Quinlan, R. J.; Sweeney, M. D.; Lo Leggio, L.; Otten, H.; Poulsen, J.-C. N.; Johansen, K. S.; Krogh, K. B. R. M.; Jorgensen, C. I.; Tovborg, M.; Anthonsen, A.; Tryfona, T.; Walter, C. P.; Dupree, P.; Xu, F.; Davies, G. J.; Walton, P. H. Insights into the oxidative degradation of cellulose by a copper metalloenzyme that exploits biomass components. *Proc. Natl. Acad. Sci. U.S.A.* **2011**, *108*, 15079−15084.

(12) Phillips, C. M.; Beeson, W. T.; Cate, J. H.; Marletta, M. A. Cellobiose dehydrogenase and a copper-dependent polysaccharide monooxygenase potentiate cellulose degradation by *Neurospora crassa*. *ACS Chem. Biol.* **2011**, *6*, 1399−1406.

(13) Kjaergaard, C. H.; Qayyum, M. F.; Wong, S. D.; Xu, F.; Hemsworth, G. R.; Walton, D. J.; Young, N. A.; Davies, G. J.; Walton, P. H.; Johansen, K. S.; Hodgson, K. O.; Hedman, B.; Solomon, E. I. Spectroscopic and computational insight into the activation of O_2 by the mononuclear Cu center in polysaccharide monooxygenases. *Proc. Natl. Acad. Sci. U.S.A.* **2014**, *111*, 8797−8802.

(14) Walton, P. H.; Davies, G. J. On the catalytic mechanisms of lytic polysaccharide monooxygenases. *Curr. Opin. Chem. Biol.* **2016**, *31*, 195−207.

(15) Bissaro, B.; Røhr, Å. K.; Müller, G.; Chylenski, P.; Skaugen, M.; Forsberg, Z.; Horn, S. J.; Vaaje-Kolstad, G.; Eijsink, V. G. H. Oxidative cleavage of polysaccharides by monocopper enzymes depends on H_2O_2. *Nat. Chem. Biol.* **2017**, *13*, 1123−1128.

(16) Jones, S. M.; Transue, W. J.; Meier, K. K.; Kelemen, B.; Solomon, E. I. Kinetic analysis of amino acid radicals formed in H_2O_2-driven CuI LPMO reoxidation implicates dominant homolytic reactivity. *Proc. Natl. Acad. Sci. U.S.A.* **2020**, *117*, 11916−11922.

(17) Bissaro, B.; Várnai, A.; Røhr, Å. K.; Eijsink, V. G. H. Oxidoreductases and reactive oxygen species in conversion of lignocellulosic biomass. *Microbiol. Mol. Biol. Rev.* **2018**, *82*, No. e00029.

(18) Kuusk, S.; Bissaro, B.; Kuusk, P.; Forsberg, Z.; Eijsink, V. G. H.; Sørlie, M.; Väljamäe, P. Kinetics of H_2O_2-driven degradation of chitin by a bacterial lytic polysaccharide monooxygenase. *J. Biol. Chem.* **2018**, *293*, 523−531.

(19) Kont, R.; Bissaro, B.; Eijsink, V. G. H.; Väljamäe, P. Kinetic insights into the peroxygenase activity of cellulose-active lytic polysaccharide monooxygenases (LPMOs). *Nat. Commun.* **2020**, *11*, 5786.

(20) Hedison, T. M.; Breslmayr, E.; Shanmugam, M.; Karnpakdee, K.; Heyes, D. J.; Green, A. P.; Ludwig, R.; Scrutton, N. S.; Kracher, D. Insights into the H_2O_2-driven catalytic mechanism of fungal lytic polysaccharide monooxygenases. *FEBS J.* **2021**, *288*, 4115−4128.

(21) Hangasky, J. A.; Iavarone, A. T.; Marletta, M. A. Reactivity of O_2 versus H_2O_2 with polysaccharide monooxygenases. *Proc. Natl. Acad. Sci. U.S.A.* **2018**, *115*, 4915−4920.

(22) Petrović, D. M.; Várnai, A.; Dimarogona, M.; Mathiesen, G.; Sandgren, M.; Westereng, B.; Eijsink, V. G. H. Comparison of three seemingly similar lytic polysaccharide monooxygenases from *Neurospora crassa* suggests different roles in plant biomass degradation. *J. Biol. Chem.* **2019**, *294*, 15068−15081.

(23) Hegnar, O. A.; Petrovic, D. M.; Bissaro, B.; Alfredsen, G.; Várnai, A.; Eijsink, V. G. H. pH-Dependent relationship between catalytic activity and hydrogen peroxide production shown via characterization of a lytic polysaccharide monooxygenase from Gloeophyllum trabeum. *Appl. Environ. Microbiol.* **2019**, *85*, No. e02612.

(24) Stepnov, A. A.; Forsberg, Z.; Sørlie, M.; Nguyen, G.-S.; Wentzel, A.; Røhr, Å. K.; Eijsink, V. G. H. Unraveling the roles of the reductant and free copper ions in LPMO kinetics. *Biotechnol. Biofuels* **2021**, *14*, 28.

(25) Filandr, F.; Man, P.; Halada, P.; Chang, H.; Ludwig, R.; Kracher, D. The H_2O_2-dependent activity of a fungal lytic polysaccharide monooxygenase investigated with a turbidimetric assay. *Biotechnol. Biofuels* **2020**, *13*, 37.

(26) Kittl, R.; Kracher, D.; Burgstaller, D.; Haltrich, D.; Ludwig, R. Production of four Neurospora crassa lytic polysaccharide monooxygenases in Pichia pastoris monitored by a fluorimetric assay. *Biotechnol. Biofuels* **2012**, *5*, 79.

(27) Caldararu, O.; Oksanen, E.; Ryde, U.; Hedegård, E. D. Mechanism of hydrogen peroxide formation by lytic polysaccharide monooxygenase. *Chem. Sci.* **2019**, *10*, 576−586.

(28) Wang, B.; Walton, P. H.; Rovira, C. Molecular mechanisms of oxygen activation and hydrogen peroxide formation in lytic polysaccharide monooxygenases. *ACS Catal.* **2019**, *9*, 4958−4969.
(29) Frandsen, K. E. H.; Simmons, T. J.; Dupree, P.; Poulsen, J.-C. N.; Hemsworth, G. R.; Ciano, L.; Johnston, E. M.; Tovborg, M.; Johansen, K. S.; Von Freiesleben, P.; Marmuse, L.; Fort, S.; Cottaz, S.; Driguez, H.; Henrissat, B.; Lenfant, N.; Tuna, F.; Baldansuren, A.; Davies, G. J.; Lo Leggio, L.; Walton, P. H. The molecular basis of polysaccharide cleavage by lytic polysaccharide monooxygenases. *Nat. Chem. Biol.* **2016**, *12*, 298−303.
(30) Courtade, G.; Ciano, L.; Paradisi, A.; Lindley, P. J.; Forsberg, Z.; Sørlie, M.; Wimmer, R.; Davies, G. J.; Eijsink, V. G. H.; Walton, P. H.; Aachmann, F. L. Mechanistic basis of substrate-O_2 coupling within a chitin-active lytic polysaccharide monooxygenase: An integrated NMR/EPR study. *Proc. Natl. Acad. Sci. U.S.A.* **2020**, *117*, 19178.
(31) Breslmayr, E.; Hanžek, M.; Hanrahan, A.; Leitner, C.; Kittl, R.; Šantek, B.; Oostenbrink, C.; Ludwig, R. A fast and sensitive activity assay for lytic polysaccharide monooxygenase. *Biotechnol. Biofuels* **2018**, *11*, 79.
(32) Loose, J. S. M.; Arntzen, M. Ø.; Bissaro, B.; Ludwig, R.; Eijsink, V. G. H.; Vaaje-Kolstad, G. Multipoint precision binding of substrate protects lytic polysaccharide monooxygenases from self-destructive off-pathway processes. *Biochemistry* **2018**, *57*, 4114−4124.
(33) Courtade, G.; Forsberg, Z.; Heggset, E. B.; Eijsink, V. G. H.; Aachmann, F. L. The carbohydrate-binding module and linker of a modular lytic polysaccharide monooxygenase promote localized cellulose oxidation. *J. Biol. Chem.* **2018**, *293*, 13006−13015.
(34) Isaksen, T.; Westereng, B.; Aachmann, F. L.; Agger, J. W.; Kracher, D.; Kittl, R.; Ludwig, R.; Haltrich, D.; Eijsink, V. G. H.; Horn, S. J. A C4-oxidizing lytic polysaccharide monooxygenase cleaving both cellulose and cello-oligosaccharides. *J. Biol. Chem.* **2014**, *289*, 2632−2642.
(35) Borisova, A. S.; Isaksen, T.; Dimarogona, M.; Kognole, A. A.; Mathiesen, G.; Várnai, A.; Røhr, Å. K.; Payne, C. M.; Sørlie, M.; Sandgren, M.; Eijsink, V. G. H. Structural and functional characterization of a lytic polysaccharide monooxygenase with broad substrate specificity. *J. Biol. Chem.* **2015**, *290*, 22955−22969.
(36) Müller, G.; Chylenski, P.; Bissaro, B.; Eijsink, V. G. H.; Horn, S. J. The impact of hydrogen peroxide supply on LPMO activity and overall saccharification efficiency of a commercial cellulase cocktail. *Biotechnol. Biofuels* **2018**, *11*, 209.
(37) Kuusk, S.; Kont, R.; Kuusk, P.; Heering, A.; Sørlie, M.; Bissaro, B.; Eijsink, V. G. H.; Väljamäe, P. Kinetic insights into the role of the reductant in H_2O_2-driven degradation of chitin by a bacterial lytic polysaccharide monooxygenase. *J. Biol. Chem.* **2019**, *294*, 1516−1528.
(38) Rieder, L.; Ebner, K.; Glieder, A.; Sørlie, M. Novel molecular biological tools for the efficient expression of fungal lytic polysaccharide monooxygenases in *Pichia pastoris*. *Biotechnol. Biofuels* **2021**, *14*, 122.
(39) Vaaje-Kolstad, G.; Houston, D. R.; Riemen, A. H. K.; Eijsink, V. G. H.; Van Aalten, D. M. F. Crystal structure and binding properties of the *Serratia marcescens* chitin-binding protein CBP21. *J. Biol. Chem.* **2005**, *280*, 11313−11319.
(40) Westereng, B.; Arntzen, M. Ø.; Aachmann, F. L.; Várnai, A.; Eijsink, V. G. H.; Agger, J. W. Simultaneous analysis of C1 and C4 oxidized oligosaccharides, the products of lytic polysaccharide monooxygenases acting on cellulose. *J. Chromatogr. A* **2016**, *1445*, 46−54.
(41) Kracher, D.; Scheiblbrandner, S.; Felice, A. K. G.; Breslmayr, E.; Preims, M.; Ludwicka, K.; Haltrich, D.; Eijsink, V. G. H.; Ludwig, R. Extracellular electron transfer systems fuel cellulose oxidative degradation. *Science* **2016**, *352*, 1098−1101.
(42) Frommhagen, M.; Westphal, A. H.; van Berkel, W. J. H.; Kabel, M. A. Distinct substrate specificities and electron-donating systems of fungal lytic polysaccharide monooxygenases. *Front. Microbiol.* **2018**, *9*, 1080.
(43) Buettner, G. R.; Jurkiewicz, B. A. Catalytic metals, ascorbate and free radicals: Combinations to avoid. *Radiat. Res.* **1996**, *145*, 532−541.
(44) Kachur, A. V.; Koch, C. J.; Biaglow, J. E. Mechanism of copper-catalyzed autoxidation of cysteine. *Free Radic. Res.* **1999**, *31*, 23−34.
(45) Severino, J. F.; Goodman, B. A.; Reichenauer, T. G.; Pirker, K. F. Is there a redox reaction between Cu(II) and gallic acid? *Free Radic. Res.* **2011**, *45*, 123−132.
(46) Zhang, X.; Wu, H.; Zhang, L.; Sun, Q. Horseradish peroxidase-mediated synthesis of an antioxidant gallic acid-g-chitosan derivative and its preservation application in cherry tomatoes. *RSC Adv.* **2018**, *8*, 20363−20371.
(47) Luo, D.; Smith, S. W.; Anderson, B. D. Kinetics and mechanism of the reaction of cysteine and hydrogen peroxide in aqueous solution. *J. Pharm. Sci.* **2005**, *94*, 304−316.
(48) Rigo, A.; Corazza, A.; Luisa Di Paolo, M.; Rossetto, M.; Ugolini, R.; Scarpa, M. Interaction of copper with cysteine: Stability of cuprous complexes and catalytic role of cupric ions in anaerobic thiol oxidation. *J. Inorg. Biochem.* **2004**, *98*, 1495−1501.
(49) Simmons, T. J.; Frandsen, K. E. H.; Ciano, L.; Tryfona, T.; Lenfant, N.; Poulsen, J. C.; Wilson, L. F. L.; Tandrup, T.; Tovborg, M.; Schnorr, K.; Johansen, K. S.; Henrissat, B.; Walton, P. H.; Lo Leggio, L.; Dupree, P. Structural and electronic determinants of lytic polysaccharide monooxygenase reactivity on polysaccharide substrates. *Nat. Commun.* **2017**, *8*, 1064.
(50) Aachmann, F. L.; Sorlie, M.; Skjak-Braek, G.; Eijsink, V. G. H.; Vaaje-Kolstad, G. NMR structure of a lytic polysaccharide monooxygenase provides insight into copper binding, protein dynamics, and substrate interactions. *Proc. Natl. Acad. Sci. U.S.A.* **2012**, *109*, 18779−18784.

https://doi.org/10.1021/acs.biochem.1c00407
Biochemistry 2021, 60, 3633−3643

Fast and specific peroxygenase reactions catalyzed by fungal mono-copper enzymes

Lukas Rieder, Anton A. Stepnov, Morten Sørlie, Vincent G.H. Eijsink*

Faculty of Chemistry, Biotechnology, and Food Sciences, Norwegian University of Life Sciences (NMBU), P.O. Box 5003, NO-1432, Ås, Norway

* For correspondence; E-mail: vincent.eijsink@nmbu.no

Supporting information

Table of contents

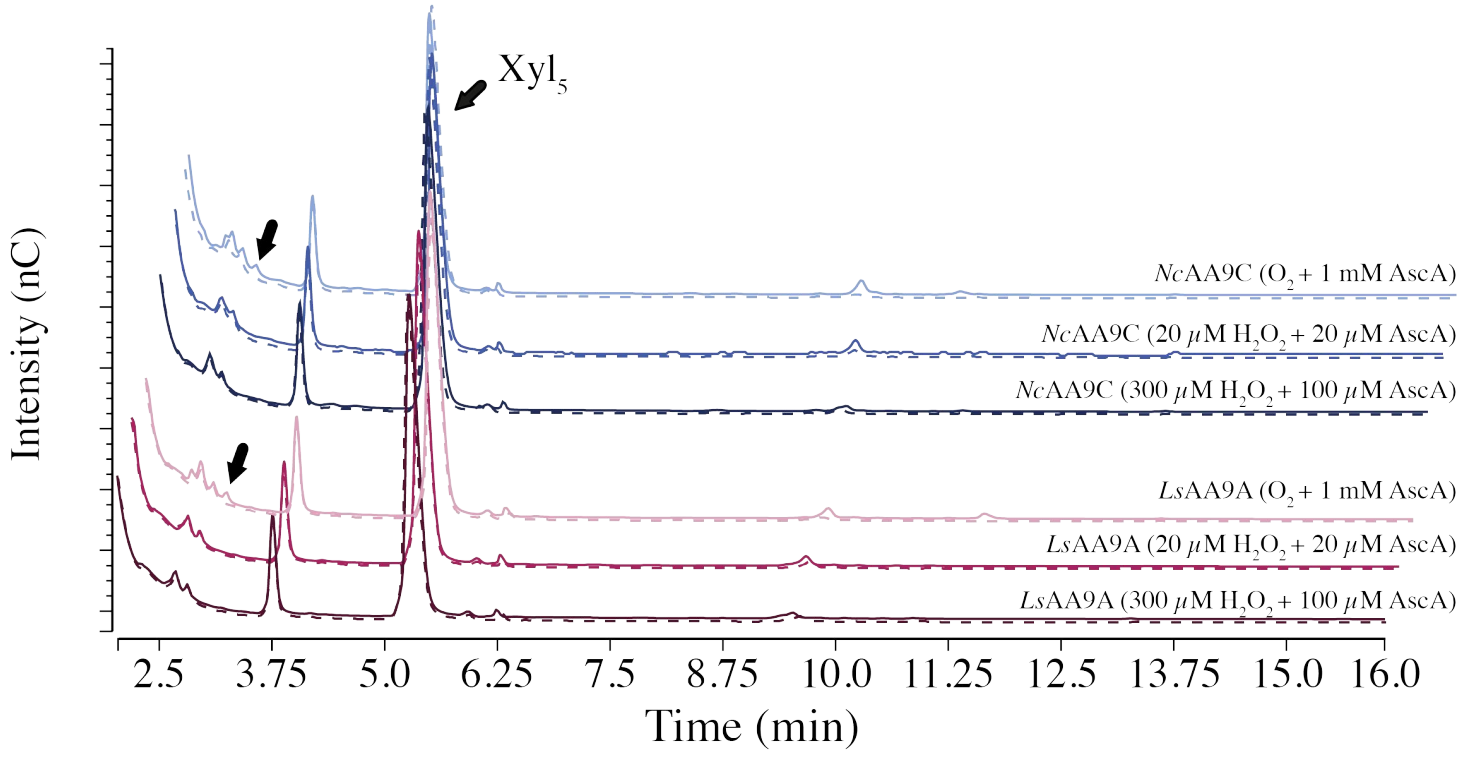

Figure S1. HPLC product profiles for reactions with 1 µM *Nc*AA9C (bluish colours) or *Ls*AA9A (purple colours) and 1 mM xylopentaose performed under standard aerobic conditions with the additions indicated in the chromatograms, and incubated overnight, at 37 °C. The dashed lines are chromatograms for corresponding reactions without AscA. Unlabeled arrows indicate minor amounts of unidentified products that may derive form oxidative cleavage of xylopentaose.

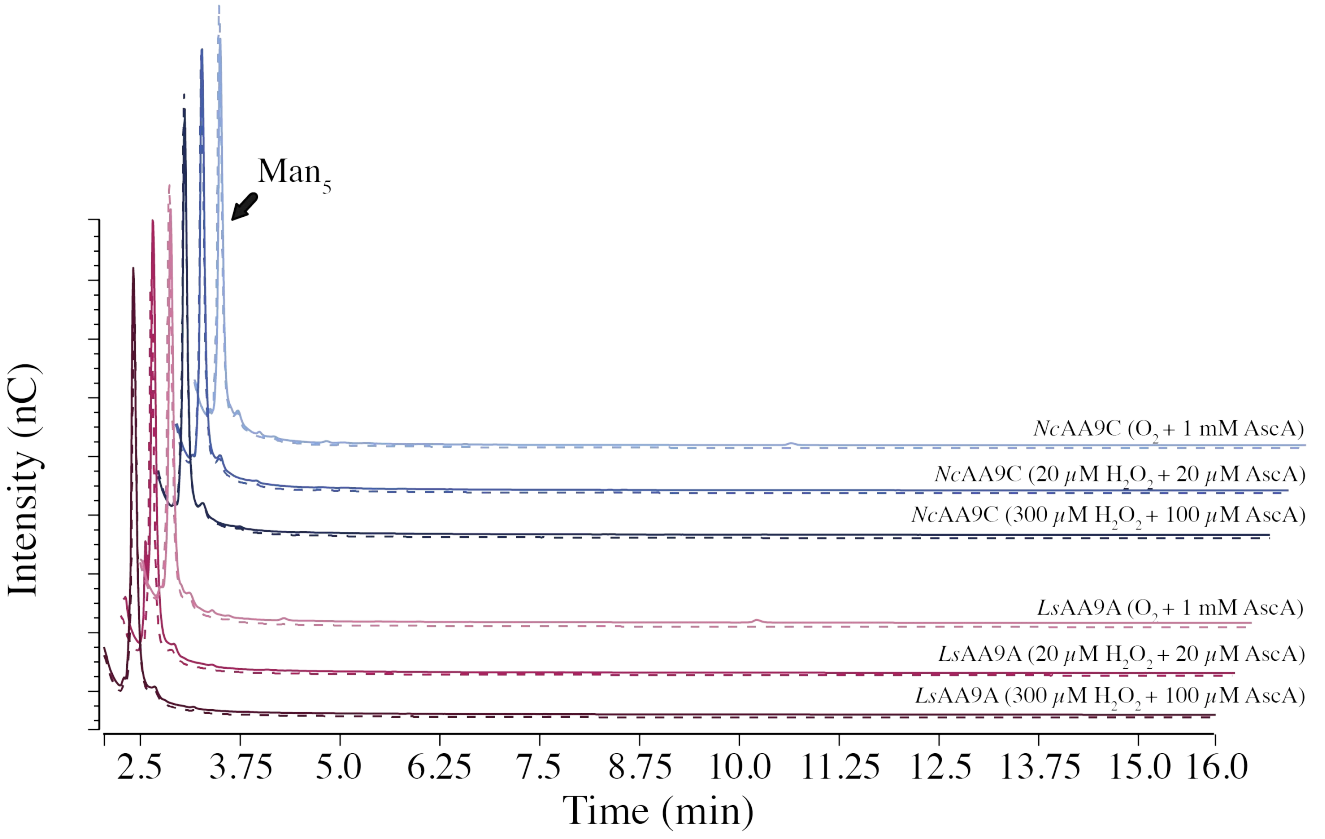

Figure S2. HPLC product profiles for reactions with 1 µM *Nc*AA9C (bluish colours) or *Ls*AA9A (purple colours) and 1 mM mannopentaose performed under standard aerobic conditions with the additions indicated in the chromatograms, and incubated overnight, at 37 °C. The dashed lines are chromatograms for corresponding reactions without AscA.

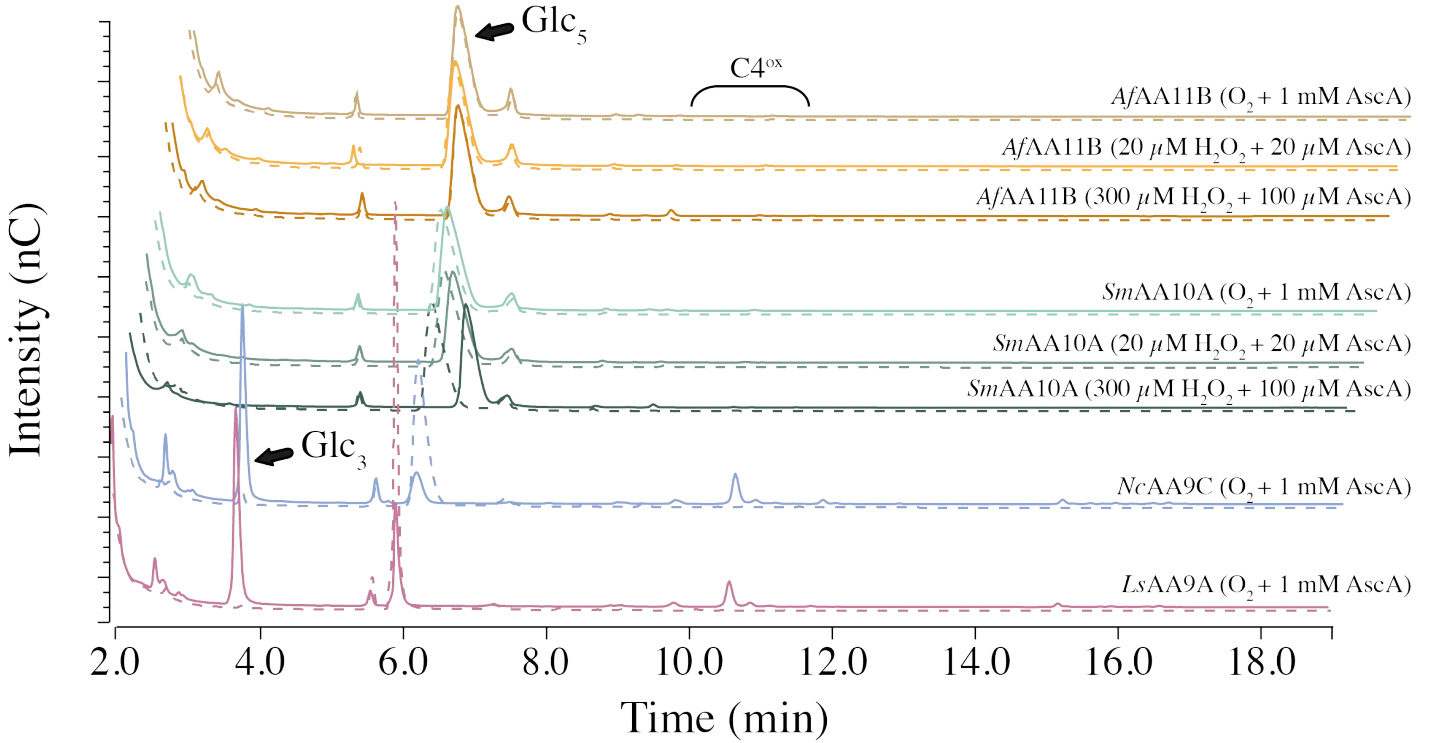

Figure S3. HPLC product profiles for reactions with 1 µM *Af*AA11B (yellow colours) or *Sm*AA10A (green colours) and 1 mM cellopentaose performed under standard aerobic conditions with the additions indicated in the chromatograms, and incubated overnight, at 37 °C. For comparison, positive controls showing products generated upon aerobic overnight reactions with *Nc*AA9C (blue) and *Ls*AA9A (purple) are included. The position of peaks corresponding to C4-oxidized products is indicated by "C4^{ox}". The dashed lines are chromatograms for corresponding reactions without AscA.

ISBN: 978-82-575-1900-1
ISSN: 1894-6402

Norwegian University
of Life Sciences

Postboks 5003
NO-1432 Ås, Norway
+47 67 23 00 00
www.nmbu.no